

**STUDIES OF LIGAND BINDING, AND THREE
DIMENSIONAL STRUCTURES OF CHITINASE A
FROM *VIBRIO HARVEYI* IN COMPLEX WITH
POTENTIAL INHIBITORS**

Supansa Pantoom



**A Thesis Submitted in Partial Fulfillment of the Requirements
for the Degree of Doctor of Philosophy in Biochemistry
Suranaree University of Technology**

Academic Year 2011

การศึกษาการจับกับลิแกนด์และโครงสร้างสามมิติเชิงซ้อนของโคติเนส เอ
จากเชื้อ *Vibrio harveyi* ที่มีตัวยับยั้งอยู่ด้วย



นางสาวสุพรรณษา ปานทุม

วิทยานิพนธ์นี้เป็นส่วนหนึ่งของการศึกษาตามหลักสูตรปริญญาวิทยาศาสตรดุษฎีบัณฑิต
สาขาวิชาชีวเคมี
มหาวิทยาลัยเทคโนโลยีสุรนารี
ปีการศึกษา 2554

**STUDIES OF LIGAND BINDING, AND THREE DIMENSIONAL
STRUCTURES OF CHITINASE A FROM *VIBRIO HARVEYI* IN
COMPLEX WITH POTENTIAL INHIBITORS**

Suranaree University of Technology has approved this thesis submitted in partial fulfillment of the requirements for the Degree of Doctor of Philosophy.

Thesis Examining Committee

(Asst. Prof. Dr. Kunwadee Rangriwatananon)

Chairperson

(Assoc. Prof. Dr. Wipa Suginta)

Member (Thesis Advisor)

(PD. Dr. Heino Prinz)

Member

(Assoc. Prof. Dr. Robert C. Robinson)

Member

(Assoc. Prof. Dr. James R. Ketudat Cairns)

Member

(Prof. Dr. Sukit Limpijumnong)

Vice Rector for Academic Affairs

(Assoc. Prof. Dr. Prapun Manyum)

Dean of Institute of Science

สุพรรณษา ปานทุม : การศึกษาการจับกับลิแกนด์และโครงสร้างสามมิติเชิงซ้อนของ
ไคตินเนส เอ จากเชื้อ *Vibrio harveyi* ที่มีตัวยับยั้งอยู่ด้วย (STUDIES OF LIGAND
BINDING, AND THREE DIMENSIONAL STRUCTURES OF CHITINASE A FROM
VIBRIO HARVEYI IN COMPLEX WITH POTENTIAL INHIBITORS)

อาจารย์ที่ปรึกษา : รองศาสตราจารย์ ดร.วิภา สุจินต์, 269 หน้า.

ไคตินเนส เอ จากเชื้อ *Vibrio harveyi* หรือ *VhChiA* จัดอยู่ในกลุ่มของไกลโคซิลไฮโดร
เลสลำดับที่ 18 ซึ่งมีส่วนประกอบของโครงสร้างหลักแบ่งเป็นสามส่วนคือ 1) โดเมนจับไคตินที่
ปลายด้านอะมิโน 2) โดเมนเร่งปฏิกิริยามีโครงสร้างแบบ $(\alpha/\beta)_8$ -TIM-barrel และ 3) โดเมนเล็ก
แทรกกระหว่างโดเมนจับไคตินกับโดเมนเร่งปฏิกิริยามีโครงสร้างแบบ $\alpha+\beta$ โดเมนจับไคตินทำ
หน้าที่สำคัญในการจับกับไคตินสายยาว ในขณะที่โดเมนเร่งปฏิกิริยามีหน้าที่สำคัญในการจับไคติน
สายสั้นและมีหน้าที่ในกระบวนการย่อยสลายไคติน งานวิจัยส่วนแรกทำการศึกษาบทบาทและ
หน้าที่ของกรดอะมิโน Ser33 Trp70 Trp231 และ Trp245 ซึ่งเป็นกรดอะมิโนที่จัดเรียงอยู่บนพื้นผิว
ของไคตินเนส การศึกษาผลของการกลายพันธุ์พบว่า กรดอะมิโน Trp70 ซึ่งอยู่ที่ปลายสุดของโดเมน
จับไคตินมีบทบาทสำคัญที่สุดในการจับและย่อยสลายไคตินสายยาว กรดอะมิโนที่มีบทบาทสำคัญ
รองลงมาคือกรดอะมิโน Ser33 ส่วนกรดอะมิโน Trp231 และ Trp245 เป็นกรดอะมิโนที่อยู่ด้าน
นอกของโดเมนเร่งปฏิกิริยามีความเกี่ยวข้องกับการย่อยสลายไคตินแต่ไม่มีบทบาทในการช่วยจับ
กับไคตินสายยาว

ในงานวิจัยส่วนที่สองตัวยับยั้งทั้งเจ็ดชนิดของไคตินเนสจากเชื้อ *V. harveyi* ได้ถูกค้นพบจาก
Library of Pharmacologically Active Compounds (LOPAC) โดยวิธี high-throughput screening
assay พบว่า ตัวยับยั้งที่มีศักยภาพดีที่สุดคือ dequalinium ซึ่งสามารถยับยั้งแอกติวิตีของเอนไซม์
VhChiA ที่ค่า K_i เท่ากับ 70 nM ซึ่งตัวยับยั้งจำนวนหกชนิดจากเจ็ดชนิด ยกเว้น PEN จัดเป็นตัว
ยับยั้งชนิดใหม่ของไคตินเนสแฟมิลี 18 จากการศึกษาโครงสร้างสามมิติเชิงซ้อน 14 โครงสร้างของ
ไคตินเนสกับตัวยับยั้งเหล่านี้พบว่า ลักษณะการจับของตัวยับยั้งนั้นครอบคลุมพื้นที่ส่วนบนของ
บริเวณเร่งและจับกับบริเวณที่ไม่มีขั้ว สองตำแหน่งคือตำแหน่ง glycone ที่บริเวณจับ -4 ถึง -2 และ
ตำแหน่ง aglycone ที่บริเวณจับ +1 ถึง +2 ซึ่งแตกต่างจากการจับของตัวยับยั้งที่ถูกค้นพบก่อนหน้านี้
โดยที่ตัวยับยั้งเหล่านี้มีลักษณะการจับคล้ายกับ reaction intermediate โดยจะจับในร่องของบริเวณ
เร่งปฏิกิริยาในตำแหน่งย่อยสลายสับสเตรทที่บริเวณ -1 ในการศึกษาพบว่า ตัวยับยั้งเข้าจับกับ
เอนไซม์ดั้งเดิมในตำแหน่ง aglycone กับกรดอะมิโน Trp275 และ Trp397 ด้วยสัมพรรคภาพสูง
เนื่องจากแสดงแผนที่ความหนาแน่นอิเล็กตรอนของตัวยับยั้งอย่างเด่นชัด ขณะที่ตัวยับยั้งจับที่

ตำแหน่ง glycone กับกรดอะมิโน Trp168 และ Val205 เป็นการจับแบบไม่แน่นอนเนื่องจากมีแผนที่ความหนาแน่นอิเล็กตรอนที่ไม่ชัดเจน แสดงให้เห็นว่าการจับที่ตำแหน่ง glycone มีสัมพรรคภาพต่ำ การเปลี่ยนกรดอะมิโน Trp275 ไปเป็นกรดอะมิโน Gly ส่งผลให้สัมพรรคภาพในการจับของตัวยับยั้งลดลงอย่างมากและมีการเปลี่ยนรูปแบบของการจับของตัวยับยั้ง โดยที่ตัวยับยั้งทั้งสองจะจับกันแบบ stacking และจับกับกรดอะมิโน Trp397 ที่ตำแหน่ง aglycone การศึกษากลไกการจับของตัวยับยั้งกับไคตินเนสโดยวิธี isothermal microcalorimetry พบว่า มีสามกลไก คือ 1) a single-site-binding mode 2) a two-independent-site binding mode และ 3) a two-sequential-site binding mode ตัวยับยั้งที่มีศักยภาพในการยับยั้งดีที่สุดคือ dequalinium ซึ่งสามารถยับยั้งได้ที่ความเข้มข้นระดับ nM ถือเป็นตัวยับยั้งที่น่าสนใจเป็นอย่างยิ่งที่จะนำไปพัฒนาการรักษาโรคในคนที่มีพยาธิสภาพเกี่ยวข้องกับไคตินเนส



สาขาวิชาชีวเคมี
ปีการศึกษา 2554

ลายมือชื่อนักศึกษา _____
ลายมือชื่ออาจารย์ที่ปรึกษา _____
ลายมือชื่ออาจารย์ที่ปรึกษาร่วม _____

SUPANSA PANTOOM : STUDIES OF LIGAND BINDING, AND THREE
DIMENSIONAL STRUCTURES OF CHITINASE A FROM *VIBRIO*
HARVEYI IN COMPLEX WITH POTENTIAL INHIBITORS.

THESIS ADVISOR : ASSOC. PROF. WIPA SUGINTA, Ph.D. 269 PP.

CHITIN BINDING DOMAIN/CHITINASE INHIBITORS/*VIBRIO HARVEYI*
CHITINASE A/LOPAC LIBRARY

Vibrio harveyi chitinase A or *VhChiA* (EC 3.2.1.14) is a member of family-18 glycoside hydrolases. The structure of *VhChiA* comprises three main domains: i) the *N*-terminal chitin binding domain (ChBD); ii) the $(\alpha/\beta)_8$ TIM barrel catalytic domain (CatD); and iii) the $\alpha+\beta$ small insertion domain. The ChBD is important for binding to long-chain substrates, while the CatD is important for binding to chitooligosaccharides and participating in enzyme catalysis. In the first part of this study, four surface-exposed residues (Trp70, Ser33, Trp231, and Tyr245) were investigated. Mutational analysis suggested that Trp70 located at the end of the ChBD is crucial for binding and catalytic activities of *VhChiA* towards chitin polymer. Ser33 located nearby also showed binding effects, but to a lesser extent. The other two residues, Trp231 and Tyr245, which are located outside the substrate-binding cleft, are involved in chitin hydrolysis, but do not play a major role in the chitin binding process.

In the second part of this study, seven inhibitors against *VhChiA* were identified from the Library of Pharmacologically Active Compounds (LOPAC) by a high throughput screening assay, with dequalinium being the most active with the K_i of 70 nM. Six out of the seven inhibitors are novel in their inhibitory effects against

family-18 chitinases. Fourteen *VhChiA*-inhibitor complexes revealed that all the inhibitor molecules only occupied the upper part of the substrate binding cleft in two hydrophobic areas (the glycone area around subsites -4 to -2 and the aglycone area around subsites +1 and +2). Such findings are different from the previously-reported inhibitors that mimicked the reaction intermediate by occupying the bottom of the chitinase's active site at subsite -1. The binding of the inhibitors to the wild-type enzyme at the aglycone sites are well defined and tightly associated with the two important aromatic residues Trp397 and Trp275, whereas interactions at the glycone sites are connected with two consensus residues, Trp168 and Val205, and are patchy with an ill-defined inhibitor density, indicating lower affinity of binding at the glycone subsites. When Trp275 was substituted with glycine (mutant W275G), the binding affinities towards all the inhibitors dramatically decreased and in most structures two inhibitor molecules were found to stack against Trp397 at the aglycone binding site. Isothermal microcalorimetry confirmed that the inhibitors occupied the active site of *VhChiA* in three different binding modes, including 1) a single-site-binding mode 2) a two-independent-site binding mode; and 3) a two-sequential-site binding mode. From chemical biology point of view, dequalinium, the most potent inhibitor with the inhibitory effect at low nM level, could serve as an extremely attractive lead compound for plausible development of therapeutics against human diseases involving chitinase-mediated pathologies.

School of Biochemistry

Student's Signature _____

Academic Year 2011

Advisor's Signature _____

Co-adviser's Signature _____

ACKNOWLEDGEMENTS

I would like to express my gratitude to my supervisor Assoc. Prof. Dr. Wipa Suginta for giving me the opportunity to work on this project. Her guidance, support and ideas made this work interesting for me and gave me a lot of inspiration. Throughout the work, she provided her valuable time for guiding and correcting me, which made this thesis successful.

Furthermore, I would like to thank my co-supervisors at the Max-Planck Institute of Molecular Physiology (MPI), Dortmund, Germany:

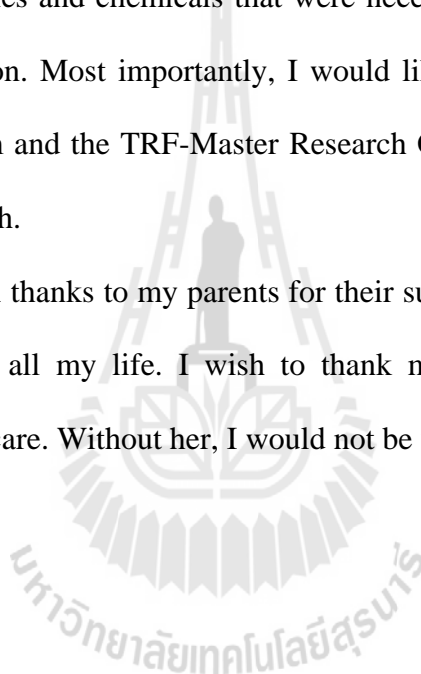
- 1) PD.Dr. Heino Prinz from the Department of Chemical Biology for his supervision on enzyme kinetics and enzyme-ligand binding assays. His great support and effort helped me to perform all the experiments properly. Also, I am grateful for his kind support throughout my time in Germany.
- 2) Dr. Ingrid Vetter from the Department of Physical Biochemistry for passing on her great expertise in protein crystallization and structural determination. Also, her help with the data collection at the Swiss Light Source at the Paul Scherrer Institute, Switzerland is acknowledged.

I would like to thank all the lecturers of the School of Biochemistry at Suranaree University of Technology (SUT) for passing on to me their biochemistry knowledge and biochemical lab techniques, which were later found to be useful for my project development.

I wish to extend my warmest thanks to my colleagues at the Biochemistry-Electrochemistry Research Unit, SUT for helping me to get through the difficult times, and for all the emotional support, friendship, entertainment, and caring that they provided.

I would like to express my gratitude to the Biochemistry-Electrochemistry Research Unit and the MPI-Dortmund for providing research facilities, including equipment, consumables and chemicals that were necessary for enzyme kinetics and structural determination. Most importantly, I would like to thank the Royal Golden Jubilee Ph.D. Program and the TRF-Master Research Grant for the financial support throughout my research.

Finally, special thanks to my parents for their support, understanding and love they provide through all my life. I wish to thank my grandmother for her great support, her love and care. Without her, I would not be what I am today.



Supansa Pantoom

CONTENTS

	Page
ABSTRACT IN THAI.....	I
ABSTRACT IN ENGLISH	III
ACKNOWLEDGEMENTS.....	V
CONTENTS.....	VII
LIST OF TABLES.....	XV
LIST OF FIGURES	XVIII
CHAPTER	
I INTRODUCTION.....	1
1.1 Chitin and applications.....	1
1.2 Classification of chitinases	2
1.3 Catalytic mechanism of family-18 chitinases	4
1.4 Function of chitin binding protein.....	9
1.5 Interactions of chitin substrates in the substrate binding cleft of family-18 chitinases.....	12
1.6 Studies of chitinase inhibitors.....	14
1.7 Studies of <i>V. harveyi</i> chitinase A.....	25
1.8 Research objectives.....	27
II MATERIALS AND METHODS	29
2.1 Chemicals and reagents.....	29

CONTENTS (Continued)

	Page
2.1.1 Bacterial strains and plasmids.....	29
2.1.2 Site directed mutagenesis and plasmid purification.....	29
2.1.3 Protein expression and purification	30
2.1.4 Enzyme kinetics	30
2.1.4.1 Reagents and buffers.....	30
2.1.4.2 Substrates for chitinase assays	31
2.1.4.3 Chitinase inhibitors	31
2.1.5 Protein crystallization	31
2.1.5.1 Crystallization screening and optimization.....	31
2.1.5.2 Buffers and precipitants	32
2.2 Instrumentation	32
2.2.1 Instrumentation used at Suranaree University of Technology (SUT), Thailand.....	32
2.2.2 Instrumentation used at the Max-Planck-Institut für Molekulare Physiologie (MPI), Dortmund, Germany	33
2.3 Analytical programs.....	34
2.4 PCR primers.....	34
2.5 Mutational design and site-directed mutagenesis	35
2.6 Structure-based sequence alignment and homology modeling.....	37
2.7 Expression and purification of chitinase A variants	38
2.8 High-throughput screening	39

CONTENTS (Continued)

	Page
2.9 Determination of dose-response curves	40
2.10 Determination of three-dimensional structures	
of chitinase-inhibitor complexes	41
2.10.1 Protein crystallization of the wild type chitinase and mutants W275G and W397F	41
2.10.2 Cryocrystallization and crystal storage	43
2.10.3 Data collection and processing	44
2.10.4 Phase determination by the molecular replacement method.....	45
2.10.5 Model rebuilding and structural refinement	45
2.10.6 Validation of the quality of the model	48
2.11 Determination of chitinase activity	48
2.11.1 Chitinase activity assay using the dimethylaminoborane (DMAB) method	48
2.11.2 Chitinase activity assay using the dinitrosalicylic acid (DNS) method	49
2.11.3 Chitinase activity assay using <i>p</i> NP-glycosides.....	49
2.11.4 Chitinase activity assay using 4MU-glycosides	50
2.12 Steady-state kinetics.....	50
2.13 Chitin binding assay and determination of adsorption	
binding isotherm	51

CONTENTS (Continued)

	Page
2.14 Determination of the inhibitor binding modes using isothermal microcalorimetry (ITC)	52
2.15 Determination of chitinase-inhibitor interactions using fluorescence spectroscopy	53
III RESULTS	55
PART I	55
3.1 Homology modeling and sequence analysis	55
3.2 Mutational design and site-directed mutagenesis	59
3.3 Expression and purification of <i>VhChiA</i> and mutants	59
3.4 Effects of point mutations on chitin binding activity of <i>VhChiA</i>	60
3.5 Effects of point mutations on hydrolytic activity of <i>VhChiA</i>	65
3.6 Steady-state kinetics of <i>VhChiA</i> and mutants	67
PART II	70
3.7 Expression and purification of wild-type chitinase and mutants W275G and W397F	70
3.8 Screening of potential chitinase inhibitors from a drug library	72
3.9 Crystallization of the wild-type chitinase and mutants W275G and W397F	77
3.9.1 Crystallization of the wild-type <i>VhChiA</i>	78
3.9.1.1 Initial screening and optimization	78

CONTENTS (Continued)

	Page
3.9.1.2 Crystal soaking and co-crystallization	
with the identified inhibitors	86
3.9.1.3 Data collection, processing and structure solution.....	88
3.9.2 Crystallization of <i>VhChiA</i> mutant W275G	92
3.9.2.1 Initial screening and optimization.....	92
3.9.2.2 Crystal soaking and co-crystallization	
with the identified inhibitors	100
3.9.2.3 Data collection, processing and structure solution.....	101
3.9.3 Crystallization of <i>VhChiA</i> mutant W397F.....	103
3.9.3.1 Initial screening and optimization.....	103
3.10 Structural comparison of the apo form of the wild-type	
<i>VhChiA</i> and mutant W275G.....	107
3.11 The structures of complexes of wild-type <i>VhChiA</i> and	
the newly-identified chitinase inhibitors.....	113
3.11.1 The structure of the complex of wild-type <i>VhChiA</i>	
with dequalinium (DEQ)	115
3.11.2 The structure of the complex of WT <i>VhChiA</i>	
with sanguinarine (SAN)	117
3.11.3 The structure of the complex of wild-type <i>VhChiA</i>	
with chelerythrine (CHE).....	119

CONTENTS (Continued)

	Page
3.11.4 The structure of the complex of wild-type <i>VhChiA</i> with idarubicin (IDA).....	122
3.11.5 The structure of the complex of wild-type <i>VhChiA</i> with 2-(imidazolin-2-yl)-5-isothiocyanatobenzofuran (IMI).....	124
3.11.6 The structure of the complex of wild-type <i>VhChiA</i> with pentoxifylline (PEN).....	127
3.11.7 The structure of the complex of wild-type <i>VhChiA</i> with propentofylline (PRO)	129
3.12 The structures of the complexes of mutant W275G with the newly identified inhibitors	133
3.13 Effects of the inhibitors on hydrolytic activity of the wild-type <i>VhChiA</i> against soluble and insoluble substrates	141
3.14 Binding study by fluorescence titration spectroscopy	143
3.15 Isothermal titration microcalorimetry (ITC) experiments	146
IV DISCUSSION	154
4.1 Investigation of the role of surface-exposed residues on substrate binding and catalytic activities of <i>VhChiA</i>	154
4.2 High throughput screening of the chitinase inhibitors from the LOPAC library	157

CONTENTS (Continued)

	Page
4.3 Crystallization of <i>VhChiA</i> and mutants	
W275G and W397F	159
4.4 Inhibitory effects and binding mechanisms of the newly identified inhibitors against <i>VhChiA</i>	162
4.5 A structural comparison between the WT-inhibitor complexes and W275G-inhibitor complexes.....	168
4.6 A structural comparison between the wild-type bound with the substrate and with the inhibitors	174
4.7 Implications of structural and mechanistic studies of <i>VhChiA</i> -inhibitor complexes on therapeutics of asthma and inflammation	176
V CONCLUSION	179
REFERENCES	184
APPENDICES	207
APPENDIX A PREPARATION OF COMPETENT CELLS AND PLASMID TRANSFORMATION.....	208
APPENDIX B DETERMINATION OF PROTEIN CONCENTRATION...211	
APPENDIX C PREPARATION OF SOLUTIONS AND REAGENTS.....213	
APPENDIX D STANDARD CURVES	229
APPENDIX E DNA SEQUENCING AND AMINO ACID SEQUENCE ALIGNMENT.....	232

CONTENTS (Continued)

	Page
APPENDIX F PUBLICATIONS.....	236
CURRICULUM VITAE.....	269



LIST OF TABLES

Table	Page
1.1 A comparison of sequence identity and the D _{xx} D _x D _x E conserved motifs of family-18 glycoside hydrolases.....	8
1.2 Substitutions of allosamidin and its derivatives.....	16
1.3 A summary of inhibitory effects and binding affinities of family-18 chitinase inhibitors identified to date	24
2.1 Primers for site-directed mutagenesis.....	35
2.2 The PCR reaction used for site-directed mutagenesis	36
2.3 The PCR conditions used for site-directed mutagenesis.....	37
3.1 Specific hydrolytic activity of <i>VhChiA</i> and mutants	66
3.2 Kinetic parameters of substrate hydrolysis by chitinase A wild-type and mutants.....	69
3.3 IC_{50} from the dose response curves using the <i>pNP</i> assay with <i>pNP</i> -GlcNAc ₂ as substrate for wild-type and mutant W397F and <i>pNP</i> -GlcNAc ₃ for mutant W275G	76
3.4 A summary of positive conditions obtained from crystallization of the wild-type <i>VhChiA</i> within 8 days of incubation	79
3.5 A grid screening of <i>VhChiA</i> with 1.0 M ammonium sulfate at various pH values.....	80

LIST OF TABLES (Continued)

Table	Page
3.6 A grid screening of PEG 4000, propanal in 0.1 M sodium citrate tribasic dihydrate, pH 5.6, for crystallization of wild-type chitinase A....	82
3.7 A refined screening of the condition containing 20% (w/v) PEG 4000, and propanol in 0.1 M tribasic sodium citrate dihydrate, pH 5.0	83
3.8 A grid screening of MPD in 0.2 ammonium phosphate at various pH values and concentrations of ammonium phosphate at 75% (v/v) MPD for crystallization of wild-type chitinase A	85
3.9 Data collection statistics for <i>VhChiA</i> wild-type in complex with seven inhibitors identified from the LOPAC library	91
3.10 A summary of positive conditions obtained from the microbatch technique for crystallization of W275G within 38 days of incubation ...	93
3.11 A grid screening of PEG 4000 in 0.1 M ammonium acetate with various pH values for crystallization of W275G	95
3.12 A refined screening of the condition containing PEG 4000 in 0.1 M ammonium acetate, pH 5.5, obtained from Table 3.10	97
3.13 Data collection statistics for the <i>VhChiA</i> mutant W275G in complex with six inhibitors identified from the LOPAC library	102
3.14 A summary of positive conditions obtained from the commercial screening kits using the microbatch technique for crystallization of W397F within 30 days incubation at 22°C	104

LIST OF TABLES (Continued)

Table	Page
3.15 A grid screening of ethylene imine polymer (EIP) in 0.5 M sodium chloride in 0.1 M sodium citrate tribasic dihydrate, pH 5.6.....	105
3.16 A grid screening of PEG 4000, 0.5 M sodium chloride in 0.1 M sodium citrate tribasic dihydrate, pH 5.6	106
3.17 Numbers of amino acid residues observed in the <i>VhChiA</i> -inhibitor complexes	111
3.18 A summary of the interactions between the inhibitors and the binding residues in the substrate-binding cleft of the wild-type <i>VhChiA</i>	132
3.19 A summary of the interactions between the inhibitors and the binding residues in the substrate-binding cleft of mutant W275G	139
3.20 The inhibition effects of the inhibitors on specific activity of the wild-type <i>VhChiA</i> against soluble and insoluble substrates, as determined by the DMAB assay	142
3.21 Parameters used for the calculation of theoretical ITC curves	153
4.1 IC_{50} and K_D values obtained from four different assays	167

LIST OF FIGURES

Figure	Page
1.1 Ribbon representation of the main fold of the catalytic domain of the family 18 (PDB code: 1NH6) and family 19 (PDB code: 3CQL) chitinases.....	3
1.2 The catalytic cycle of family-18 glycoside hydrolases.....	6
1.3 A model of crystalline β -chitin hydrolysis by <i>B. circulans</i> ChiA	12
1.4 Positions of the aromatic residues in the catalytic binding cleft of CatDChiA1 from <i>B. circulans</i> complexed with GlcNAc ₇	13
1.5 The chemical structures of oxazolinium ion intermediate and allosamidin	17
1.6 Argifin and argadin in two-dimensional structures	18
1.7 Chemical structures of argifin-derived peptides	20
1.8 The chemical structures of allosamidin and cyclic dipeptides.....	21
1.9 Structures of AMCcase inhibitors identified by HTS, FBS, VS, and SSS ..	23
3.1 Swiss-model 3D-structure of <i>VhChiA</i>	57
3.2 Structure-based alignment of <i>VhChiA</i> with <i>S. marcescens</i> chitinase A and <i>B. circulans</i> chitinase A1.....	58
3.3 Agarose gel electrophoresis of the PCR products of <i>VhChiA</i> DNA fragment obtained by site-directed mutagenesis	59
3.4 SDS-PAGE analysis of <i>VhChiA</i> and its mutants.....	60

LIST OF FIGURES (Continued)

Figure	Page
3.5 Time-course of binding of <i>VhChiA</i> variants to colloidal chitin	61
3.6 Binding of <i>VhChiA</i> and mutants to insoluble chitin	63
3.7 Equilibrium adsorption isotherms of the wild-type and mutated <i>VhChiA</i> to colloidal chitin	64
3.8 Michaelis-Menten plots of the wild-type and mutated <i>VhChiA</i> to chitohexaose and colloidal chitin.....	68
3.9 Purification of chitinase A mutant W275G using a Ni-NTA agarose, followed by a HisTrap™ affinity chromatography	71
3.10 Dose response curves of the wild type chitinase against the inhibitors newly identified from the LOPAC library.....	73
3.11 The chemical structures of the chitinase inhibitors identified from the LOPAC library.....	74
3.12 Optimization of the wild-type crystal grown under the condition A4 from JBScreen HTSII	81
3.13 Optimization of wild-type crystal growth from the condition 40 from Crystal Screen HR2-110	84
3.14 Optimization of wild-type crystals grown from the condition 43 from Crystal Screen HR2-112	86
3.15 Single crystals obtained from co-crystallization with DEQ and PRO using the micro-seeding technique.....	87
3.16 Diffraction images of the wild-type crystal	90

LIST OF FIGURES (Continued)

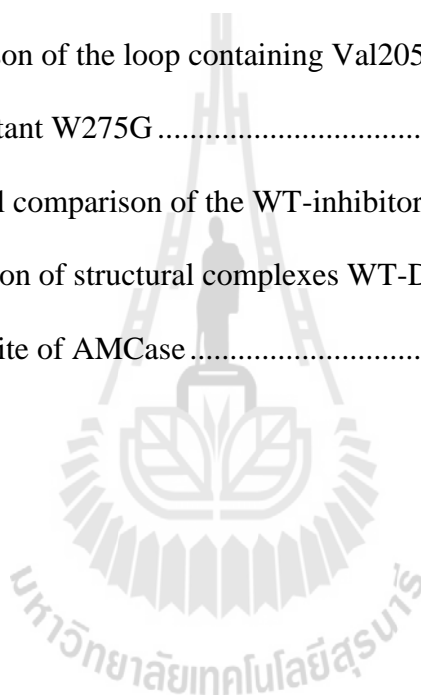
Figure	Page
3.17 Optimization of W275G crystal growth from the condition 9 of Crystal Screen HR2-112.....	96
3.18 Plate clusters of W275G obtained from a grid screening of PEG 4000 in 0.1 M ammonium acetate with various pH values	98
3.19 Crystals of W275G obtained from the streak-seeding technique	99
3.20 Single crystals of W275G obtained from pipetting seeding technique..	100
3.21 Optimization of W397F crystal growth from the condition 16 of Crystal Screen HR2-112 and the condition 40 of Crystal Screen HR2-110.....	107
3.22 A comparison of the overall structure of wild-type <i>VhChiA</i> and mutant W275G.....	109
3.23 Docking of GlcNAc ₆ (E315M+NAG ₆ , PDB code: 3b9a) to the apo form of the <i>VhChiA</i> structure.....	112
3.24 Surface representation of the structural complexes of the wild-type <i>VhChiA</i> with seven different inhibitors.....	114
3.25 The-structure of the complex of wild-type <i>VhChiA</i> with DEQ	116
3.26 The structure of the complex of wild-type <i>VhChiA</i> with SAN	118
3.27 The first structure of the complex of wild-type <i>VhChiA</i> with CHE	120
3.28 The second structure of the complex of wild-type <i>VhChiA</i> with CHE .	121
3.29 The structure of the complex of wild-type <i>VhChiA</i> with IDA	123
3.30 The first structure of the complex of the wild-type <i>VhChiA</i> with IMI..	125

LIST OF FIGURES (Continued)

Figure	Page
3.31 The second structure of the complex of the wild-type <i>VhChiA</i> with IMI	126
3.32 The structure of the complex of wild-type <i>VhChiA</i> with PEN	128
3.33 The structure of the complex of wild-type <i>VhChiA</i> PRO	130
3.34 The structures of the complexes of mutant W275G with six inhibitors	135
3.35 The electron density maps of all the inhibitors in active site of W275G.....	137
3.36 Details of the interactions of PEN and PRO in the active site of W275G.....	140
3.37 A protein-inhibitor binding study by intrinsic fluorescence spectroscopy	144
3.38 Binding curves determined for each inhibitor	145
3.39 Thermographic binding isotherms of wild-type with DEQ, SAN and PEN	147
3.40 Thermographic binding isotherms of W275G with DEQ, SAN and PEN	150
3.41 Thermographic binding isotherms of W397F with DEQ, SAN and PEN	152
4.1 A summary of <i>VhChiA</i> -inhibitor interactions as revealed by crystallographic data	169

LIST OF FIGURES (Continued)

Figure	Page
4.2 Different binding behaviors of the inhibitors in the active site of the wild-type and mutant W275G, when compare with the binding of GlcNAc ₆	171
4.3 A comparison of the loop containing Val205 in the wild-type and the mutant W275G	173
4.4 A structural comparison of the WT-inhibitors and the WT-GlcNAc ₆	175
4.5 Superposition of structural complexes WT-DEQ with the active site of AMCcase	177



CHAPTER I

INTRODUCTION

1.1 Chitin and applications

Chitin is a homopolysaccharide chain of *N*-acetylglucosamine (GlcNAc) combined together with β 1-4 glycosidic linkages. It is the second most abundant polymer in nature and a common constituent of fungal cell walls, shells of crustaceans, and exoskeletons of insects (Yuli *et al.*, 2001). Chitin has intra- and intermolecular hydrogen bonds that make it a water insoluble material, which limits its use (Je and Kim, 2006). Several strategies have been developed to convert chitin into small derivatives that can be used in various fields, such as medicine, and the agriculture, pharmaceutical and food industries (Yuli *et al.*, 2001). For medical applications, deacetylated chitooligomers are potentially used for fatty acid absorption, decreasing LDL and increasing HDL cholesterols (Koide *et al.*, 1998), activating immune response, lowering blood pressure, and enhancing calcium absorption (Koide, 1998; DeNardis *et al.*, 2006). In the food industry, chitin and chitosan derivatives are used as food and drink supplements (Qin *et al.*, 2006). In the pharmaceutical field, chitin degradation products are used as anti-cancer, anti-bacteria, and anti-aging agents (Kim and Rajapakse, 2005). In agriculture, chitin derivatives are used to increase quality and quantity of agricultural products and to protect the products by eliminating pests (Chang *et al.*, 2007). Furthermore,

monomers of chitin degradation, (*N*-acetylglucosamine and glucosamine), are effective agents for osteoarthritis treatment as their biocompatible property could reduce inflammation (John *et al.*, 1995; Breborowicz *et al.*, 2006), as well as stimulate innate immunity (Nishiyama *et al.*, 2006). Chitin is hydrolyzed into oligomers and monomers by chemical or enzymatic processes (Ilankovan *et al.*, 2006). However, the enzymatic process is preferable since types, quantity and quality of the oligomeric products can be selectively controlled. In addition, the enzymatic reaction occurs quickly and completely with less time consumed, lower cost and no pollutants released to the nearby environment.

1.2 Classification of chitinases

Chitinases are a diverse group of enzymes that catalyze the conversion of insoluble chitin to soluble oligosaccharides. Chitinases are found in a wide variety of organisms including bacteria, fungi, insects, plants and animals (Balsubramanium *et al.*, 2003; Yu *et al.*, 1991; Merzendorfer and Zimoch, 2003; Donnelly and Barnes, 2004). Chitinolytic enzymes include chitinases (endochitinases and exochitinases) (EC 3.2.1.14) and β -*N*-acetylglucosaminidases (GlcNAcases) (EC 3.2.1.52) (Sahai and Manocha, 1993; Hiroshi *et al.*, 2002). Endochitinases randomly hydrolyze a chitin chain at internal sites into chito oligomers, yielding GlcNAc₂ as the major product. On the other hand, exochitinases exolytically hydrolyze a chitin chain in a sequential manner from the non-reducing end to produce GlcNAc₂ as the final end product. GlcNAc₂ is further hydrolyzed by GlcNAcases to GlcNAc. Finally, GlcNAc is then taken up in to bacterial cells and used as their carbon and nitrogen sources (Wu *et al.*, 2001).

In the Carbohydrate Active Enzyme database (CAZY) (<http://www.cazy.org/>), chitinases are classified into glycoside hydrolases family-18 (GH-18) and family-19 (GH-19) (Henrissat, 1991). Family-18 chitinases are found in a wide range of species, such as bacteria, viruses, fungi, plants, insects, and mammals whereas family-19 chitinases are found mainly in higher plants and in some Gram-positive bacteria, such as *Streptomyces sp.* (Iseli *et al.*, 1996).

Three-dimensional (3D) structures of family-18 and family-19 enzymes reveal differences in their catalytic domains. The catalytic domain of family-18 chitinases, such as *Serratia marcescens* chitinase A (*SmChiA*), contains a typical $(\alpha/\beta)_8$ TIM barrel structure consisting of eight α -helices and eight β -strands (Terwisscha van Scheltinga *et al.*, 1994; Perrakis *et al.*, 1994; Papanikolau *et al.*, 2001; Papanikolau *et al.*, 2003; Aronson *et al.*, 2003) (Figure 1.1). On the other hand, the catalytic domain of family-19 chitinases comprises two lobes, each of which is rich in α -helical structure. From a docking calculation of barley chitinase (a GH-19 chitinase) with GlcNAc₆, the substrate binding cleft of this enzyme was predicted to lie between the two lobes (Figure 1.1) (Davies and Henrissat, 1995; Henrissat and Davies, 2000).

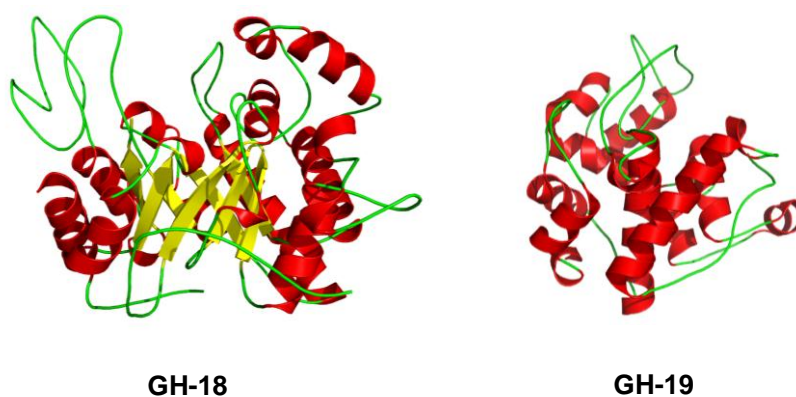


Figure 1.1 Ribbon representation of the main fold of the catalytic domain of the family 18 (PDB code: 1NH6) and family-19 (PDB code: 3CQL) chitinases.

For family-18 chitinases, the TIM barrel domain contains two sub-regions, namely CatDI and CatDII, that are flanked by a small $\alpha+\beta$ insertion domain. A recent study showed that removal of the small insertion domain from *SmChiA* led to a decrease in thermal stability, binding and catalytic activity of the enzyme, in addition to a shift of the pH optimum to more acidic value (Zees *et al.*, 2009). *S. marcescens* ChiA and ChiB, *B. circulans* chitinase A1, and *Aspergillus fumigatus* chitinase B1 (PDB code: 1W9P), all are members of family-18 chitinases, have a long deep groove substrate-binding clefs, containing multiple binding sites referred to subsites (-4), (-3), (-2), (-1), (+1) and (+2). Subsites (-4) to (-2) are located on the glycone part, whereas subsites (+1) and (+2) are on the aglycone part. The cleavage site is located between subsites (-1) and (+1) (van Aalten *et al.*, 2001; Horn *et al.*, 2006; Watanabe *et al.*, 2003; Sikorski *et al.*, 2006; Songsiriritthigul *et al.*, 2008).

1.3. Catalytic mechanism of family-18 chitinases

The structural (Tew *et al.*, 1997) and stereochemical studies of chitin hydrolysis (Armand *et al.*, 1994; Terwissha van Scheltinga *et al.*, 1995; Brameld *et al.*, 1998; Honda *et al.*, 2000; Suginta *et al.*, 2005) revealed that family-18 chitinases catalyze hydrolysis through substrate-assisted catalysis, in which the substrate is forced to distort to a boat geometry at subsite -1 prior to protonation, leading to glycosidic bond cleavage and formation of the oxazolinium intermediate. From a sequence comparison, all family-18 chitinases share a conserved D_{xx}D_xD_xE motif, which contains the catalytic residue Glu315 in *SmChiA* or Glu144 in *SmChiB* which acts as proton donor, and donates a proton to oxygen O4 of the +1 subsite sugar unit,

thus cleaving the glycosidic C1(-1)-O4(+1) bond (Kolstad *et al.*, 2004; Kolstad *et al.*, 2002; Perrakis *et al.*, 1994; Papanikolau *et al.*, 2001).

The substrate-assisted catalysis by family-18 chitinases is essentially achieved via the catalytic cycle involving three neighboring acidic residues in the D_xD_xE motif. The structural complexes of *SmChiA* and *SmChiB* with oligo-NAG were solved (Papanikolau *et al.*, 2001; van Aalten *et al.*, 2001) and the data revealed that in the resting enzyme, the side chain of the second carboxylate Asp313 in *SmChiA* (Asp142 in *SmChiB*), which is close to the proton donor Glu315, points towards Asp311 (Asp140 in *SmChiB*). Subsequent substrate binding causes distortion of -1NAG, leading to a conformational change of the stable ⁴C₁ chair conformation to a ^{1,4}B boat and a rotation of Asp313 (Asp142 in *SmChiB*) towards Glu315 (Glu144 in *SmChiB*). The rotation of the protonated Asp313 residues is not only for stabilizing the developing positive charge of the intermediate oxazolinium ion, but also for donating a proton (Figure 1.2B). The rotation of Asp313 also caused lowering of *pKa* of Glu315, which promotes the proton transfer to the oxygen in the scissile glycosidic bond. At this stage, one water molecule is H-bonded with Tyr390 (Tyr214 in *SmChiB*) and the -1 acetamido group. Then, the proton from the water molecule was taken up by the γ -carboxylate of Glu315 and the remaining hydroxide anion was taken up by the C₁ carbon of the subsite -1 sugar. (Papanikolau *et al.*, 2001; van Aalten *et al.*, 2001; Kolstad *et al.*, 2002). The catalytic cycle of family-18 chitinase is completed in Figure 1.2.

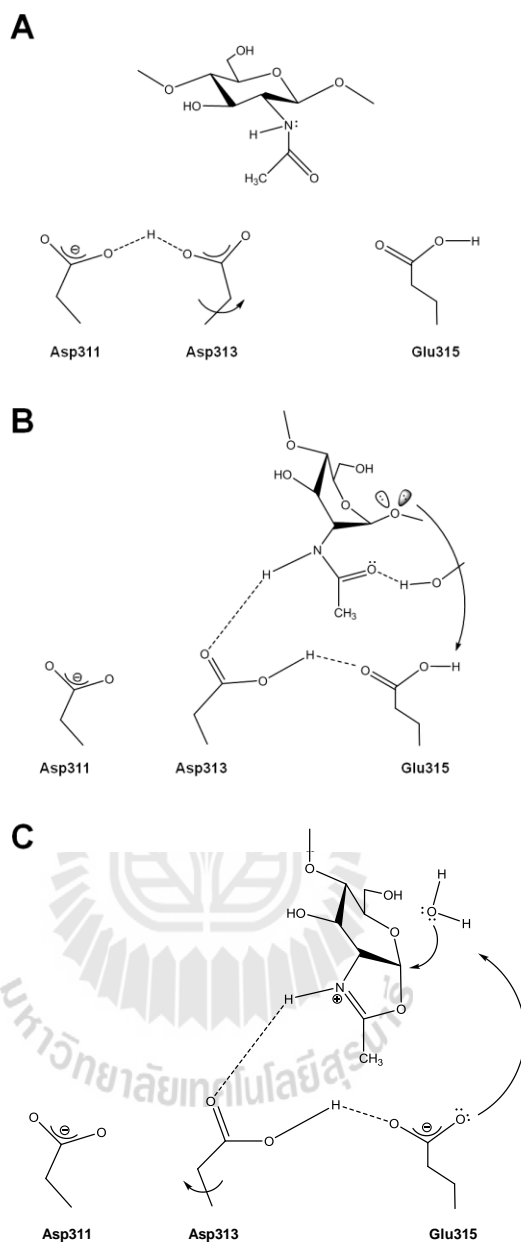


Figure 1.2 The catalytic cycle of family-18 chitinases.

(A) Substrate-binding. (B) Substrate distortion and protonation of the glycosidic bond.

(C) Formation of the oxazolinium ion intermediate and departure of the leaving group, while a water molecule approaches the anomeric carbon. (Modified from Papanikolua *et al.*, 2001; van Aalten *et al.*, 2001).

The catalytic mechanism of other known family-18 chitinases are also reported to adopt the substrate assisted catalysis. For example, the crystal structure of *Coccidioides immitis* chitinase (CiX1) revealed that Glu171 acts as the proton donating group, and the positive charge built up on the sugar at subsite -1 was stabilized by interactions with its own *N*-acetyl group, forming an oxazolinium intermediate, whereas Asp169 rotated to form an ion pair with the oxazolinium cation (Bortone *et al.*, 2002). The polysaccharide chain was rotated and bent between sugars at subsites -1 and +1, thus facilitating distortion of the sugar at subsite -1 towards a high energy boat conformation. A study of the catalytic domain of hevamine chitinase suggested that Glu127 acted as the proton donating residue, whereas Asp125 and Tyr18 contributed to catalysis by positioning the carbonyl oxygen of the *N*-acetyl group near to the C₁ atom (Andersen *et al.*, 1997). The X-ray structures of mutant (E315M) *VhChiA* complexed with hexaNAG revealed that the catalytic cleft of *VhChiA* has a long, deep groove, which contains six chitooligosaccharide binding subsites (-4)(-3)(-2)(-1)(+1)(+2). *VhChiA* is presumed to catalyze substrate hydrolysis following the “slide and bend” mechanism (Songsiriritthigul *et al.*, 2008). First, subsite +2 binding residues, such as Trp275, Asp392, Trp397, and Tyr435, act in substrate recognition, then the sugar chain slides forward towards the reducing end. This action causes distortion of the sugar unit at position -1 and bending of the sugar chain. Twist of the scissile bond, together with bending of -1NAG, renders the linking glycosidic oxygen accessible to the catalytic residue Glu315 located at the bottom of the substrate binding cleft. After cleavage, the GlcNAc₂ moiety at the product (aglycone) side is released and diffuses away.

The D_{xx}D_xD_xE motif is well conserved in the catalytic domain of all family-18 chitinases. However, aside from mammalian chitinases, mammals have other groups of proteins that contain the TIM barrel domain like family-18 chitinases but lack chitinase activity due to the replacement of the aspartic acid residues, and glutamate acid in the conserved motif are replaced by other amino acid residues as shown in Table 1.1. These proteins are referred to chitinase-like proteins (CLPs), which include YKL39, YKL40 (also named HCgp39), mouse YM1/2 and stabilin-1 chitinase like protein (SI-CLP) (Fusetti *et al.*, 2003; Houston *et al.*, 2003; Sun *et al.*, 2001).

Table 1.1 A comparison of sequence identity and the D_{xx}D_xD_xE conserved motifs of family-18 glycoside hydrolases.

Enzyme	Sequence identity (%)	Amino acid length	Conserved motif	Enzyme activity	PDB code
hCHT	100	366(22-387)	D ₁₃₃ XXD ₁₃₆ XD ₁₃₈ XE ₁₄₀	Detectable	1GUV
AMCase	53	379(22-400)	D ₁₃₃ XXD ₁₃₆ XD ₁₃₈ XE ₁₄₀	Detectable	3FXY
<i>Vh</i> ChiA	18	449(139-587)	D ₃₀₉ XXD ₃₁₁ XD ₃₁₃ XE ₃₁₅	Detectable	3B9A
<i>Sm</i> ChiA	21	424(138-561)	D ₃₀₉ XXD ₃₁₁ XD ₃₁₃ XE ₃₁₅	Detectable	1CTN
<i>Sm</i> ChiB	21	496(3-498)	D ₁₃₇ XXD ₁₄₀ XD ₁₄₂ XE ₁₄₄	Detectable	1E15
Hevamine	16	273(1-273)	D ₁₂₀ XXD ₁₂₃ XD ₁₂₅ XE ₁₂₇	Detectable	2HVM
CiX1	22	392(36-427)	D ₁₆₄ XXD ₁₆₇ XD ₁₆₉ XE ₁₇₁	Detectable	1LL7
YKL40	54	362(22-387)	D ₁₃₃ XXD ₁₃₆ XA ₁₃₈ XL ₁₄₀	N/A	1NWS
YM1	47	373(22-395)	D ₁₃₃ XXN ₁₃₆ XD ₁₃₈ XQ ₁₄₀	N/A	1E9L
SI-CLP	13	359(13-371)	D ₁₆₅ XXV ₁₆₈ XE ₁₇₀ V ₁₇₁ XN ₁₇₃	N/A	3BXW

N/A indicates that there is no detectable chitinase activity.

1.4 Function of chitin binding proteins

Family-18 chitinases usually contain one or two chitin binding domains (ChBDs) which are responsible for binding to chitin polysaccharides. Previous studies showed that the ChBD helps to increase enzyme concentration at the substrate surface and guide a chitin chain into the substrate binding cleft (Linder and Teeri, 1997; Watanabe *et al.*, 2001; Imai *et al.*, 2002; Watanabe *et al.*, 2003).

In CAZy (<http://www.cazy.org/>), the protein domains with chitin binding properties are classified into several families of the carbohydrate binding modules, including families 1, 2, 12, 14, 18, 19, and 33 (Kolstad *et al.*, 2005; Cantarel *et al.*, 2009). Marine bacteria that are attached to chitin, such as *V. harveyi*, *V. paraheamolyticus* and *V. alginolyticus* (Montgomery and Kirchman, 1993), have been reported to express chitin binding proteins at their outer membrane. These proteins are required for attachment of the bacterial surface to chitin that is abundant in the marine environment (Pruzzo *et al.*, 1996; Keyhani and Roseman, 1999; Tsujibo *et al.*, 2002). The function of the chitin binding domain was demonstrated in *B. circulans* chitinase A1. This enzyme comprises an N-terminal catalytic domain, two fibronectin-type domains, and a ChBD (namely ChBD_{chiA1}). A polysaccharide binding assay study suggested that ChBD_{chiA1} bound to various forms of chitin, but not to other polysaccharides, such as chitosan, cellulose, and starch (Hardta and Roger, 2004). Loss of the ChBD deprived the enzyme of its ability to bind and to hydrolyze insoluble chitin. Mutants of ChBD_{chiA1}, including W687A and E688K/P689A, showed very low affinity towards chitin substrates (Hardta and Roger, 2004). Aside from chitinases, the chitin binding protein (CBP21) identified from *S. marcescens* was found to adsorb chitin but did not contain chitinase activity (Watanabe *et al.*, 1997).

CBP21 contains four surface-exposed aromatic amino acids, two of which (Trp69 and Trp33) were located in the *N*-terminal domain, while the other two (Trp245 and Phe232) were located near the TIM barrel domain. Such residues appear to be essential for binding to polysaccharides via hydrophobic interactions (Poole *et al.*, 1993; Uchiyama *et al.*, 2001).

Functional significance of the ChBD was also revealed for the *ChiA* gene product of *V. harveyi* (Svitil and Kirchman, 1998). The full length enzyme (ChiA1) was found to bind and to hydrolyze chitin, whereas the truncated ChiA without the ChBD (ChiA2) did not bind to chitin and showed poor ability to degrade chitin. In addition, ChiA1 diffused more slowly in agarose containing colloidal chitin than ChiA2, but the diffusion of the two proteins in agarose without colloidal chitin was similar. The results indicated that the ChBD helped to determine the movement of chitinase along *N*-acetylglucosamine strands (Svitil and Kirchman, 1998).

Additional studies of the ChBD were from *B. circulans* ChiA (Watanabe *et al.*, 1994), *Clostridium parapatrificum* ChiB (Morimoto *et al.*, 1997; Hashimoto *et al.*, 2000), *S. olivaceoviridis* exoChiO1 (Blaak and Schrempf, 1995), *Alteromonas* sp. strain O-7 ChiC (Tsujiho *et al.*, 1998), *S. marcescens* ChiC (Suzuki *et al.*, 1999), *Pyrococcus kadakaraensis* KOD1 ChiA (Tanaka *et al.*, 1999) and *Aeromonas hydrophila* JP101 Chi 92 (Wu *et al.*, 2001). Reports showed that the chitinases lacking the ChBD lose much of their binding and hydrolytic activities towards insoluble chitins. Site-directed mutagenesis of Tyr56 to Ala (mutant Y56A) and Trp53 to Ala (mutant W53A) of *B. circulans* ChiA1 demonstrated that the two residues played a critical role in binding to β -chitin (Watanabe *et al.*, 2003).

Mutations of Trp59 and Trp60 to alanine in the ChBD of *S. griseus* chitinase C also suggested that these two residues were important for binding and hydrolysis of colloidal chitin, as mutants W59A, W60A and a double mutant W59A/W60A abolished the binding activity of chitinase C to colloidal chitin and decreased its hydrolytic activity towards colloidal chitin and soluble substrates (Itoh *et al.*, 2000).

The mechanisms of crystalline β -chitin hydrolysis has been proposed based on the structure of *S. marcescens*, especially from the positions of the aromatic residues. Binding of *SmChiA* to the crystalline β -chitin surface is presumably achieved through interactions among three aromatic residues (Trp69, Trp33, and Trp245) with GlcNAc residues in a single chitin chain on the crystalline β -chitin surface. The chitin chain interacting with the three aromatic residues was introduced into the catalytic cleft from the reducing end side of the chain through the interaction with Phe232. In the catalytic cleft, the introduced chitin chain slides through the cleft to the catalytic site, where the second linkages from the reducing end are progressively cleaved, releasing GlcNAc₂ units (Figure 1.3) (Uchiyama *et al.*, 2001).

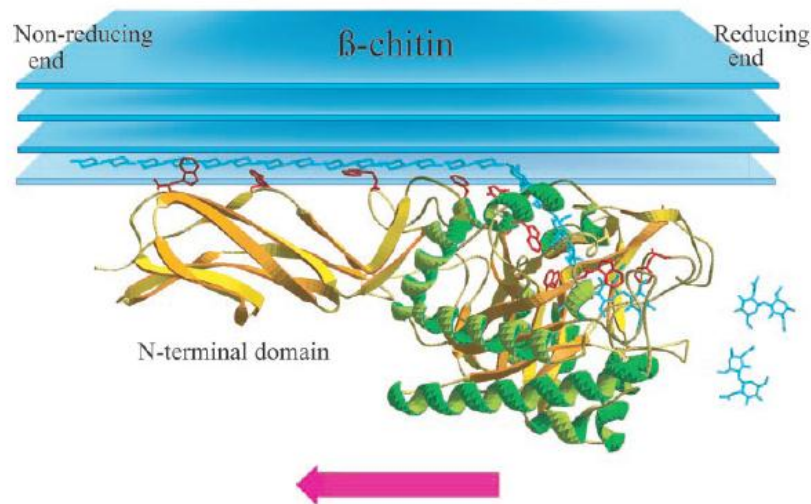


Figure 1.3 A model of crystalline β -chitin hydrolysis by *B. circulans* ChiA (Uchiyama *et al.*, 2001).

1.5 Interactions of chitin substrates in the substrate binding cleft of family-18 chitinases

Superposition of the positions of aromatic residues in *SmChiA* and *CatDChiA1* from *B. circulans* complexed with GlcNAc_7 revealed a number of conserved aromatic residues that linearly aligned on the surface of the substrate binding cleft and play an important role as sugar binding residues (Matsumoto *et al.*, 1999; Uchiyama *et al.*, 2001). In the structure of *B. circulans* chitinase A1 (*ChiA1*) complexed with GlcNAc_7 (Figure 1.4), six aromatic residues, Tyr56, Trp53, Trp433, Trp164, Tyr279, and Trp285 were found to interact with the sugar rings from subsites -5 to +2, respectively (Watanabe *et al.*, 2001). The results of hydrolytic activity against soluble and insoluble substrates revealed that Tyr56 and Trp53 of *B. circulans* *ChiA1* were required only for crystalline chitin hydrolysis, but not for soluble substrates. On the other hand, Trp164, and Trp285 were important for crystalline

chitin hydrolysis and also participated in hydrolysis of soluble substrates. Trp433 at subsite -1 was suggested to play a major role in the catalytic reaction by holding the GlcNAc moiety at subsite -1, in a boat conformation. Another aromatic residue, Tyr279, is in the position to interact with the *N*-acetyl group of -1 GlcNAc and has been assumed to assist the formation of the oxazolinium ion intermediate (Watanabe *et al.*, 2003; Uchiyama *et al.*, 2001).

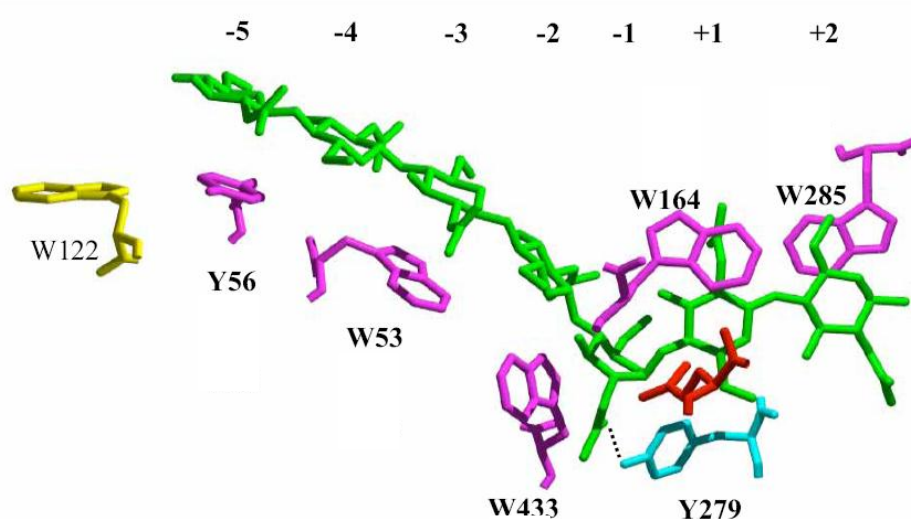


Figure 1.4 Positions of the aromatic residues in the catalytic binding cleft of CatDChiA1 from *B. circulans* complexed with GlcNAc₇. The relative positions of Tyr56, Trp53, Trp433, Trp164, Trp285, and Tyr279 are shown in grey, with the bound GlcNAc₇ in light grey (Watanabe *et al.*, 2001).

The crystal structure of *SmChiA* mutant E315L complexed with hexasaccharide showed that the oligosaccharide occupied subsites -4 to +2, which interacted with Tyr418 and Phe396 at the +2 site and Trp275 at the +1 site. Tyr418 appears to mark the end of the cleft, but it does not interfere with the extension of the reducing end beyond the +2 site. Mutations of Phe396 and Trp275 to alanine,

indicated that the substrates GlcNAc₅ and GlcNAc₆ only occupied subsites -2 to +2 and one (for GlcNAc₅) or two (for GlcNAc₆) GlcNAc residues at the reducing end of the substrate are not bound during the hydrolysis (Aronson *et al.*, 2003). A study of binding and hydrolytic activities of mutants W275G and W397F (equivalent with Trp396 in *SmChiA*) of *VhChiA* suggested that these two residues were involved in defining the binding selectivity of the enzyme to soluble substrates (Suginta *et al.*, 2007; Suginta *et al.*, 2009).

1.6 Studies of chitinase inhibitors

Chitinase inhibitors have been shown to have activity against several pathogens, such as *Candida albicans* (Dickinson *et al.*, 1989), insects (Cohen, 1993; Sakuda *et al.*, 1987) and the human malaria parasite *Plasmodium falciparum* (Bhatnagar *et al.*, 2003). Recently, two human family-18 chitinases (human acidic chitinase and human macrophage chitinase) have been identified (Zhu *et al.*, 2004; Fusetti *et al.*, 2002). Both are highly expressed in asthmatic lungs and believed to contribute to the pathogenic process through recruitment of inflammatory cells (Mayumi *et al.*, 2007). Therefore chitinases seem to be an interesting target for the design of effective agents against human diseases, including malaria, asthma and inflammation.

Allosamidin, a natural product isolated from *Streptomyces sp.*, was the first identified chitinase inhibitor (Sakuda *et al.*, 1987; Sakuda and Sakurada, 1998). This compound showed K_i values in a range of 0.48 nM to 3.1 mM for different chitinases (Houston *et al.*, 2002A; Rao *et al.*, 2003). Allosamidin has a unique pseudotriscarbohydride structure consisting of two units of *N*-acetyl-*D*-allosamine

connected with one unit of an aminocyclitol derivative with a cyclopentanoid skeleton being fused with an aminooxazolinium ring (Figure 1.5A) The first structural complex of allosamidin with family-18 chitinase was solved for hevamine, a plant family-18 chitinase (Terwisscha van Scheltinga *et al.*, 1995). After that, several structural complexes of this compound with other family-18 chitinases were further elucidated, such as chitinase 1 from *C. immitis* (CiX1) (Bortone *et al.*, 2002), *S. marcescens* chitinase B (*SmChiB*) (van Aalten *et al.*, 2001; Kolstad *et al.*, 2004), *S. marcescens* chitinase A (*SmChiA*) (Papanikolau *et al.*, 2003), *A. fumigatus* chitinase B1 (*AfChiB1*) (Roa *et al.*, 2005A) and human macrophage chitinase (Rao *et al.*, 2003). All known structural complexes of allosamidin with family-18 chitinases show that the inhibitor bound from subsites -3 to -1, with the allosamizolinium ring always occupies subsite -1. Several hydrogen bonds and hydrophobic interactions with aromatic residues were shown to be responsible for tight binding of the allosamidin to chitinases (Rao *et al.*, 2003; Rao *et al.*, 2005A; Kolstad *et al.*, 2004). Since allosamidin exhibits high affinity towards all family-18 chitinases, several allosamidin derivatives were synthesized and their binding affinities evaluated. The crystal structures of the human macrophage chitinase complexed with allosamidin (ALLO) and other three derivatives, demethylallosamidin (DEME), methylallosamidin (METH), and glucoallosamidin B (GLCB) showed that the allosamidin derivatives mainly occupied the same positions of allosamidin at subsites -3 to -1 (Table 1.2).

Table 1.2 Substitutions of allosamidin and its derivatives.

	R₁	R₂	R₃	R₄
Allosamidin (ALLO)	CH ₃	H	OH	H
Demethylallosamidin (DEME)	H	H	OH	H
Methylallosamidin (METH)	CH ₃	CH ₃	OH	H
Glucoallosamidin (GLCB)	H	CH ₃	H	OH

Demethylallosamidin is a demethylated form of allosamizoline moiety. The study of inhibitory effects against human macrophage chitinase showed that the binding affinity of demethylallosamidin was increased about 20-fold compared to that of allosamidin. On the other hand, modifications of the -2 and -3 *N*-acetylglucosamine residues (methylallosamidin and glucoallosamidin B) appeared to bind more strongly than allosamidin due to the displacement of ordered water molecules, which leading to increased hydrogen bonding with human macrophage chitinase (Rao *et al.*, 2003). In addition, structural analyses showed that allosamidin and its derivatives inhibited chitinase activity by mimicking the oxazolinium ion reaction intermediate (Houston *et al.*, 2002A). The crystal of chitinase CiX1 complexed with allosamidin suggested that it interacted with this enzyme at the subsites -3 to -1 and inhibited CiX1 with a K_i of 60 nM (Bortone *et al.*, 2002). The moiety bound to the -1 subsite is an allosamizoline, which resembles the reaction intermediate (Figure 1.5B) (Kolstad *et al.*, 2004). Also, the structural complex of *SmChiA* with allosamidin revealed that allosamidin was located deep in the substrate binding cleft of the enzyme by interacting with three important residues, Asp313, Glu315, and Tyr390 (Papanikolau *et al.*, 2003). Investigation of the structural complexes of the human macrophage chitinase with

allosamidin revealed two allosamidin molecules in the active site. The first molecule was occupied at subsites -3 to -1, whereas the second molecule bound near subsites +1 and +2 (Rao *et al.*, 2003).

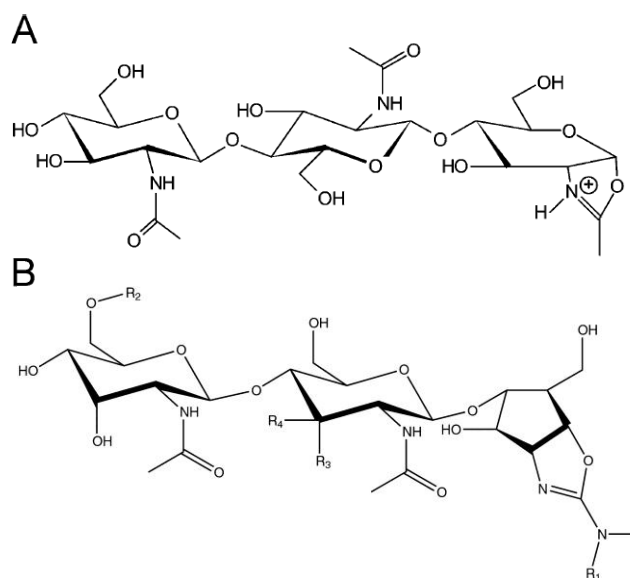


Figure 1.5 The chemical structures of oxazolinium ion intermediate and allosamidin. (A) The proposed positively charged reaction intermediate (oxazolinium ion). (B) Allosamidin.

Synthesis of allosamidin and its derivatives is difficult and costly due to their complex chemistry, thus making such compounds as suitable candidates for further optimization as a chemotherapeutical drug against human chitinase-mediated pathogens. Further screening for natural products with potent chitinase inhibitory activity has been reported, including cyclic pentapeptides (Houston *et al.*, 2002B). Argadin was isolated from *Clonostachys* sp. (Arai *et al.*, 2000), while argifin was isolated from *Gliocladium* sp. (Shiomi *et al.*, 2000). Other natural products that showed chitinase inhibitory effects, included styloguanidine and derivatives from the

marine sponge *Stylotella aurantium* (Kato *et al.*, 1995), cyclo(Arg-Pro) peptidic compounds from the marine bacterium *Pseudomonas sp.* (Izumida *et al.*, 1996), (Kolstad *et al.*, 2004) and psammaplins also from the marine sponge *Aplysinella rhax* (Tabudravu *et al.*, 2002).

Recently, the peptidic inhibitors have received much attention as inhibitor-based drug targets, as they offer improved stability toward peptidolytic breakdown, but still retain high potency. Argifin and argadin (for their chemical structures see Figure 1.6) are the most widely-studied peptidic inhibitors (Shiomi *et al.*, 2000). Structural studies of *SmChiB* complexed with argifin and argadin revealed that these two peptides bound the enzyme by occupying subsites -1, +1 and +2. Both, argifin and argadin were found to interact with the side chains of the essential residues, such as Asp142, Glu144, Tyr214, Trp97, and Trp220 at subsites -1, +1 and +2.

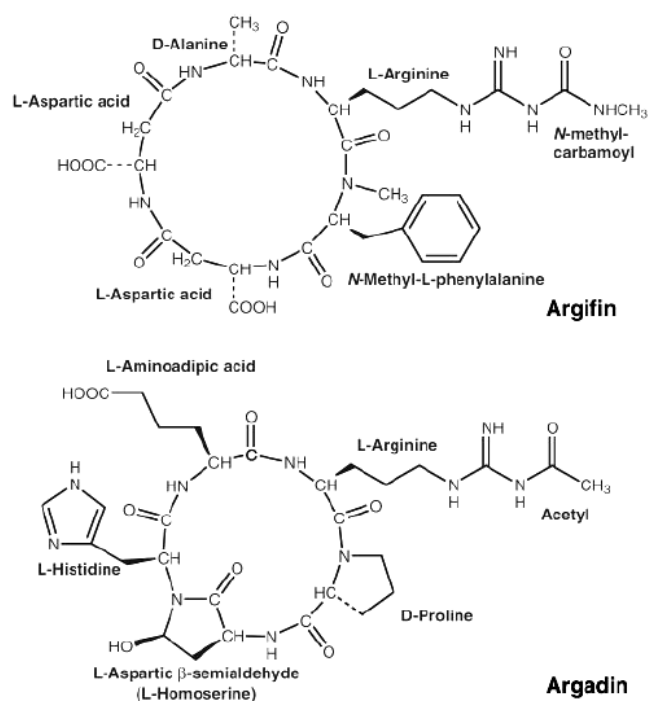


Figure 1.6 Argifin and argadin in two-dimensional structures (Houston *et al.*, 2002B).

When tested with *SmChiB*, argifin showed weaker inhibition ($K_i = 33 \mu\text{M}$) than allosamidin ($K_i = 450 \text{ nM}$), whereas argadin showed approximately 20-fold stronger inhibition ($K_i = 20 \text{ nM}$) (Houston *et al.*, 2002B). Argadin was conformationally more restricted than argifin. Therefore, it bound deeper in the active site of *SmChiB* (van Aalten *et al.*, 2001). The structural complexes of *AfChiB1* chitinase, and human chitotriosidase (hCMT) with argadin and argifin also showed that both inhibitors occupied the sugar binding subsites -1, +1 and +2, whereas allosamidin bound to subsites -3, -2, and -1 (Rao *et al.*, 2005B). The inhibitory effects of argifin revealed high affinity of binding, with an IC_{50} of 27 nM against *AfChiB1* (Dixon *et al.*, 2005), and 4.5 μM human chitotriosidase (hCMT), respectively (Rao *et al.*, 2005B).

Although argadin and argifin are peptidic derivatives, they contain several unusual modifications, such as acetylation and cyclization (Andersen *et al.*, 2008). When the cyclopentapeptide was progressively dissected down to four linear peptides (tetra-, tri-, di-, and mono-peptides) and dimethylguanylyurea (Figure 1.7), the inhibitory effects against *AfChiB1* were in the following orders: tetrapeptide > tripeptide > dipeptide > mono-peptide > dimethylguanylyurea (Table 1.3). Noticeably, the (tiny) dimethylguanylyurea fragment was found to harbor all significant interactions with the protein and bound with high efficiency (Andersen *et al.*, 2008).

Recently, the solid-phase synthesis of the argifin scaffold revealed that the compounds referred to as MeTyr(Bn) for MePhe, had the highest affinity, with an IC_{50} of 11 nM towards *AfChiB1* (Dixon *et al.*, 2009).

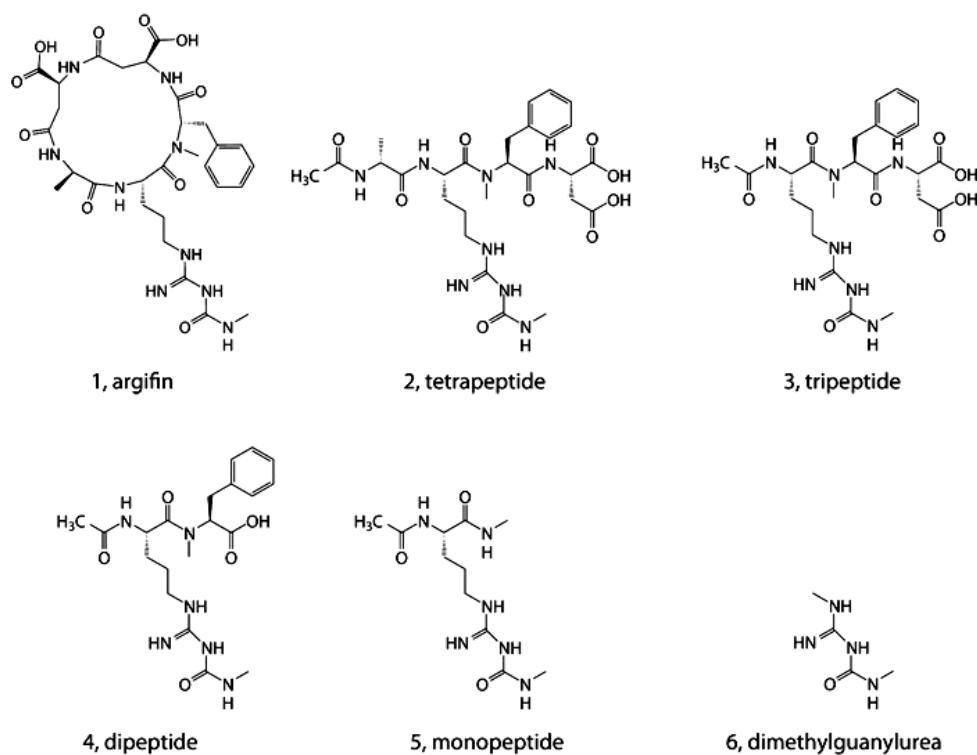


Figure 1.7 Chemical structures of dissected argifin-derived peptides (Dixon *et al.*, 2009).

A simple peptide *cyclo*-(L-Arg-D-Pro) (CI-4) has also been reported as a natural-product produced by the marine bacterium *Pseudomonas sp.* IZ208 (Izumida *et al.*, 1996). It has activity against the fungal pathogen *C. albicans*. In 2002, the structural complex of *SmChiB* and CI-4 was solved (Houston *et al.*, 2002A). Like other peptidic inhibitors, CI-4 inhibits family 18 chitinases through structural mimicry of the reaction intermediate (oxazolinium ion). The inhibitor only covered a small area in the active site of *SmChiB* (subsites -1 to -2) and lacked key interactions with the catalytic residue Asp142, thus explaining its weak binding affinity (IC_{50} 1.2 mM) compared with allosamidin (K_i 0.45 μ M) (Houston *et al.*, 2002A; Houston *et al.*, 2004). The CI-4 structure contains two domains, the *cyclo*-(Gly-Pro) backbone and

the Arg side chain. The structural complex of *SmChiB* and CI-4 showed that only the cyclo-(Gly-Pro) backbone was sufficient for the binding. In 2004, the structural-based optimization of CI-4 was studied (Houston *et al.*, 2004) (Figure 1.8) to investigate the role of the cyclic backbone and the Arg side chain. Three stereoisomers of CI-4: cyclo-(L-Arg-L-Pro), cyclo-(L-His-L-Pro), and cyclo-(L-Tyr-L-Pro) were generated. However, their inhibitory effects on chitinases were moderate with cyclo-(L-His-L-Pro) having the IC_{50} of 1.1 mM, followed by CI-4, cyclo-(L-Tyr-L-Pro), cyclo-(Gly-L-Pro), and cyclo-(L-Arg-L-Pro) with the IC_{50} values of 1.2 mM, 2.4 mM, 5.0 mM and 6.3 mM, respectively (Table 1.3) (Houston *et al.*, 2004).

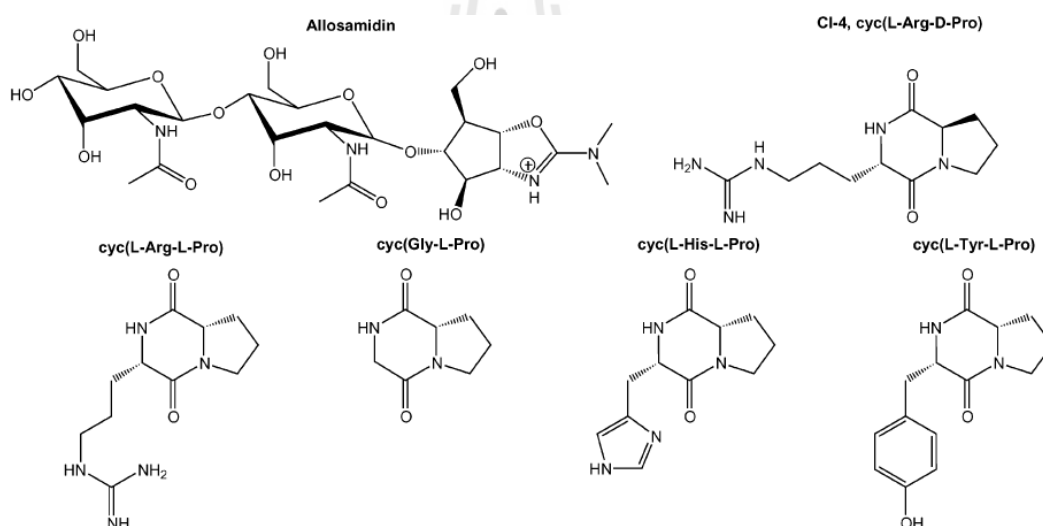


Figure 1.8 The chemical structures of allosamidin and cyclic dipeptides (Houston *et al.*, 2004).

In 2005, Rao *et al.* reported a screening of chitinase inhibitors against *AfChiB1* from a commercial drug library (Rao *et al.*, 2005A) based on the methylxanthine (MET) scaffold. Three identified drugs: theophylline (THE), caffeine (CAF), and pentoxifylline (PEN) containing the 1,3 dimethylxanthine substructure were

identified, with PEN being the most potent inhibitor against *AfChiB1* with K_i of 37 μM .

The structural complex of *AfChiB1* with PEN revealed two molecules of PEN bound in the active site as PEN1 bound at subsites -1 to -2 at the glycone region, with its xanthine ring making favorable π - π interactions with Trp385, while PEN2 bound around subsites +1 and +2 of the aglycone region (Rao *et al.*, 2005A).

Binding of CAF showed three molecules of CAF in the active site of *AfChiB1*. CAF1 and CAF2 were found at subsites -3 to -1, while CAF3 bound around subsites +1 and +2. For theophylline (THE), four molecules were observed. The first two molecules, THE1 and THE2 occupied subsites -3 and -1 at the glycone region, whereas the other two molecules, THE3 and THE4, formed stacking structures with the key residues Trp137 and Trp251 at subsites +1 and +2 at the aglycone region.

Other inhibitors were also reported. A novel aspartic protease inhibitor (API) isolated from *B. licheniform* inhibited *SmChiA* with the IC_{50} of 600 nM and K_i of 510 nM (Kumar and Rao, 2010). The recently reported chitinase inhibitors are chitobiose and chitotriose thiazoline analogues (Macdonald *et al.*, 2010). Such compounds were synthesized as stable mimics of the oxazolinium intermediate. Kinetic analysis revealed that they inhibited the chitinase activity of Chi18A from *S. marcescens* with a K_i range of 0.15 to 30 μM .

In 2010, novel AMCase inhibitors were screened using a combination of high-throughput screening (HTS), fragment-based screening (FBS), and virtual screening techniques (VS) (Derek *et al.*, 2010). The compounds were characterized by enzyme inhibition using colorimetric assay, NMR and Biacore binding experiments. Four potent compounds were identified from different screening techniques, including one

compound identified from the substructure search (SSS). As seen in Figure 1.9, compound 1 is the most potent showing the IC_{50} at 200 nM against AMCase. This compound was further characterized and shown to be orally active by reducing the AMCase activity in the BAL fluid of allergen challenged mice.

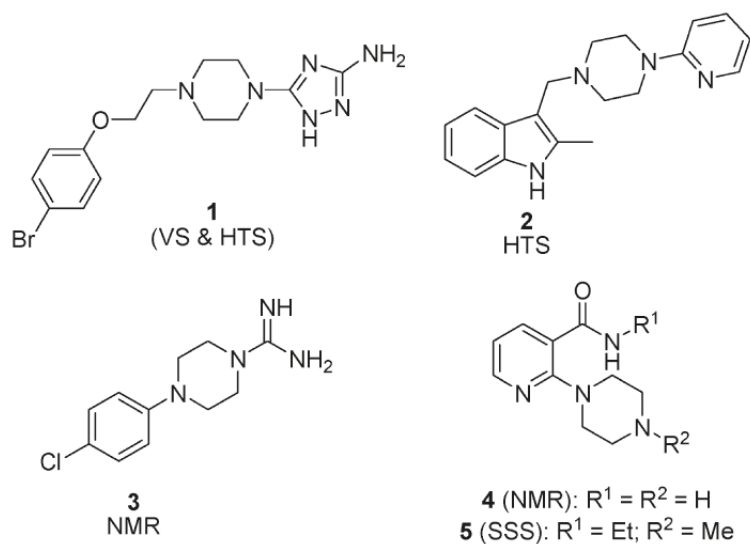


Figure 1.9 Structures of the AMCase inhibitors identified by HTS, FBS, VS, and SSS.

Table 1.3 A summary of inhibitory effects and binding affinities of family-18 chitinase inhibitors identified to date.

Chitinase enzyme	Source	Inhibitor	Kinetic parameter	Reference
<i>B.mori</i> chitinase	<i>Bombyx mori</i>	allosamidin	0.075 μM (K_i)/ 0.386 μM (IC_{50})	Koga <i>et al.</i> , 1987
<i>SmChiB</i>	<i>S. marcescens</i>	allosamidin	450 nM (K_i)	Houston <i>et al.</i> , 2002A
<i>SmChiB</i>	<i>S. marcescens</i>	argifin	33 μM (K_i)	Houston <i>et al.</i> , 2002B
<i>SmChiB</i>	<i>S. marcescens</i>	argadin	20 nM (K_i)	Houston <i>et al.</i> , 2002B
CiX1	<i>C. immitis</i>	allosamidin	60 nM (K_i)	Bortone <i>et al.</i> , 2002
<i>SmChiB</i>	<i>S. marcescens</i>	psammaphin A	148 μM (K_i)	Tabudravu <i>et al.</i> , 2002
<i>SmChiB</i>	<i>S. marcescens</i>	CI-4 [cyclo-(L-His-L-Pro)]	1.1 mM (IC_{50})	Houston <i>et al.</i> , 2004
<i>SmChiB</i>	<i>S. marcescens</i>	CI-4 [cyclo-(L-Arg-D-pro)]	1.2 mM (IC_{50})	Houston <i>et al.</i> , 2004
<i>SmChiB</i>	<i>S. marcescens</i>	CI-4 [cyclo-(L-Tyr-L-Pro)]	2.4 mM (IC_{50})	Houston <i>et al.</i> , 2004
<i>SmChiB</i>	<i>S. marcescens</i>	CI-4 [cyclo-(Gly-L-Pro)]	5.0 mM (IC_{50})	Houston <i>et al.</i> , 2004
<i>SmChiB</i>	<i>S. marcescens</i>	CI-4 [cyclo-(L-Arg-L-Pro)]	6.3 mM (IC_{50})	Houston <i>et al.</i> , 2004
<i>SmChiB</i>	<i>S. marcescens</i>	HM508	45 μM (K_i)	Kolstad <i>et al.</i> , 2004
<i>AfChiB1</i>	<i>A. fumigates</i>	theophylline	1500 μM (IC_{50})	Rao <i>et al.</i> , 2005A
<i>AfChiB1</i>	<i>A. fumigates</i>	caffeine	469 μM (IC_{50})	Rao <i>et al.</i> , 2005A
<i>AfChiB1</i>	<i>A. fumigates</i>	pentoxifylline	37 μM (K_i)/126 μM (IC_{50})	Rao <i>et al.</i> , 2005A
<i>AfChiB1</i>	<i>A. fumigates</i>	argifin	27 nM (IC_{50})	Dixon <i>et al.</i> , 2005
human chitotriosidase (hCHT)	Gaucher spleen	argifin	4.5 μM (IC_{50})	Rao <i>et al.</i> , 2005B
<i>AfChiB1</i>	<i>A. fumigates</i>	argadin	0.5 μM (IC_{50})	Rao <i>et al.</i> , 2005B
human recombinant chitotriosidase (hCHT)	Gaucher spleen	argadin	0.013 μM (IC_{50})	Rao <i>et al.</i> , 2005B

Table 1.3 A summary of inhibitory effects and binding affinities of family-18 chitinase inhibitors identified to date (Continued).

Chitinase enzyme	Source	Inhibitor	Kinetic parameters	Reference
AfChiB1	<i>A. fumigates</i>	tetrapeptide	4.3 μ M (IC_{50})	Andersen <i>et al.</i> , 2008
AfChiB1	<i>A. fumigates</i>	tripeptide	5.1 μ M (IC_{50})	Andersen <i>et al.</i> , 2008
AfChiB1	<i>A. fumigates</i>	dipeptide	12 μ M (IC_{50})	Andersen <i>et al.</i> , 2008
AfChiB1	<i>A. fumigates</i>	monopeptide	81 μ M (IC_{50})	Andersen <i>et al.</i> , 2008
AfChiB1	<i>A. fumigates</i>	dimethylguanylurea	500 μ M (IC_{50})	Andersen <i>et al.</i> , 2008
SmChiA	<i>B. licheniform</i>	API	510 nM (K_i)/600 nM (IC_{50})	Kumar and Rao, 2010
Chi18A	<i>S. marcescens</i>	chitobiose thiazoline	25 μ M (K_i)	Macdonald <i>et al.</i> , 2010
Chi18A	<i>S. marcescens</i>	chitobiose thiazoline thioamide	30 μ M (K_i)	Macdonald <i>et al.</i> , 2010
Chi18A	<i>S. marcescens</i>	chitotriose thiazoline	0.25 μ M (K_i)	Macdonald <i>et al.</i> , 2010
Chi18A	<i>S. marcescens</i>	chitotriose thiazoline dithioamide	0.15 μ M (K_i)	Macdonald <i>et al.</i> , 2010

1.7 Studies of *V. harveyi* chitinase A

Chitinase A isolated from marine bacteria such as, *V. harveyi* and *V. alginolyticus* 283 were found to be highly expressed upon induction with chitin (Suginta *et al.*, 2000; Suginta, 2007). *V. harveyi* chitinase A (or *VhChiA*) was active as a monomer of M_r 63,000 (Suginta *et al.*, 2000). Analysis of chitin hydrolysis using the viscosity assay and HPLC-ESI MS suggested that this enzyme acted as an endochitinase (Suginta *et al.*, 2004) and had a broad range of substrate specificity with various chitin oligomers (Suginta *et al.*, 2005). The X-ray structure of wild-type *VhChiA* revealed that the overall structure of *VhChiA* consists of three domains, the N-terminal chitin-binding domain (ChBD), the catalytic (α/β)₈ TIM-barrel domain

(CatD), and the small ($\alpha+\beta$) insertion domain. The structure of *VhChiA* mutant E315M complexed with GlcNAc₆ revealed that the active site of this enzyme contained six substrate binding sites, designated subsites -4, -3, -2, -1, +1 and +2 (Songsiriritthigul *et al.*, 2008), where subsites -4 to -2 are the glycone sites, subsites +1 and +2 are the aglycone sites. The cleavage site is located between subsites -1 and +1. Mutation of Glu315 to Gln and Met (mutants E315Q and E315M) led to a complete loss of chitinase activity which suggested that Glu315 is an essential residue in enzyme catalysis. Mutation of Asp392 to Asn retained significant chitinase activity on the gel activity assay, suggesting that the Asp392 mutant did not directly participate in the catalysis (Suginta *et al.*, 2005).

Effects of point mutation of the aromatic residues located within the substrate binding cleft of *VhChiA* were studied. These residues included Trp168, Tyr171, Trp275, Trp397, and Trp570. Substitutions of Trp168, Tyr171, and Trp570 to Gly abolished the hydrolyzing activity against colloidal chitin almost completely and greatly reduced the hydrolyzing activity against the *p*NP-GlcNAc₂. Mutant W570G showed the most severe effects on the hydrolyzing activity, having no activity against colloidal chitin. In the modeled 3D structure of inactive mutant E315M in complex with GlcNAc₆, Trp570 was closest to the sugar ring at subsite -1, which suggested that it is likely to be responsible for holding the GlcNAc ring at this position in place so that cleavage of the glycosidic bond between subsites -1 and +1 can occur (Songsiriritthigul *et al.*, 2008). A time course study of GlcNAc₆ hydrolysis using thin-layer chromatography assay exhibited distinct hydrolytic patterns between wild-type and mutants W275G and W397F, but no difference in colloidal chitin hydrolysis. This modification of the cleavage patterns of chito oligomers suggested that residues

Trp275 and Trp397 play the critical role in the substrate binding at the subsites -1, +1, and +2 (Suginta *et al.*, 2007). A more recent report suggested that both Trp275 and Trp397 are also involved in the anomer selectivity of soluble substrates and involved in the feeding process, which facilitates a degradation of chitin polymer in progressive manner (Suginta *et al.*, 2009).

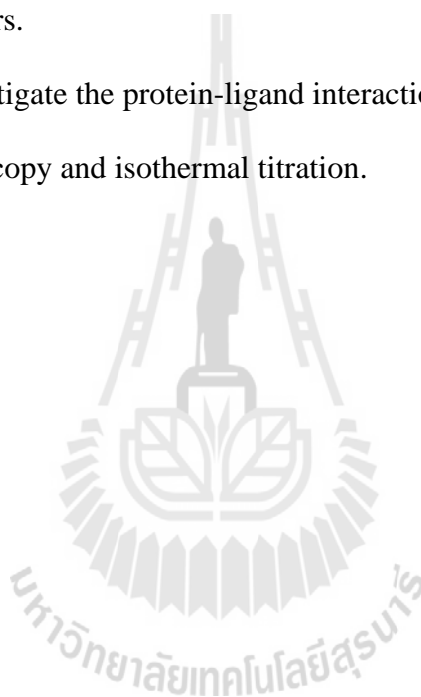
1.8 Research objectives

Since the structural data suggest that bacterial family-18 chitinases contained several surface-exposed residues located near or within the ChDB which may contribute to chitin binding, the first part of this study focused on site-directed mutagenesis and functional characterization to demonstrate the influence of such residues on the enzymatic properties of *VhChiA*.

The second part of the study attempted to identify new inhibitor molecules which are effective against family-18 chitinases. In this study, seven *VhChiA* inhibitors were identified from the Library of Pharmacological Active Compounds (LOPAC) via a high throughput screening technique. These compounds showed IC_{50} values as submicromolar concentrations, and included chelerythrine, dequalinium, Idarubicin, 2-(imidazolin-2-yl)-5-isothiocyanatobenzofuran, pentoxifylline, propentofylline, and sanguinarine. The effects of the inhibitors on *VhChiA* activity were investigated by means of enzyme activity assays, dose response curves, intrinsic fluorescence spectroscopy, isothermal titration calorimetric assay and 3D structures of the enzyme-inhibitor complexes. The objectives of this study include:

1. To mutate the surfaced-exposed residues located near the ChBD or outside the CatD which are important for chitin binding and hydrolysis

- by the site-directed mutagenesis technique.
2. To highly express, and purify the mutated proteins in *E. coli* M15.
 3. To investigate the effects of the mutations on binding and hydrolytic activities of *VhChiA* using appropriate biochemical techniques.
 4. To identify the newly *VhChiA* inhibitors and determine the crystal structures of *VhChiA* wild-type and mutant W275G in complex with inhibitors.
 5. To investigate the protein-ligand interactions with intrinsic fluorescence spectroscopy and isothermal titration.



CHAPTER II

MATERIALS AND METHODS

2.1 Chemicals and reagents

2.1.1 Bacterial strains and plasmids

Escherichia coli strain DH5 α was used as a routine host for amplification of recombinant plasmids. XL1-Blue supercompetent cells were used as a host for transformation of the recombinant plasmid harboring the mutated DNAs. *E. coli* type strain M15(pREP4) cells carrying the pREP4 repressor plasmid was used for overexpression of the lac repressor protein (QIAGEN GmbH., Hilden, Germany). The pQE-60 expression vector harboring the *V. harveyi chitinase A* gene fragment was used for high-level expression of recombinant chitinases.

2.1.2 Site-directed mutagenesis and plasmid purification

PfuTurbo[®] DNA polymerase, 10 \times *Pfu* DNA polymerase reaction buffer and *Dpn* I restriction enzyme were purchased from Stratagene (Stratagene Corp., CA, USA); dATP, dCTP, dGTP, dTTP, and QIAprep[®] Spin Miniprep kit were purchased from QIAGEN (QIAGEN GmbH., Hilden, Germany). Ethidium bromide, agarose, and HyperLadder[™] I DNA marker were products of Bioline (Bioline USA Inc., Taconic MA, USA).

2.1.3 Protein expression and purification

Consumables and chemicals used for protein expression and purification were obtained from the following sources: disposable columns for Ni-NTA agarose chromatography (1.0 x 10 cm) from Biorad, (Bio-Rad Laboratories, Inc., CA, USA), Ni-NTA agarose resin from QIAGEN and ultrafiltration membrane concentrators (M_r 10,000 cut-off) from Vivascience (Vivascience, Hanover, Germany), HisTrap™ HP column (5.0 x 1.0 ml) was from GE Healthcare (GE Healthcare, WI, USA); dialysis cassette (0.5 x 3.0 ml; M_r 30,000 cut-off) from Thermo Fisher Scientific (Thermo Fisher Scientific Inc., MA, USA), ampicillin, kanamycin, bovine serum albumin (BSA), isopropyl- β -D-thiogalactopyranoside (IPTG), hen egg white lysozyme, phenylmethylsulfonyl fluoride (PMSF), bacto tryptone and bacto yeast extract from USB (Affymetrix, Inc., OH, USA), calcium chloride, potassium chloride, sodium chloride, disodium ethylene diamine tetraacetate (EDTA), glycerol, glycine, imidazole, tris base, SDS, acrylamide, *N,N'*-methylene bisacrylamide, TEMED, ammonium persulfate, coomassie brilliant blue R-250, 2-mercaptoethanol, glacial acetic acid, bromophenol blue and methanol from Sigma-Aldrich (Sigma-Aldrich Inc., MO, USA).

2.1.4 Enzyme kinetics

2.1.4.1 Reagents and buffers

p-Dimethylaminobenzaldehyde (DMAB), dinitrosalicylic acid (DNS) sodium tetraborate, sodium acetate, sodium hydroxide, ammonium acetate, sodium citrate, citric acid, monobasic sodium phosphate, and dibasic sodium phosphate were

purchased from Carlo Erba (Carlo Erba Réactifs-SDS, Peypin, France). Triton X-100 was a product of USB.

2.1.4.2 Substrates for chitinase assays

N-acetyl-chitooligosaccharides (di-*N*-acetyl-chitobiose, tri-*N*-acetyl-chitotriose, tetra-*N*-acetyl-chitotetraose, penta-*N*-acetyl-chitopentaose, hexa-*N*-acetyl-chitohexaose), and *p*-nitrophenyl-di-*N*-acetyl-chitobioside (*p*NP-GlcNAc₂) were products of Seikagaku (Seikagaku Corp., Tokyo, Japan). 4-Methylumbelliferyl β -*N,N'*-diacetylchitobioside (4MU-GlcNAc₂), 4-Methylumbelliferyl β -*N,N',N''*-triacetylchitotriose (4MU-GlcNAc₃), *p*-nitrophenyl-tri-*N*-acetyl-chitotriose (*p*NP-GlcNAc₃), and chitin flakes were purchased from Sigma-Aldrich.

2.1.4.3 Chitinase inhibitors

Chelerythrine (CHE), dequalinium (DEQ), idarubicin (IDA), 2-(imidazolin-2-yl)-5-isothiocyanatobenzofuran (IMI), pentoxifyllin (PEN), propentofylline (PRO), sanguinarine (SAN), methysergide maleate (MET), and 2-bromo- α -ergocryptine methanesulfonate (BRO) were purchased from Sigma-Aldrich.

2.1.5 Protein crystallization

2.1.5.1 Crystallization screening and optimization

20 mm siliconized glass cover, 20 micron CryoLoops™, CrystalCap Magnetic™ with vial, Glass Dewar, CryoCane, CryoSleeve, Magnetic Crystal Wand™, vial Curved Clamp™, Long CryoTongs™, CrystalWand™, microbatch

crystallization oils and Dow Corning[®] vacuum grease were products of Hampton Research (Hampton Research Corp., CA, USA). MicroWell[™] MiniTrays (60-well microwell plates) were from Nunc[™] (Thermo Fisher Scientific Inc., MA, USA). Linbro Plates (24-well tissue culture plates) with cover were from Linbro[®] (Linbro Division, Flow laboratories Inc., CA, USA). Crystal Screen HR2-110 and Crystal Screen HR2-112 were products of Hampton Research and JBScreen HTS II was a product of Jena Bioscience (Jena Bioscience GmbH., Jena, Germany).

2.1.5.2 Buffers and precipitants

Sodium citrate tribasic dihydrate, sodium acetate hydrate and 2-propanol were obtained from Carlo Erba. Ammonium phosphate monobasic, ammonium sulfate, ammonium acetate, calcium acetate hydrate, sodium cacodylate trihydrate, MES (2-(*N*-morpholino) ethanesulfonic acid), MOPS (3-(*N*-morpholino) ethanesulfonic acid), PIPES (piperazine-1,4-bis(2-ethanesulfonic acid), HEPES (*N*-(2-hydroxyethyl) piperazine-*N*-(2-ethanesulfonic acid)), triton X-100, PEG 400, PEG 1500, PEG 4000 and PEG 20000 were purchased from USB. (+/-)-2-Methyl-2,4-pentanediol (MPD) was purchased from Hampton Research.

2.2 Instrumentation

2.2.1 Instrumentation used at Suranaree University of Technology (SUT), Thailand

All instruments required for molecular cloning, recombinant protein expression, protein purification, protein characterization and preliminary crystallization are located at the Center for Scientific and Technology Equipment at

Suranaree University of Technology, Nakhon Ratchasima, Thailand. These instruments include a Sonopuls Ultrasonic homogenizer with a 6-mm diameter probe, microtiter plate reader (Applied Biosystems, CA, USA), Mastercycler® personal PCR thermocycler (Eppendorf AG., Hamburg, Germany), DNA gel apparatus (Pharmacia Biotech, SF, USA), Gemini EM microplate fluorometer (Sunnyvale, CA, USA), Jenway UV-VIS spectrophotometer (Bibby Scientific Ltd., Staffordshire, UK), Olympus CX40 stereomicroscope (Olympus Optical Co., Ltd., Tokyo, Japan), Gel-Doc 2000 Gel document system (Bio-Rad Laboratories, CA, USA), and an LS-50 fluorescence spectrometer (PerkinElmer Ltd., Instruments & Life Sciences, Bangkok, Thailand).

2.2.2 Instrumentation used at the Max-Planck-Institut für Molekulare Physiologie (MPI), Dortmund, Germany

The instruments required for protein expression and purification and protein characterization included HC-2000 microfluidizer (Microfluidics, Lampertheim, Germany), ÄKTA purifier system (GE Healthcare), Tecan GENios Pros microplate reader (Tecan Group Ltd., Männedorf, Switzerland), Thermomixer Comfort (Eppendorf AG., Hamburg, Germany), ITC-200 system (MicroCal, Inc., MA, USA), a Zeiss stemi 200-C stereo microscope (Carl Zeiss MicroImaging GmbH., Göttingen, Germany), mounted with a color video camera (Sony Corp., Tokyo, Japan). Protein crystallography instruments required for initial data collection are located at the MPI, Dortmund, Germany. These include a Rigaku Micromax HF-007 rotating anode generator and two MAR Research image plate detectors on a Nonius FR-591 generator (Rigaku Corp., Berlin, Germany). Data collections were performed at the

beamline PX-II of the Swiss Light Source located in Villigen, Switzerland using a MAR Research CCD detector. Some data sets were collected on a Bruker Microstar rotating anode generator (Bruker ASX Inc., WI, USA) equipped with Xenocs Fox mirrors (Xenocs SA., Sassenage, France) and a MAR Research DTB image plate detector.

2.3 Analytical programs

The crystallographic programs used for data scaling, processing, model rebuilding and structural refinement included XDS program (Kabsch, 1993), MOLREP (CCP4, 1994), REFMAC (CCP4, 1994), COOT (Emsley and Cowtan, 2004), Maestro (www.schrödinger.com), PRODRG servers (Schüttelkopf, 2004), PROCHECK (Laskowski, 1993), WHAT IF (Vriend, 1990), PYMOL (www.pymol.org) and LIGPLOT (Wallace, 1995). All of these programs were operated under the Linux operating system.

2.4 PCR primers

The oligonucleotide primers used for generation of recombinant chitinase A mutations of Ser33→Ala (S33A), Ser33→Trp (S33W), Trp70→Ala (W70A), Trp231→Ala (W231A), Trp231→Phe (W231F), Tyr245→Ala (Y245A), and Tyr245→Trp (Y245W) are shown in Table 2.1. Such oligonucleotides were synthesized by BioService Unit (BSU), the National Science and Technology Development Agency (NSTDA), Thailand.

Table 2.1 Primers for site-directed mutagenesis.

Mutation	Primers
Ser33→Ala (S33A)	Forward 5'-CGATATGTACGGT <u>GCG</u> ^a AATAACCTTCAATTTTC-3' Reverse 5'-GAAAATTGAAGGTTATT <u>CGC</u> ACCGTACATATCG-3'
Trp70→Ala (W70A)	Forward 5'-GAAATTTAACCAG <u>GCG</u> AGTGGCACATCTG-3' Reverse 5'-CAGATGTGCCACT <u>CGC</u> CTGGTTAAATTTTC-3'
Trp231→Ala (W231A)	Forward 5'-GTTATCCATGAT ^b <u>CCGGCGGC</u> AGCTTATC-3' Reverse 5'-GATAAGCTGCC <u>GCCGAT</u> CATGGATAAC-3'
Tyr245→Ala (Y245A)	Forward 5'-GTCATGAAG <u>CGAGC</u> ACGCCAATCAAG-3' Reverse 5'-CTTGATTGGCGTGCT <u>CGC</u> TTCATGAC-3'
Ser33→Trp (S33W)	Forward 5'-CGATATGTACGGT <u>TGGA</u> AATAACCTGCAATTTTC-3' Reverse 5'-GAAAATTGCAGGTTATT <u>CCA</u> ACCGTACATATCG-3'
Trp231→Phe (W231F)	Forward 5'-GGTTATCCATGACCCG <u>TTTGC</u> AGCTTATCAG-3' Reverse 5'-CTGATAAGCTGCA <u>AA</u> CGGGTCATGGATAACC-3'
Tyr245→Trp (Y245W)	Forward 5'-CAGGTCATGAAT <u>TGGAGC</u> ACGCCAATCAAG-3' Reverse 5'-CTTGATTGGCGTGCT <u>CCAT</u> TTCATGACCTG-3'

^aSequences underlined indicate the mutated codons. ^bSequences in bold represent the codon being modified to achieve the T_m value as required for Quick-Change Site-Directed Mutagenesis.

2.5 Mutational design and site-directed mutagenesis

A comparison of the putative amino acid sequence of *VhChiA* with other bacterial sequences displayed several surface-exposed residues located near the ChBD and could potentially act as chitin binding residues. Such residues included Ser33, Trp70, Trp231, and Tyr245. To demonstrate the effects of these residues on the chitin binding and enzymatic properties of *VhChiA*, they were mutated using the Quick-Change Site-Directed Mutagenesis kit (Stratagene). The PCR reaction mix and PCR conditions used in the mutagenic reactions are shown in Table 2.2 and Table 2.3, respectively. The pQE60 plasmid harboring the *chitinase A* DNA lacking the residues

598-850 C-terminal fragment was used as DNA template. Mutations of the desired nucleotides were carried out using the PCR-based strategy, employing the mutagenic primers presented in Table 2.1. The PCR amplification product was verified by agarose gel electrophoresis. The PCR products were digested with *Dpn* I restriction enzyme for 1 hour at 37°C to remove the non-mutated DNAs. The *Dpn* I-treated DNAs were transformed to XL1-Blue super competent cells. Afterwards, the transformed cells were spread on LB-agar containing 100 µg/ml ampicillin. Plasmids obtained from positive colonies were extracted with QIAGEN Plasmid Miniprep. After the mutated DNAs were confirmed by automatic DNA sequencing, the plasmids harboring the mutated DNAs were transformed to *E. coli* M15 cells for high level of recombinant protein expression.

Table 2.2 The PCR reaction used for site-directed mutagenesis.

Reagent	Volume	Final concentration
<i>Pfu</i> Turbo DNA polymerase (2.5 U/µl)	0.5 µl	0.05 U/µl
10 x reaction buffer	2.5 µl	1X
Oligonucleotide forward primer	0.625 µl	0.25 µM
Oligonucleotide reward primer	0.625 µl	0.25 µM
DNA template	2.0 µl	Variable
dNTP mix	0.5 µl	0.2 mM
Total volume		25 µl

Table 2.3 The PCR conditions used for site-directed mutagenesis.

PCR step	Cycle	Temperature	Time
Hot start	1	97°C	5 seconds
Denaturation start	1	97°C	30 seconds
Denaturation		97°C	30 seconds
Annealing	1-18	55°C	1 minute
Extension		68°C	5.3 minutes

2.6 Structure-based sequence alignment and homology modeling

Amino acid sequence alignment was constructed by the program MegAlign using the CLUSTAL method algorithm in the DNASTAR package (Biocompare, Inc., CA, USA) and displayed in Genedoc (www.psc.edu/biomed/genedoc). The amino acid sequence of the *VhChiA* was aligned with five selected bacterial chitinase sequences available in the Swiss-Prot or TrEMBL database. The secondary structure elements of *VhChiA* were obtained by the PHD method available in PredictProtein (www.predictprotein.org). The modeled tertiary structure of the *VhChiA* was built by Swiss-Model using the X-ray crystal structure of *SmChiA* E315L mutant complex with hexaNAG (PDB code: 1NH6) as structure template. The co-ordinates of GlcNAc₆ were modeled into the active site of the *Vibrio* enzyme and the target residues were located by superimposing the C_α atoms of 459 residues of *VhChiA* with the equivalent residues of *SmChiA* E315L complex, using the program Superpose available in the CCP4 suit. The predicted structure was viewed with Pymol (www.pymol.org).

2.7 Expression and purification of chitinase A variants

For preparation of the recombinant enzymes, single colonies of *E. coli* M15 (pREP4) cells were picked and grown at 37°C in 1 ml of Luria–Bertani (LB) medium, containing 100 µg/ml ampicillin and 25 µg/ml kanamycin (LB/Amp/Kana). After 5-6 hours of incubation, cell culture (20 µl) was transferred to 20 ml LB/Amp/Kana medium, then further incubated overnight at 37°C for 16-18 hours. In the next step, 10 ml of the overnight cell culture was transferred to 1 liter of LB/Amp/Kana, then incubated at 37°C until the OD₆₀₀ reached 0.6. Then, isopropyl thio-β-D-galactoside (IPTG) was added to the cell culture to a final concentration of 0.5 mM for induction of the recombinant chitinase. Incubation was continued at 25°C overnight with shaking. The cells were then harvested by centrifugation at 6000 rpm for 15-20 min at 4°C and then disrupted in lysis buffer: (20 mM Tris-HCl buffer, pH 8.0, 150 mM NaCl) with a HC-2000 Microfluidizer. Unbroken cells and cell debris were removed by centrifugation, while the soluble chitinase was purified from the supernatant by affinity chromatography. The crude supernatant containing 20 mM imidazole was applied under gravity onto a Ni-NTA agarose column (5.0 x 1.0 ml; QIAGEN). To remove unspecific proteins, the column was washed with 10 CV of equilibration buffer (20 mM Tris-HCl buffer, pH 8.0, 150 mM NaCl), followed by 20 mM imidazole in the equilibration buffer. The column was eluted with 250 mM imidazole in the equilibration buffer, and then applied onto a Vivaspin-20 ultrafiltration membrane concentrator (M_r 10,000 cut-off, Vivascience AG.) to obtain a small volume of the enzyme and for removal of imidazole. For protein crystallization experiments, the concentrated enzyme obtained from the first Ni-NTA agarose column was further purified by a HisTrap™ HP column (5.0 x 1.0 ml; GE Healthcare,

Munich, Germany) connected to an ÄKTA purifier system (GE Healthcare). The running buffer was 20 mM Tris-HCl, pH 8.0, containing 150 mM NaCl. A flow rate of 1.0 ml/min was maintained. The protein was eluted with a linear gradient from 0 to 300 mM imidazole in the running buffer. Fractions of 1.0 ml were collected and fractions containing chitinase were pooled, exchanged into 10 mM Tris-HCl buffer, pH 8.0, and concentrated in a Vivaspin-20 ultrafiltration membrane concentrator (M_r 10,000 cut-off). Purity of the enzyme was verified by SDS-PAGE, following the method of Laemmli (Laemmli, 1970). The final concentration of the protein was determined by Bradford's method (Bradford, 1976) with a calibration curve of BSA (0-25 μ g).

2.8 High-throughput screening

Potential chitinase inhibitors were screened from the "Library Of Pharmacologically Active Compounds" or "LOPAC" (Sigma-Aldrich). The general set-up of the primary screen was described by Prinz and Schönichen, 2008. Briefly, 5 μ l of 1 mM substrate (*p*NP-GlcNAc₂) were added to 5 μ l of the purified chitinase and 200 μ M of the respective inhibitor. The reaction buffer consisted of 50 mM Tris-HCl, pH 7.5, 50 mM NaCl, 1 mM dithiothreitol (DTT), and 0.025% (v/v) nonyl phenoxy polyethoxy ethanol (NP-40). Formation of *p*-nitrophenylate (*p*NP) as a result of *p*NP-GlcNAc₂ hydrolysis by *VhChiA* was monitored continuously for 30 min by absorbance measurement at 405 nm (A_{405}). The reaction rate without enzyme was taken as 0% activity and without inhibitor as 100% activity. Dose-response curves of the inhibitors obtained from the initial screen were generated either from the *p*NP

assay (Tabatabai and Bremner, 1969; Sinsabaugh and Linkins, 1990) or from the DMAB assay (Boller and Mauch, 1988).

2.9 Determination of dose-response curves

Dose-response curves were carried out using chitohexaose with the reaction containing 0-500 μM substrate and *VhChiA* (50 μg of wild-type, 250 μg of W275G or 0.4 μg of W397F) in 100 mM sodium acetate buffer, pH 5.5. The reaction mixture was titrated with a two-fold dilution series to obtain a concentration range of 1 nM to 1 mM of each inhibitor. Residual chitinase activity was assessed by the DMAB assay. Similar dose-activity curves were measured independently by hydrolysis of *pNP-GlcNAc*₂. A two-fold dilution series of inhibitor was incubated with 0.25 μM chitinase in 20 mM Tris-HCl buffer, pH 7.5, containing 100 mM ammonium acetate and 0.025% (v/v) Triton X-100, for 10 min before the substrate was added to a final concentration of 125 μM . The progress of the reaction (A_{405}) was monitored continuously at 28°C for 16 min in the Tecan GENios Pros microplate reader. The slope obtained from a linear portion of the reaction curve was taken as the initial velocity using the standard calibration curve of *pNP* (0.4-25 nmol). For mutant W275G, 2 μM of the enzyme and 250 μM of *pNP-GlcNAc*₃ were used. The IC_{50} value for each inhibitor was estimated from the dose response curves (Figure 3.10) using the 4-parameter logistic (4PL) fit. The mathematical equation used of 4PL fit is

$$y = y_{max} + \frac{y_{min} - y_{max}}{\left[1 + \left(\frac{[I]}{IC_{50}}\right)^{HillSlope}\right]}$$

where y is the fractional activity of the enzyme in the presence of inhibitor at the concentration $[I]$, y_{max} is the maximum value of y that is observed at zero inhibitor concentration, y_{min} is the minimum value of y that is

observed at very high inhibitor concentration, and HillSlope describes the steepness of the curve. This variable is called the Hill slope, the slope factor, or the Hill coefficient.

2.10 Determination of three-dimensional structures of chitinase-Inhibitor complexes

2.10.1 Protein crystallization of the wild type chitinase and mutants

W275G and W397F

Crystallization screening experiments were carried out by the microbatch method using the screening kits: Crystal Screen HR2-110 and Crystal Screen HR2-112 (Hampton Research).

The microbatch screening was carried out manually. Each well of 60-well microwell plates (NUNC™) was filled with 10 μ l paraffin oil (Hampton Research). One microliter of the precipitate solution was transferred to each well, then 1 μ l of the chitinase solution (10 mg/ml freshly-prepared in 10 mM Tris-HCl buffer, pH 8.0) was added to each well without mixing. The protein samples were protected from evaporation, contamination and physical shock by covering with the paraffin oil. To prevent dust and debris contamination, the crystallization plate was covered with a cover slide and placed on a moist sponge in a plastic box to minimize the evaporation rate of the water through the oil. The plate was incubated at 22°C. Protein drops were immediately examined after the screen setting under the stereomicroscope mounted with a video camera. Crystal growth was examined under the microscope daily for one week, and continued once a week afterwards.

After positive conditions were obtained, the hanging drop technique was used for further optimization. Optimization experiments were setup using a Linbro® Tissue culture multi-well plate with cover. The positive conditions obtained from the microbatch under oil were optimized by varying pH of buffer, concentrations of salt and precipitant, protein concentrations and temperatures. A crystallization droplet of 2 μl was prepared by pipetting 1 μl of the chitinase solution on a 20 mm glass cover slide, and then mixing with 1 μl of the required buffer and the precipitant. The droplet was subsequently inverted and placed over a 1000 μl reservoir containing high concentrations of the same buffer and the precipitant to allow the system to be equilibrated properly. The protein droplet prepared on a covered slide sealed with high-vacuum grease was incubated at 22°C and examined regularly until small crystals, plates, rods, needle clusters or single crystals were observed.

To obtain X-ray quality single crystals, further optimization was carried out by microseeding using either a manual pipetting or streak seeding technique. For microseeding, the seed crystals obtained from the positive conditions from the hanging drop method were crushed in a few microliters of the mother liquor, then the seed solution was pipetted to a 1/2 or 1/10 dilution series in a proper precipitating solution. For streak seeding, a whisker glued to a small rod was dragged into the seed solution to pick up a small amount of the liquid containing microcrystals. The whisker was then dipped into the pre-equilibrated drops containing different concentrations of the chitinase. Crystals were allowed to grow in the drops with sufficiently high precipitant concentration at 4°C.

Alternatively, macroseeding was used for optimization. A single seed was washed with the mother liquor in a plastic petri dish, then placed in a pre-equilibrated

drop of the mother liquor and the protein solution. The petri dish was gently swirled to dissolve microcrystals.

After seeding, growth of crystals was observed in the crystallization plates until the X-ray quality single crystals were obtained. The crystals were then mounted in a nylon loop of the proper size for soaking experiment and for further data collection.

2.10.2 Cryocrystallization and crystal storage

A cryotechnique was employed to prevent crystal damage from ice formation and to stabilize the crystals during flash cooling and protect them from X-ray radiation damage. The cryoprotection solution was prepared by addition of 10% (w/v) glycerol while keeping the concentration of the crystallization precipitant unchanged. For the crystallization condition containing the precipitant, which already served as the cryoprotectant, such as 2-propanol, MPD ((+/-)-2-methyl-2,4-pentanediol) and DMSO, the concentration of the precipitant was then increased slightly to enhance its cryoprotectant property. To perform shock-cooling, the crystal was carefully picked by a suitable size of a cryoloop, then the crystal was immediately immerse into liquid nitrogen before X-ray diffraction was performed.

2.10.3 Data collection and processing

Preliminary data were collected on a home source. The crystals that provided high-quality datasets were then further analyzed at the synchrotron light source. For in-house X-ray diffraction, the diffraction data were collected either on a MAR desktop beamline image plate detectors, operating on a Rigaku Micromax HF-007 rotating anode generator or on a MAR research image plate detector on a Nonius FR-591 generator. All the detector systems were equipped with Oxford Cryostream devices. One of the MAR systems was equipped with an automatic sample changer was located at the Max-Planck Institute for Molecular Physiology, Dortmund, Germany. To perform data collection, the flash-frozen crystal was mounted on the goniometer head, which was adjusted to the beam center with one side of the crystal being perpendicular to the X-ray beam. The distances between crystal and the detector were varied from 100 to 150 mm. The exposure times were varied between 1 to 15 min to ensure that the diffraction spots were still visible at high background. Once a satisfactory image was visualized, it was further analyzed by DENZO software (Otwinowski and Minor, 1997) to obtain preliminary data about the crystal quality, the unit-cell dimensions, the space group, the lattice type, the unit cell parameters, the crystal orientation and the completeness. The data were collected using the rotation method to obtain a complete data set.

For crystals complexed with the inhibitors, the best diffracted crystals, in which the electron density of the inhibitor was observed in the active site, were collected on beamline PX-II of the Swiss Light Source, as mentioned earlier. Some data sets were collected on a Bruker Microstar rotating anode generator equipped with Xenocs Fox mirrors and a MAR Research DTB image plate detector with

1° oscillations. The data sets were integrated and processed using program *XDS* (Kabsch, 1993). The maximum resolution to which a crystal diffracted was determined by analyzing the ratio of the measured intensity to its standard deviation, $I/\sigma(I)$. All the data sets were scaled using the maximum resolution range of 2.45 to 1.16 Å. Other criteria to assess the quality of the measured data were the completeness, the redundancy, and the merging R -factor (R_{merge}) (Rhodes, 2000).

2.10.4 Phase determination by the molecular replacement method

In this study, the molecular replacement method was employed to obtain phase information using the program MOLREP (Vagin and Teplyakov, 1997; CCP4, 1994). The first data set of the apo form of native *VhChiA* was solved using the crystal structure of *VhChiA* inactive mutant E315M complexed with chitohexaose (E315M+GlcNAc₆) (PDB ID 3B9A, Songsiriritthigul *et al.*, 2008) as a search model. For the structures of the WT-inhibitor complexes and the W275G-inhibitor complexes, the final model of native *VhChiA* was employed to obtain the phases of all the data sets of the *VhChiA*-inhibitor complexes.

2.10.5 Model rebuilding and structural refinement

The COOT program (Emsley, 2004) was used to manually rebuild the model structure. The search model E315M, complexed with chitohexaose (E315M+GlcNAc₆) (PDB ID 3B9A), was placed into a new unit cell, then an electron density map was calculated using model phases and the observed structure factor amplitudes (Rhodes, 2000). The Fourier difference maps ($F_o - F_c$ and $2F_o - F_c$ maps) were generated from the observed structure-factor amplitudes ($|F_{\text{obs}}|$) and the calculated amplitudes

($|F_{\text{calc}}|$), where each $|F_{\text{obs}}|$ is derived from the measured reflection intensity and each $|F_{\text{calc}}|$ is the amplitude of the corresponding structure factor calculated from the current model. Model rebuilding was carried out based on those two maps which were re-calculated for each cycle of rebuilding and refinement with the program REFMAC5 (Murshudov *et al.*, 1997) available in the CCP4 suit. The atomic positions and the B-factors of all atoms were refined to fit the observed diffraction data. The agreement was measured by R_{factor} which is defined as;

$$R = \frac{\sum \left| |F_{\text{obs}}| - |F_{\text{calc}}| \right|}{\sum |F_{\text{obs}}|} \quad (1)$$

The crystallographic model of the apo form of the native *VhChiA* obtained by the molecular replacement method using the search model (PDB ID 3B9A) as further refined using REFMAC5 to the resolution of 2.7 Å. The final model which had an R_{value} of 21.5% and R_{free} of 31.5%, was then used as the template to solve the other structural complexes with rigid body refinement. For rigid body refinement, these models were divided into three domains. Domain 1 covers the residues 22 to 40; domain 2 covers the residues 61 to 134; and domain 3 covers the residues 135 to 588. These domains were moved as rigid units. The electron density maps were calculated from the observed structure factor amplitudes of the structural model, then the models were refined further to give the best fit to the density, while maintaining good geometry with restrained refinement.

Molecular topologies of the inhibitors were created using Maestro (www.schrödinger.com) and the PRODRG server (Schüttelkopf and van Aalten, 2004). The inhibitors were modeled into the corresponding $2F_o - F_c$ and $F_o - F_c$ maps.

During refinement, water molecules positioned within hydrogen bonding distance of the model were identified from the electron density peaks in the F_o-F_c map and included in the subsequent refinement steps.

Progress of the refinement was measured by R_{factor} and R_{free} values. The crystallographic R_{factor} measures the agreement between the structure factors calculated for the existing model and for the observed structure factors. A more demanding and revealing criterion of model quality and of improvements during refinement is the R_{free} . To compute the R_{free} , the data were divided into a work set and a test set. The test set comprised a random selection of 5% of the observed reflections. Only the work set was used to refine the model. The R_{free} was computed from the test set, which was not included in the refinement process using the same equation. If the structure was improved during refinement, both R_{factor} and R_{free} should decrease. The R_{factor} usually ranges between 0.6 (a random set of reflections with given model) and 0.2 (a well-refined model at a resolution of 2 Å). The R_{free} should be approximately the resolution in Ångstroms divided by 10. Thus, a data set with 2 Å resolution should yield a final R_{free} of roughly 0.2.

From this study, the final refinement of all the structures were completed with R_{factor} of 14.3% to 19.8% and R_{free} of 17.7% to 25.9%, (Table 3.9 and 3.13), which indicated that all the modeled structures were well refined.

2.10.6 Validation of the quality of the model

To build the correct atomic model into the electron density, initial validation was done in COOT (Emsley, 2004). The Ramachandran plot (Ramachandran *et al.*, 1963), which validates the torsional angles of a protein chain from a plot of the dihedral angles ψ against ϕ of amino acid residues in protein structure was evaluated. Water molecules that did not fit the electron density were deleted. The un-modeled blobs of the electron density which were not accounted for by existing atoms were also removed. Rotamers, were checked for unusual side-chain conformations. Finally, the geometry of the structure was analyzed using the program PROCHECK (Laskowski *et al.*, 1993), and the hydrogen bond analysis was carried out with WHAT_ IF (Vriend, 1990).

2.11 Determination of chitinase activity

2.11.1 Chitinase activity assay using the dimethylaminoborane (DMAB) method

Chitinase activity was measured by the DMAB method using chitohexaose, colloidal chitin and crystalline α chitin as substrates. The reaction mixture (500 μ l), containing 100 μ M GlcNAc₆ or 1% (w/v) colloidal chitin, or crystalline α chitin, 50 μ g of native enzyme or 200 μ g of W275G or 0.4 μ g of W397F, and 0.1 M sodium acetate, pH 5.5, were incubated at 37°C in a Thermomixer Comfort. After 15 min of incubation, the reaction was terminated by heating at 100°C for 5 min. A 200 μ l aliquot was then subjected to the DMAB assay. Release of the amino sugars was detected spectrophotometrically at 585 nm and was converted to molar concentrations using a standard calibration curve of GlcNAc₂ (0-8.75 mM) (Pantoom *et al.*, 2008).

2.11.2 Chitinase activity assay using the dinitrosalicylic acid (DNS) method

Kinetic measurements were determined in a microtiter plate using GlcNAc₅, GlcNAc₆, and colloidal chitin as substrates. A reaction mixture (100 µl), containing 0-500 µM substrate and chitinase (50 µg of wild type, 250 µg of W275G or 0.4 µg of W397F) in 0.1 M sodium acetate buffer, pH 5.5, was incubated at 37°C for 15 min. After boiling to 100°C for 3 min, the entire reaction mixture was subjected to the reducing sugar assay using dinitrosalicylic acid (DNS) reagent, as described by Miller (Miller, 1959). For colloidal chitin, the reaction was carried out the same way as the other substrates, but concentrations of colloidal chitin were varied from 0 to 5% (w/v) and 150 µg of wild type, 700 µg of W275G, or 200 µg of W397F chitinase was used. The amounts of the reaction products were determined from a standard curve of GlcNAc₂ (0-500 nmol). The kinetic values were evaluated from the experiments carried out in triplicate using the non linear regression function available in GraphPad Prism version 5.0 (GraphPad Software Inc., SDG, USA).

2.11.3 Chitinase activity assay using *p*NP-glycosides

The *p*NP assay was carried out in 0.1 M acetate buffer, pH 5.5 using *p*NP-GlcNAc₂ or *p*NP-GlcNAc₃ as substrates. A reaction mixture contained 25 µl of 500 µM substrate, 65 µl of 0.1 M sodium acetate buffer, pH 5.5, and 10 µl of the purified enzyme. The reaction mixture was incubated at 37°C for 10 min, then 50 µl of 1.0 M Na₂CO₃ was added to stop the reaction. Absorbance at 405 nm (A_{405}) was measured and molar concentrations of *p*NP were calculated using the *p*NP standard curve. One unit of enzyme is defined as the amount releasing 1 nmol of *p*NP in 1 min at 37°C.

2.11.4 Chitinase activity assay using 4MU-glycosides

A reaction mixture (50 μ l) was prepared in a 96 well plate compatible with a Gemini EM microplate fluorometer. The reaction contained 0.1 M sodium citrate/citric acid, 0.2 M phosphate buffer, pH 5.5, 0.025% (v/v) Triton X-100 and the fluorogenic substrate 4MU-GlcNAc₂ or 4MU-GlcNAc₃ at a concentration of 0.125 μ M. The pre-mixed reaction without enzyme was pre-incubated at 28°C for 10 min and then 25 nM of the wild type or 650 nM of W275G was added, then the reaction was measured immediately at the excitation wavelength of 360 nm and the emission wavelength of 450 nm. The progress was monitored for 30 min and the data were analyzed using SoftMax Pro version 5.3 (SOFTmax PRO, Molecular Devices, Sunnyvale, CA, USA). The amount of released 4-methylumbelliferone (4MU) was converted to a molar quantity using the standard curve of 4MU (0.625-10 nM). The kinetic values (k_{cat} , K_m , and k_{cat}/K_m) were evaluated using a nonlinear regression function available in GraphPad Prism version 5.0.

2.12 Steady-state kinetics

Kinetic parameters of the chitinase variants were determined using chitohexaose or colloidal chitin as substrates. For chitohexaose, a reaction mixture (200 μ l), containing 0-500 μ M GlcNAc₆, and 50 μ g of enzyme in 0.1 M sodium acetate buffer, pH 5.5, was incubated at 37°C for 10 min. After boiling at 100°C for 3 min, the entire reaction mixture was subjected to the DMAB assay. For colloidal chitin, the reaction was carried out the same way as the DNS assay, but concentrations of colloidal chitin were varied from 0 to 5.0% (w/v). The amounts of the reaction products produced from both substrates were determined from a standard curve of

GlcNAc₂ (0-1.75 μ mol). The kinetic values were evaluated from the experiments carried out in triplicate using the nonlinear regression function obtained from the GraphPad Prism software.

2.13 Chitin binding assay and determination of adsorption binding

isotherm

The chitin binding assay was assayed at 0°C to minimize hydrolysis. For the time course study, a reaction mixture (500 μ l), containing 1.0 μ mol enzyme, and 1.0 mg of chitin in 20 mM Tris-HCl buffer, pH 8.0, was incubated for 1.25, 2.5, 5, 10, 15, 20, 25, and 30 min, and then the supernatant was collected by centrifugation at 12000 x g at 4°C for 10 min. The concentration of the remaining enzyme (E_f) in the supernatant was determined by Bradford's method, while the concentration of the bound enzyme (E_b) was calculated from the difference between the initial protein concentration (E_i) and the free protein concentration (E_f) after binding. The chitin binding assay was also carried out with crystalline α chitin and colloidal chitin. A reaction (set as above) was incubated for 60 min at 0°C, then the chitin-bound enzyme was removed by centrifugation, and the concentration of the free enzyme was determined. For adsorption isotherm experiments, the reaction assay (also prepared as described above) containing varied concentrations of the chitinase from 0 to 7.0 μ M was incubated for 60 min at 0°C. After centrifugation, the concentration of free enzyme in the supernatant was determined. A plot of [E_b] vs [E_f] was subsequently constructed and the binding dissociation constants (K_D) of wild-type and mutants were estimated using a nonlinear regression function in the GraphPad Prism software.

2.14 Determination of the inhibitor binding modes using isothermal microcalorimetry (ITC)

ITC experiments were performed with the ITC-200 system. Measurements were carried out at 25°C with a stirring speed at 1000 rpm. After the baseline was set with distilled water, 4 µl of 250 µM DEQ or 500 µM SAN or PEN was injected into the 300 µl calorimeter cell containing 20 mM sodium acetate, pH 5.5, and 25 µM enzyme. The injections were repeated 20 times over 90 sec intervals. The background was measured by injecting the inhibitor into the cell containing only buffer. The ITC experiments of the mutated *VhChiA* were performed as described for the wild-type experiments with higher concentrations of the reaction components 100 µM of the W275G enzyme with 1mM DEQ or 2 mM SAN or PEN and 50 nM of W397F with 500 µM DEQ or 100 µM SAN and PEN were used. All the measurements of mutant W275G were conducted at 18°C in 20 mM sodium acetate buffer, pH 5.5, as the similar condition as the measurement of W397F with DEQ and SAN. The only exception was the measurement of W397F with PEN, which was done in 20 mM Tris-HCl buffer, pH 8.0. After subtracting the background, titration curves were fitted using the most appropriate algorithms supplied with the instrument.

The ITC data were evaluated using MicroCal Origin vs 7.0 software. All the data were corrected by subtracting heat released from titration of inhibitor in buffer without enzyme. The data were fitted to a theoretical titration curve using the most appropriate model by Origin version 8.0. The measured heat changes as a function of ligand concentrations, provided information on the binding enthalpy (ΔH) in kcal mol⁻¹, and the binding affinity by means of the equilibrium association constant (K_A)

from the maximal slope of the sigmoidal part and the number of binding sites (n) from the positions of the inflection point relative to protein concentrations. The equilibrium dissociation constant (K_D) was calculated from $1/K_A$. The Gibbs free energy was obtained from the equation: $\Delta G = \Delta H - T\Delta S = RT\ln(K_D)$. Where, ΔG , ΔH , and ΔS are the changes in the Gibbs' free energy, enthalpy, and entropy of binding, respectively. R represents the gas constant ($1.98 \text{ cal K}^{-1}\text{mol}^{-1}$) and T the absolute temperature in kelvin (K).

The quantity $c = K_A M_t(0)$, where $M_t(0)$ is the initial macromolecule concentration of importance in titration microcalorimetry. All experiments were performed with the c values set between $1 < c < 500$.

2.15 Determination of chitinase-inhibitor interactions using fluorescence spectroscopy

The purified wild-type chitinase ($0.25 \text{ } \mu\text{M}$) was titrated with different concentrations of the inhibitors ($0.005\text{-}100 \text{ } \mu\text{M}$) in 20 mM Tris-HCl , pH 8.0, at 25°C . Changes in intrinsic tryptophan fluorescence were monitored directly on a LS-50 fluorescence spectrometer. The excitation wavelength of 295 nm and emission intensities were collected over $310\text{-}450 \text{ nm}$ with the excitation and emission slit widths being kept at 5 nm . Each protein spectrum was corrected for the buffer spectrum. The fluorescence intensity data were analyzed by a nonlinear regression function available in Prism version 5.0 using the following single-site binding model:

$$F/F_0 = \left(F_0/F_0 - NS \right) e^{-K_D[L_0]} + NS$$

Where F and F_0 refer to the fluorescence intensity in the presence and absence of ligand, respectively, $[L_0]$ is the initial ligand concentration, K_D is the equilibrium dissociation constant and NS is the non specific binding that does that dissociated (plateau).



CHAPTER III

RESULTS

PART I

FUNCTIONAL ROLE OF THE SURFACE-EXPOSED RESIDUES ON THE BINDING AND HYDROLYTIC ACTIVITIES OF CHITINASE A FROM *VIBRIO HARVEYI*

3.1 Homology modeling and sequence analysis

Studies of the substrate binding residues revealed a number of conserved aromatic residues which are located in the active site of *VhChiA*. These residues include Trp168, Tyr171, Trp275, Trp397, and Trp570. These residues were found to be important in binding to chitooligosaccharide substrates (Suginta *et al.*, 2007; Songsiriritthigul *et al.*, 2008). There are also the surface-exposed residues positioned outside the substrate binding cleft and extending towards the *N*-terminal ChBD that are conserved and their function may be relevant to binding and hydrolysis of crystalline chitin (Watanabe *et al.*, 2001; Uchiyama *et al.*, 2001). Figure 3.1 represents the modeled 3D-structure of *VhChiA* that was built based on the crystal structure of *SmChiA* mutant E315L complexed with GlcNAc₆. In the modeled

structure, four surface-exposed residues (Trp70, Ser33, and Trp231, and Tyr245) are found to align linearly with each other. Trp70 and Ser33 are positioned at the end of the *N*-terminal ChBD, whilst Trp231 and Tyr245 are found outside the substrate binding cleft where they are part of the TIM barrel catalytic domain. A structure-based alignment (Figure 3.2A) of the *N*-terminal ChBD of *Vibrio* and *Serratia* chitinases with the *C*-terminal fragment that covers the ChBD of *Bacillus* WL-12 chitinase A1 (ChBDChiA1), showed that the residues Trp656 and Trp687 of the ChBDChiA1 are well aligned with Ser33 and Trp70 of *V. harveyi* chitinase A. With respect to the alignment of the catalytic domain (Figure 3.2B), Trp231 of the *Vibrio* chitinase is equivalent to Trp122 and to Phe232 of the *Bacillus* and *Serratia* chitinases. For Tyr245, this residue is replaced by Trp134 and Trp245 in the *B. circulans* and *S. marcescens* sequences, respectively. The residues Trp245 and Tyr231 are found as part of the catalytic $(\alpha/\beta)_8$ TIM barrel. In this study, the functional roles of the four amino acid residues (Ser33, Trp70, Trp231, and Tyr245) located on the surface of *V. harveyi* chitinase A were investigated.

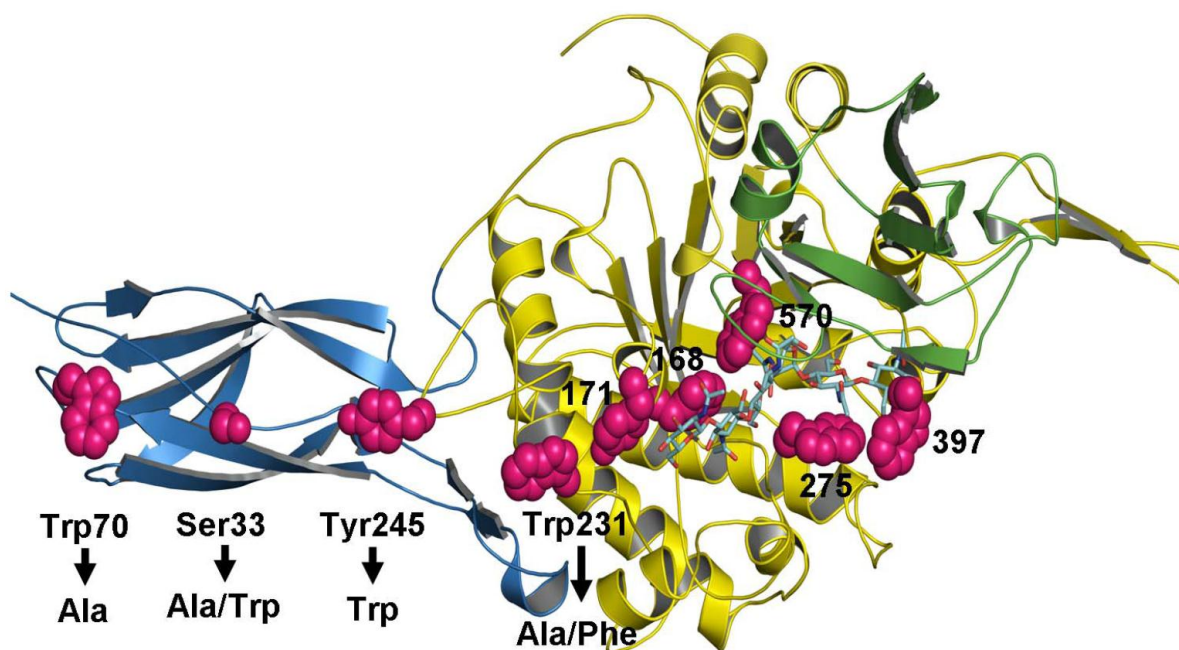


Figure 3.1 Swiss-model 3D-structure of *VhChiA*.

A ribbon representation of the 3D-structure of *VhChiA* chitinase A was constructed based on the X-ray structure of *SmChiA* E315L mutant as described in the text. The *N*-terminal ChBD is presented in cyan, the TIM barrel domain in yellow and the small insertion domain in green. The coordinates of GlcNAc₆ that are modeled in the active site of the *Vibrio* enzyme are shown as a stick model with N atoms in blue and O atoms in red. The mutated residues (Ser33, Trp70, Trp231, and Tyr245) and other substrate binding residues are also presented in stick model (magenta).

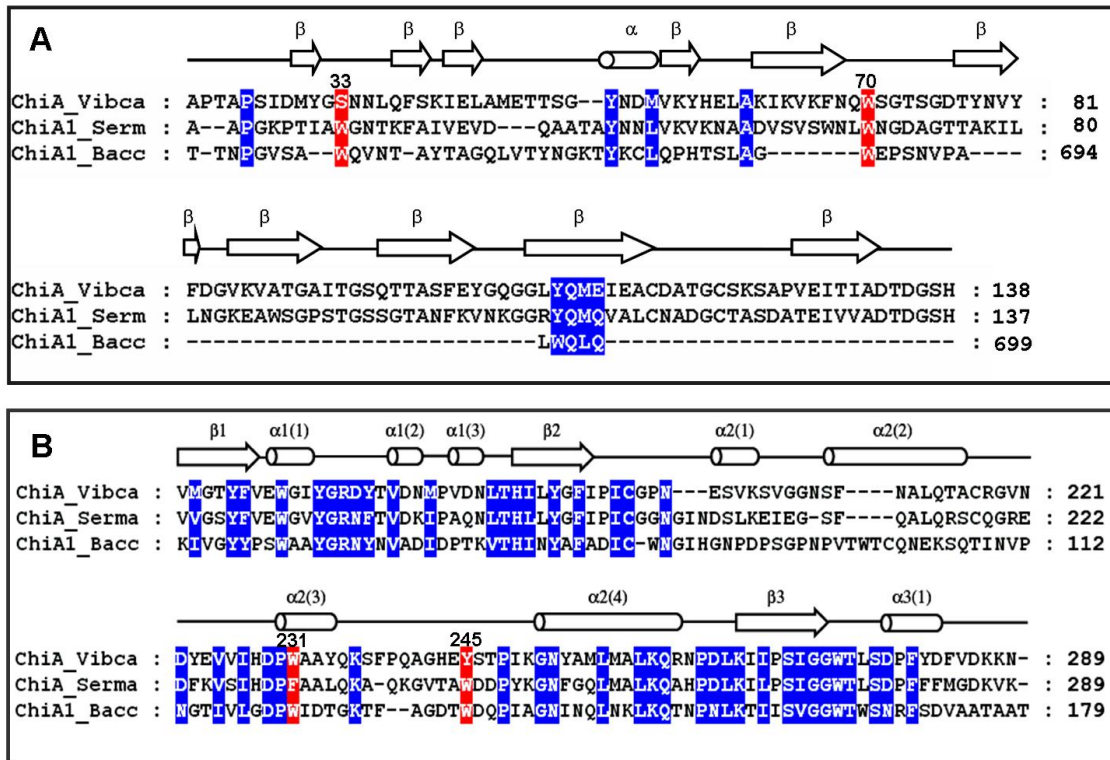


Figure 3.2 Structure-based alignment of *Vh*ChiA with *S. marcescens* chitinase A and *B. circulans* chitinase A1.

(A) The *N*-terminal ChBDs of *Vh*ChiA (residues 22-138) and *Sm*ChiA (residues 24-137) are aligned with the *C*-terminal fragment (residues 648-699), covering the ChBD of *B. circulans* WL-12 chitinase A1. (B) An alignment of the catalytic domain of the three bacterial chitinases with residues 160 to 289 of *Vh*ChiA are displayed. Conserved residues are shaded in blue, whereas the residues that are aligned with Ser33, Trp70, Trp231, and Tyr245 of *Vh*ChiA are shaded in red. ChiA_Vibca: *Vh*ChiA (Q9AMP1), ChiA_Serma: *Sm*ChiA (P07254), and ChiA1_Bacc: *B. circulans* chitinase A1 (P20533). β -strand is represented by an arrow, α -helix by a cylinder and loop by a straight line.

3.2 Mutational design and site-directed mutagenesis

To investigate the functional roles of Ser33, Trp70, Trp231, and Tyr245 on binding and hydrolytic activities of *VhChiA*, they were mutated by site-directed mutagenesis using the QuickChange Site-Directed Mutagenesis kit (Stratagene). The pQE60 plasmid harboring the *ChiA* DNA lacking the residues 598-850 C-terminal fragment, was used as DNA template. The PCR products of the mutated DNAs had the expected size of 5.2 kb, which is the sum of the sizes of the pQE60 plus the wild-type DNA together (Figure 3.3). The mutated DNAs were sequenced by automated DNA sequencing (BSU, Bangkok, Thailand) to verify the correct mutations.

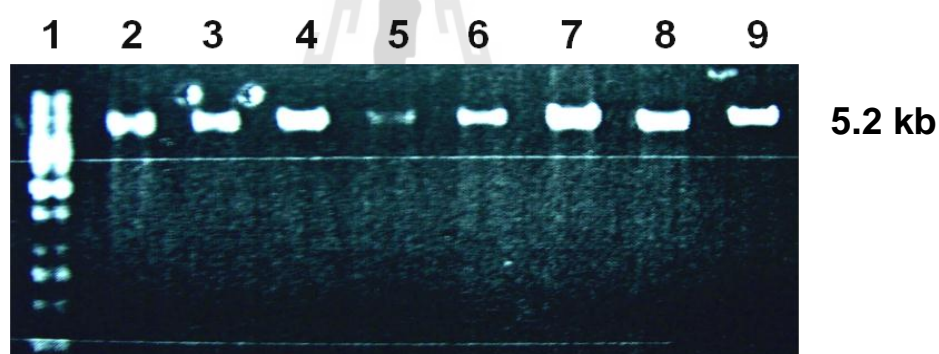


Figure 3.3 Agarose gel electrophoresis of the PCR products of *VhChiA* DNA fragment obtained by site-directed mutagenesis. Lane 1, 1-kb DNA markers; lane 2, wild-type chitinase A; lane 3, S33A; lane 4, S33W; lane 5, W231A; lane 6, W231F; lane 7, W70A; lane 8, Y245A, and lane 9, Y245W.

3.3 Expression and purification of *VhChiA* and mutants

The chitinase A wild-type and all the mutants (Ser33A, S33W, Trp70A, Trp231A, Trp231W, and Try245W) were expressed as the C-terminally (His)₆ tagged

fusion protein. After a single-step purification by Ni-NTA agarose affinity chromatography, the yields of the purified proteins were estimated to be approx. 20 to 25 mg/ml per liter of bacterial culture. All the mutated proteins displayed a single band of molecular weight of 63 kDa as shown in Figure 3.4 which is identical to the molecular weight of the wild-type enzyme.

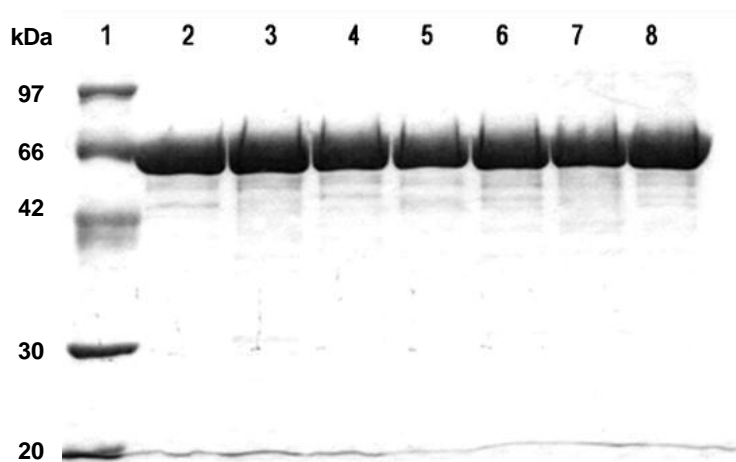


Figure 3.4 SDS-PAGE analysis of *VhChiA* and its mutants.

The mutated enzymes were purified by Ni-NTA agarose affinity column chromatography, as described in Section 2.7. Protein purity was confirmed on a 12% SDS-PAGE gel, and stained with Coomassie brilliant blue R-250. Lane 1, low MW protein markers (Invitrogen); lane 2, wild-type chitinase A; lane 3, S33A; lane 4, S33W; lane 5, W70A; lane 6, W231A; lane 7, W231F, and lane 8, Y245W.

3.4 Effects of point mutations on chitin binding activity of *VhChiA*

Chitin binding activity of chitinase variants was measured as a function of time using colloidal chitin as substrate. To minimize hydrolysis, all the binding experiments were carried out on ice. The unbound enzymes were measured at different

time points from 0 to 30 min. The results in Figure 3.5 shows a rapid decrease in concentrations of the unbound enzyme remained in the supernatant of the reaction mixture after centrifugation, and the equilibrium was reached within 5 min. Relative binding activity of each mutant to colloidal chitin follows the order: W231A > S33W > WT \cong W231F > S33A > Y245W > W70A.

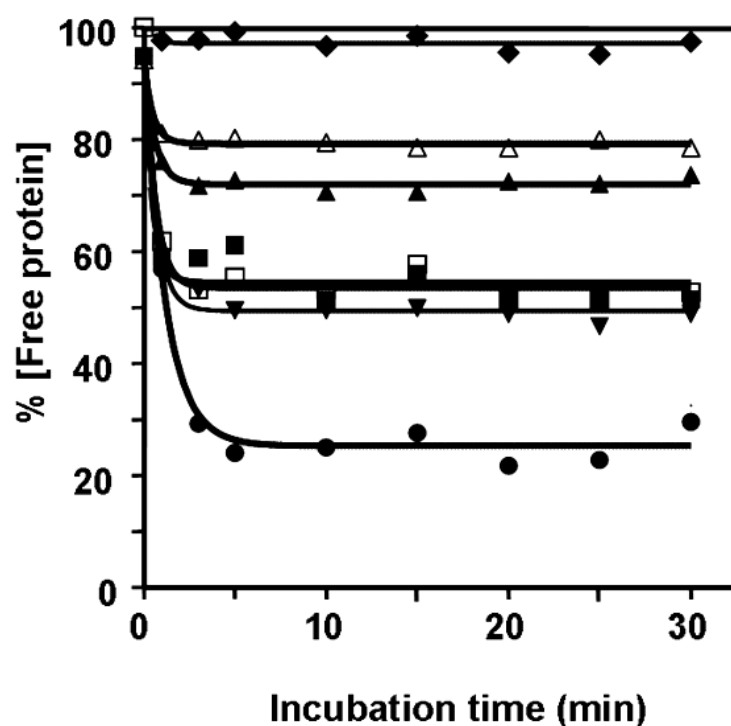


Figure 3.5 Time-course of binding of *VhChiA* variants to colloidal chitin. Chitinases (1 μ mol in 100 mM sodium acetate buffer, pH 5.5) was incubated with 1.0 mg colloidal chitin at 0°C. Decreases in the free enzyme concentrations were determined at different time points from 0-30 min by Bradford's method. Each data value was calculated from the binding experiments carried out in triplicate. Symbols: wild-type (black square); S33A (black upward-pointing triangle); S33W (black downward-pointing triangle); W70A (black diamond); W231A (black circle); W231F (open square); and Y245W (open triangle).

Binding activity of the individual mutants was further examined in relation to that of the wild-type enzyme with colloidal chitin and crystalline α -chitin at a single time point of 60 min (Figure 3.6). In general, the wild-type and mutated chitinases displayed greater binding activity towards colloidal chitin than crystalline α -chitin. For both polysaccharides, W70A and Y245W displayed lower binding activity than the wild-type enzyme. Mutants S33A and W231F showed the modest increase in binding to crystalline α -chitin and a decreased level of binding to colloidal chitin. On the other hand, mutants S33W and W231A displayed higher effectiveness in binding to both substrates. Of all, mutant W231A displayed the highest binding activity, while mutant W70A exhibited the lowest activity. Especially, no detectable binding to crystalline α -chitin was observed with mutant W70A. To determine the equilibrium dissociation binding constant (K_D), adsorption isotherm experiments of the chitinase variants were carried out towards colloidal chitin substrate.

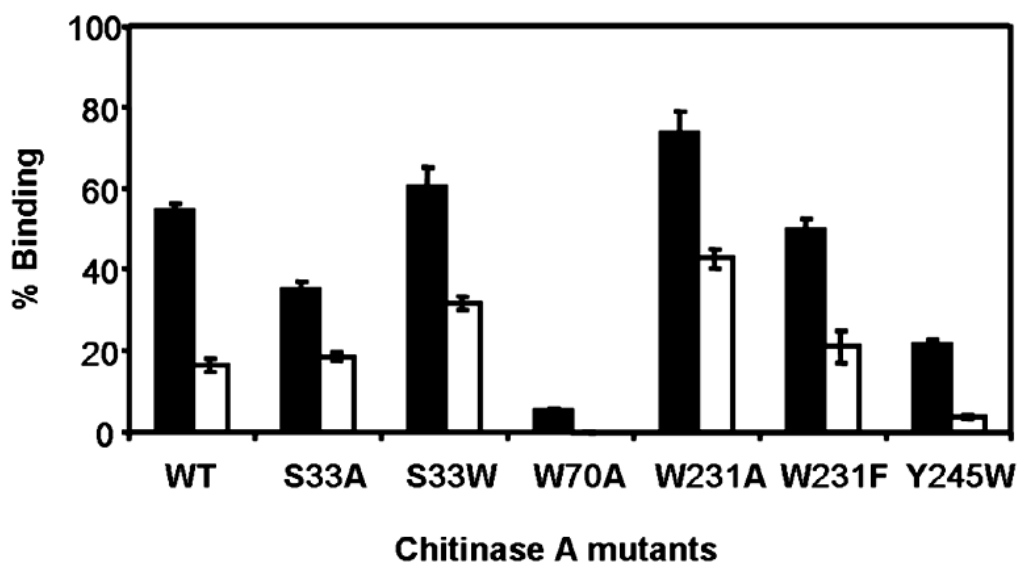


Figure 3.6 Binding of *VhChiA* and mutants to insoluble chitin.

The binding assay was carried out with crystalline α -chitin or colloidal chitin at a single time point of 60 min. % binding = $\left[\frac{E_t - E_f}{E_t} \right]$; where E_t is the initial enzyme concentration and E_f is the free enzyme concentration after binding. Closed and open bars represent the percents of binding to colloidal chitin and crystalline α -chitin, respectively. The presented data are mean values obtained from the experiments done in triplicate.

A nonlinear plot of the adsorption isotherms obtained at a fixed concentration of colloidal chitin and varied concentrations of the enzyme is shown in Figure 3.7. In comparison to the wild-type enzyme, mutants S33W and W231A exhibited significantly higher binding activity, whereas mutants W70A, S33A, W231F, and Y245W had notably decreased binding activity. The K_D value of wild-type ($0.95 \pm 0.11 \mu\text{M}$) estimated from the nonlinear regression function, was slightly larger than the K_D of S33W ($0.84 \pm 0.09 \mu\text{M}$) and W231F ($0.88 \pm 0.09 \mu\text{M}$), but remarkably

greater than the value of W231A ($0.26 \pm 0.03 \mu\text{M}$). In contrast, significantly higher K_D values than the wild-type value were observed with S33A ($1.50 \pm 0.11 \mu\text{M}$), W70A ($2.30 \pm 0.25 \mu\text{M}$), and Y245W ($1.60 \pm 0.16 \mu\text{M}$). These estimated K_D values gave a notation of the enzyme's binding strength in the following order: W231A > S33W > W231F > wild-type > S33A > Y245W > W70A. Such results are in accordance with the binding activities determined by the chitin binding assay and the kinetic data as shown in Table 3.2.

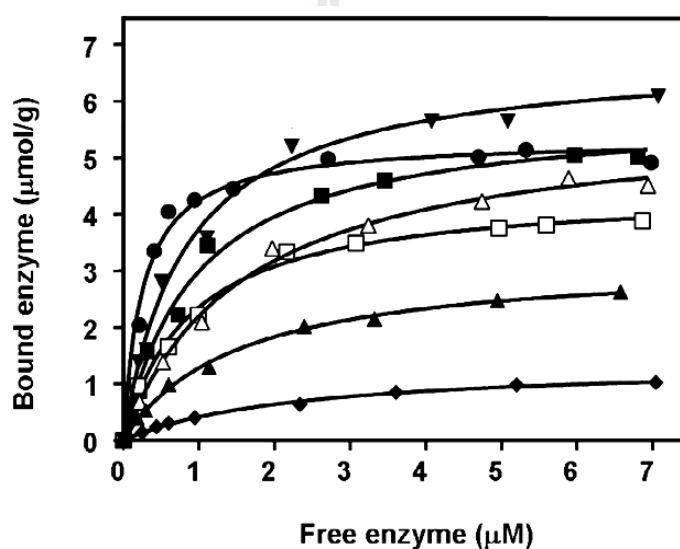


Figure 3.7 Equilibrium adsorption isotherms of the wild-type and mutated *VhChiA* to colloidal chitin.

The reaction assay (500 μl) contained 1.0 mg chitin and varied concentrations of enzyme from 0 to 7.0 μM . After 60 min of incubation at 0°C , the reaction mixture was centrifuged and concentrations of E_b and E_f were determined as described in the text. Symbols: wild-type (black square); S33A (black upward-pointing triangle); S33W (black downward-pointing triangle); W70A (black diamond); W231A (black circle); W231F (open square); and Y245W (open triangle).

3.5 Effects of point mutations on hydrolytic activity of *VhChiA*

To investigate the effects of mutations on hydrolytic activity of the enzyme, specific activities towards three different substrates (*p*NP-GlcNAc₂, colloidal chitin and crystalline α -chitin) were evaluated. From all the mutants, only W231A displayed a slightly reduced specific activity against the *p*NP substrate with 90% of the specific activity of the wild-type enzyme as shown in Table 3.1. In contrast with the *p*NP-glycoside, strong effects on hydrolytic activity were observed with the insoluble substrates. Specific activity against crystalline α -chitin was completely abolished in case of mutants S33A, W70A, and W231A/F, but improved for mutants S33W and Y245W at levels of 166% and 250% of the wild-type activity, respectively. A similar trend was also seen when colloidal chitin was used as substrate. Specific activity of S33A, W70A, and W231A/F were markedly decreased, while S33W and Y245W displayed higher activity than wild-type enzyme. The most severe loss of specific activity towards colloidal chitin was detected for mutant W70A.

Table 3.1 Specific hydrolytic activity of *VhChiA* and mutants.

The reducing sugar assay was carried out against crystalline and colloidal chitin. Release of the hydrolytic products was calculated from a standard curve of GlcNAc₂. On the other hand, specific hydrolyzing activity against *p*NP-GlcNAc₂ was determined from a standard curve of *p*NP.

Chitinase variant	Specific hydrolyzing activity (U/μmol protein) ^a		
	Crystalline α chitin	Colloidal chitin	<i>p</i> NP-GlcNAc ₂
Wild-type	0.6 ± 0.02(100) ^b	12.9 ± 0.2 (100)	50.5 ± 1.1 (100)
S33A	n.d. ^c	8.5 ± 0.5 (66)	58.0 ± 1.1 (115)
S33W	1.00 ± 0.1 (166)	15.3 ± 0.3 (119)	54.0 ± 2.6 (107)
W70A	n.d.	4.3 ± 0.2 (33)	52.8 ± 2.1 (105)
W231A	n.d.	1.0 ± 0.3 (51)	45.2 ± 2.0 (90)
W231F	n.d.	9.2 ± 0.5 (71)	54.3 ± 2.9 (108)
Y245W	1.5 ± 0.1 (250)	19.6 ± 0.5 (152)	53.6 ± 1.6 (106)

^a One unit of chitinase is defined as the amount of enzyme that releases 1 μmol of GlcNAc₂ or 1 nmol of *p*NP per min at 37°C.

^b Values in parentheses represent relative specific hydrolyzing activities (%).

^c Non-detectable activity.

3.6 Steady-state kinetics of *VhChiA* and mutants

Steady-state kinetics of *VhChiA* and mutants were determined with chitohexaose and colloidal chitin as substrates. All kinetic parameters were determined from the Michaelis-Menten curves as shown in Figures 3.8A and 3.8B. The kinetic parameters presented in Table 3.2 indicate concomitant decreases in both K_m and k_{cat} against hexachitooligomer. For all the mutants, the overall catalytic efficiency (k_{cat}/K_m) was not much different to the value observed for the wild-type enzyme. In contrast, the kinetic properties of the enzyme against colloidal chitin were significantly modified by the mutations. K_m values of S33A (20.7 mg ml⁻¹), W70A (22.6 mg ml⁻¹), and Y245W (18.2 mg ml⁻¹) were higher than the wild-type K_m (17.4 mg ml⁻¹), whereas S33W (15.8 mg ml⁻¹) and W231A (10.1 mg ml⁻¹) had considerably lower K_m values compared to the reference value. Mutants that displayed decreases in k_{cat} , were S33A, W70A, and W231A, and W231F, whereas mutants S33W and Y245W displayed elevated k_{cat} values instead. The overall catalytic efficiency (k_{cat}/K_m) that was calculated for the hydrolysis of colloidal chitin was to more or less extent either reduced (for S33A, W70A, W231A, and W231F) or increased (for S33W and Y245W).

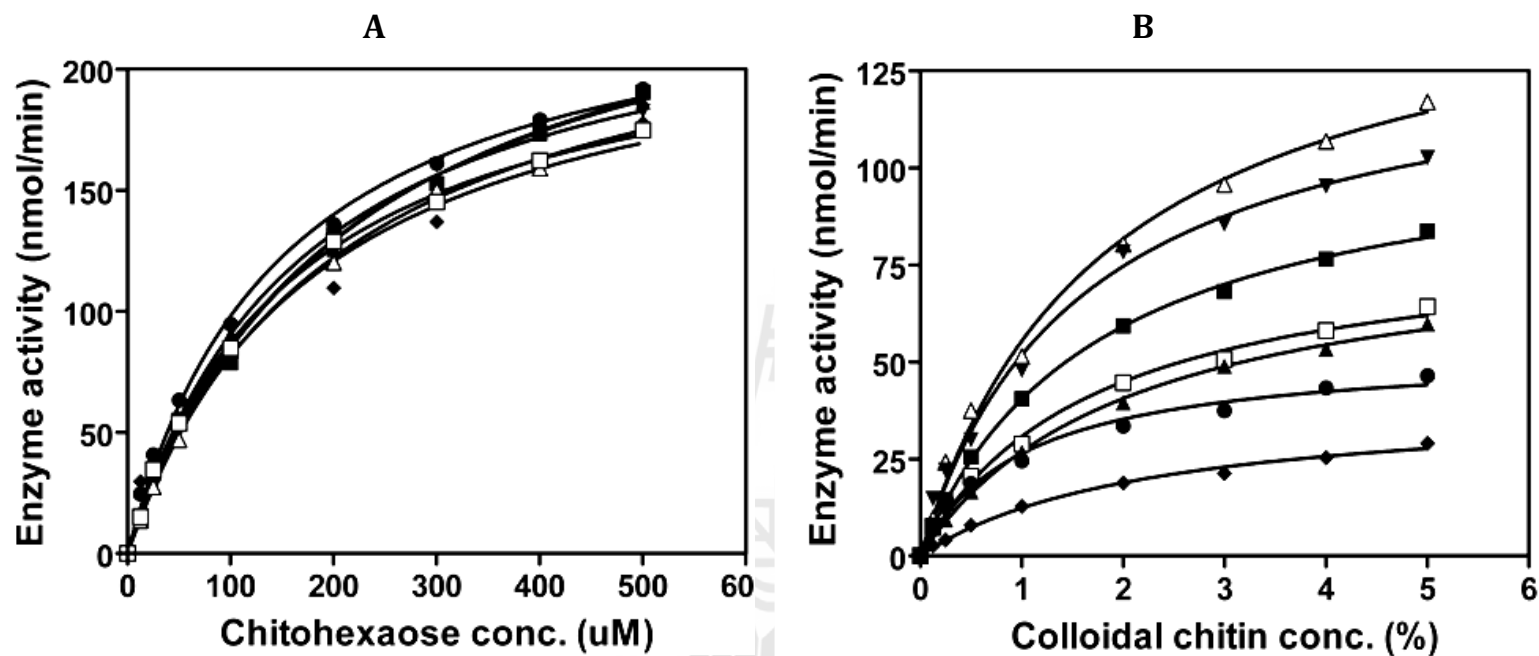


Figure 3.8 Michaelis-Menten plots of the wild-type and mutated *VhChiA* to chitohexaose (A) and colloidal chitin (B).

The reaction assay (200 µl) containing 0-500 µM (GlcNAc)₆ or 0 to 5% (w/v) colloidal chitin, and 50 µg enzyme in 100 mM sodium acetate buffer, pH 5.5, was incubated at 37°C for 10 min. Chitinase activity was determined by the DMAB method. Symbols: wild-type (black square); S33A (black upward-pointing triangle); S33W (black downward-pointing triangle); W70A (black diamond); W231A (black circle); W231F (open square); and Y245W (open triangle).

Table 3.2 Kinetic parameters of chitin hydrolysis by chitinase A wild-type and mutants.

A kinetic study was carried out using 0-5% (w/v) colloidal chitin or 0-500 μM GlcNAc₆ as substrates. After 10 minutes of incubation at 37°C, the amounts of the reaction products were determined from a standard curve of GlcNAc₂.

Chitinase A variant	GlcNAc ₆			Colloidal chitin		
	K_m (μM)	k_{cat} (s^{-1})	k_{cat}/K_m ($\text{S}^{-1}\text{M}^{-1}$)	K_m (mg/ml)	k_{cat} (s^{-1})	k_{cat}/K_m ($10^{-1}\text{s}^{-1}/\text{mg}/\text{ml}^{-1}$)
Wild-type	218 \pm 22.0	2.9 \pm 0.12	1.3 X10 ³ (100) ^a	17.4 \pm 0.1	1.2 \pm 0.02	0.7 (100) ^d
S33A	171 \pm 20.5	2.6 \pm 0.12	1.5 X10 ³ (115)	20.7 \pm 0.2	0.9 \pm 0.03	0.4 (57)
S33W	210 \pm 15.4	2.8 \pm 0.10	1.3 X 10 ³ (100)	15.8 \pm 0.2	1.4 \pm 0.07	0.9 (129)
W70A	185 \pm 22.0	2.5 \pm 0.08	1.3 X 10 ³ (100)	22.6 \pm 0.4	0.4 \pm 0.03	0.2 (29)
W231A	189 \pm 13.2	2.6 \pm 0.05	1.4 X10 ³ (108)	10.1 \pm 0.2	0.6 \pm 0.04	0.6 (86)
W231F	163 \pm 10.3	2.4 \pm 0.20	1.5 X 10 ³ (115)	17.0 \pm 0.2	0.9 \pm 0.03	0.6 (71)
Y245W	201 \pm 13.1	2.6 \pm 0.07	1.3X 10 ³ (99)	18.2 \pm 0.2	1.7 \pm 0.07	0.9 (129)

^a Relative catalytic efficiencies (%) are shown in parentheses.

PART II

THREE DIMENSIONAL STRUCTURES OF CHITINASE A FROM *VIBRIO HARVEYI* IN COMPLEX WITH THE NEWLY IDENTIFIED INHIBITORS AND BINDING MECHANISMS

Novel inhibitors of *VhChiA* were screened from the Library of Pharmacological Active compounds (LOPAC). Previous studies revealed that the residues Trp275 and Trp397 acted as the key binding residues at subsites +1 and +2 (the aglycone subsites) and were also important for the anomeric selectivity of soluble substrates (Suginta *et al.*, 2007; Suginta *et al.*, 2009). Thus, the study of mutational effects of Trp275 and Trp397 could help to gain more information on protein-ligand interactions around the aglycone subsites.

3.7 Expression and purification of wild-type chitinase and mutants W275G and W397F

The wild-type *VhChiA* and its two mutants W275G and W397F were highly expressed as the C-terminal (His)₆ tagged polypeptides, which could be purified by affinity chromatography. Protein purification began with a gravity flow Ni-NTA agarose column, followed by HisTrap™ HP column connected with an ÄKTA Purifier system. Figure 3.9 shows SDS-PAGE analysis of mutant W275G purification. It is seen that the protein was mainly purified by the first Ni-NTA affinity column (lane 6). Contaminated proteins could be subsequently removed after a second affinity column. Eluted fractions (lanes 7-12) obtained from the HisTrap™

affinity column operated on an FPLC system showed a single protein band of 63-kDa, which was corresponded to the size of *VhChiA* as observed previously (Suginta *et al.*, 2004). Purification of the other two chitinase variants (wild-type and mutant W397F) also gave similar results.

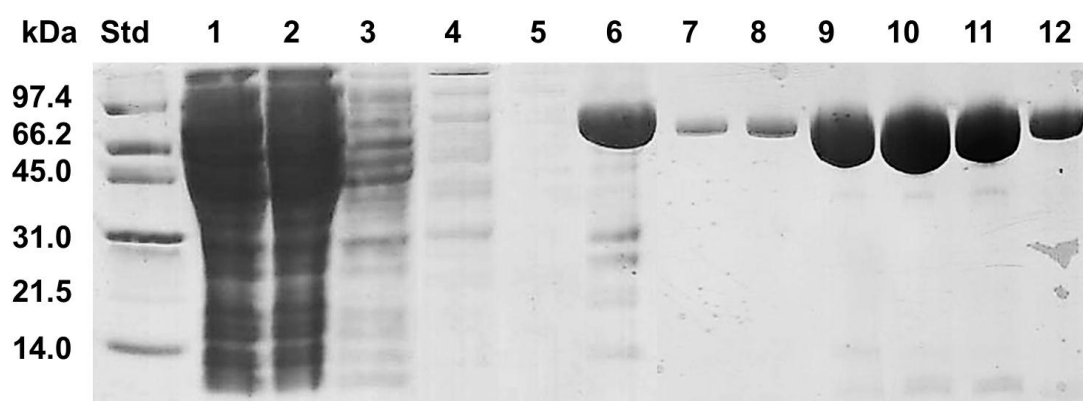


Figure 3.9 Purification of chitinase A mutant W275G using a Ni-NTA agarose, followed by a HisTrapTM affinity chromatography.

Lanes: Std, low molecular weight protein markers; 1, *E. coli* cells harboring the recombinant plasmid after 0.5 mM IPTG induction; 2, crude supernatant; 3, flow through; 4, 20 mM imidazole washed fraction; 5, the first fraction eluted with 250 mM imidazole; 6, the second fraction eluted with 250 mM imidazole; and 7-12 fractions eluted with a linear gradient of 0-250 mM imidazole from a HisTrapTM HP column connected to an ÄKTA purifier system.

The final yields of the purified chitinases after purification were about 20-40 mg per one liter culture. The freshly prepared enzymes obtained from the two affinity steps were immediately subjected to functional studies or crystallization experiments.

3.8 Screening of potential chitinase inhibitors from a drug library

Potential chitinase inhibitors were screened from the Library of Pharmacological Active Compounds (LOPAC) using *p*NP-GlcNAc₂ as substrate. In the *p*NP assay, formation of *p*-nitrophenolate (*p*NP) released as an action of *p*NP-GlcNAc₂ hydrolysis by the wild-type *VhChiA* was monitored at absorption wavelength of 405 nm (A_{405}). Since the phenolate ion is only formed at detectable concentrations at neutral or basic pH values, the enzymatic hydrolysis was performed at pH 7.5 (although the pH optimum of *VhChiA* was determined to be between 5.5 and 6.0). Screening of 1,280 compounds in the commercial LOPAC library initially identified nine hits, including chelerythrine (CHE), dequalinium (DEQ), idarubicin (IDA), 2-(imidazolin-2-yl)-5-isothiocyanatobenzofuran (IMI), pentoxifyllin (PEN), propentofylline (PRO), sanguinarine (SAN), 2-bromo- α -ergocryptine methanesulfonate (BRO) and methysergide maleat (MET).

These nine compounds were subjected to further screening for obtaining their IC_{50} values. Dose response curves were obtained from a reaction mixture containing the wild-type *VhChiA* with 100 μ M GlcNAc₆ in 0.1 M sodium acetate, pH 5.5, and 1 nM-1 mM of inhibitor. The remaining activity was assessed by the DMAB method. IC_{50} values for each inhibitor were estimated from the dose response curves (Figure 3.10) derived from the 4-parameter logistic (4PL) fit.

From the secondary screening results, DEQ was the most potent inhibitor against the wild-type chitinase A with an IC_{50} of $3.91 \pm 1.1 \mu$ M, followed by IDA, SAN, CHE, IMI, PEN and PRO with the IC_{50} values of $6.4 \pm 1.1 \mu$ M, $7.6 \pm 1.3 \mu$ M, $10.47 \pm 1.1 \mu$ M, $21.0 \pm 1.5 \mu$ M, $59.2 \pm 1.2 \mu$ M, and $83.0 \pm 1.0 \mu$ M, respectively. Of the nine, MET showed poorest inhibition with an IC_{50} of $2,995 \pm 2.8 \mu$ M and BRO

showed no inhibitory effect up to 1 mM of the inhibitor used. Thus, only seven compounds, which displayed IC_{50} values less than 100 μ M, were selected as potential chitinase inhibitors for further studies.

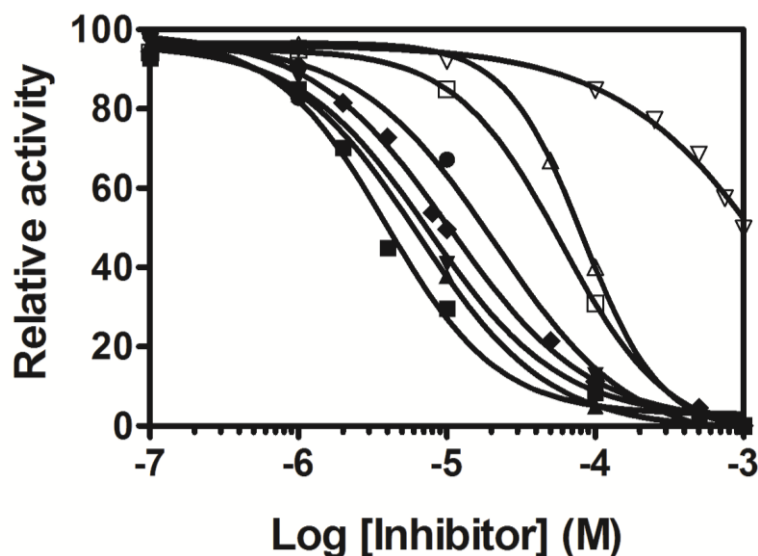


Figure 3.10 Dose response curves of the wild type chitinase against the inhibitors newly identified from the LOPAC library.

Dose-response curves were determined by the DMAB assay using chitohexaose as the substrate. Plots are made between relative activity (%) versus log concentrations of the inhibitor in M units. Symbols: DEQ (black square), IDA (black upward-pointing triangle), SAN (black downward-pointing triangle), CHE (black diamond), IMI (black circle), PEN (open square), PRO (open upward-pointing triangle), and MET (open downward-pointing triangle).

The chemical structures of the seven potential inhibitors are shown in Figure 3.11. It is worth mentioning that propentofylline (PRO) and pentoxifyllin (PEN) are xanthine derivatives, and only PEN was reported previously to inhibit enzymatic activity of the fungal chitinase *Aspergillus fumigatus* chitinase B1 (*AfChiB1*) with an IC_{50} of 126 μ M (Rao *et al.*, 2005).

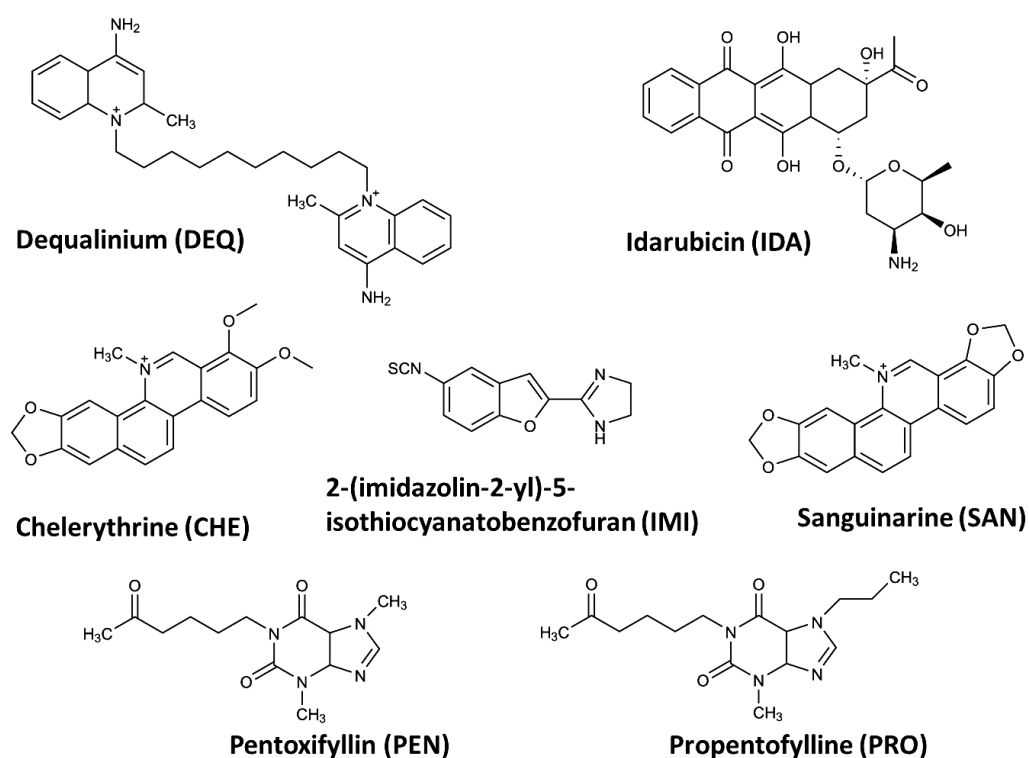


Figure 3.11 The chemical structures of the chitinase inhibitors identified from the LOPAC library.

Abbreviations: chelerythrine (CHE), dequalinium (DEQ), idarubicin (IDA), 2-(imidazolin-2-yl)-5-isothiocyanatobenzofuran (IMI), pentoxifyllin (PEN), propentofylline (PRO), and sanguinarine (SAN).

Effects of the seven inhibitors against the mutants W275G and W397F were studied in comparison with wild-type enzyme using the *p*NP assay. For wild-type and W397F, *p*NP-GlcNAc₂ was used as substrate, while *p*NP-GlcNAc₃ was used as substrate for W275G. After the enzyme was titrated with 0.06-125 μM of each inhibitor, release of the *p*NP was measured at absorbance 405 nm (A_{405}) every 30 sec for 30 min at 25°C. Dose response curves were obtained from the plots between relative activity (%) versus log concentrations of the inhibitor. The curves were fitted using the 4-Parameter-Logistic (4PL) nonlinear model and the IC_{50} values were estimated from the plots are presented in Table 3.3.

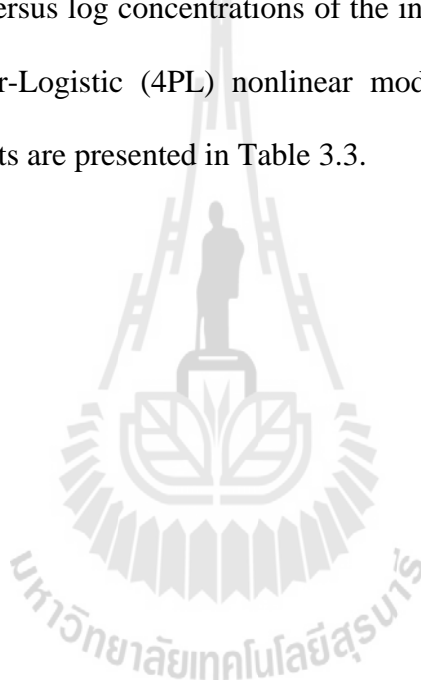


Table 3.3 IC_{50} from the dose response curves using the *p*NP assay with *p*NP-GlcNAc₂ as substrate for wild-type and mutant W397F and *p*NP-GlcNAc₃ for mutant W275G. Each data value was calculated from the experiments carried out in triplicate.

	Wild-type	W397F	W275G
Inhibitor	IC_{50} (μ M)	IC_{50} (μ M)	IC_{50} (μ M)
DEQ	0.4 ± 0.1	9 ± 1	68 ± 28
IDA	0.9 ± 0.2	15 ± 4	270 ± 33
SAN	2.3 ± 0.3	30 ± 2	71 ± 26
CHE	2.2 ± 0.01	48 ± 4	95 ± 34
PRO	3.7 ± 0.9	56 ± 3	360 ± 42
PEN	3.5 ± 0.5	32 ± 2	260 ± 21
IMI	15 ± 3.2	66 ± 5	160 ± 78

Based on the IC_{50} values presented in Table 3.3, the most effective inhibitor against wild-type and the two mutants was DEQ with IC_{50} values of 0.4 μM , 8.8 μM and 68 μM for wild-type, W397F and W275G, respectively. The IC_{50} of the seven inhibitors are in following order: DEQ < IDA < SAN < CHE < PEN < PRO < IMI. It is noticeable that IDA, which acts as the second most potent inhibitor for wild-type and W397F (IC_{50} values of 0.9 μM and 14.6 μM , respectively) showed weak inhibition against W275G with IC_{50} of 270 μM (see Table 3.3). The IC_{50} values of mutants W397F and W275G obtained from the *p*NP assay were about 10 and 100 time weaker than that of wild-type, respectively.

3.9 Crystallization of the wild-type chitinase and mutants W275G and W397F

To investigate how the identified inhibitors interact structurally with the *VhChiA*, crystals of the wild-type *VhChiA* were grown and then soaked or co-crystallized with the inhibitors. Our recent structural data (Songsiriritthigul *et al.*, 2008) already suggested that Trp275 and Trp397 were important for maintaining the molecular interactions with the substrate around subsites (+1/+2). Site-directed mutagenesis data revealed that both residues were crucial for the binding selectivity toward short-chain substrates, such as tetra-, penta-, and hexa-chitooligosaccharides (Suginta *et al.*, 2007). Therefore, crystallization trials of both W275G and W397F were also made. However, only mutant W275G could be crystallized. The availability of the crystal complexes of W275G-inhibitors helps to evaluate how Trp275 contributes to the binding affinity of the enzyme towards the identified inhibitors.

3.9.1 Crystallization of the wild-type *VhChiA*

3.9.1.1 Initial screening and optimization

Initial crystallization of wild-type *VhChiA* was screened using Crystal Screen HR2-110, Crystal Screen HR2-112 (Hampton Research) and JBScreen HTS II using the hanging drop technique. A protein concentration of 20 mg/ml was freshly prepared in 10 mM Tris-HCl, pH 8.0. Positive conditions are shown in Table 3.4. Needle clusters were obtained within 8 days of incubation at 22°C in the condition A4 from JBScreen HTS II (1.0 M ammonium sulfate in 0.1 M Tris-HCl, pH 8.5), and the condition 40 from HR2-110 (20% (v/v) 2-Propanol, 20% (w/v) PEG 4000 in 0.1 M sodium citrate tribasic dihydrate, pH 5.6), whereas thin plates were obtained from the condition 43 of Crystal Screen (HR2-112) (50% (v/v) (+/-)-2-methyl-2,4-pentanediol, 0.2 M ammonium phosphate monobasic in 0.1 M Tris-HCl, pH 8.5).

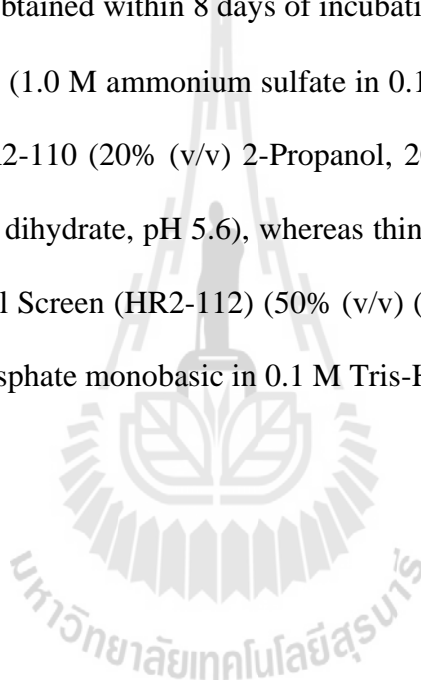


Table 3.4 A summary of positive conditions obtained from crystallization of the wild-type *VhChiA* within 8 days of incubation.

Screen kit	Precipitant condition	Precipitant composition	Temperature (°C)	Crystal morphology
Crystal Screen HR2-110 (Hampton Research)	40	20% (v/v) 2-propanol, 20% (w/v) PEG 4000 in 0.1 M sodium citrate tribasic dihydrate, pH 5.6	18	Needle clusters ^a
Crystal Screen HR2-112 (Hampton Research)	43	50% (v/v) (+/-)-2-methyl-2,4-pentanediol, 0.2 M ammonium phosphate monobasic in 0.1 M Tris-HCl, pH 8.5	18	Plates ^a
Crystal Screen (JBScreen HTS II)	A4	1.0 M ammonium sulfate in 0.1 M Tris-HCl, pH 8.0	18	Needle clusters ^a

^a The conditions used for further optimization.

The condition A4 from Table 3.4 was further optimized by the hanging-drop vapor-diffusion method. A protein drop of 1 μ l chitinase A solution (10 mg/ml in 20 mM Tris-HCl buffer, pH 8.0) mixed with 1 μ l of various concentrations of precipitants (ammonium sulfate concentrations of 0.9, 1.0, 1.1, 1.2, 1.3, and 1.4 M in 0.1 M Tris-HCl buffer, pH 7.5, 8.0, and 8.5, and 0.1 M MOPS, pH 8.5) was equilibrated over 1.0 ml of the same precipitant.

Table 3.5 A grid screening of *VhChiA* with 1.0 M ammonium sulfate at various pH values.

Buffer	Concentration of ammonium sulfate (M)					
Tris-HCl, pH 7.5	0.9 M	1.0 M	1.1 M ^a	1.2 M ^a	1.3 M ^a	1.4 M ^a
Tris-HCl, pH 8.0	0.9 M	1.0 M	1.1 M ^a	1.2 M ^a	1.3 M ^a	1.4 M ^a
Tris-HCl, pH 8.5	0.9 M	1.0 M	1.1 M ^{a,b}	1.2 M ^a	1.3 M ^a	1.4 M ^a
Tris-HCl, pH 7.5	0.9 M	1.0 M	1.1 M	1.2 M	1.3 M	1.4 M

^aThe condition that produced crystals.

^bThe condition used for further optimization.

As presented in Table 3.5, rod and needle clusters obtained from the positive conditions, appeared after 7 days of incubation at 22°C. To produce single crystals, the condition containing 1.1 M ammonium sulfate, 0.1 M Tris-HCl buffer, pH 8.5, were used for streak seeding or pipetting technique. At protein concentrations of 2.5 and 5 mg/ml and under 1/10 and 1/100 dilutions of the seed solution, single crystals appeared after 2 days of incubation (Figure 3.12B).

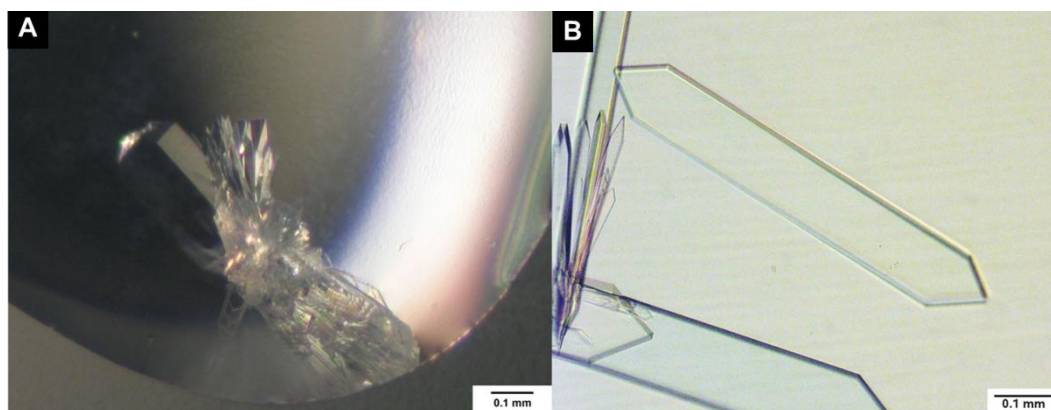


Figure 3.12 Optimization of the wild-type crystals grown under the condition A4 from JBScreen HTSII. (A) Rod clusters obtained from the condition: 1.1 M ammonium sulfate in 0.1 M Tris-HCl buffer, pH 8.5, after grid screening (see Table 3.5); (B) Single crystals obtained from the same condition as (A) after 2 days of incubation at 22°C using a pipetting seeding technique with a protein concentration of 2.5 mg/ml and 1/100 dilution of the seed solution.

The condition 40 obtained from Crystal Screen HR2-110 was also optimized by varying the percentages of PEG 4000 from 5 to 30% (w/v) and percentages of propanol from 5 to 25 % (v/v) using the hanging drop technique (Table 3.6).

Table 3.6 A grid screening of PEG 4000, propanol in 0.1 M sodium citrate tribasic dihydrate, pH 5.6, for crystallization of the wild-type chitinase A.

% (v/v) Propanol	% (w/v) PEG 4000					
	5%	10%	15%	20%	25%	30%
5%	0.1 M	0.1 M	0.1 M	0.1 M	0.1 M	0.1 M
15%	0.1 M	0.1 M	0.1 M	0.1 M	0.1 M	0.1 M
20%	0.1 M	0.1 M	0.1 M	0.1 M	0.1 M	0.1 M
25%	0.1 M	0.1 M	0.1 M	0.1 M	0.1 M ^{a,b}	0.1 M

^aThe conditions that produced crystals.

^bThe condition used for the refined screening.

From Table 3.6, only the condition containing 25% (v/v) 2-propanol and 25% (w/v) PEG 4000 in 0.1 M sodium citrate tribasic dihydrate, pH 5.6, yielded rod cluster crystals. To optimize further, percentages of 2-propanol and PEG 4000 were varied as shown in Table 3.7.

Table 3.7 A refined screening of the condition containing 20% (w/v) PEG 4000, and propanol in 0.1 M tribasic sodium citrate dihydrate, pH 5.0.

% (v/v) Propanol	% (w/v) PEG 4000					
	16%	18%	20%	22%	24%	26%
21%	0.1 M ^{a,b}	0.1 M ^a	0.1 M ^a	0.1 M ^a	0.1 M	0.1 M
23%	0.1 M ^a	0.1 M ^a	0.1 M ^a	0.1 M ^a	0.1 M ^a	0.1 M
25%	0.1 M ^a	0.1 M ^a	0.1 M ^a	0.1 M ^a	0.1 M	0.1 M
28%	0.1 M ^a	0.1 M ^a	0.1 M ^a	0.1 M	0.1 M	0.1 M

^aThe conditions that produced crystals.

^bThe condition used for further micro-seeding optimization.

From all the conditions presented in Table 3.7, needles and plate clusters were seen in the condition A1 (16% (w/v) PEG 4000, 21% (v/v) propanol in 0.1 M sodium citrate tribasic dihydrate, pH 5.6) within 7 days of incubation at 22°C. This condition was used for further optimization using the streak seeding technique, single crystals appeared after 2 days of incubation at 22°C at protein concentrations of 5.0 mg/ml and 7.5 mg/ml under 1/10 and 1/100 dilutions of the seed solution (Figure 3.13).

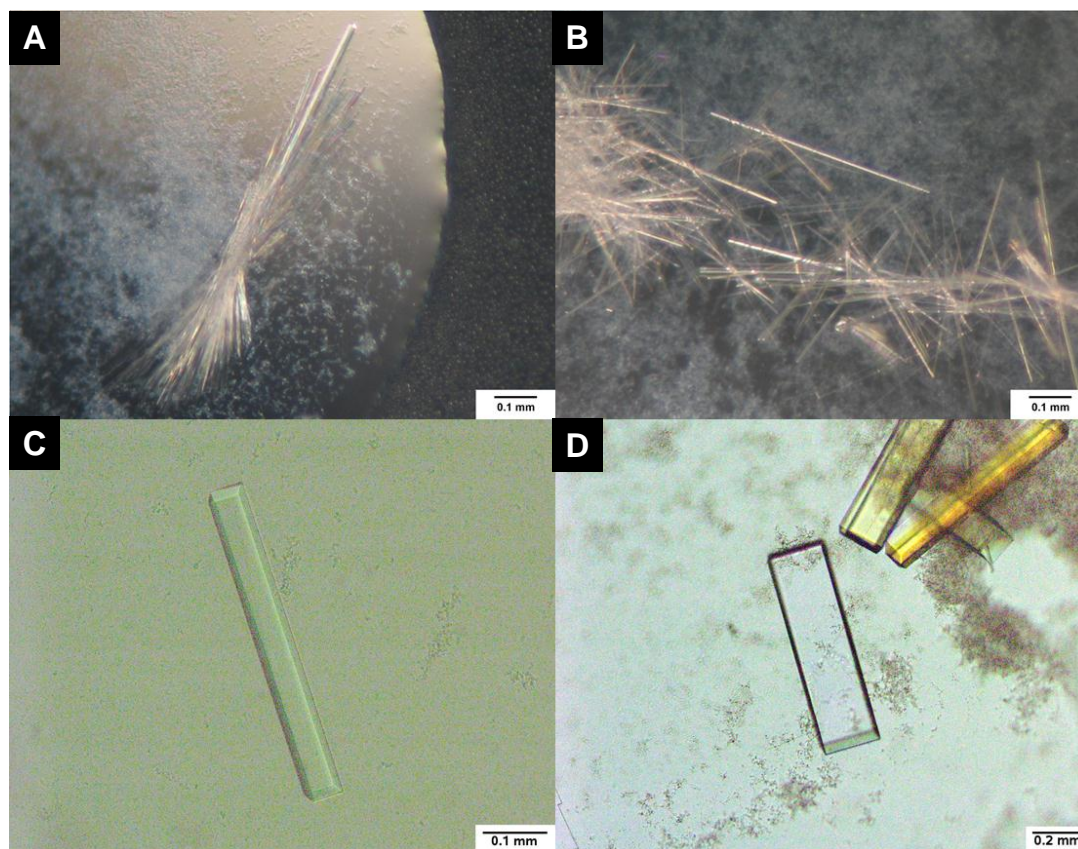


Figure 3.13 Optimization of the wild-type crystals grown under the condition 40 from Crystal Screen HR2-110.

(A) Rod clusters of wild-type obtained from the condition A1: (16% (w/v) PEG 4000, 21% (v/v) propanol in 0.1 M sodium citrate tribasic dihydrate, pH 5.6) after refined screening (see Table 3.7) by the hanging drop technique; (B) needle-like crystals obtained after optimization of the condition A1 were observed after 2 days of incubation at 22°C using the steak seeding technique; (C) and (D) single crystals obtained after optimization of the condition A1 were observed after 2 days of incubation using the pipetting seeding technique.

The condition 43 from Crystal Screen HR2-112 containing (50% (v/v) (+/-)-2-methyl-2,4-pentanediol, 0.2 M ammonium phosphate monobasic in 0.1 M Tris-HCl, pH 8.5) (Table 3.4) was further optimized by varying concentrations of (+/-)-2-methyl-2,4-pentanediol (MPD) from 5% (v/v) to 75% (v/v) and Tris-HCl, pH 7.0 to 9.5 in the hanging drop technique. In addition, ammonium phosphate monobasic was also varied from 0.05 to 0.3 M at 30% (w/v) PEG 4000 (as shown in Table 3.8). Figure 3.14A shows plate crystals obtaining after 30 days under the condition C4 (50% (v/v) MPD in 0.1 M Tris-HCl, pH 8.0). Figure 3.14B shows single crystals obtained under the same condition after 7 days of incubation with protein concentrations of 1.25, 2.5, 5.0, and 10 mg/ml and 1/10 and 1/100 dilutions of the seed solution.

Table 3.8 A grid screening of MPD in 0.2 ammonium phosphate at various pH values and concentrations of ammonium phosphate at 75% (v/v) MPD for crystallization of wild-type chitinase A.

Buffer	% (v/v) MPD					Ammonium phosphate (M)
	5%	15%	30%	50%	75%	75%
Tris-HCl, pH 7.0	0.2 M	0.2 M	0.2 M	0.2 M	0.2 M	0.05 M
Tris-HCl, pH 7.5	0.2 M	0.2 M	0.2 M	0.2 M	0.2 M ^a	0.1 M
Tris-HCl, pH 8.0	0.2 M	0.2 M	0.2 M	0.2 M ^{a,b}	0.2 M ^a	0.2 M
Tris-HCl, pH 9.5	0.2 M	0.2 M	0.2 M	0.2 M ^a	0.2 M	0.3 M

^aThe condition that produced crystals.

^bThe condition used for further micro-seeding optimization.

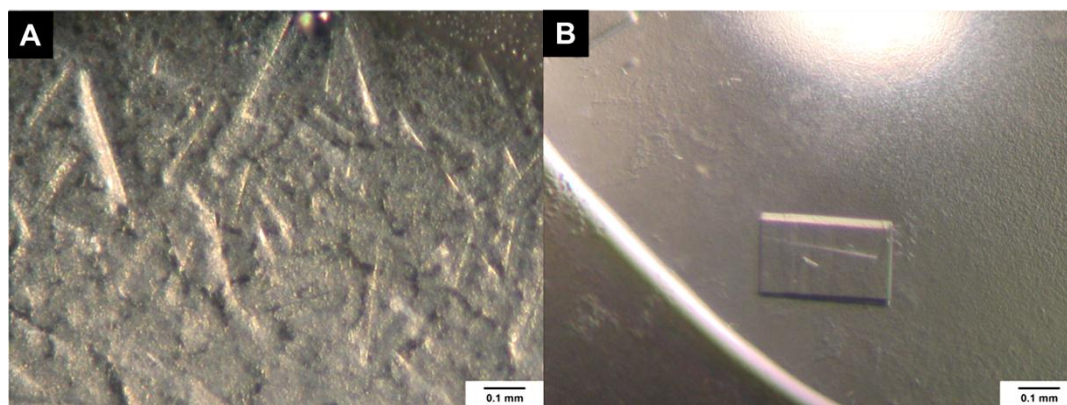


Figure 3.14 Optimization of the wild-type crystals grown under the condition 43 from Crystal Screen HR2-112.

(A) Plate crystals of wild-type obtained from the condition containing 50% (v/v) (+/-)-2-methyl-2,4-pentanediol, 0.2 M ammonium phosphate monobasic in 0.1 M Tris-HCl, pH 8.0 after optimization by the hanging drop technique; (B) single crystals appeared after 7 days of incubation at 22°C using the streak seeding technique.

3.9.1.2 Crystal soaking and co-crystallization with the identified inhibitors

The wild-type crystals obtained from the precipitant containing 1.1 M ammonium sulfate in 0.1 M Tris-HCl, pH 8.5, and the precipitant containing 16% (w/v) PEG 4000, 21% (v/v) propanol in 0.1 M sodium citrate tribasic dihydrate, pH 5.6, were soaked overnight at 22°C with 5-15 mM of IDA, SAN, CHE, IMI, and PEN. The crystals survived without cracking after soaking overnight in the presence of 10% (v/v) *tert*-butyl alcohol for the condition containing 1.1 M ammonium sulfate in 0.1 M Tris-HCl, pH 8.5, and in addition 2% concentration of PEG 4000 for the condition containing 16% (w/v) PEG 4000, 21% (v/v) propanol in 0.1 M sodium citrate tribasic dihydrate, pH 5.6. The soaked crystals obtained from these two

conditions were transferred to the cryo-solution containing the soaking solution with additional 10% (v/v) glycerol. Then, the soaked crystals were transferred to the cryo-solution for a few seconds and immediately frozen in liquid nitrogen and then stored in the cryo-condition for data collection. However, co-crystallization technique was used with DEQ and PRO, as the complexes with the two inhibitors were not successfully obtained by soaking. For DEQ, the solubility of this inhibitor was poor with the maximum solubility limited to 4 mM. For PRO, the inhibitor exhibited weak binding affinity against the wild-type enzyme with IC_{50} of 3.7 μ M (Table 3.3).

For co-crystallization, the wild-type protein was crystallized in both conditions containing 400 μ M of the inhibitors, DEQ and PRO. After microseeding, single crystals appeared after 2 days of incubation in 22°C (Figure 3.15).

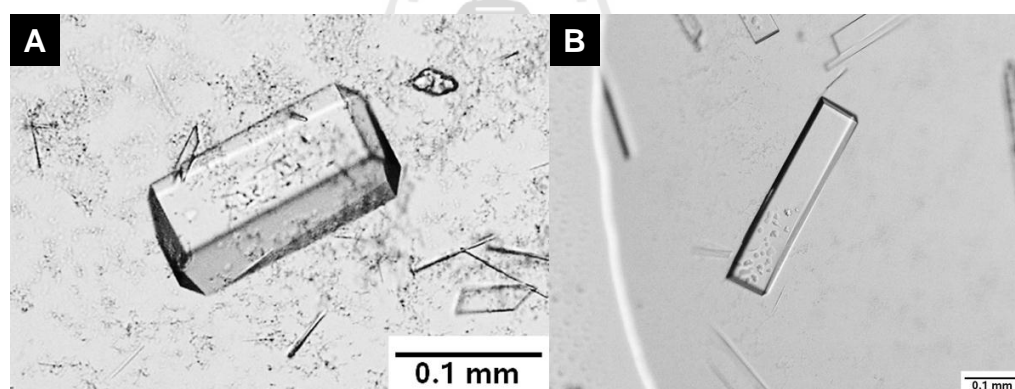


Figure 3.15 Single crystals obtained from co-crystallization with DEQ and PRO using the micro-seeding technique.

(A) Co-crystallization of wild-type chitinase A with DEQ under the condition 16% (w/v) PEG 4000, 21% (v/v) propanol in 0.1 M sodium citrate tribasic dihydrate, pH 5.6; (B) Co-crystallization of the chitinase with PRO under the condition 16% (w/v) PEG 4000, 21% (v/v) propanol in 0.1 M sodium citrate tribasic dihydrate, pH 5.6. The concentration of the inhibitors used was 400 μ M.

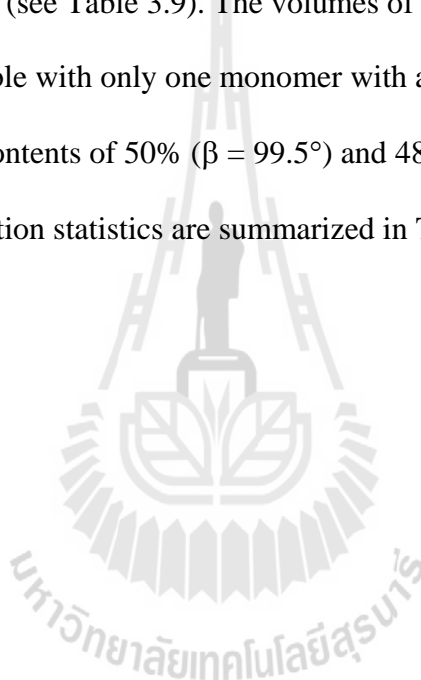
3.9.1.3 Data collection, processing and structure solution

Diffraction quality of the crystals was initially evaluated using an in-house X-ray generator located at the MPI-Dortmund, Germany. Following initial refinement, electron density of each inhibitor in the active site of the enzyme was evaluated. Once the density of the inhibitor was observed, the diffraction data were further collected at the Synchrotron Swiss Light Source located in Villigen, Switzerland. Some data sets were collected on a Bruker Microstar rotating anode generator equipped with Xenocs Fox mirrors and a MAR Research DTB image plate detector with 1° oscillations. Initial diffraction data of the wild-type crystals revealed weak diffraction at the resolution of more than 2.5 Å. The diffraction spots were smeared and ice rings were observed (Figure 3.16A).

To improve the quality of the diffraction data, the crystal was annealed by blocking with a cryo-stream for 5 to 20 seconds. After annealing, clear and strong intensity of the diffraction data was observed at the resolution of less than 2.5 Å without appearance of the ice ring (Figure 3.16B). The highest resolution of 1.16 Å was obtained from the crystal of wild-type complexed with PRO (Figure 3.16C). The structures complexes of DEQ, IDA, SAN, CHE, PEN, PRO and IMI were obtained from crystal soaking and co-crystallization (for DEQ and PRO) from condition containing 16% (w/v) PEG 4000, 21% (v/v) propanol in 0.1 M sodium citrate tribasic dihydrate, pH 5.6. The other two structural complexes: WT-PEN and the second structure complex of WT-IMI were obtained from crystal soaking under the condition containing 1.1 M ammonium sulfate in 0.1 M Tris-HCl, pH 8.5.

All the crystal complexes of the wild-type with DEQ, IDA, SAN, CHE, PRO, PEN, and IMI belonged to the primitive monoclinic space group P2₁.

The crystal complexes of the wild-type with PEN and IMI obtained from the condition: 1.1 M ammonium sulfate in 0.1 M Tris-HCl, pH 8.5, contained different unit cell dimensions ($a = 60.0 \text{ \AA}$, $b = 85.3 \text{ \AA}$, $c = 63.0 \text{ \AA}$, $\beta = 112.9 \text{ \AA}$) when compared to crystal complexes of wild-type and DEQ, SAN, CHE and PRO obtained from the condition: 16% (w/v) PEG 4000, 21% (v/v) propanol in 0.1 M sodium citrate tribasic dihydrate, pH 5.6, that gave the unit cell dimensions: $a = 65.1 \text{ \AA}$, $b = 50.9 \text{ \AA}$, $c = 93.2 \text{ \AA}$, $\beta = 99.5 \text{ \AA}$ (see Table 3.9). The volumes of the asymmetric unit of all the crystals were compatible with only one monomer with a molecular weight of 63 000 Da, with the solvent contents of 50% ($\beta = 99.5^\circ$) and 48% ($\beta = 112.9^\circ$) (Matthews, 1968). The data collection statistics are summarized in Table 3.9.



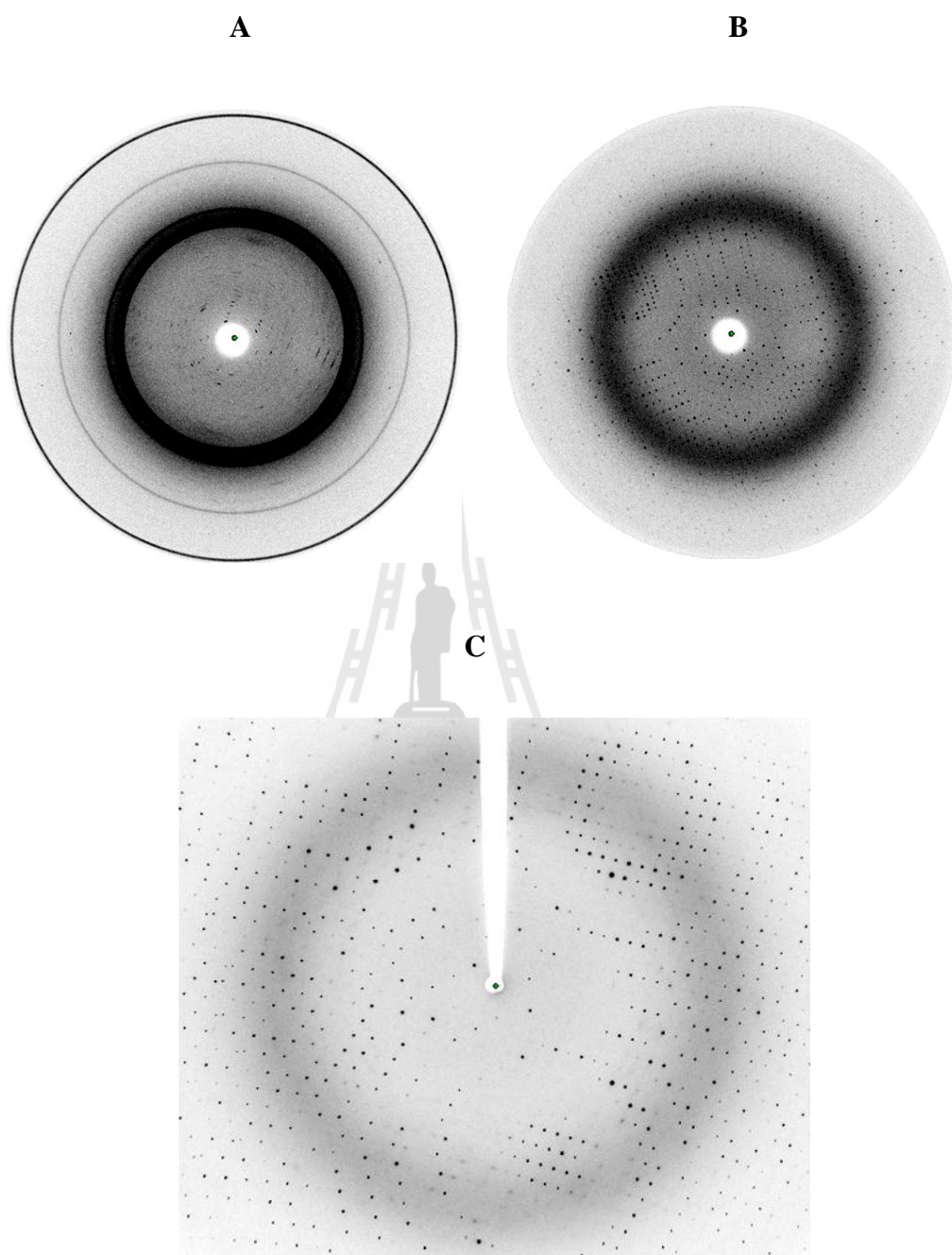


Figure 3.16 Diffraction images of the wild-type crystal.

(A) A diffraction image of the wild-type crystal before annealing; (B) A diffraction image of the wild-type crystal after annealing; (C) A diffraction image of wild-type complexed with PRO at 1.16 Å resolution.

Table 3.9 Data collection statistics for *VhChiA* wild-type in complex with seven inhibitors identified from the LOPAC library.

Crystal	WT-APO	WT-DEQ	WT-IDA	WT-SAN	WT-CHE	WT-PEN	WT-IMI	WT-PRO	
	<i>P</i> 2 ₁	<i>P</i> 2 ₁							
Space group	a = 65.1 b = 50.9 c = 93.2 β = 99.5	a = 65.1 b = 50.9 c = 93.2 β = 99.5	a = 65.1 b = 50.9 c = 93.2 β = 99.5	a = 65.1 b = 50.9 c = 93.2 β = 99.5	a = 65.1 b = 50.9 c = 93.2 β = 99.5	a = 65.1 b = 50.9 c = 93.2 β = 99.5	a = 60.0 b = 85.3 c = 63.0 β = 112.9	a = 60.0 b = 85.3 c = 63.0 β = 112.9	a = 65.1 b = 50.9 c = 93.2 β = 99.5
Resolution range (Å)	19.82-2.22 (2.28-2.22)	19.96-1.55 (1.59-1.55)	19.90-1.5 (1.54-1.5)	38.04-1.50 (1.54-1.50)	39.81-1.50 (1.54-1.50)	19.95-1.65 (1.69-1.65)	19.94-1.82 (1.87-1.82)	40.66-1.16 (1.19-1.16)	
No of observed reflections	68816	291154	698077	344568	268054	211087	158556	786080	
No of unique reflections	28030	82238	95004	95064	90870	66052	49568	199166	
Redundancy	2.46	3.54	7.3	3.62	2.95	3.20	3.20	3.78	
<i>I</i> /σ(<i>I</i>)	15.91(6.34)	19.14(3.50)	23.76(7.19)	16.79(8.33)	14.86(4.04)	12.80(4.21)	13.72(4.16)	12.88(3.76)	
Completeness (%)	94.7(85.8)	93.4 (77.0)	98.3 (95.1)	98.0 (91.8)	94.0 (74.8)	93.8 (88.0)	94.2 (89.5)	95.8 (79.1)	
R _{merge} (%)	5.7(15.3)	4.2(28.5)	7.1(47.5)	6.3(15.0)	5.1(27.0)	6.9(42.0)	6.0(40.8)	5.9(27.6)	
R _{cryst} , R _{free}	14.3,21.6	14.6,18.7	14.5,18.4	14.4,17.7	15.3,19.0	14.3,18.8	14.8,19.1	16.0,18.5	
Rmsd from ideal geometry	0.021	0.029	0.029	0.029	0.029	0.029	0.027	0.034	
Bonds (Å)	1.828	2.391	2.335	2.437	2.427	2.368	2.109	2.602	
Angles (°)									
B factor (Å ²)									
Bonded,	14.1	16.8	15.0	15.2	17.7	19.2	25.1	17.4	
mainchain	11.6	12.9	10.8	10.6	12.4	14.4	20.8	11.9	
 protein ^a	12.4	14.1	12.2	12.1	14.1	16.5	23.3	13.3	
 ligands ^a	-	17.8	22.0	46.6	29.7	35.8	79.9	26.4	
 water ^a	25.5	30.7	29.7	29.4	34.4	35.4	38.9	33.9	

^a Values in parentheses refer to the corresponding values of the highest resolution shell.

^b $R_{\text{merge}} = \frac{\sum_{hkl} \sum_i |I_i(hkl) - \langle I(hkl) \rangle|}{\sum_{hkl} \sum_i I_i(hkl)}$ where I_i is the intensity for the i th measurement of an equivalent reflection with indices hkl .

^c $R_{\text{factor}} = \frac{\sum ||F_{\text{obs}}| - |F_{\text{calc}}||}{\sum |F_{\text{obs}}|}$ where F_{obs} and F_{calc} are the observed and calculated structure-factors.

^d $R_{\text{free}} = \frac{\sum ||F_{\text{obs}}| - |F_{\text{calc}}||}{\sum |F_{\text{obs}}|}$ calculated from 5% of the reflections selected randomly and omitted from the refinement process.

3.9.2 Crystallization of *VhChiA* mutant W275G

3.9.2.1 Initial screening and optimization

Crystallization of mutant W275G was screened from Crystal Screen HR2-110 and Crystal Screen HR2-112 (Hampton Research) using the microbatch under oil technique. W275G was freshly prepared to a concentration of 20 mg/ml in 10 mM Tris-HCl, pH 8.0. Several positive conditions, which yielded microcrystals, were obtained as summarized in Table 3.10.



Table 3.10 A summary of positive conditions obtained from the microbatch technique for crystallization of W275G within 38 days of incubation.

Screening kit	Precipitant number	Precipitant composition	Temperature (°C)	Crystal morphology
Crystal Screen HR2-110 (Hampton Research)	9	30% (w/v) PEG 4000, 0.2 M ammonium acetate in 0.1 M sodium citrate tribasic dihydrate, pH 5.6.	18	Plates ^a
Crystal Screen HR2-110 (Hampton Research)	46	18% (w/v) PEG 8000, 0.2 M calcium acetate hydrate in 0.1 M sodium cacodylate trihydrate, pH 6.5	18	Plate clusters
Crystal Screen HR2-112 (Hampton Research)	2	0.01 M hexadecyltrimethyl ammonium bromide, 0.5 M sodium chloride and 0.01 M magnesium chloride hexahydrate	18	Needle clusters
Crystal Screen HR2-112 (Hampton Research)	16	2% (v/v) ethylene imine polymer, 0.5 M sodium chloride in 0.1 M sodium citrate tribasic dihydrate, pH 5.6.	18	Plate clusters
Crystal Screen HR2-112 (Hampton Research)	18	10% (v/v) jeffamine M-600®, 0.01 M iron (III) chloride hexahydrate in 0.1 M sodium citrate tribasic dihydrate, pH 5.6	18	Plate clusters
Crystal Screen HR2-112 (Hampton Research)	22	12% (w/v) PEG 20000 in 0.1 M MES monohydrate, pH 6.5	18	Plate clusters

^a The condition that was used for further optimization.

From Table 3.10, only the condition 9 from Crystal Screen HR2-110 (Hampton Research) gave plate crystals, and thus it was used for further screening by the hanging drop technique. Concentrations of the precipitants, the additives and pH of the buffer solutions were varied. Concentrations of PEG 4000 were varied from 15% to 30% (w/v) with pH varied from 5.0 to 6.0. In addition, concentrations of ammonium acetate were varied from 0.05 to 0.3 M at 30% (w/v) PEG 4000 (Table 3.11). Within 30 days of the incubation at 22°C, plate crystals were obtained in the condition containing 25% (w/v), 30% (w/v), and 35% (w/v) PEG 4000, 0.1 M ammonium acetate in 0.1 M sodium citrate tribasic dihydrate, pH 5.6 (Figure 3.17). These three conditions were further refined (Table 3.12), by varying PEG 4000 from 22% (w/v) to 34% (w/v) in 0.1 M sodium acetate tribasic dihydrate, pH 5.0, 5.6, 6.0, and 0.1 M MES, pH 6.5. From all the optimized conditions, larger plate crystals appeared within 2 weeks (Figure 3.18) in the conditions: 26% (w/v) PEG 4000 in 0.1 M sodium citrate tribasic dihydrate, pH 5.6, 28% (w/v) PEG 4000 in 0.1 M sodium acetate tribasic dihydrate, pH 5.0 and pH 6.0, 30% (w/v) PEG 4000 in 0.1 M sodium acetate tribasic dihydrate, pH 5.0 and pH 5.6, and 32% (w/v) PEG 4000 in 0.1 M sodium acetate tribasic dihydrate, pH 5.6 and pH 6.0. To obtain single crystals, the condition 26% (w/v) and 28% (w/v) of PEG 4000 in 0.1 M sodium acetate tribasic dihydrate, pH 5.6 and 6.0, were further screened either by pipetting and streak seeding. Single crystals were obtained from both techniques after 2 days of incubation at 22°C with protein concentrations of 2.5 and 5.0 mg/ml and 1/10 and 1/100 times seed dilutions (Figures 3.19 and 3.20).

Table 3.11 A grid screening of PEG 4000 in 0.1 M ammonium acetate with various pH values for crystallization of W275G.

Buffer	% (w/v) PEG 4000					Ammonium acetate (M)
Sodium citrate, pH 5.0	15%	20%	25%	30%	35%	30%
	0.1 M	0.1 M	0.1 M	0.1 M	0.1 M	0.05
Sodium citrate, pH 5.6	15%	20%	25%	30%	35%	30%
	0.1 M	0.1 M	0.1 M	0.1 M	0.1 M	0.1
Sodium citrate, pH 6.0	15%	20%	25%	30%	35%	30%
	0.1 M	0.1 M	0.1 M	0.1 M	0.1 M	0.2
Sodium acetate, pH 5.5	15%	20%	25% ^{a,b}	30% ^{a,b}	35% ^{a,b}	30%
	0.1 M	0.1 M	0.1 M	0.1 M	0.1 M	0.3

^aThe conditions that produced crystals.

^bThe conditions that was used for refined screening.

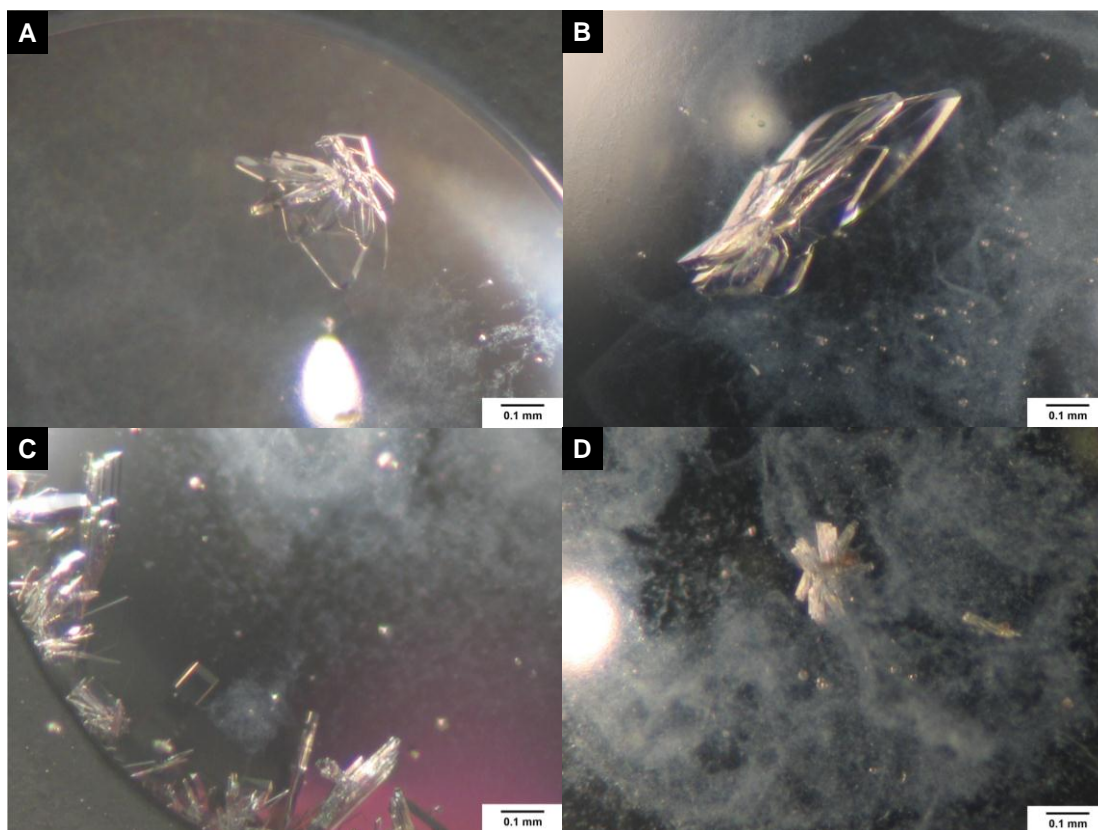


Figure 3.17 Optimization of W275G crystal grown under the condition 9 from Crystal Screen HR2-112. Plate clusters were observed from the precipitant containing 25% (w/v) PEG 4000, 0.1 M sodium acetate, pH 5.6, with a protein concentration of (A) 10 mg/ml; (B) 20 mg/ml; (C) Plate clusters appeared under the condition 30% (w/v) PEG 4000, 0.1 M sodium acetate, pH 5.6, and 20 mg/ml of the enzyme within 23 days of incubation at 22°C; and (D) Plates clusters appeared under the condition of 35% (w/v) PEG 4000, 0.1 M sodium acetate, pH 5.6, in 0.1 M ammonium acetate and protein concentration of 20 mg/ml at 30 days of incubation at 22°C.

Table 3.12 A refined screening of the condition containing PEG 4000 in 0.1 M ammonium acetate, pH 5.5, obtained from Table 3.10.

Buffer	% (w/v) PEG 4000					
Sodium acetate, pH 5.0	22%	24%	26%	28% ^a	30% ^a	34%
	0.1 M	0.1 M	0.1 M	0.1 M	0.1 M	0.1 M
Sodium acetate, pH 5.6	22%	24%	26% ^{a,b}	28%	30% ^a	34% ^a
	0.1 M	0.1 M	0.1 M	0.1 M	0.1 M	0.1 M
Sodium acetate, pH 6.0	22%	24%	26%	28% ^{a,b}	30%	34% ^a
	0.1 M	0.1 M	0.1 M	0.1 M	0.1 M	0.1 M
MES, pH 6.5	22%	24%	26%	28%	30%	34%
	0.1 M	0.1 M	0.1 M	0.1 M	0.1 M	0.1 M

^aThe conditions that produced crystals.

^bThe conditions that used for further optimization.

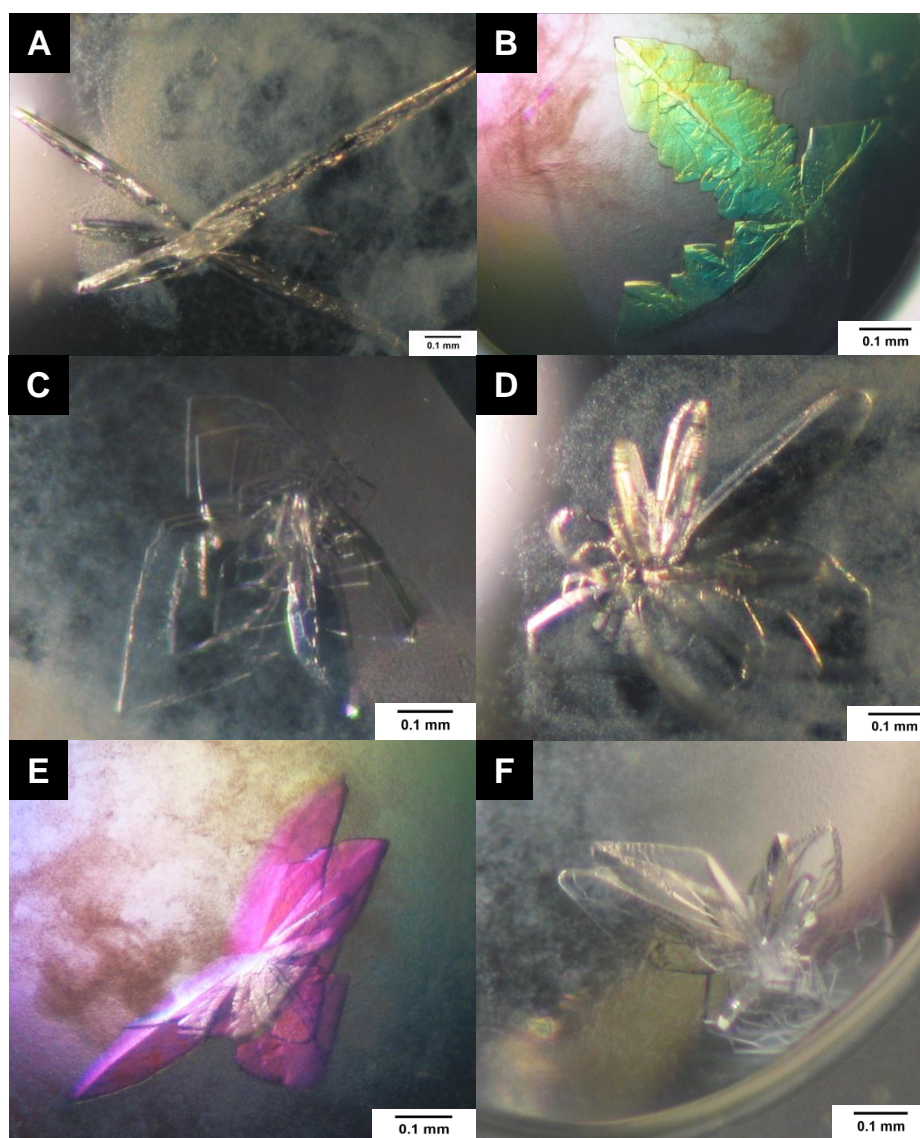


Figure 3.18 Plate clusters of W275G obtained from a grid screening of PEG 4000 in

0.1 M ammonium acetate with various pH values.

(A) Condition A4: 28% (w/v) PEG 4000, pH 5.0; (B) condition A5: 30% (w/v) PEG 4000, pH 5.0; (C) condition B3: 26% (w/v) PEG 4000, pH 5.6; (D) condition B5: 30% (w/v) PEG 4000, pH 5.6; (E) condition B6: 32% (w/v) PEG 4000, pH 5.6; and (F) condition C4: 28% (w/v) PEG 4000, pH 6.0. All crystals were appeared after 2 weeks of incubation at 22°C.

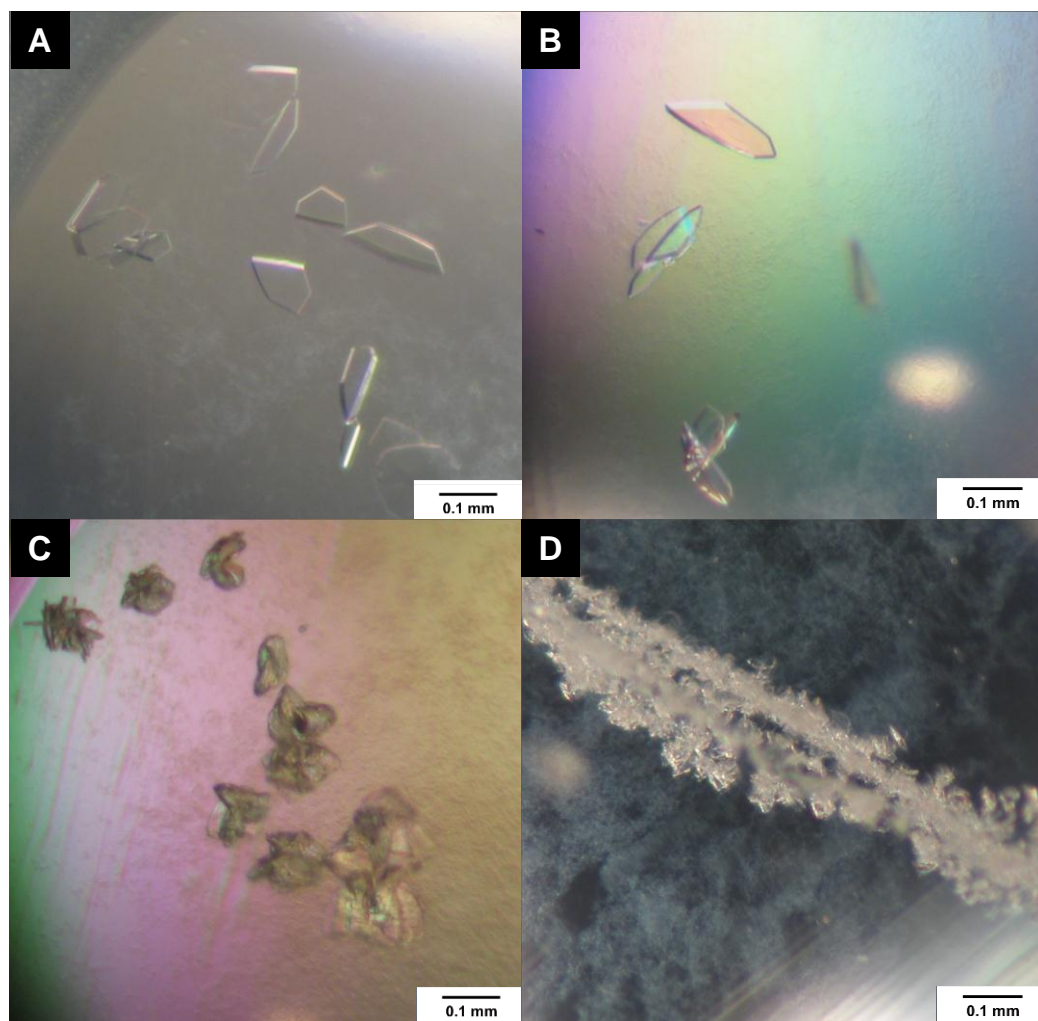


Figure 3.19 Crystals of W275G obtained from the streak-seeding technique. The condition used for crystal growth was 28% (w/v) PEG 4000 in 0.1 M sodium acetate tribasic dihydrate, pH 6.0. (A) A pre-equilibrated drop containing a protein concentration of 2.5 mg/ml was streaked using a 1/100 dilution of the seed solution; (B) protein concentration of 5.0 mg/ml and a 1/10 dilution of the seed solution; (C) protein concentration of 7.5 mg/ml and a 1/10 dilution of the seed solution; and (D) protein concentration of 7.5 mg/ml and the seed stock. Single crystals were obtained within 2 days of the incubation at 22°C.

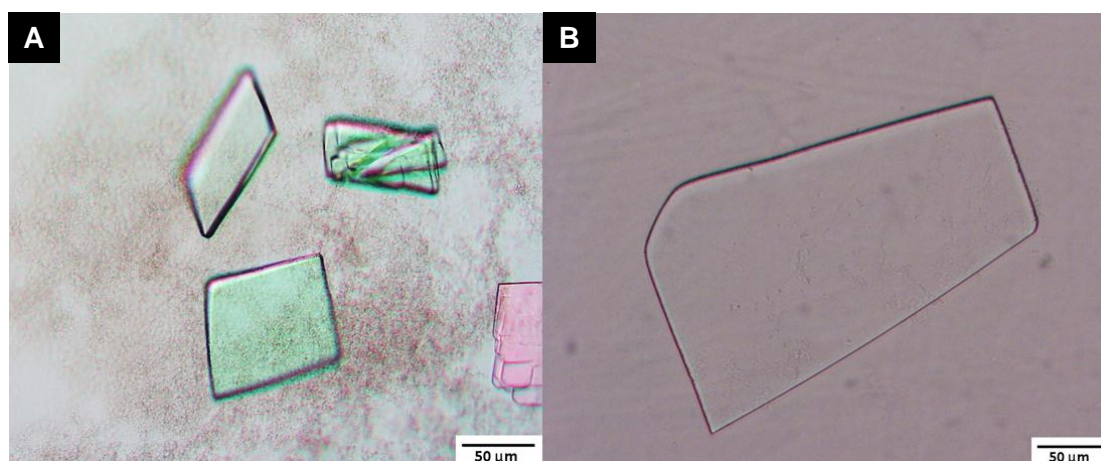


Figure 3.20 Single crystals of W275G obtained from the pipetting seeding technique. The condition for crystal growth was 26% (w/v) PEG 4000 in 0.2 M sodium acetate tribasic dihydrate, pH 5.6. The crystals appeared after 2 days of incubation at 22°C.

3.9.2.2 Crystal soaking and co-crystallization with the identified inhibitors

Single crystals of W275G obtained from the condition 26% (w/v) PEG 4000, 0.2 M ammonium acetate in 0.1 M sodium acetate, pH 5.6, were soaked overnight in the soaking solution containing 5-15 mM inhibitor and 2% (w/v) PEG 4000 from 26% (w/v) to 28% (w/v) at 22°C. The crystals survived in the soaking solution overnight without cracking or shrinking. The crystals soaked with the inhibitors were then immersed in a cryo-protectant containing 10% (v/v) glycerol in the identical buffer used for crystal growth. For with DEQ and IDA, co-crystallization was performed, since the electron densities of DEQ and IDA were not seen by the soaking experiment.

3.9.2.3 Data collection, processing and structure solution

X-ray diffraction data were collected at the in house X-ray source, located at the MPI-Dortmund, Germany. Similar to the wild-type diffraction data, the first shot of the W275G crystal showed an extremely poor diffraction pattern. After the annealing step, the diffraction quality was greatly improved. The crystals, for which the inhibitor density could be identified within the active site of W275G, were sent for data collection on the beamline PX-II of the Swiss Light Source located in Villigen, Switzerland. The crystals of W275G diffracted at the resolutions between 2.4 to 1.8 Å. All the data were processed by *XDS* (Kabsch, 1993). The best data set was obtained from the crystal complex of W275G with PEN. After the data processing, all the crystal-inhibitor complexes belonged to the orthorhombic space group $P2_12_12_1$ with the volumes of the asymmetric unit compatible with only one subunit. All the crystals have the same unit cell dimensions of $a = 66.6$, $b = 83.9$, and $c = 102.4$. The crystal volumes per protein weight (V_m) were estimated as $2.29 \text{ \AA}^3 \text{ Da}^{-1}$ with a solvent content of 46.3% (Matthews, 1968). Phase determination was carried out using the molecular replacement method and the *VhChiA* mutant E315M-GlcNAc₆ complex (PDB code: 3B9A) was used as the structural model. The refinement began with the rigid body refinement and then restrained refinement was used to modify the atomic model together with the model building performed in COOT program. (Emsley and Cowtan, 2004). The refinement statistics are shown in Table 3.13.

Table 3.13 Data collection statistics for the *VhChiA* mutant W275G in complex with six inhibitors identified from the LOPAC library.

Crystal	W275G-APO	W275G-DEQ	W275G-SAN	W275G-CHE	W275G-PRO	W275G-IMI	W275G-PEN
Space group	<i>P</i> 2 ₁ :2 ₁ :2 ₁						
Resolution range (Å)	19.78-2.45 (2.51-2.45)	19.9-2.23 (2.29-2.23)	33.43-2.0 (2.05-2.0)	19.96-2.0 (2.05-2.0)	36.49-1.80 (1.85-1.80)	46.58-2.4 (2.5-2.4)	40.62-1.90 (1.95-1.90)
No of observed reflections	67399	119424	311975	268938	210243	90927	343052
No of unique reflections	19696	27041	38365	39084	51578	22493	45190
Redundancy	3.42	4.16	8.13	6.88	4.08	4.04	7.59
<i>I</i> / σ (<i>I</i>)	14.47(4.08)	18.45(6.09)	19.21(6.45)	13.27(5.43)	16.78(4.38)	13.54(6.54)	18.32(8.14)
Completeness (%)	91.0 (67.5)	94.1 (67.4)	97.4 (94.1)	96.9 (93.5)	96.1 (89.5)	97.1 (93.7)	98.3 (95.8)
<i>R</i> _{merge} (%)	8.2(30.3)	7.8(29.6)	8.3(38.2)	13.2(48.5)	6.1(35.1)	11.2(44.7)	11.9(34.9)
<i>R</i> _{cryst} , <i>R</i> _{free}	19.8,25.9	16.2,22.9	14.5,19.7	15.3,20.5	15.0,19.6	15.4,23.0	14.4,19.6
Rmsd from ideal geometry	0.006	0.021	0.024	0.025	0.025	0.019	0.024
Bonds (Å)	0.865	1.765	1.903	1.862	2.019	1.748	1.981
Angles (°)							
B factor (Å ²)	19.6	16.7	21.6	19.7	18.8	22.9	15.3
Bonded, mainchain	19.6	14.5	18.9	16.5	15.1	20.9	11.6
 protein ^a	19.6	14.9	20.2	17.8	16.6	22.2	13.0
 ligands ^a	-	61.6	51.6	76.3	52.4	75.8	39.6
 water ^a	20.7	23.6	32.2	30.7	30.2	26.4	28.2

^a Values in parentheses refer to the corresponding values of the highest resolution shell.

^b $R_{\text{merge}} = \frac{\sum_{hkl} \sum_i |I_i(hkl) - \langle I(hkl) \rangle|}{\sum_{hkl} \sum_i I_i(hkl)}$ where *I_i* is the intensity for the *i*th measurement of an equivalent reflection with indices *hkl*.

^c $R_{\text{factor}} = \frac{\sum \| |F_{\text{obs}}| - |F_{\text{calc}}| \|}{\sum |F_{\text{obs}}|}$ where *F_{obs}* and *F_{calc}* are the observed and calculated structure-factors.

^d $R_{\text{free}} = \frac{\sum \| |F_{\text{obs}}| - |F_{\text{calc}}| \|}{\sum |F_{\text{obs}}|}$ calculated from 5% of the reflections selected randomly and omitted from the refinement process.

3.9.3 Crystallization of chitinase A mutant W397F

3.9.3.1 Initial screening and optimization

Like W275G, crystallization trials of W397F mutant were carried out using Crystal Screen HR2-110 and Crystal Screen HR2-112 (Hampton Research) by the microbatch technique. A protein concentration of 20 mg/ml was freshly prepared in 10 mM Tris-HCl, pH 8.0. Positive conditions, which produced small crystals, were obtained in many conditions as summarized in Table 3.14. From all the conditions tested, only the condition 16 from Crystal Screen HR2-112 and the condition 40 from HR2-110 produced clusters crystals as indicated in Tables 3.15 and 3.16, respectively.

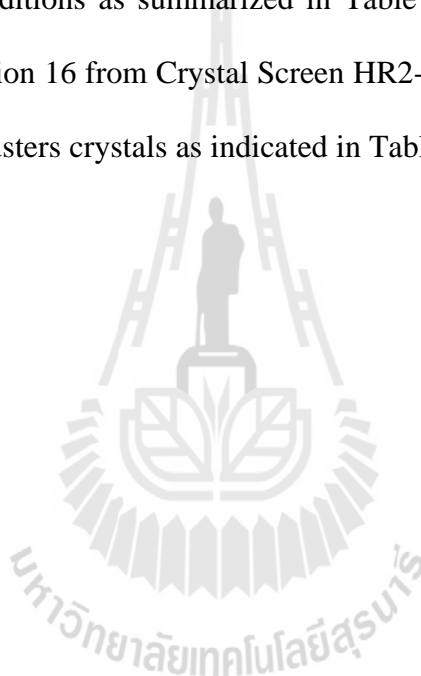


Table 3.14 A summary of positive conditions obtained from the commercial screening kits using the microbatch technique for crystallization of W397F within 30 days incubation at 22°C.

Commercial screening kit	Precipitant number	Precipitant composition	Temperature (°C)	Crystal morphology
Crystal Screen HR2 110 (Hampton Research)	3	0.4 M ammonium phosphate monobasic	18	Needle
Crystal Screen HR2 110 (Hampton Research)	23	30% (v/v) PEG 400, 0.2 M magnesium chloride hexahydrate in 0.1 M HEPES sodium, pH 7.5	18	Needle
Crystal Screen HR2 110 (Hampton Research)	40	20% (v/v) 2-propanol , 20% (w/v) PEG 4000 in 0.1 M sodium citrate tribasic dihydrate, pH 5.6	18	Needle
Crystal Screen HR2 110 (Hampton Research)	43	30% (w/v) PEG 1500	18	Needle
Crystal Screen HR2 112 (Hampton Research)	2	0.01 M hexadecyltrimethylammonium bromide, 0.5 M sodium chloride and 0.01 M magnesium chloride hexahydrate	18	Needle
Crystal Screen HR2 112 (Hampton Research)	16	2% (v/v) ethylene imine polymer, 0.5 M sodium chloride in 0.1 M sodium citrate tribasic dihydrate, pH 5.6	18	Needle

Table 3.15 A grid screening of ethylene imine polymer (EIP) in 0.5 M sodium chloride and 0.1 M sodium citrate tribasic dihydrate, pH 5.6.

Buffer	% (v/v) EIP					
	0.5 %	1.0 %	1.5 %	2.0 %	2.5 %	4.0 %
Sodium acetate, pH 5.0	0.1 M	0.1 M	0.1 M	0.1 M	0.1 M	0.1 M ^{a,b}
Sodium acetate, pH 5.6	0.1 M	0.1 M	0.1 M	0.1 M	0.1 M ^a	0.1 M ^a
MES, pH 6.0	0.1 M	0.1 M	0.1 M	0.1 M	0.1 M ^a	0.1 M ^a
MES, pH 5.5	0.1 M	0.1 M	0.1 M	0.1 M	0.1 M	0.1 M ^a

^aThe conditions that produced crystals.

^bThe conditions used for further optimization.

Needle clusters obtained from the condition 4% (v/v) ethylene imine polymer, 0.5 M sodium chloride in 0.1 M sodium acetate tribasic dehydrate, pH 5.0 appeared after 30 days of incubation (Figure 3.21A). Therefore, this condition was used for further screening by the hanging drop vapor diffusion technique.

The condition 40 from Crystal Screen HR2 110: 20% (v/v) 2-propanol, 20% (w/v) PEG 4000 in 0.1 M sodium citrate tribasic dihydrate, pH 5.6, was further optimized. As seen in Table 3.15, only 20% (v/v) 2-propanol, 20% (w/v) PEG 4,000 in 0.1 M sodium citrate tribasic dihydrate, pH 5.6, generated plate crystals (Figure 3.21B). However, after several rounds of optimization, single crystals of W397F were not obtained. Therefore, no further attempt had been made to try to obtain single crystals of this mutant.

Table 3.16 A grid screening of PEG 4000, 0.5 M sodium chloride in 0.1 M sodium citrate tribasic dihydrate, pH 5.6.

	% (v/v) Propanol		% (w/v) PEG 4000		
	5 %	10 %	15 %	20 %	
5 %	0.1 M	0.1 M	0.1 M	0.1 M	
10 %	0.1 M	0.1 M	0.1 M	0.1 M	
15 %	0.1 M	0.1 M	0.1 M	0.1 M	
20 %	0.1 M	0.1 M	0.1 M	0.1 M ^a	

^aThe conditions that produced crystals.

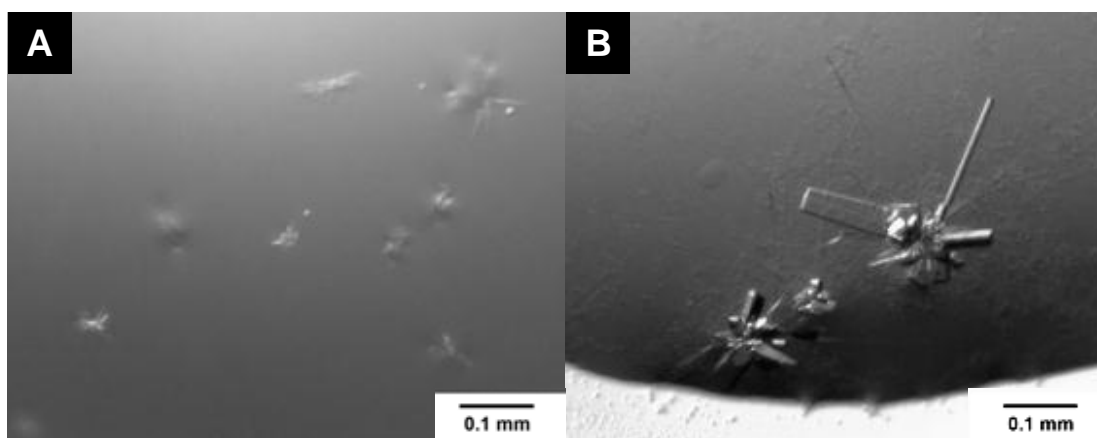


Figure 3.21 Optimization of W397F crystal growth from the condition 16 of Crystal Screen HR2-112 and the condition 40 of Crystal Screen HR2-110.

(A) Needle clusters of W397F obtained by the hanging drop after 30 days of incubation from the condition 4% (v/v) ethylene imine polymer, 0.5 M sodium chloride in 0.1 M sodium acetate tribasic dihydrate, pH 5.0. (B) Plate clusters of W397F obtained by the hanging drop after 30 days of incubation from the condition 20% (v/v) 2-propanol, 20% (w/v) PEG 4000 in 0.1 M sodium citrate tribasic dehydrate, pH 5.6.

3.10 Structural comparison of the apo form of the wild-type *VhChiA* and mutant W275G

After final refinement, the overall structure of the wild-type and mutant W275G in the absence of ligand were evaluated and found to be almost identical. As already described by Songsiriritthigul *et al.*, 2008, *VhChiA* comprises three distinct domains (Figure 3.22A). The *N*-terminal chitin binding domain (ChBD, blue) contains mostly β -strands and covers residues 22-139. The catalytic domain (green) has a $(\alpha/\beta)_8$ -TIM barrel fold consisting of eight β -strands (B1-B8) tethered to eight α -

helices (A1-A8) by loops and is made up of two parts, referred to as CatD I (residues 160-460) and CatD II (residues 548-588). The catalytic residue (Glu315) is positioned in the loop of strand B4, which is part of a DxxDxDxE conserved motif. Two important binding residues Trp275 and Trp397 are located in the loop of strands B3 and B6, respectively (Figure 3.22B). The ChBD domain is connected to the CatD domain by a hinge which comprises 21 amino acid residues (residues 140 to 159). The third domain has an α/β fold which inserts between CatI and CatII and is made up of six anti-parallel β -strands flanked by short α helices (residues 461-547). Although the overall structures of wild-type and the W275G were almost identical with the least R.M.S. value of 0.262 Å, minor conformational changes in the Val205-loop of the CatD domain are observed. In the wild-type, the loop containing Val205 forms one “wall” of the glycone binding sites, whereas Trp168 is the counterpart on the other side. In the mutant, the cleft formed between those two residues is more open compared to the wild-type. Another visible variation in the wild-type and the W275G structures is the tilt between the ChBD of WT and of W275G. This tilt had been observed previously (Songsiriritthigul *et al.*, 2008) and it was an indication of the flexible movement of the chitin binding domain compared to the catalytic domain (Figure 3.22A).

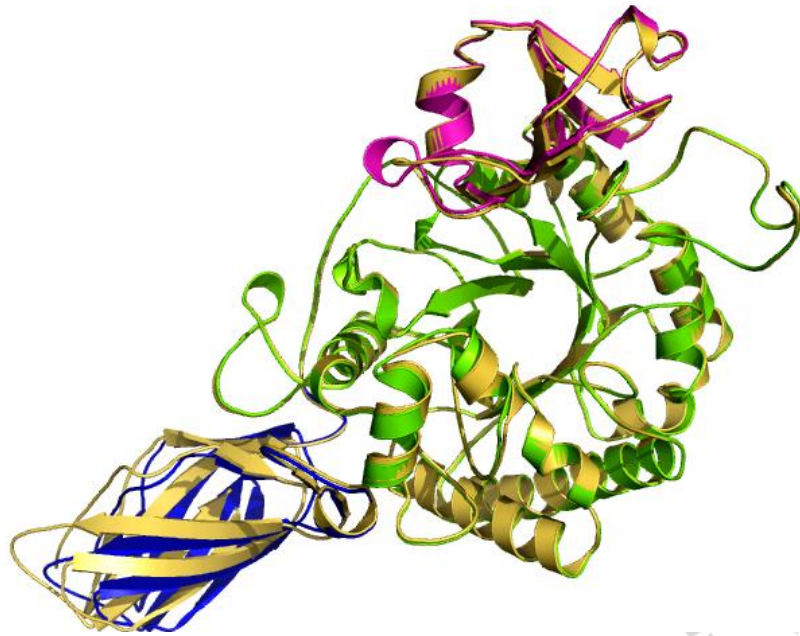
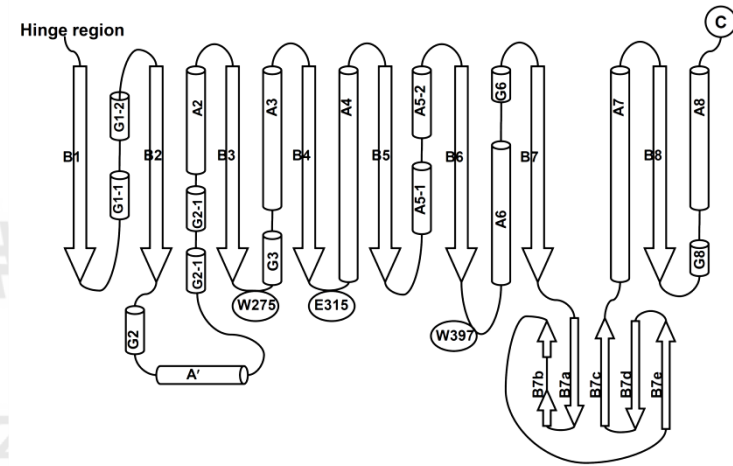
A**B**

Figure 3.22 A comparison of the overall structure of wild-type *VhChiA* and mutant W275G.

(A) A ribbon representation of wild-type *VhChiA* superimposed with W275G. The ChBD of wild-type is colored in blue, the CatD domain is colored in green and the small insertion domain is in pink. The structure of W275G is colored in yellow; (B) a topology diagram of the CatD domain of *VhChiA*, indicating three important residues Trp275, Glu315, and Trp397 located at loop B3, B4, and B6, respectively.

In the final models of the WT-inhibitor complexes obtained from the condition: 1.1 M ammonium sulfate in 0.1 M Tris-HCl, pH 8.5, and all of the W275G-inhibitor complexes, the C-terminal residues starting from Gly588 and the C-terminal hexahistidine tag were not observed. In contrast, the wild-type crystals grown under 16% (w/v) PEG 4000, 21% (v/v) propanol in 0.1 M sodium citrate tribasic dihydrate, pH 5.6, showed clear electron density up to residues 595 or 596. Noticeably, the apo form of native *VhChiA* crystals grown from the condition: 16% (w/v) PEG 4000, 21% (v/v) propanol in 0.1 M sodium citrate tribasic dihydrate, pH 5.6, showed the electron density up to 601, including three histidine residues of the hexahistidine tag (599-601) (Table 3.17).

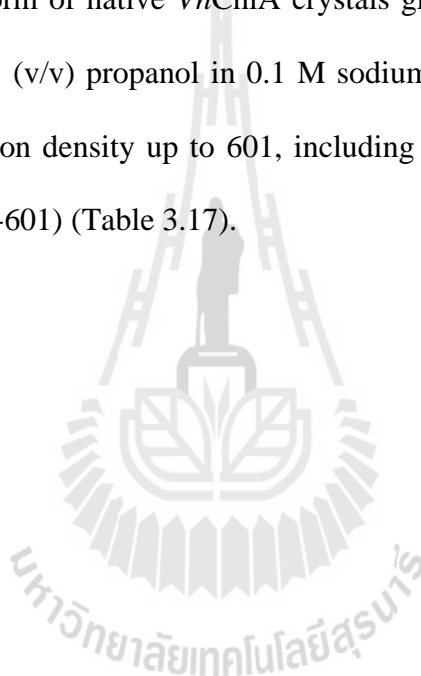


Table 3.17 Numbers of amino acid residues observed in the *VhChiA*-inhibitor complexes.

Enzyme	Condition for crystal Growth	Number of residues	Inhibitors
Wild-type	PEG 4000 ^a	579 (22-601)	Native
"	PEG 4000 ^a	574 (22-596)	DEQ
"	PEG 4000 ^a	574 (22-596)	IDA
"	PEG 4000 ^a	574 (22-596)	SAN
"	PEG 4000 ^a	574 (22-596)	CHE
"	PEG 4000 ^a	573 (22-595)	CHE
"	Ammonium sulfate ^b	566 (22-588)	PEN
"	PEG 4000 ^a	574 (22-596)	IMI
"	Ammonium sulfate ^b	566 (22-588)	IMI
"	PEG 4000 ^a	573 (22-595)	PRO
W275G	PEG 4000 ^c	566 (22-588)	Native
"	PEG 4000 ^c	566 (22-588)	DEQ
"	PEG 4000 ^c	566 (22-588)	SAN
"	PEG 4000 ^c	566 (22-588)	CHE
"	PEG 4000 ^c	566 (22-588)	PEN
"	PEG 4000 ^c	566 (22-588)	IMI
"	PEG 4000 ^c	566 (22-588)	PRO

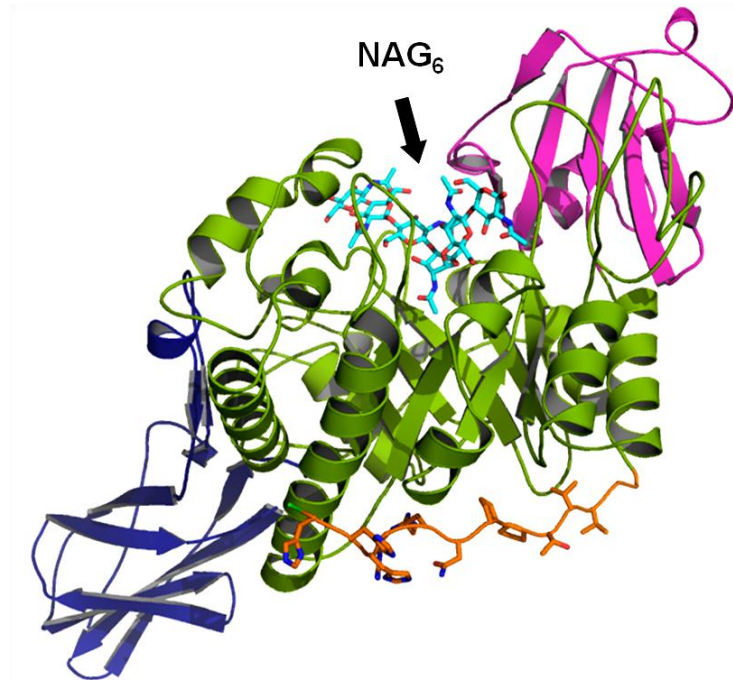
^a The crystallization condition was 16% (w/v) PEG 4000, 21% (v/v) propanol in 0.1 M sodium citrate tribasic dihydrate, pH 5.6.

^b The crystallization condition was 1.1 M ammonium sulfate in 0.1 M Tris-HCl, pH 8.5.

^c The crystallization condition was 26% (w/v) PEG 4000, 0.2 M ammonium acetate in 0.1 M sodium citrate tribasic dihydrate, pH 5.6.

The final structure of the apo form of the native *VhChiA*, showing the C-terminal end attached with the three histidine residues of the His₆ tag (starting from Gly588), which made up a elongating loop at the opposite side of the catalytic domain and extended towards the N-terminal ChBD domain (Figure 3.23A). This observation is in contrast with the *VhChiA* structure determined previously by Songsiriritthigul *et al.* (2008) that reported the hexaHis residues were embedded in the active site of the wild-type enzyme and interacted with many important residues for binding to GlcNAc₅ and GlcNAc₆.

A



B

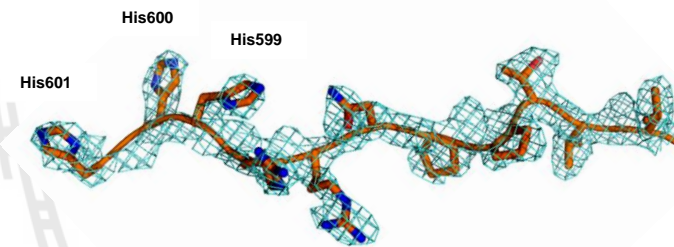


Figure 3.23 Docking of GlcNAc₆ (E315M+NAG₆, PDB code: 3B9A) to the apo form of the *VhChiA* structure.

(A) A cartoon representation of GlcNAc₆ docked into the active site of the wild-type enzyme. GlcNAc₆ and the residues 589-602 in the apo form of *VhChiA* are indicated as the stick model with carbon atoms labeled as cyan and orange, respectively; (B) The electron density map of the C-terminal end of the wild-type structure including residues 589-601 connected with three histidine residues from the His₆ tag. A $2F_o - F_c$ map was calculated from the refined model and contoured at 1.0σ .

3.11 The structures of complexes of the wild-type *VhChiA* and the newly-identified chitinase inhibitors

Thorough crystallographic analysis demonstrated that the inhibitors bound to the wild-type chitinase mainly at two locations, one is between Trp275 and Trp397 at the aglycone binding sites (subsites +1/+2), and the other one is near Trp168 and Val205 at the glycone binding sites (subsites -3/-4). Figure 3.24 shows that two molecules of SAN, IMI, PEN, and PRO were bound to the active site of the wild-type enzyme. One was located at subsites +1 and +2 with well-defined electron density, while the electron density of the second molecule at subsites (-4) and (-3) are always much less well-defined, with relatively higher temperature factors. The crystallographic data gave an implication of weak affinity of binding at the glycone binding sites. The backbone of two molecules of SAN, IMI, PEN, and PRO were oriented in the active site of wild-type with torsional angles of 51 to 74 degree from each other. For IDA and CHE, no interpretable density was found at the glycone sites, thus only one molecule of IDA and CHE was found at the aglycone sites. For PRO and PEN, either superimposition of multiple binding stances or less well-defined aliphatic substituents were observed. In contrast to the other inhibitors, only one molecule of DEQ was found in the active site of the wild type enzyme, and it occupied subsites -3 to +2 with the two head groups acting like two separated molecules bound at two different locations.

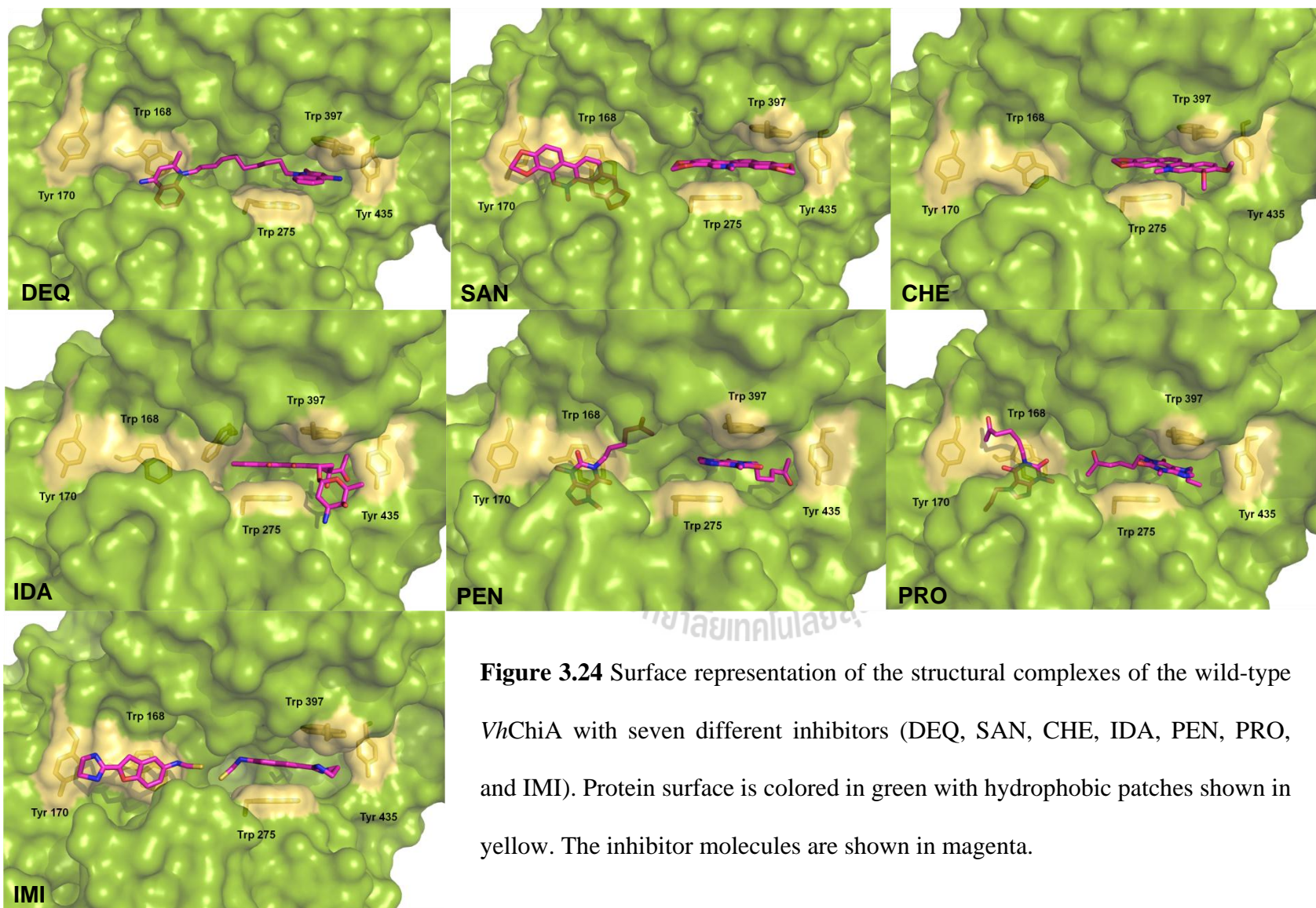


Figure 3.24 Surface representation of the structural complexes of the wild-type *VhChiA* with seven different inhibitors (DEQ, SAN, CHE, IDA, PEN, PRO, and IMI). Protein surface is colored in green with hydrophobic patches shown in yellow. The inhibitor molecules are shown in magenta.

3.11.1 The structure of the complex of wild-type *VhChiA* with dequalinium (DEQ)

As mentioned above, only one molecule of DEQ was found in the active site of the wild-type enzyme (Figure 3.24). The electron density map of the refined structure of WT-DEQ complex clearly showed that DEQ occupied subsites -3 to +2 (Figure 3.25A). DEQ contains two symmetrical 4-amino-2-methylquinolinium head groups connected with each other by a long flexible C_{10} -linker. The structural complex of WT-DEQ revealed that the two head groups are oriented with torsional angle of 62 degree. DEQ interacts with the active site residues by three hydrophobic interactions, which are maintained mainly by tryptophan residues and a few other hydrophobic residues as shown in Ligplot (Figure 3.25B). One head group of DEQ at the subsites +1/+2 is sandwiched between Trp275 and Trp397, as well as Asp392, while the other head group interacts at subsites -2/-3 with Trp168 and other surrounding residues, including Trp570, Thr276, and Leu277 at subsite -2 and Val 205 and His228 at subsite -3.

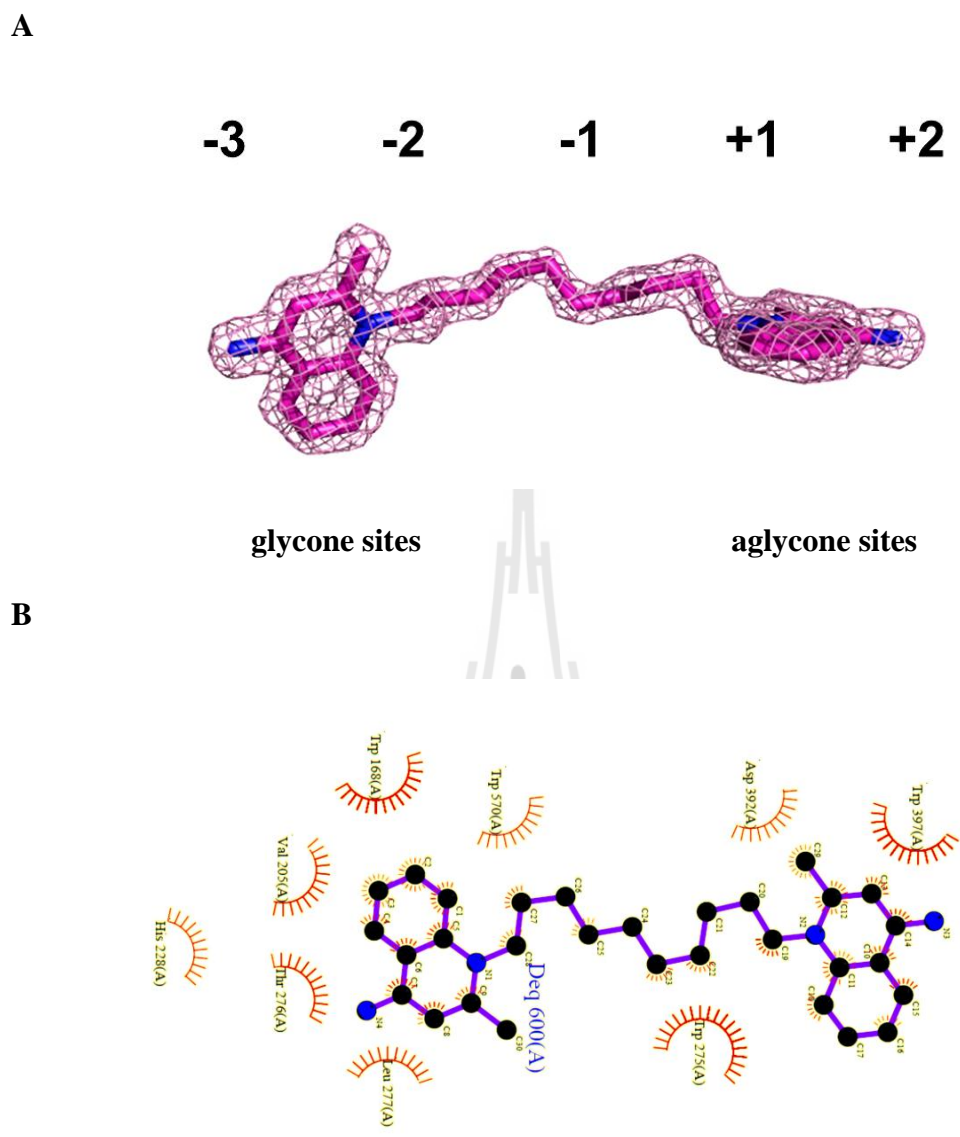


Figure 3.25 The structure of the complex of wild-type *VhChiA* with DEQ.

(A) The electron density map of DEQ in the structure of WT-DEQ complex.

The $2F_o - F_c$ map was calculated from the refined model and contoured at 1.0σ .

The inhibitor molecule was shown in sticks with carbon atoms labeled in magenta.

(B) Protein-ligand interactions was calculated by LIGPLOT.

3.11.2 The structure of the complex of WT *VhChiA* with sanguinarine (SAN)

The structural complex of WT-SAN showed two molecules of SAN in the active site of the enzyme (Figure 3.26A). SAN1 located at subsites -1 to +2 had a well-defined electron density, whereas SAN2 located at subsites -4 to -2 had less defined density. For SAN1, the benzodioxole ring orients to the direction of the glycone sites, while the dioxolane part orients towards the aglycone sites. For SAN2, its benzodioxole ring also points towards the direction of glycone sites, but its dioxolane ring points downward into the binding pocket without interacting with the three residues essential for catalysis (Asp311, Asp313, and Glu315) as found for allosamidin and its derivatives (Roa *et al.*, 2003; Roa *et al.*, 2005; Vaaje-Kolstad *et al.*, 2004; Houston *et al.*, 2002). SAN1 and SAN2 are aligned with each other with a 74 degree torsional angle. SAN1 was sandwiched between with Trp275 and Trp397 via π - π interaction, while SAN2 formed hydrophobic interactions with Trp168 and other surrounding residues including Tyr171, Phe192, Val205, and Leu277 at subsites -2/-3. Thus, the main interactions of the two molecules of SAN are hydrophobic interactions as shown in Figure 3.26B. Only one hydrogen bond was observed. This bond links between O ^{γ 1} of the side chain of Tyr276 and the O²⁴ of the benzodioxole group of SAN2 at the glycone sites.

3.11.3 The structure of the complex of wild-type *VhChiA* with chelerythrine (CHE)

Only one molecule of CHE showed a well-defined electron density at the aglycone sites, while the electron density of the second CHE molecule at the glycone sites was too weak to be modeled with confidence. The structure of CHE is similar to SAN (see Figure 3.11 for the chemical structure) with the dioxolane ring of CHE being open at the position C¹⁹. The refined structure of the WT-CHE complex showed that the orientation of CHE was similar to SAN1. However, there are different relative orientations between WT-SAN1 and WT-CHE, by which the benzodioxole part of CHE points towards the glycone sites, whereas this part of SAN1 points towards the aglycone sites. Moreover, a structure of WT-CHE was also solved, and it showed that the orientation of CHE was different from the first complex as the benzodioxole part of CHE in the second complex points toward the aglycone sites as shown in Figures 3.28A. Hydrophobic interactions which are similar the WT-CHE are also major interactions, which is similar to WT-SAN. However, the number of residues that interact with CHE are smaller than SAN (Figure 3.27B).

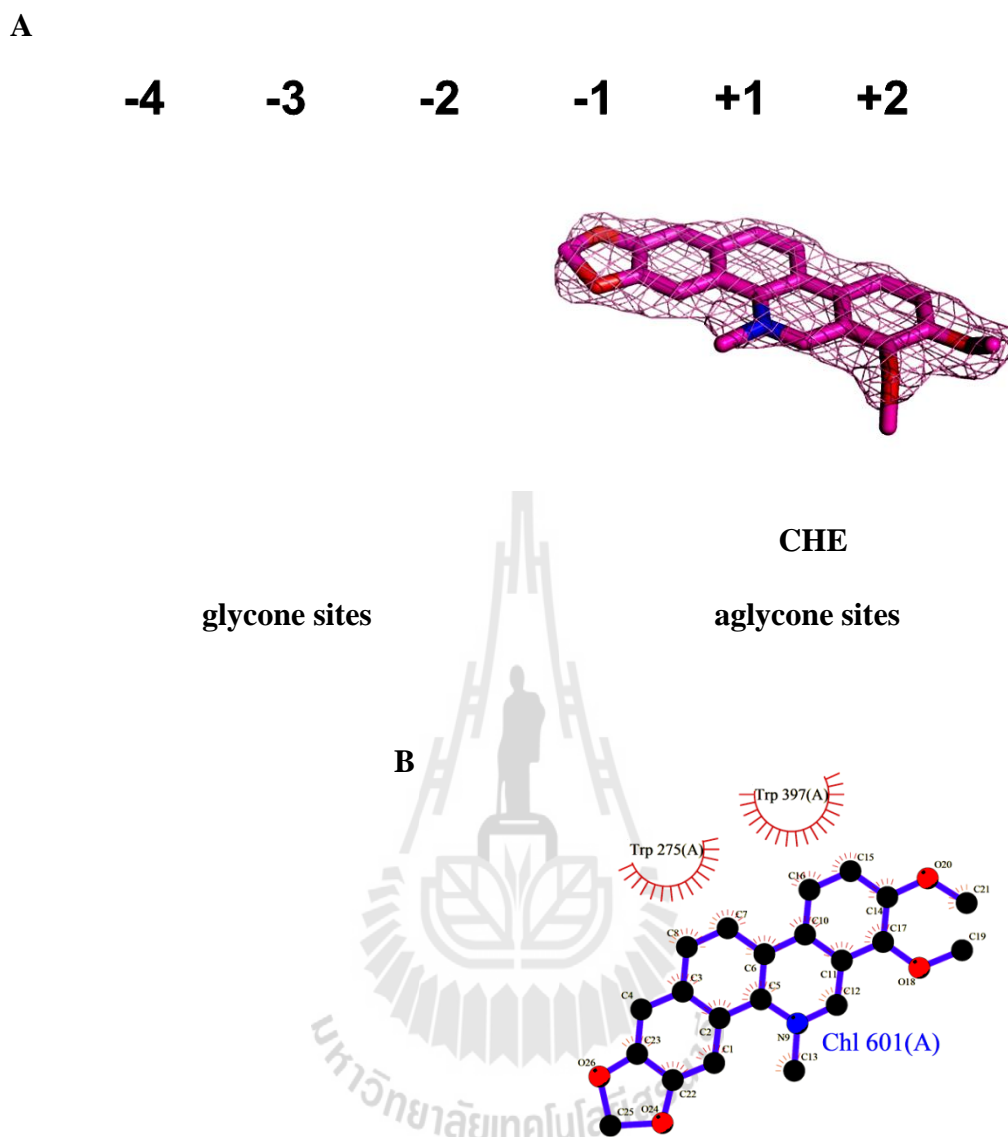


Figure 3.27 The first structure of the complex of wild-type *VhChiA* with CHE.

(A) The electron density map of CHE in the structure of WT-CHE complex.

The $2F_o - F_c$ map was calculated from the refined model and contoured at 1.0σ .

The inhibitor molecule is shown in sticks with carbon atoms labeled in magenta.

(B) Protein–ligand interactions was calculated by LIGPLOT.

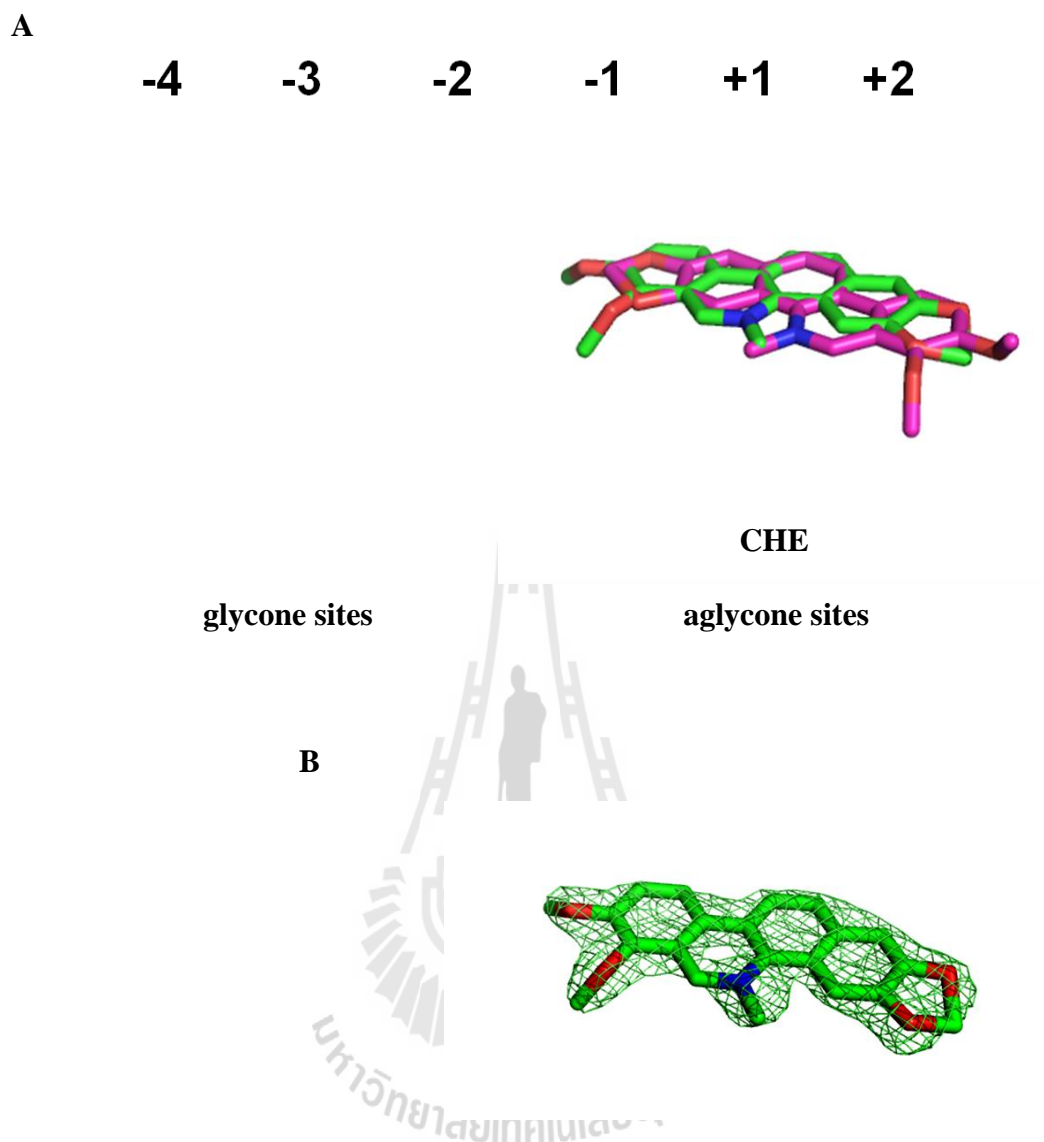
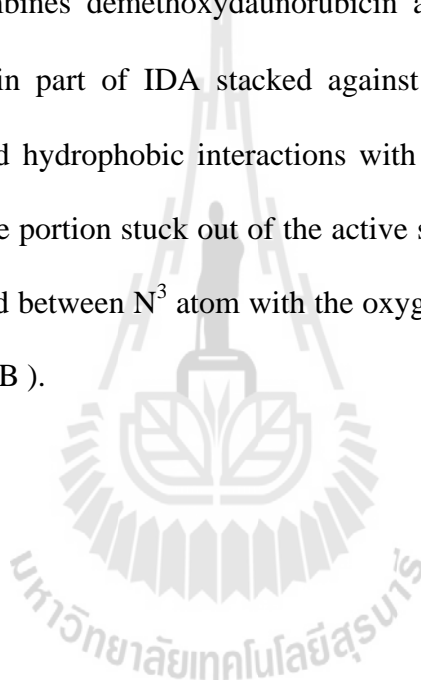


Figure 3.28 The second structure of the complex of wild-type *VhChiA* with CHE.

(A) Superposition of two structural complexes. The inhibitor molecules are shown in stick model and carbon atoms of CHE in first complex are labeled in magenta, while carbon atoms of CHE in the second complex are labeled in green. (B) The $2F_o - F_c$ map of CHE in the second complex was calculated from the refined model and contoured at 1.0σ .

3.11.4 The structure of the complex of wild-type *VhChiA* with idarubicin (IDA)

Similar to the WT-CHE complex, only one molecule of IDA showed a well-defined electron density at the aglycone binding sites, while the electron density around the glycone binding sites was very weak and could only be seen in the $2F_o-F_c$ map with a σ value set to lower than 0.5 (Figure 3.29A). IDA comprises an aromatic backbone, which combines demethoxydaunorubicin and cytosine arabinoside. The demethoxydaunorubicin part of IDA stacked against Trp275 and Trp397 via π - π interaction and formed hydrophobic interactions with Tyr435 at the aglycone sites, whereas its arabinoside portion stuck out of the active site beyond subsites +1/+2 and forms a hydrogen bond between N³ atom with the oxygen atom of the carbonyl group of Gly321 (Figure 3.29B).



3.11.5 The structure of the complex of wild-type *VhChiA* with 2-(imidazolin-2-yl)-5-isothiocyanatobenzofuran (IMI)

Two structures of complexes with WT-IMI were obtained from two different crystallization conditions. The first complex was obtained from the condition 26% (w/v) PEG 4000, 0.2 M ammonium acetate in 0.1 M sodium citrate tribasic dihydrate, pH 5.0, while the second complex was obtained from the condition 1.1 M ammonium sulfate in 0.1 M Tris-HCl, pH 8.5. Both complexes showed two molecules of IMI in the active site of *VhChiA*. IMI1 was located at the aglycone sites and IMI2 at the glycone sites. The electron densities of both molecules of IMI were well-defined as seen in Figures 3.30A and 3.31B. The orientations of IMI from both complexes were slightly different as shown in Figure 3.31A. In addition, there are some different orientations between IMI2 of the first complex and IMI2 of the second complex as the imidazole head group of the first structure points toward the glycone sites, whereas this head group of IMI2 of the second complex points towards the aglycone sites. No hydrogen bond was observed in both complexes. The main interactions of both complexes are again hydrophobic interactions (see LIGPLOT, Figure 3.30B). The benzofuran ring of IMI1 at the aglycones sites was sandwiched only by Trp275 and Trp397, while the benzofuran ring of IMI2 at the glycone sites formed hydrophobic interactions with Trp168, Val205, and Tyr171.

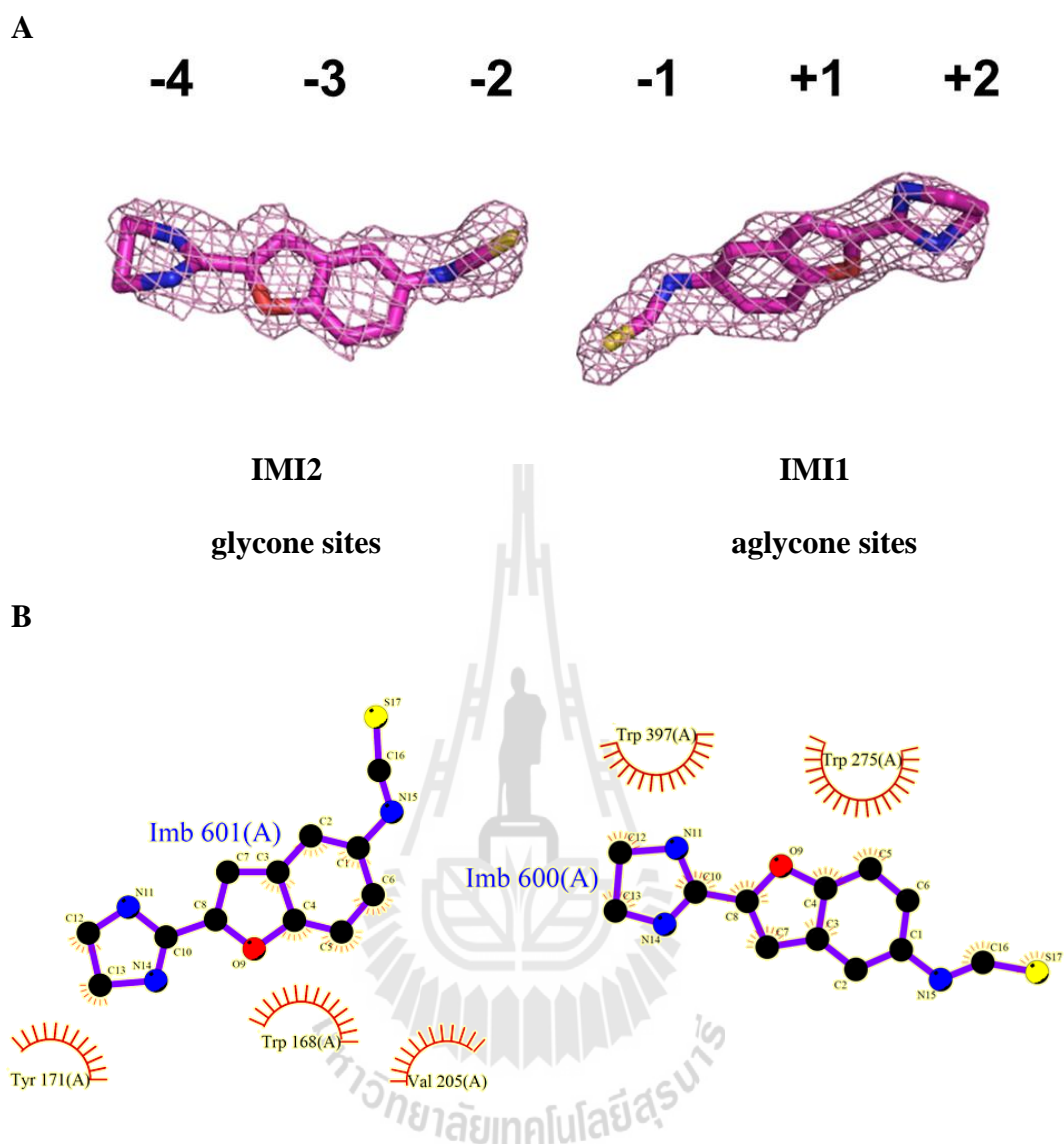


Figure 3.30 The first structure of the complex of the wild-type *VhChiA* with IMI.

(A) The electron density map of IMI in the first complex of WT-IMI1+IMI2.

The $2F_o - F_c$ map was calculated from the refined model and contoured at 1.0σ . The inhibitor molecules are shown in sticks and carbon atoms are labeled in magenta.

(B) Protein–ligand interactions was calculated by LIGPLOT.

3.11.6 The structure of the complex of wild-type *VhChiA* with pentoxifylline (PEN)

Two molecules of PEN at different locations (one on the glycone sites and other one on the aglycone sites) were refined, both showed well-defined electron densities as shown in Figure 3.32A. PEN has a xanthine backbone, which stacks against the aromatic side chains of the binding residues in the enzyme's active site. In the refined model of the WT-PEN1-PEN2 complex, PEN1 was sandwiched by Trp275 and Trp397 via π - π interaction, while PEN2 made its main interaction with Trp168. Moreover, hydrophobic interactions of the surrounding residues with PEN1 were observed at the aglycone sites, including Phe393 and Tyr435. At the glycone sites, additional residues, including Val205, His228, and Leu227, made hydrophobic interactions with PEN2. Two hydrogen bonds were observed at glycone sites: one between the oxygen atom of the oxohexyl tail of PEN2 and the Nⁿ side chain of Lys 370 and another one between the nitrogen backbone of Gly367 and the oxygen atom of the oxohexyl tail of PEN2 (Figure 3.32B).

3.11.7 The structure of the complex of wild-type *VhChiA* with propentofylline (PRO)

Two molecules of PRO were also found in the active site of the wild-type enzyme, with the electron density of PRO2 at the glycone sites being less well-defined (Figure 3.33A). The chemical structure of PRO (Figure 3.10) is similar to PEN, which also contains a xanthine backbone. The difference is PRO comprises a bulky substitute (N⁹ linked 7-propyl moiety), while PEN contains a small N⁷ linked methyl group. Like other inhibitors described earlier, the main interactions of both molecules of PRO are hydrophobic interactions. PRO1 was stacked by Trp275 and Trp397, while PRO2 made hydrophobic contact with Trp168. Moreover, PEN1 also made hydrophobic interactions with the surrounding residues, including Lys370 and Arg463 at subsites +1/+2, and Tyr276 at subsite -2, while Val205, His228, Ser209, Tyr171, and Arg173 interacted with PEN2 at subsites -2 to -4. No hydrogen bond was observed in the structural complex of WT-PRO (see Ligplot, Figure 3.33B).

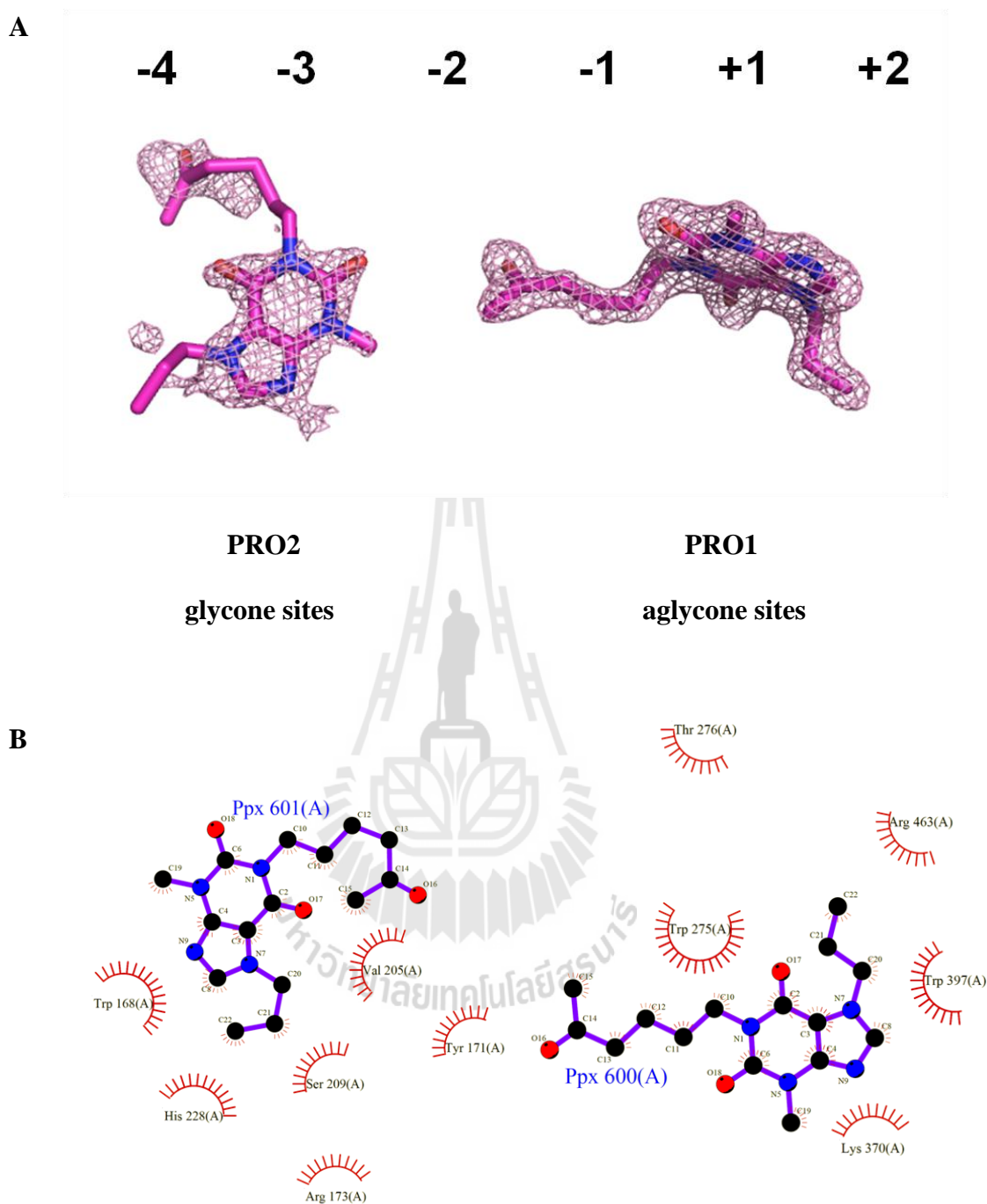


Figure 3.33 The structure of the complex of wild-type *VhChiA* PRO.

(A) The electron density map of IMI in complex with WT-PRO1-PRO2. The $2F_o - F_c$ map was calculated from the refined model and contoured at 1.0σ . The inhibitor molecules are shown in sticks and carbon atoms are labeled in magenta;

(B) Protein–ligand interactions was calculated by LIGPLOT.

All the interactions found in the WT-inhibitor complexes are summarized in Table 3.18, which shows that all the inhibitors are maintained in the active site of the wild-type chitinase mainly by hydrophobic residues and a few other surrounding interactions with a very few hydrogen bonds involved in the interactions. In addition, the inhibitors were found to occupy the surface of the substrate binding cleft of *VhChiA* covering subsites -4 to +2, but no interaction found at subsite -1. These findings are different from other inhibitors reported previously (Roa *et al.*, 2003; Roa *et al.*, 2005; Vaaje-Kolstad *et al.*, 2004; Roa *et al.*, 2005; Houston *et al.*, 2002).



Table 3.18 A summary of the interactions between the inhibitors and the binding residues in the substrate-binding cleft of the wild-type *VhChiA*.

Binding subsite	WT-DEQ	WT-IDA	WT-SAN	WT-CHE	WT-PEN	WT-PRO	WT-IMI
+2	Trp275 ¹ , Asp392 ¹ , Trp397 ¹	Trp275 ¹ , Gly321 ^{1,H} , Trp397 ¹ , Tyr435 ¹	Trp275 ¹ , Trp397 ¹	Trp275 ¹ , Trp397 ¹	Trp275 ¹ , Gly367 ^{1,H} , Lys370 ^{1,H} , Trp397 ¹ , Phe393 ¹ , Tyr435 ¹	Trp275 ¹ , Trp397 ¹	Trp275 ¹ , Trp397 ¹
+1	Trp275 ¹ , Asp392 ¹	Trp275 ¹	Trp275 ¹	Trp275 ¹	Trp275 ¹	Trp275 ¹ , Lys370 ¹ , Arg463 ¹	Trp275 ¹
-1						Arg463 ¹	
-2	Thr276 ² , Leu227 ² , Trp570 ²		Phe192 ² , Leu227 ² , Thr276 ^{2,H}		Leu227 ² ,	Thr276 ²	
-3	Trp168 ² , Val205 ² , His228 ²		Trp168 ² , Val205 ²		Trp168 ² , Val205 ² , His228 ²	Trp168 ² , Arg173 ² , Val205 ² , His228 ² , Ser209 ²	Trp168 ² , Val205 ²
-4			Tyr171 ²			Tyr171 ² , Arg173 ²	Tyr171 ²

¹The residues interacted with the first inhibitor at the aglycone sites.

²The residues interacted with the second inhibitor at the glycone sites.

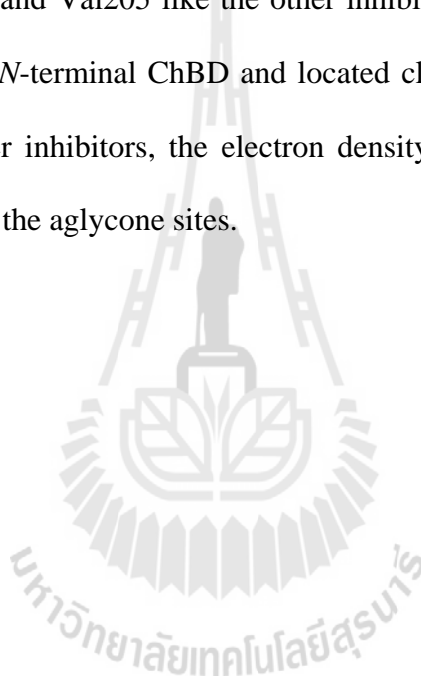
^HThe residues that hydrogen bonded with the inhibitors.

3.12 The structures of the complexes of mutant W275G with the newly identified inhibitors

The refined structures of the complexes of W275G with the inhibitors also revealed, if not all, two molecules of inhibitors but their binding behaviors are different from that of the wild-type enzyme. With the exception of DEQ, the complexes of W275G with the inhibitors SAN, CHE, PEN, and IMI showed two inhibitor molecules in only the aglycone location. The first molecule of the inhibitors formed hydrophobic interactions with Trp397 as in the wild-type complex, while the second molecule stacked against the first molecule, in exactly the place of where the indole ring of Trp275 was missing (Figure 3.34). Moreover, the backbone of the loop containing Gly321 interacts with the second inhibitor molecule via hydrophobic interactions and/or hydrogen bonds (see Ligplot, Figure 3.34 for DEQ and for IMI). Both inhibitor molecules that stack against one another at the aglycone sites were likely to orient in the same direction with similar well defined electron densities (Figure 3.35).

However, binding of DEQ to the mutant W275G (Figure 3.34DEQ) is different from binding of DEQ to the wild-type enzyme and to the other inhibitors to the mutant W275G for three reasons: (1) inspection of the $2F_o-F_c$ and F_o-F_c maps revealed two DEQ molecules in the W275G's active site instead of one molecule as observed in wild-type (Figure 3.24, DEQ): (2) the two DEQ molecules are located at the opposite sides of the substrate binding cleft: one is at the aglycone subsites, while the other one reaches outside the glycone subsites: and (3) both molecules adopt completely different conformations. At the aglycone subsites, the DEQ molecule (DEQ1) apparently folds onto itself, allowing one of the quinolinium head groups to

stack against the other head group, which concomitantly substitutes for the eliminated side-chain of Trp275 in a structure reminiscent of the double stack described for two separate inhibitor molecules. The electron density of the first molecule at the aglycone position was very weak for the head groups and even weaker for the linker. In contrast, the second molecule of DEQ is in an open conformation and stretches along the enzyme's surface starting from the glycone position, where one aromatic moiety interacts with Trp168 and Val205 like the other inhibitors, while the other moiety is extended towards the *N*-terminal ChBD and located close to Trp231 and Tyr171. In contrast with the other inhibitors, the electron density at the glycone sites is more clearly defined than at the aglycone sites.



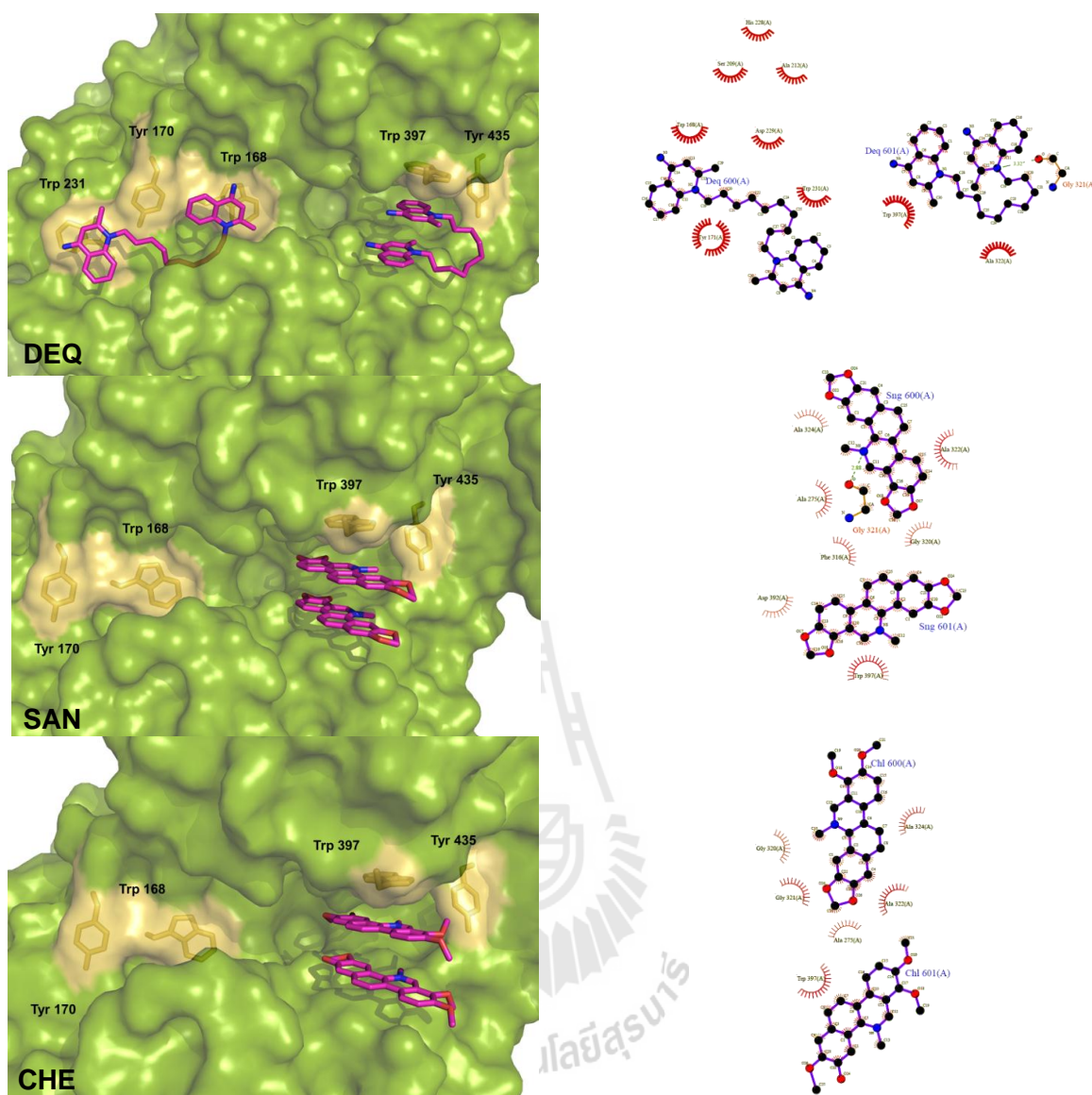


Figure 3.34 The structure of mutant W275G with six inhibitors identified inhibitors from LOPAC library. Right panels: Surface representation of the complexes of mutant W275G with the inhibitors (DEQ, SAN, CHE, PEN, PRO, and IMI). The protein surface is colored in green with hydrophobic patches and stick models of corresponding aromatic residues shown as yellow. The inhibitor molecules are shown in magenta. Left panel: Ligplot schematic diagrams showing protein–ligand interactions of the W275G-inhibitor complexes.

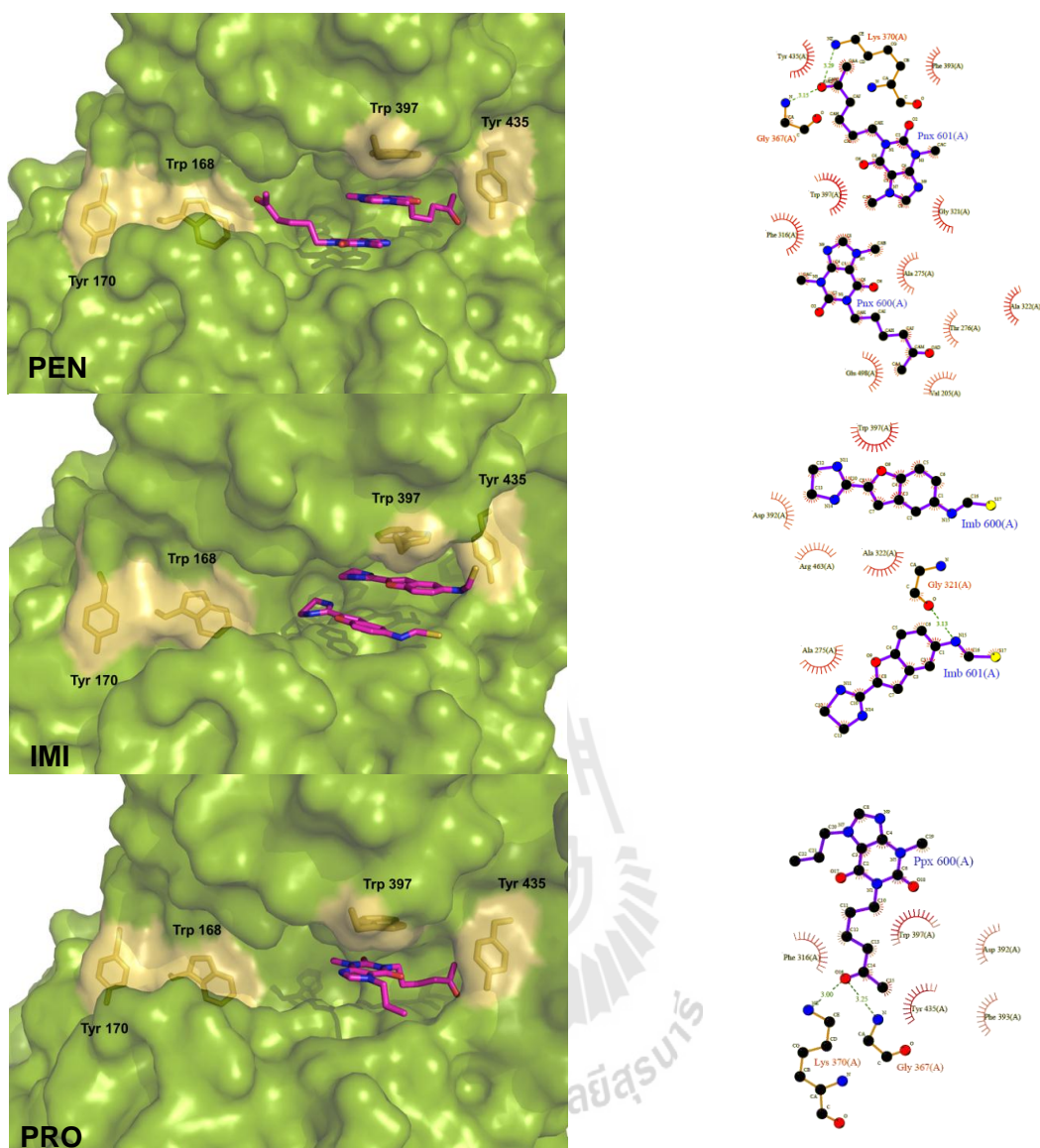


Figure 3.34 The structure of mutant W275G with six inhibitors identified inhibitors from LOPAC library. Right panels: Surface representation of the complexes of mutant W275G with the inhibitors (DEQ, SAN, CHE, PEN, PRO, and IMI). The protein surface is colored in green with hydrophobic patches and stick models of corresponding aromatic residues shown as yellow. The inhibitor molecules are shown in magenta. Left panel: Ligplot schematic diagrams showing protein–ligand interactions of the W275G-inhibitor complexes (Continued).

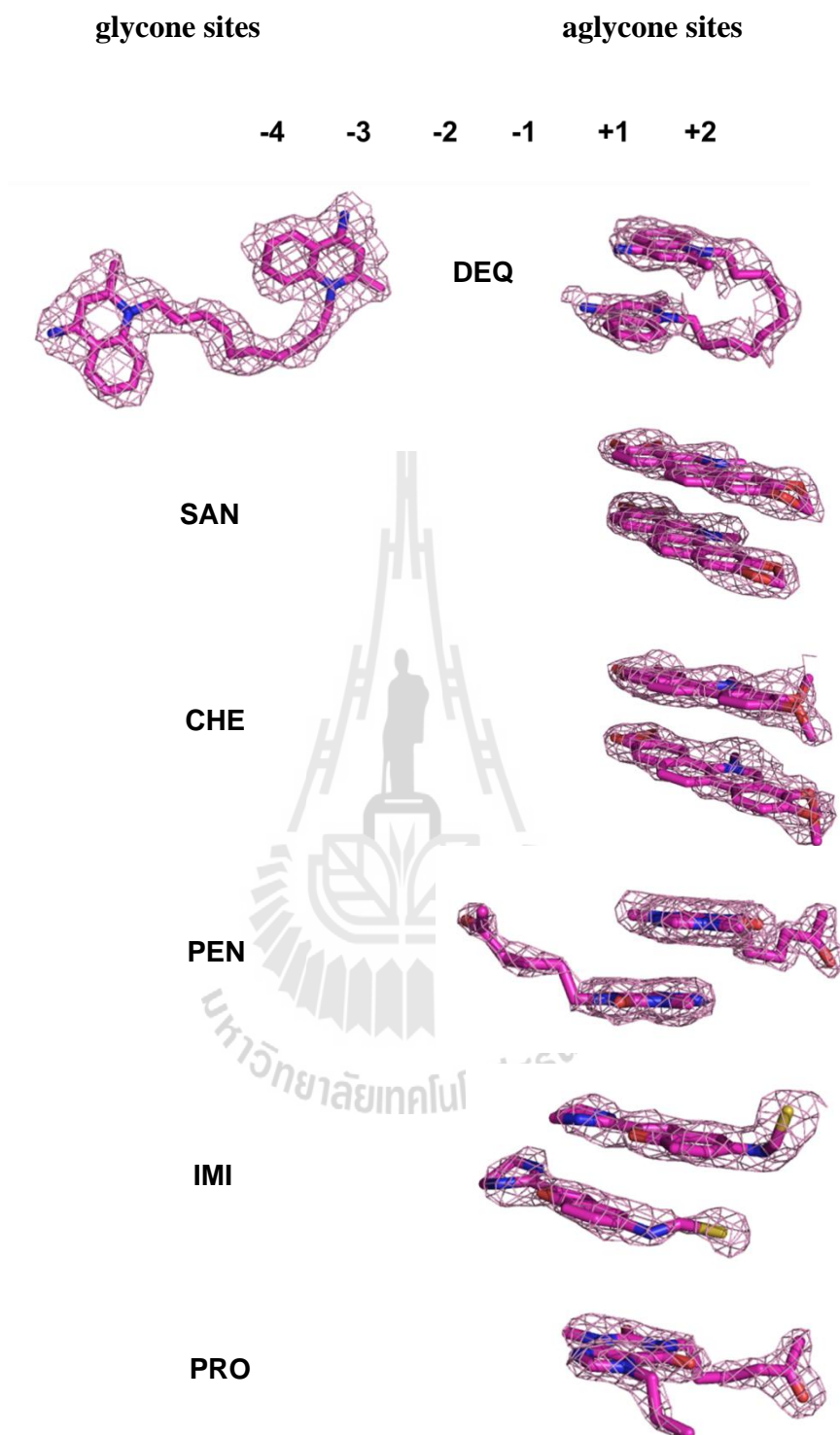


Figure 3.35 The electron density maps of the six inhibitors in active site of W275G. The substrate binding cleft of the enzyme is indicated as subsites -4, -3, -2, -2, +1, and +2. The $2F_o - F_c$ maps were calculated from the refined model and contoured at 1.0σ .

Although both PEN and PRO have a xanthine backbone (Figure 3.11), their binding behaviors to the mutant W275G are different as two molecules of PEN formed a double sandwich with Trp397 at the aglycone position, with well-defined density just like the other inhibitors. On the other hand, only one molecule of PRO was found to stack against Trp397. This is most likely due to a steric clash of the 7-propyl moiety of PRO that protrudes towards the site of the mutation W275G, thus preventing stacking (Figure 3.36).

There is also a sign of the third molecule of PEN in the active site of mutant W275G at the glycone sites in a similar area as PEN2 bound to the wild-type enzyme (Figure 3.24). However, its electron density was relatively weak. Similar evidence of the second molecule of IMI was observed at the glycone sites of W275G's active site.

The main interactions of W275G-inhibitors are hydrophobic interactions with a few hydrogen bonds involved as shown in Ligplot (Figure 3.34, left panel). A summary of the interactions between the binding residues in the active site of W275G and the inhibitors is presented in Table 3.19.

Table 3.19 A summary of the interactions between the inhibitors and the binding residues in the substrate-binding cleft of mutant W275G.

Binding subsites	WG-DEQ	WG-SAN	WG-CHE	WG-PEN	WG-PRO	WG-IMI
+2	Gly231 ^{1,H} ,Gly275 ¹ ,Ala322 ¹	Gly275 ² ,Gly320 ² ,Gly321 ^{2,H} ,Ala322 ² ,Ala324 ² , Asp392 ¹ ,Trp397 ¹	Gly275 ² ,Gly320 ² ,Gly321 ^{2,H} ,Ala322 ² ,Ala324 ² ,Trp397 ¹	Gly275 ² ,Gly321 ² ,Gly367 ^{1,H} ,Phe393 ¹ ,Lys370 ^{1,H} ,Trp397 ¹ ,Try435 ¹	Trp397 ¹ ,Lys370 ^{1,H} ,Try435 ¹ ,Phe393 ¹	Trp275 ² ,Ala322 ² ,Trp397 ¹ ,Asp392 ¹
+1		Trp275 ¹ ,Phe316 ^{1,2} ,Asp392 ¹		Gly 275 ² ,Phe316 ^{1,2}	Phe316 ¹ ,Asp392 ¹	Gly275 ²
-1						Arg463 ²
-2				Thr276 ²		
-3	Trp168 ² ,His228 ²			Val205 ² ,His228 ²		
-4	Ser209 ² ,Ala212 ² ,Tyr171 ²					
-5	Asp229 ² ,Tyr171 ²					
-6	Trp231 ²					

¹The residues interacted with the first inhibitor at the aglycone sites.

²The residues interacted with the second inhibitor at the glycone sites.

^HThe residues that hydrogen bonded with the inhibitors.

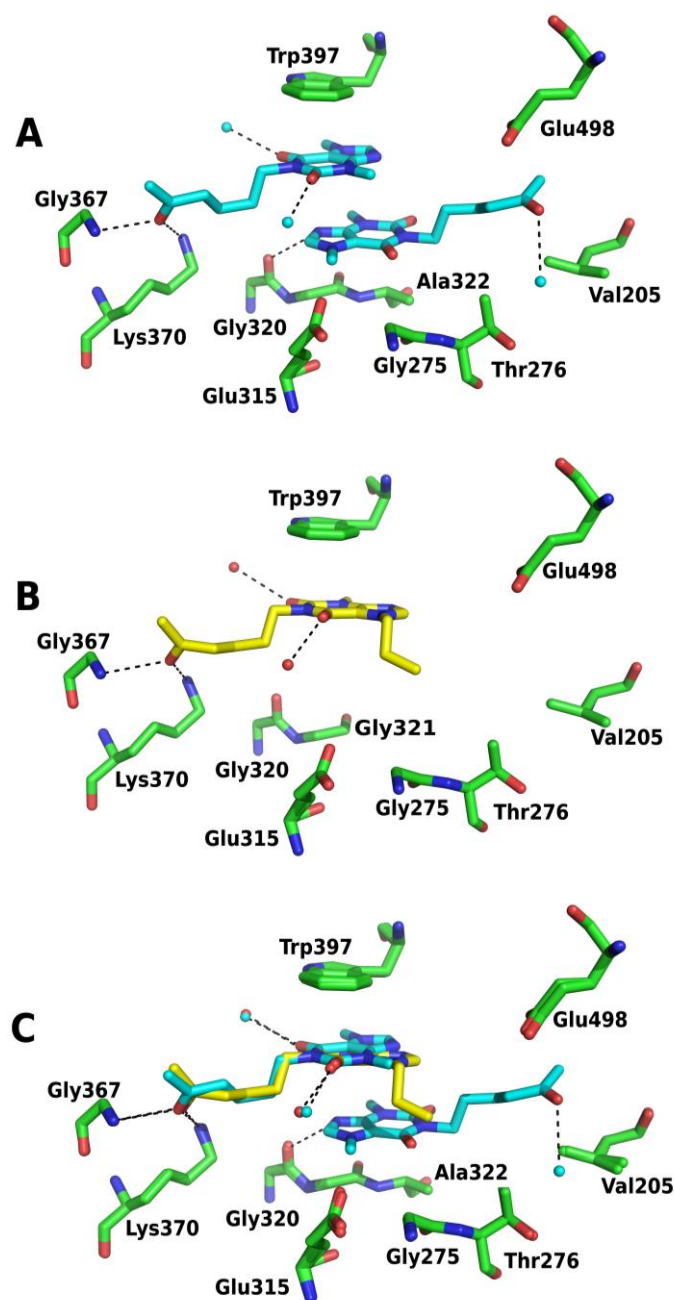


Figure 3.36 Details of the interactions of PEN and PRO in the active site of W275G.

The structures of mutant W275G in complex with (A) PEN; (B) PRO.

PEN is shown in cyan and PRO in yellow. Hydrogen bonds are presented as dashed lines, water molecules as blue spheres; and (C) Superposition of the two complexes showing the potential clash of the 7-propyl moiety of PRO that most likely prevents binding of a second PRO molecule at the aglycone subsites.

3.13 Effects of the inhibitors on hydrolytic activity of the wild-type *VhChiA* against soluble and insoluble substrates

The effects of the inhibitors on chitinase activity were evaluated by assaying the specific activity values towards soluble (GlcNAc₆) or insoluble (colloidal chitin and crystalline α chitin) substrates using the DMAB assay (Table 3.20). The results showed that at a fixed concentration of the inhibitor of 3.9 μ M, the wild-type activity against chitohexaose was inhibited by DEQ by 50%. This concentration was in an agreement with the IC_{50} of DEQ determined by the dose-response curve presented earlier (see Table 3.3). All other inhibitors were found to inhibit the wild-type activity less efficiently than DEQ. Especially, PEN, PRO and MET showed no inhibition on the wild-type activity against chitohexaose. All the inhibitors showed similar effects on enzyme activity against colloidal chitin and crystalline α chitin. The orders of the inhibition are DEQ > IDA > SAN > CHE > IMI > PRO > PEN.

Table 3.20 The inhibition effects of the inhibitors on specific activity of the wild-type *VhChiA* against soluble and insoluble substrates as determined by the DMAB assay.

	Specific hydrolyzing activity (U/nmol protein) ^a		
	Crystalline chitin	Colloidal chitin	Chitohexaose
No inhibitor	1.6 ± 0.1 (100) ^b	19 ± 0.3(100)	47 ± 0.5 (100)
DEQ	0.5 ± 0.1 (31)	10 ± 0.9 (53)	24 ± 0.3 (51)
IDA	0.6 ± 0.1 (38)	12 ± 0.6 (53)	28 ± 2.9 (59)
SAN	0.6 ± 0.02 (38)	13 ± 0.7 (68)	30 ± 1.0 (64)
CHE	0.7 ± 0.1 (44)	13 ± 0.7 (68)	32 ± 1.5 (68)
IMI	0.8 ± 0.1 (50)	16 ± 0.4 (84)	43 ± 1.0 (91)
PEN	0.8 ± 0.02 (50)	15 ± 0.2 (79)	46 ± 1.6 (98)
PRO	0.8 ± 0.1 (50)	15 ± 0.5 (79)	46 ± 0.3 (98)
MET	0.8 ± 0.1 (50)	15 ± 0.3 (79)	46 ± 0.5 (98)

^aOne unit of chitinase is defined as the amount of enzyme that releases 1 μmol of GlcNAc₂ or 1 nmol of *p*NP per min at 37°C.

^bValues in parentheses represent relative specific hydrolyzing activities (%).

3.14 Binding study by fluorescence titration spectroscopy

Intrinsic fluorescence titration spectroscopy was used to assess the binding affinity of all the inhibitors towards the wild-type *VhChiA*. Changes in the intrinsic protein fluorescence intensity after adding different concentrations of the inhibitors were measured at the excitation wavelength of 295 nm and at the emission wavelength between 310-450 nm. Decreases in the fluorescence intensity were found to correspond to increases in the concentrations of the inhibitors (Figure 3.37). A plot of relative fluorescence (F/F_0) as a function of inhibitor concentrations yielded a well-defined exponential decay curve, allowing the equilibrium dissociation constant (K_D) of each corresponding inhibitors to be estimated using a single site binding model (Figure 3.38).

The corresponding binding curves were fitted with a single binding site model;

$$F/F_0 = \left(\frac{F_0}{F_0} - NS \right) e^{-K_D [L_0]} + NS$$

where F and F_0 refer to the fluorescence intensity in the presence and absence of ligand respectively, L_0 is the initial ligand concentration, K_D is the equilibrium dissociation constant and NS is the non specific binding that does that dissociated (plateau).

In agreement with the data obtained from the dose-response curves, DEQ acts as the most potent inhibitor with the K_D of 0.2 μM , followed by IDA (K_D of 0.4 μM), SAN (K_D of 0.6 μM), CHE (K_D of 0.7 μM), IMI (K_D of 1.0 μM), PEN (K_D of 4.0 μM), and PRO (K_D of 4.7 μM), respectively. The K_D of MET at 33.4 μM indicated that this inhibitor was the weakest inhibitor compared to the other inhibitors.

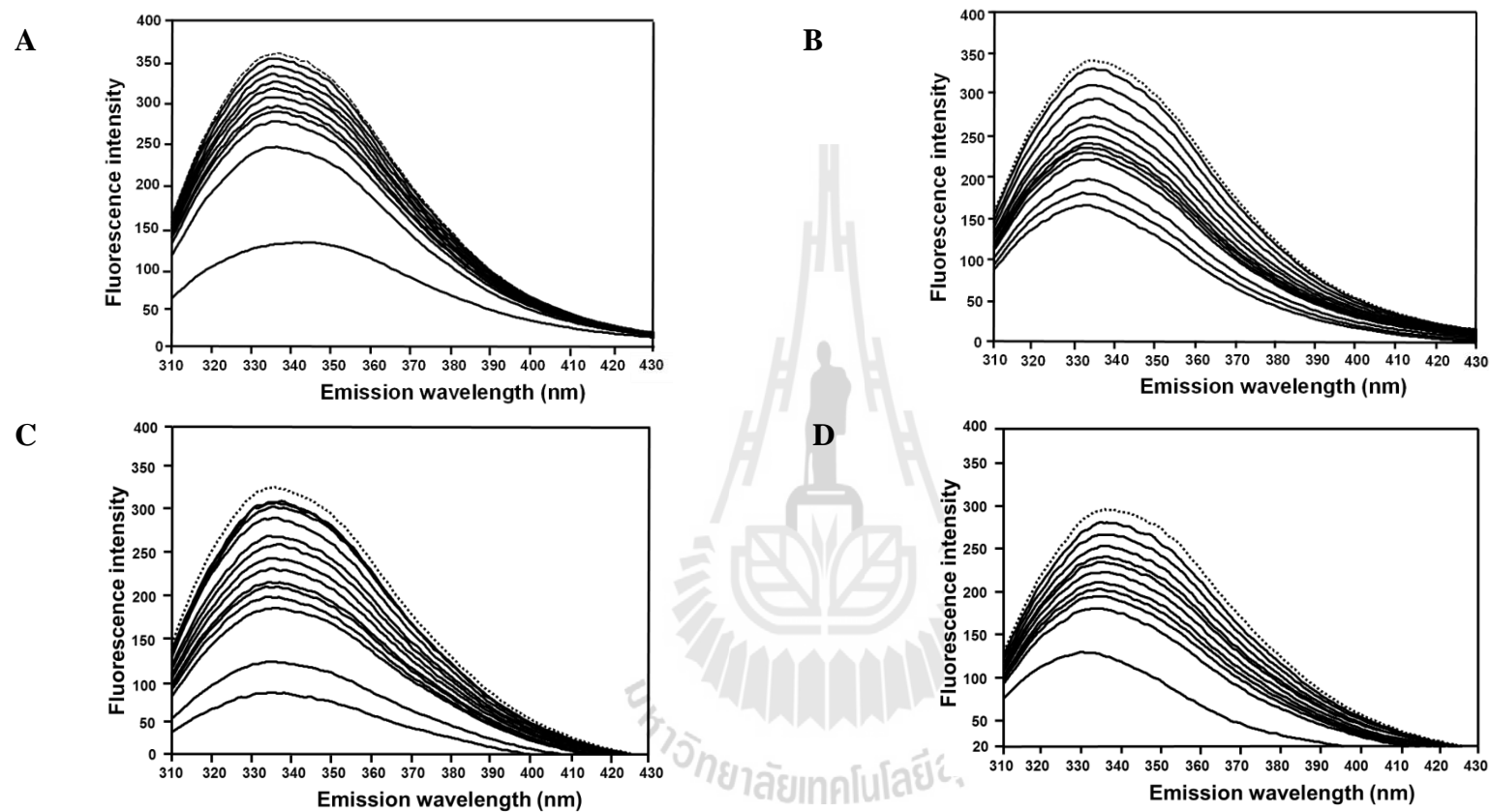


Figure 3.37 A protein-inhibitor binding study by intrinsic fluorescence spectroscopy. Increased concentrations of (A) DEQ; (B) IDA; (C) SAN from 0-3 μM ; and (D) PEN from 0-10 μM were added to 0.25 μM of the purified wild-type *VhChiA* in 20 mM Tris-HCl, pH 8.0. The emission spectra were collected from 310-450 nm upon excitation at 295 nm. Dash line indicates 0 μM of the inhibitors.

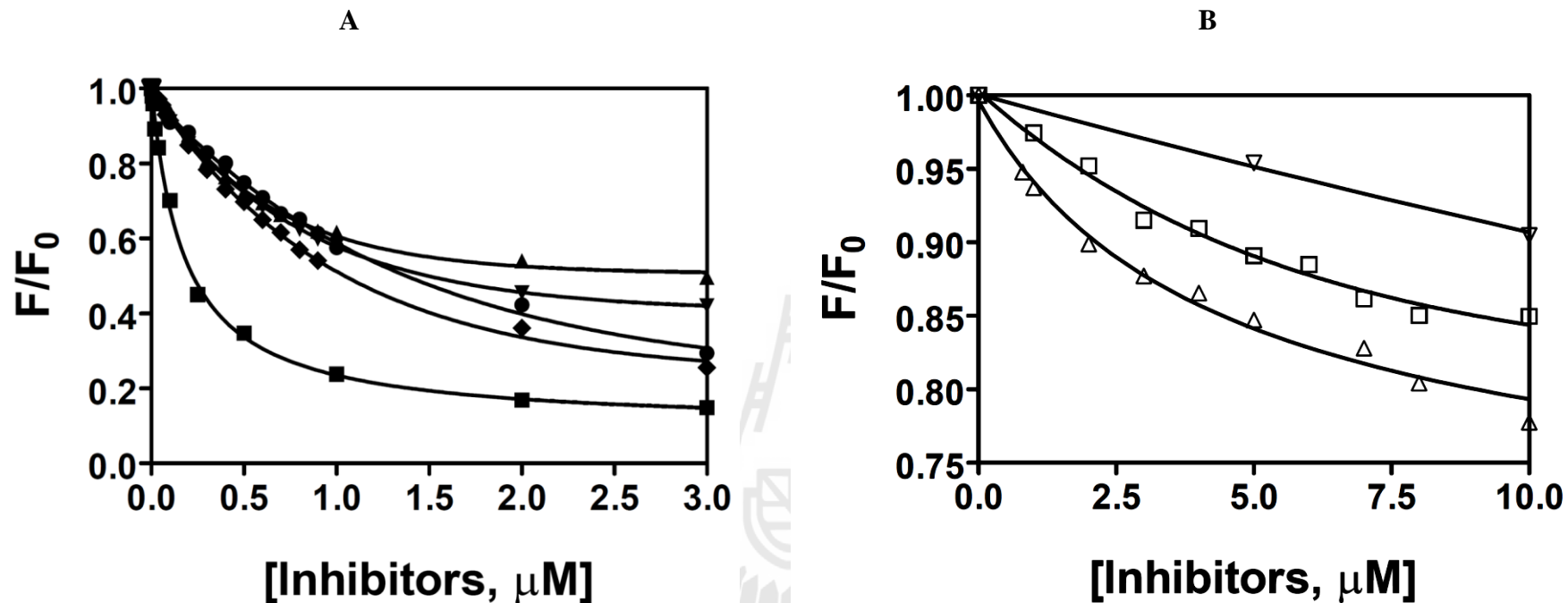


Figure 3.38 Binding curves determined for each inhibitor. The binding curves of (A) DEQ, IDA, SAN, CHE, and IMI; and (B) PEN, PRO and MET. Symbols: DEQ (black square), IDA (black upward-pointing triangle), SAN (black downward-pointing triangle), CHE (black diamond), IMI (black circle), PEN (open square), PRO (open upward-pointing triangle), and MET (open downward-pointing triangle).

3.15 Isothermal titration microcalorimetry (ITC) experiments

ITC experiments of wild-type, mutants W275G and W397F against three inhibitors (DEQ, PEN and SAN) were carry out. The reason for selecting these three inhibitors for ITC experiments was because they exhibited different binding behaviors, which represent three different binding modes as proposed based on the ITC and structural data.

The ITC experiments were carried out at two different pH values (pH 5.5 and pH 8.0). The results showed that the three inhibitors bound with the enzymes at pH 5.5, while the heat changes, indicating ligand binding upon addition of DEQ and SAN, could not be observed for the wild-type and the mutated enzymes at pH 8.0.

Together with the structural data of wild-type and W275G complexed with the inhibitors, fitting the ITC data implicated that the inhibitors occupied the enzyme's active site in three different binding modes. The first binding mode is applicable for binding of DEQ to the wild-type chitinase as seen the structural complex of WT-DEQ (Figure 3.24, DEQ) and the ITC thermogram of the wild-type and DEQ showing the heat release as calories/mole of injectant, and plotted as a function of molar ratio of DEQ:*VhChiA* (Figure 3.39A1). The binding parameters were analyzed from the binding isothermal curve, as indicated as a solid black line in Figure 3.39A2 and revealed the number of binding site $N = 1$ (see Table 3.21). Fitting the curve using a single-site binding model yielded ΔH as $-8.7 \text{ kcal mol}^{-1}$, ΔS as 3.5 cal mol^{-1} , and K_D of 70 nM.

Wild-type with DEQ, SAN and PEN

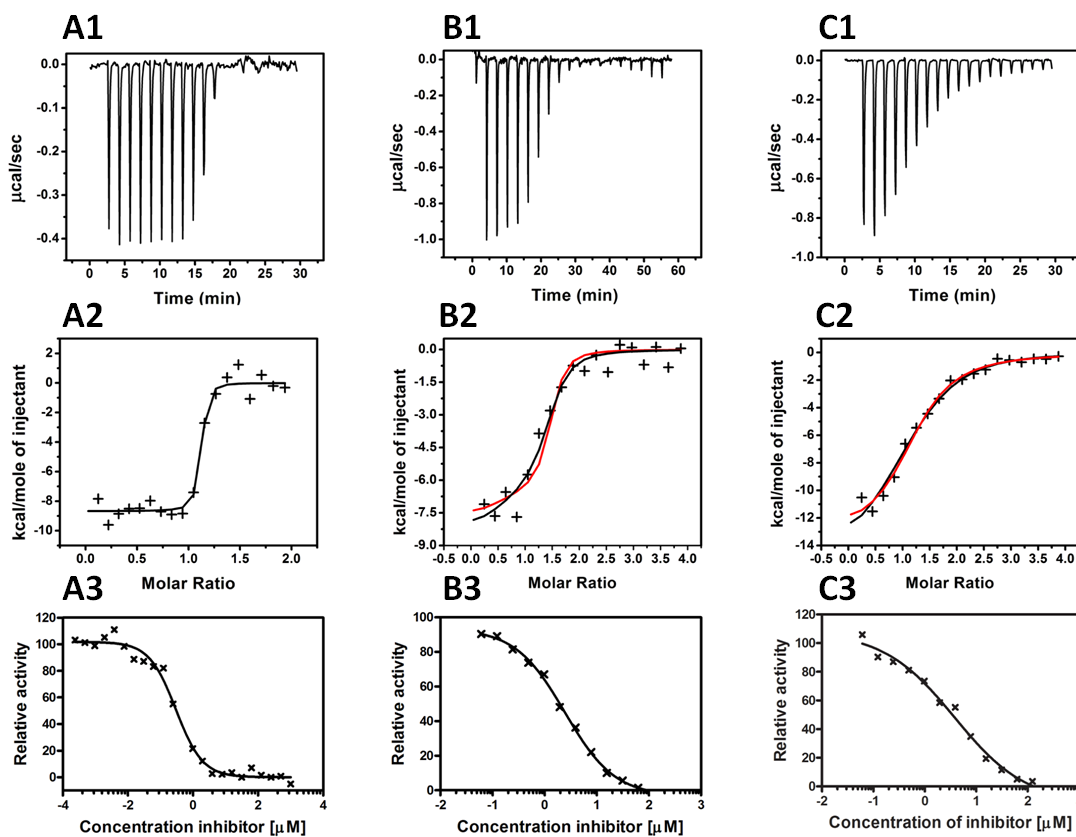


Figure 3.39 Thermographic binding isotherms (A1-C1) with theoretical fits (A2-C2) obtained from ITC experiments and the dose-response curves (A3-C3) obtained from colorimetric assays.

Thermograms and theoretical data fittings corresponding to binding of DEQ, SAN and PEN to the wild-type chitinase are shown in A1-A3, B1-B3, and C1-C3 respectively. In A2, the fitted binding curve assumes a single binding site; while theoretical curve fits assuming two-independent inhibitor binding sites are shown in B2 and C2 in red.

The second binding mode is described by two molecules of the inhibitors binding in two different locations (locations: aglycone and glycone). To understand the binding mechanism, the ITC experiments were performed with PEN and SAN against the wild-type enzyme. Although the isothermal curves of both inhibitors could be fitted with a one-site binding model, the fit displayed the number of binding sites to be larger than one ($N > 1$) (Table 3.21). This is shown in Figure 3.39B2, where a 3-parameter fit for one binding site (black solid line) gave $N = 1.3$, $\Delta H = -7.2 \text{ kcal mol}^{-1}$, $\Delta S = 3.3 \text{ cal mol}^{-1}$ and $K_D = 800 \text{ nM}$ for SAN, and $N = 1.2$, $\Delta H = -13 \text{ kcal mol}^{-1}$, $\Delta S = -18 \text{ cal mol}^{-1}$ and $K_D = 2 \text{ }\mu\text{M}$ for PEN. In addition, the one-site-binding model did not correspond to the structural findings, which revealed two inhibitor molecules bound to two sites (Figures 3.24 SAN and 3.24 PEN). Therefore, the data were then fitted with a two-independent-site model (red line, Figure 3.39B) with the number of the binding sites set to $N_1 = N_2 = 1$. Based on the two-independent-site fitting, two dissociation constants were obtained. For SAN, K_{D1} is 40 fold larger than K_{D2} ($K_{D1} = 0.2 \text{ }\mu\text{M}$ and $K_{D2} = 8.0 \text{ }\mu\text{M}$). For PEN, K_{D1} is 5 fold larger than K_{D2} ($K_{D1} = 2.0 \text{ }\mu\text{M}$ and $K_{D2} = 10 \text{ }\mu\text{M}$). The inhibitor molecule bound to the glycone sites likely has the weaker binding affinity binding than the one that bound to the aglycone sites as its electron density was less well-defined and refined with higher B-factors.

The two-independent site binding mode seems to also explain binding of DEQ to mutant W275G (Figure 3.40A1 and Figure 3.40A2), since the crystal structure of the W275G-DEQ showed two molecules of DEQ bound at two different sites (Figure 3.34 DEQ).

The third binding mode is applicable for binding of two molecules of inhibitors to W275G at the same location (location “aglycone”). As seen in Figure 3.34 SAN, CHE, PEN, and IMI. The ITC curve of SAN to W275G was a representative of this binding mode, where the first SAN molecule formed a double stack against the residue Trp397 and the second SAN molecule.

Again, the binding curve was first fitted with the one-site binding model as indicated with black line (Figure 3.40B2), and gave a number of binding sites of $N = 3.9$. The number of binding sites (N) larger than one indicates that more than one sites of the inhibitor were bound. Based on the structural data (Figure 3.34 SAN), the binding curve was re-fitted with the two-sequential-site binding model. The red line in Figure 3.40 B2 was calculated with the sequential binding model with the assumption of two molecules of the inhibitor bound to the active site of W275G. The curve fit with $N_1 = N_2 = 1$ gave K_D1 of 264 μM with ΔH_1 and ΔS_1 at $-8.0 \text{ kcal mol}^{-1}$ and $-8.6 \text{ cal mol}^{-1}$, and K_D2 of 66 μM with ΔH_2 and ΔS_2 at $-8.6 \text{ kcal mol}^{-1}$ and $-12.0 \text{ cal mol}^{-1}$. Similar results were seen with PEN binding to W275G, where its ITC binding curve was fitted by the two sequential binding model giving two different K_D values with K_D1 of 93 μM and K_D2 of 609 μM .

W275G with DEQ, SAN and PEN

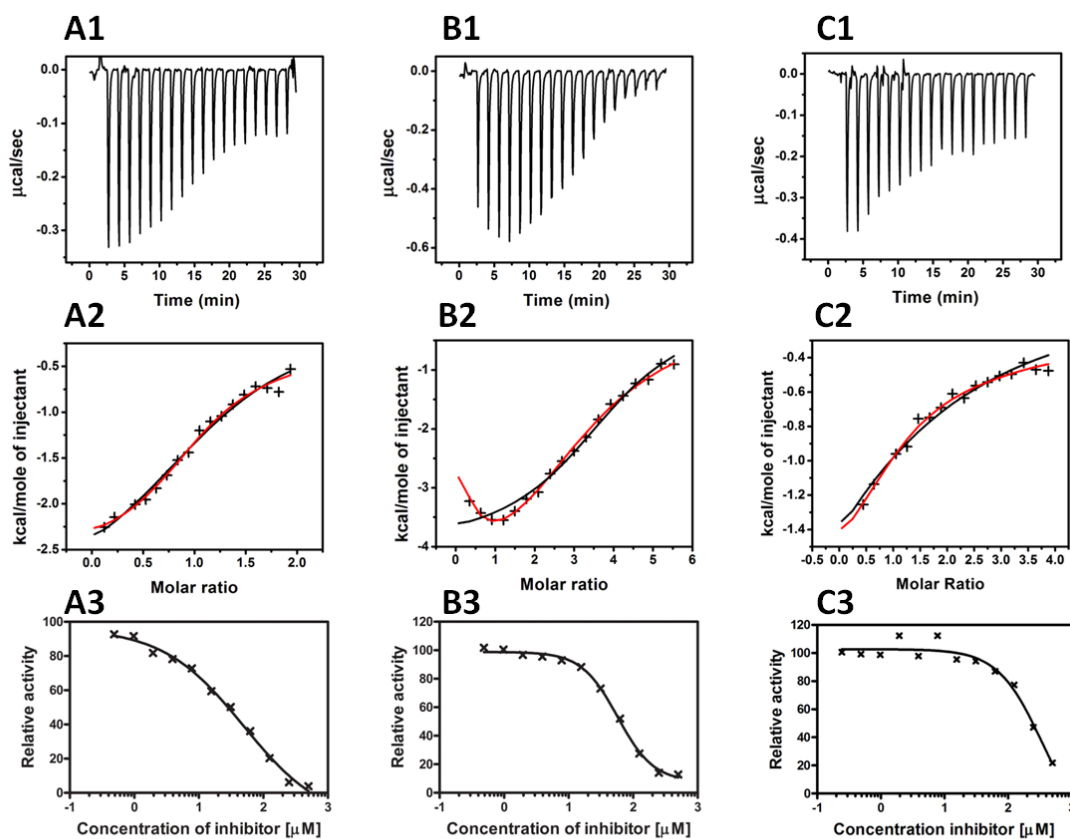


Figure 3.40 Thermographic binding isotherms (A1-C1) with theoretical fits (A2-C2) obtained from ITC experiments and the dose-response curves (A3-C3) obtained from the colorimetric assays.

Bindings of DEQ, SAN, and PEN to W275G are shown in A1-A3, B1-B3, and C1-C3, respectively. The theoretical fit to two-independent site binding of DEQ to W275G is indicated as red line in A2. The theoretical fits to two- sequential-site binding of SAN and PEN to W275G are indicated as red line in B2 and C2. The black line indicated one-site binding.

The ITC experiments of W397F were carried out even though the structural complexes of this mutant with the inhibitors were not successfully obtained. However, its binding mechanism was explained base on the structural elucidation of the wild-type and the mutant W275G with the inhibitors (Figures 3.24 and 3.34).

The isothermal binding curves were fitted as the same binding models as for the wild-type enzyme. The isothermal binding curve of DEQ to W397F gave the fit with the one site binding model (black line, Figure 3.33A1) with K_D of 3.8 μM , $\Delta H = -1.3 \text{ kcal mol}^{-1}$ and $\Delta S = -20 \text{ cal mol}^{-1}$. However, the number of binding sites is shown to be smaller than one ($N = 0.7$) (Table 3.21). For SAN and PEN, their isothermal binding curves could also be fitted to the data with a one site binding model, but the number of binding sites was not equal to one. The obtained N values indicated more than one site of the inhibitors could be bound. Thus, the binding curves were fit with the assumption of the two independent binding sites (set at $N_1 = N_2 = 1$) (red line, Figures 3.41B2 and 3.41C2). The results gave two dissociation constants with K_{D1} is 12.5 μM for SAN and 17 μM for PEN, and K_{D2} is 10 μM for SAN and 29 μM for PEN.

W397F with DEQ, SAN and PEN

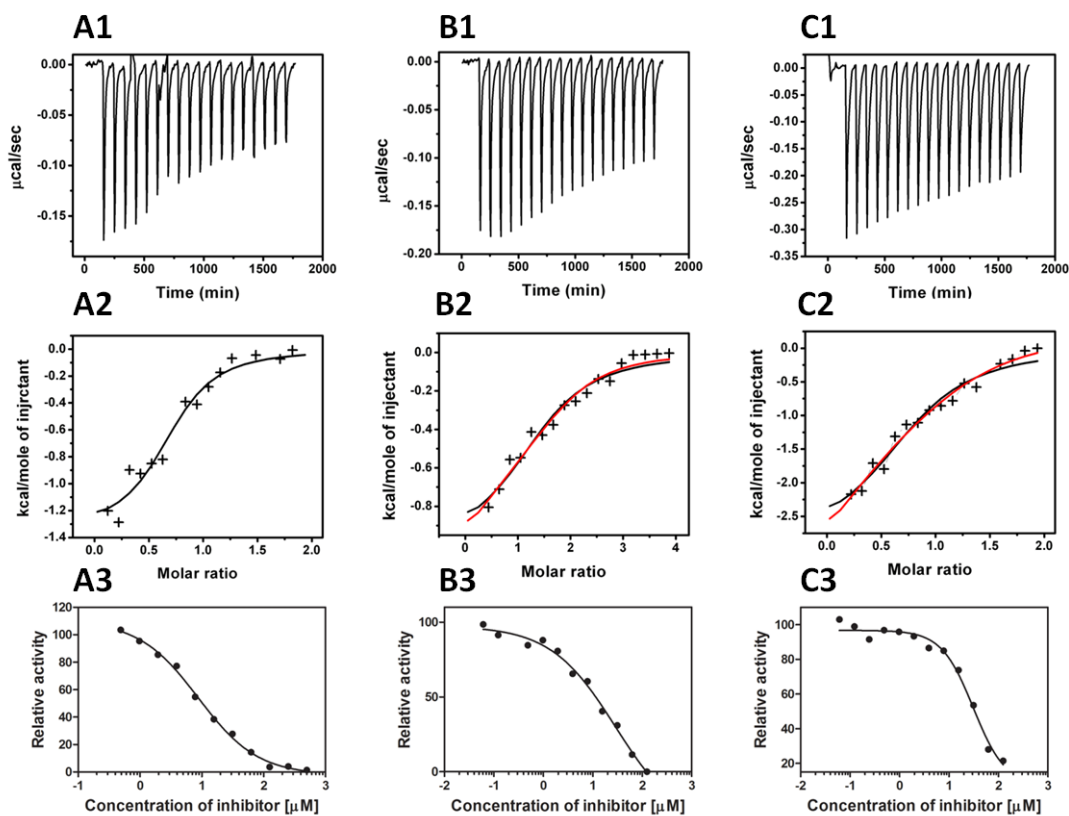


Figure 3.41 Thermographic binding isotherms (A1-C1) with theoretical fits (A2-C2) obtained from ITC experiments and the dose-response curves (A3-C3) obtained from colorimetric assays.

Binding of DEQ, SAN, and PEN to W397F chitinase are shown in A1-A3, B1-B3, and C1-C3 respectively. The theoretical fit to two independent inhibitor binding sites is indicated as red in B2 and C2, and the black line indicated a single site binding.

Table 3.21 Parameters used for the calculation of theoretical ITC curves. Equilibrium dissociation constants K_D (μM), enthalpy changes ΔH (kcal mol^{-1}), entropy changes ΔS (cal mol^{-1}), IC_{50} values (μM), and Hill coefficients n_H , which have been used for the calculation of the theoretical curves, are shown for three molecules of the inhibitors and wild-type (WT) or mutants W275G and W397F. All the ITC experiments were first fitted to the single-site binding model 1, yielding values of N , K_D and ΔH observed upon binding. Hill coefficients n_H and IC_{50} values were obtained from the four-parameter logistic fits. For two independent-site binding and two sequential-site binding mechanisms, the N values ($N1$ and $N2$) were set to 1.

	Binding to one site (black lines)				Binding to two independent or sequential sites							4 parameter fit	
	N	K_D	ΔH	ΔS	N	K_{D1}	K_{D2}	$\Delta H1$	ΔS	$\Delta H2$	ΔS	IC_{50}	n_H
DEQ WT	1.1	0.07	-8.7	3.5	-	-	-	-	-	-	-	0.4	1.4
SAN WT	1.3	0.8	-7.2	3.3	1	0.2	8	-8.3	2.6	-1.6	18	2.3	0.9
PEN WT	1.2	2	-13	-18	1	2	10	-16	-25	-1	19.5	3.5	1
DEQ W275G	1.3	24	-2.7	11.8	1	11	500	-2.5	14.1	-3.2	4.0	68	0.7
SAN W275G	3.9	50	-4.4	4.4	1	214	66	-8.0	-8.6	-8.6	-12	71	1.4
PEN W275G	1.8	200	-3.0	6.8	1	93	690	-2.6	9.2	-4.1	0.26	260	1.9
DEQ:W397F	0.7	3.8	-1.3	20	-	-	-	-	-	-	-	8.8	0.9
SAN W397F	1.4	14	-1	18.7	1	12.5	10	1.6	28	-3.0	13	30	0.9
PEN W397F	0.8	8.7	-3	13.5	1	17	29	-9.3	-9.3	8	48	32	1.2

CHAPTER IV

DISCUSSION

4.1 Investigation of the role of surface-exposed residues on substrate binding and catalytic activities of *VhChiA*

Four surface-exposed residues (Trp70, Ser33, Trp231, and Tyr245) positioned outside the substrate binding cleft and extended towards the *N*-terminal ChBD of *VhChiA* were investigated. Trp70 and Ser33 are located at the end of the *N*-terminal ChBD, whilst Trp231 and Tyr245 are found outside the substrate binding cleft, where they are part of the TIM barrel catalytic domain (Figure 3.1). Previous studies showed that these residues play an important role in the binding and hydrolysis of crystalline chitin (Watanabe *et al.*, 2001; Uchiyama *et al.*, 2001).

In this study, point mutations of Ser33, Trp70, Trp231, and Tyr245 were carried out by site-directed mutagenesis and effects of the mutations on chitin binding and catalytic activities were investigated with various chitin derivatives. The results obtained from the chitin binding assays displayed a decrease in the binding activity of the mutants S33A, W70A, and Y245W to various extents. However, the most severe effect was observed with W70A. A time course study showed that both binding and hydrolytic activities of W70A towards colloidal chitin were completely abolished, while the activities were retained in other mutants. A remarkable loss of the specific activity as well as the rate of enzyme turnover (k_{cat}) of the mutant W70A could be

explained by a loss of the binding affinity due to a substitution of Trp to Ala and an associated change in hydrophobic interactions of this residue. The results strongly suggested that Trp70 was the major determinant for insoluble chitin binding. Similar results were seen for residue Ser33, but to a lesser extent. Mutation of Ser33 to Ala also showed decreased binding activity, while its mutation to Trp improved the binding activity. This finding provided additional evidence that binding of a chitin chain to ChBD cooperatively takes place via hydrophobic interactions and is influenced by the molecular setting in this region. The most striking observations were made with Trp231. As demonstrated by the modeled 3D-structure (Figure 3.1), Trp231 is found at the edge of the catalytic surface, thereby lying close to the glycone part of the substrate binding cleft. The observed improvement in the binding efficiency of mutant W231A could be explained as a removal of the side-chain blockage. Hence, reduced specific activity of mutant W231A was unlikely influenced by changes in binding activity as a result of the alanine substitution of Trp231. Apparently, the same phenomenon was previously recognized in *S. marcescens* chitinase A (Uchiyama *et al.*, 2001), with which a mutation of Phe232 to Ala seriously diminished the hydrolytic activity but left the binding activity to both colloidal chitin and β -chitin microfibrils unchanged. When the next residue in line (Tyr245) was mutated to a bulkier side-chain (Trp), inverse effects (reduced binding but improved hydrolysis) were observed. This complimented the idea of the binding barrier around the entrance hall of the catalytic domain by Trp231 and Tyr245. Similar findings were also recognized with a cellulose degrading enzyme, *Thermobifida fusca* endoglucanase (Cel9A) (Li *et al.*, 2007).

The study reported that mutations of the surface-exposed cellulose binding residues Arg557 and Glu559 to Ala (mutant R557A/E559A) caused a severe loss in hydrolytic activity against crystalline cellulose, but a change in the binding activity was not at all observed. Residues Arg557 and Glu559 are found on the surface of the cellulose binding module (CBM), closest to the catalytic binding cleft of Cel9A. Therefore, the effects of Arg557 and Glu559 could be explained in analogy to those of Trp231 and Tyr245 in *V. harveyi* chitinase A. In marked contrast, observations made with the *Vibrio* Trp231 mutation were different to the studies of Li *et al.* on *A. caviae* Chi 1 (Li *et al.*, 2005) and of Watanabe *et al.* on *B. circulans* Chi A1 (Watanabe *et al.*, 2001). Mutations of Trp232 and Trp245 (in *A. caviae* Chi1) or Trp122 and Trp134 (in *B. circulans*) to alanine resulted in a marked loss in both binding and hydrolyzing activities, especially against crystalline β -chitin. Therefore, the reduced hydrolytic activities were likely associated with the weaker binding of the two corresponding residues. Based on their mutational data, the residues seem to participate directly in binding to crystalline chitin, and subsequently cooperatively assisting the chitin chain to penetrate through the catalytic cleft of *A. caviae* or *B. circulans* chitinase. The above-mentioned event that took place in the *A. carviae* and *B. circulans* chitinases did not seem to be the case for the *V. harveyi* chitinase A due to different behaviors of Trp231 and Tyr245 found for the *Vibrio* enzyme. Here, the data suggested that a possible action of *V. harveyi* chitinase A on insoluble chitin could proceed as follows: 1) Initial binding of a chitin chain to the ChBD. This process is mostly influenced by hydrophobic interactions set between the incoming sugar and the residue Trp70, which is located at the doorway of the ChBD: 2) Further binding of GlcNAc units. However, binding through Ser33 remains inconclusive,

since the mutational results revealed that Ser33 did not act as a powerful binding residue. Alternatively, this binding step might be made through a different surface-exposed aromatic residue located nearby and 3) Sliding of the bound sugar units of the chitin chain into the substrate binding cleft. Based on the “slide and bend” mechanism proposed by Watanabe and others (Watanabe *et al.*, 2001; Imai *et al.*, 2002 and Watanabe *et al.*, 2003), the sliding process is achieved by cooperative interactions with other surface-exposed aromatic residues located close to the entrance of the substrate binding cleft. However, our data strongly suggest that the chitin chain movement most likely takes place via interactions with different surface-exposed aromatic residues other than Tyr245 and Trp231. When *p*NP-GlcNAc₂ was used as a substrate, hydrolyzing activities of the mutated enzymes and the wild-type enzyme were almost indistinguishable. This observation and the essentially unchanged catalytic efficiency (k_{cat}/K_m) of all mutants compared to the wild-type enzyme clearly pointed out that Ser33, Trp70, Trp231, and Tyr245 do not play a major role in the process of hydrolysis of soluble chitooligosaccharides.

4.2 High throughput screening of the chitinase inhibitors from the LOPAC library

Potential chitinase inhibitors were initially screened from the Library of Pharmacologically Active Compounds (LOPAC) using the *p*NP assay, which *p*NP-GlcNAc₂ was used as substrate. Such compounds were commercially available from Sigma-Aldrich Ltd. Initial screening identified nine hits out of 1,280 namely chelerythrine (CHE), dequalinium (DEQ), idarubicin (IDA), 2-(imidazolin-2-yl)-5-isothiocyanatobenzofuran (IMI), pentoxifylline (PEN), propentofylline (PRO),

sanguinarine (SAN), 2-bromo- α -ergocryptine methanesulfonate (BRO) and methysergide maleat (MET).

All of these compounds are drugs readily used for treatment of various forms of human diseases. For an example, dequalinium has antiseptic effect against a wide range of bacteria, yeast, fungi and viruses (Kaufman, 1981; D'Auria *et al.*, 1989). Dequalinium is the active ingredient of several medications. Its commercial form, such as Dequadin®, is used for treatment of mouth and throat infections, while Fluomizin® is used for relieving vaginal bacterial conditions (Della *et al.*, 2002). This compound has been later investigated as a safe and effective agent for treatment of malaria (Rodrigues and Gamboa, 2007; Rodrigues and Gamboa, 2008). Other compounds, such as idarubicin is an antileukemic drug (Fukushima *et al.*, 1994), pentoxifylline is used for treatment of vascular diseases since 1984 (Huh *et al.*, 1985), and sanguinarine and chelerythrine are found to induce apoptotic cell death and are administrated as anti-cancer agents (Malíková *et al.*, 2006).

After the first round of screening, the nine compounds as mentioned above were subjected for further screening to confirm their binding affinities by the DMAB assay using GlcNAc₆ as substrate. The second screening displayed IC_{50} of seven compounds (DEQ, IDA, CHE, PEN, PRO, SANG, and IMI) less than 100 μ M, whereas MET showed very weak inhibition and BRO showed no inhibition effected (Table 3.3). Note that from the seven compounds, PEN was the only compound reported previously to possess the inhibitory effect against the activity of a fungal chitinase (*AfChiB1*) (Rao *et al.*, 2005A).

4.3 Crystallization of *VhChiA* and mutants W275G and W397F

Structural determination of *VhChiA* in complex with the newly identified inhibitors was performed. Previous structural data revealed that Trp275 and Trp397 were located near subsites +1 and +2 in the substrate binding cleft and their hydrophobic faces stacked against the heterocyclic rings of the corresponding sugar units (Sonsirittigul *et al.*, 2008).

In 2009, Suginta *et al.*, proposed that Trp275 and Trp397 were important for the feeding process of chitin polymer pulling the chitin chain towards subsites +1 and +2, thereby permitting the next progressive hydrolysis to occur. In addition, the kinetic studies using quantitative HPLC ESI MS/MS with two soluble substrates (GlcNAc₅ and GlcNAc₆) revealed that substitution of Trp275 to Gly and Trp397 to Phe significantly shifted the anomeric selectivity of *VhChiA* by increasing the apparent rate of the β anomer consumption. Steady-state kinetics of the hydrolytic activity of the wild-type chitinase A and mutants W275G and W397F revealed that W275G reduced the catalytic rate (k_{cat}) and the substrate specificity ($k_{\text{cat}}/K_{\text{m}}$) towards all the substrates by five to tenfold. In contrast, mutant W397F weakened the binding strength at subsite (+2), thereby speeding up the rate of the enzymatic cleavage towards soluble substrates but slowing down the rate of the progressive degradation towards insoluble chitin (Suginta *et al.*, 2007; Suginta *et al.*, 2009). Therefore, the two mutants seem to be good candidates for studying the protein-ligand binding behaviors around the aglycone binding sites in parallel with wild-type enzyme.

Conditions for *VhChiA* crystallization were initially screened using the microbatch under oil technique and further optimized by the hanging drop vapor diffusion method. In the later steps of crystal optimization, microseeding (either

streak seeding or pipetting technique) was employed to obtain high quality single crystals. After several rounds of optimization, single crystals of the wild-type enzyme were obtained from two conditions: 1) 16% (w/v) PEG 4000, 21% (v/v) propanol, 0.1 M sodium citrate tribasic dihydrate, pH 5.6, and 2) 1.1 M ammonium sulfate, 0.1 M Tris-HCl, pH 8.5. The second condition was similar with the condition used for crystallization of the wild-type *VhChiA* as described previously (1.2 M ammonium sulphate in 0.1 M Tris-HCl, pH 8.0) (Songsiritthigul *et al.*, 2008). The crystals grown under these two conditions were soaked with the inhibitors without cracking. However, soaking the crystals with DEQ and PRO did not yield visible electron density of the two compounds, due to a poor solubility property of DEQ and a weak binding affinity of PRO. Therefore, their structural complexes were obtained by co-crystallization technique instead.

The crystals of wild-type enzyme grown under the above mentioned conditions had well-defined morphology and diffracted well after the annealing were performed. The wild-type crystals diffracted to the resolutions between 1.16 to 2.22 Å. The highest resolution of 1.16 Å was obtained from the crystal of the wild-type complexed with PRO.

Eight complexes of the wild-type with the inhibitors were successfully solved. Of all, six structural complexes of the wild-type and IDA, SAN, CHE, and IMI were obtained from crystal soaking, whereas the crystal complexes of WT-DEQ and WT-PRO were obtained from co-crystallization from condition containing 16% (w/v) PEG 4000, 21% (v/v) propanol in 0.1 M sodium citrate tribasic dihydrate, pH 5.6. The other two structural complexes: WT-PEN and the second structure complex of

WT-IMI were obtained from crystal soaking under the condition 1.1 M ammonium sulfate in 0.1 M Tris-HCl, pH 8.5.

All the crystal complexes of the wild-type with inhibitors belonged to the primitive monoclinic space group $P2_1$, which were a different form from the wild-type crystal reported in a previous study by Songsirittigul *et al.*, 2008, which belonged to the triclinic P_1 space group with unit cell of $a = 60.72 \text{ \AA}$, $b = 64.24 \text{ \AA}$, $c = 83.52 \text{ \AA}$, $\alpha = 91.74 \text{ \AA}$, $\beta = 91.18$, and $\gamma = 112.91 \text{ \AA}$.

In addition, the crystal complexes of wild-type with PEN and IMI obtained from the condition 1.1 M ammonium sulfate in 0.1 M Tris-HCl, pH 8.5 contained different unit cell dimensions ($a = 60.0 \text{ \AA}$, $b = 85.3 \text{ \AA}$, $c = 63.0 \text{ \AA}$, $\beta = 112.9 \text{ \AA}$) when compared to crystal complexes of wild-type with DEQ, SAN, CHE, and PRO obtained from the condition 16% (w/v) PEG 4000, 21% (v/v) propanol in 0.1 M sodium citrate tribasic dihydrate, pH 5.6 that gave the unit cell dimension: $a = 65.1 \text{ \AA}$, $b = 50.9 \text{ \AA}$, $c = 93.2 \text{ \AA}$, $\beta = 99.5 \text{ \AA}$ (Table 3.9). This could be explained by the effect of crystal packing from different crystal growth conditions.

After optimization, single crystals of W275G were obtained from the condition: 26% (w/v) PEG 4000 in 0.1 M sodium citrate tribasic dihydrate, pH 5.5. The crystals of W275G also diffracted well after an annealing step with the resolutions from 2.45 to 1.80 \AA . The highest resolution of 1.80 \AA was obtained from the crystal of the W275G complexed with PRO. After data processing, all the W275G crystals belonged to the orthorhombic space group $P2_12_12_1$ with the volumes of the asymmetric unit compatible with only one monomer. Six structural complexes of W275G with the inhibitors DEQ, SAN, CHE, PEN, PRO, and IMI were successfully obtained. W275G-IDA was the only complex missing from this study, as both soaking

and co-crystallization methods failed to give the electron density for this compound. This coincides with the W275G mutant having relatively low affinity for IDA with an IC_{50} of 270 μM , as shown in Table 3.3. The final refinement of the fourteen complexes of wild-type and mutant W275G were completed with R_{factor} values of 14.3% to 19.8% and R_{free} values of 17.7% to 25.9%, (Tables 3.9 and 3.13), indicating that all the modeled structures were well refined.

4.4 Inhibitory effects and binding mechanisms of the newly identified inhibitors against *VhChiA*

The equilibrium dissociation constants (K_D) and the half maximal inhibitory concentrations (IC_{50}), representing the inhibitory effects of the identified inhibitors against the wild-type *VhChiA* were determined using the fluorescence quenching assay and the DMAB assay. The K_D values obtained from the fluorescence quenching assay indicated that DEQ is the most active inhibitor with a K_D of 0.2 μM , followed by IDA, SAN, CHE, IMI, PEN, and PRO. Similar results were obtained with the same order of the binding affinities when the IC_{50} values were determined by the DMAB assay.

The IC_{50} values of the mutants W397F and W275G obtained from the *pNP* assay are about 10 and 100 times weaker than that of wild-type, respectively. For W275G, it can be explained by the elimination of hydrophobic interactions by the substitution of Trp275 to Gly, thus causing a dramatic decrease in the binding affinity. Mutation of Trp397 to Phe (mutant W397F) also showed a decrease in binding affinity, but its effects were less than mutant W275G (Table 4.1). The structures of the complexes of WT with inhibitors suggested that the main contact between the

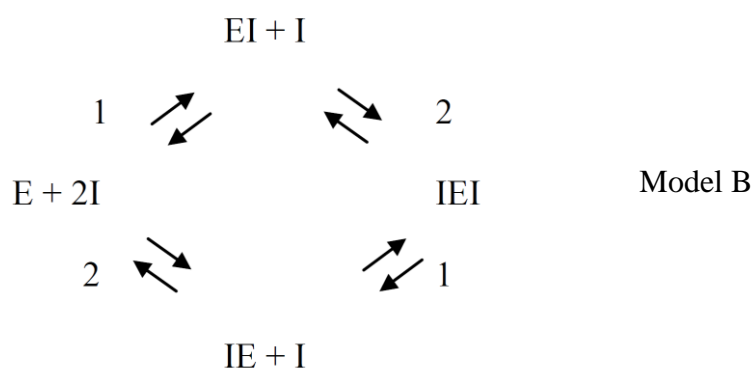
inhibitors and the enzyme around the aglycone binding sites was made by hydrophobic interactions with the indole ring of Trp275 (Figure 3.24). Both ITC and structural data support the idea that the binding site for the second inhibitor molecule was generated at the site of the missing indole ring of Trp275 at subsites +1/+2 after the first inhibitor molecule formed a stack against Trp397 (Figure 3.34). The data indicate that the binding affinity of the first inhibitor is likely to be stronger than the binding affinity of the presumed second site.

The effects of the inhibitor bindings on specific hydrolyzing activity are shown in Table 3.20. The results suggest that the inhibitors were more effective on the enzyme against insoluble substrates than soluble substrates as the inhibitory effects decreased following the order of the substrates used as $p\text{NP-GlcNAc}_2 > \text{GlcNAc}_6 > \text{colloidal chitin}$, respectively. This might reflect the accessibility of the enzyme's active site by the inhibitor molecules in a more random fashion (just like that of small chitooligosaccharides), rather than by a feeding process as observed for a chitin polymer.

When the ITC data were related to the data obtained from the dose-response curves and the structural data of the enzyme-inhibitor complexes, the binding behaviors of the inhibitors to the enzyme were classified in three different binding models. The first binding model presents a one-site-binding mechanism (model A). This model describes binding of one DEQ molecule to the wild-type enzyme (Figure 3.24DEQ). Analysis of the ITC data of DEQ bound to the wild-type confirmed a stoichiometry of $N = 1$ for one DEQ molecule bound to one enzyme molecule with a K_D of 70 nM.



The second binding mode (model B) is described by a two-independent-site binding mode which indicates two inhibitor molecules bind at two locations (aglycone and glycone). With this model, the first inhibitor molecule can bind either to site 1 (aglycone) as EI or to site 2 (glycone) to form the complex IE. A second inhibitor molecule binding to another non-occupied site will subsequently give the fully saturated complex IEI. This model corresponds to the structural complexes of the wild-type and the inhibitors SAN, PEN, PRO, and IMI. Since, no interpretable density of IDA and CHE was found at the glycone sites, model B was not verified for binding of IDA and CHE to the wild-type enzyme.



From model B, two inhibitor molecules bind with different binding affinities with $K_D1 \neq K_D2$ (Table 3.21). The structural data showed that the inhibitor bound to the aglycone sites is characterized by a well-defined electron density compared to the electron density of the other molecule at the glycone sites. Therefore, the aglycone

sites more likely act as stronger binding sites. Also, the inhibitor molecules tended to bind to the glycone subsites in different orientations such as two different orientations of IMI at the glycone sites were observed in the active site of wild-type enzyme (Figure 3.31A), indicating high flexibility of binding around the glycone sites. The model B also explains binding of two molecules of DEQ in the active site of W275G. For the W275G-DEQ complex, the first molecule occupied the position outside the glycone sites towards the ChBD, while the second molecule at the aglycone sites with its two head groups folded onto itself and behaved like two molecules as found for the other inhibitors bound to the aglycone sites of W275G.

The crystal structures of W275G with the inhibitors other than DEQ implied a completely different binding mode, in which the two binding sites are not independent. When the first inhibitor molecule has bound, a second molecule may form a stack with the first one. As such, a new binding site is created. The two dependent sites can be described using a two-sequential-site model as depicted in model C.



The ITC data representing binding of SAN and PEN to W275G were fitted successfully to model C. Although the same experimental finding could also be fitted to scheme B of a two-independent-sites model, the structural data showing a double sandwich of two inhibitor molecules and Trp397 at aglycone sites suggest that model C is the more likely mechanism.

Observation of only one PRO molecule being stacked against Trp397 at the aglycone sites in the complex of W275G-PRO, indicates higher affinity of the binding at the site close to Trp397. In the structures of the complexes of W275G with inhibitors other than PRO, the second molecule subsequently occupied the presumed “low affinity” site, providing an indication of the cooperative binding behavior at the aglycone location.

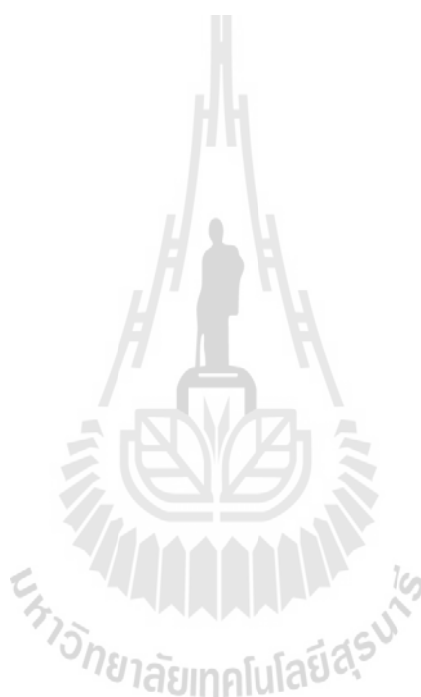


Table 4.1 IC_{50} and K_D values obtained from four different assays.

IC_{50} values (μM) were derived from competition studies with 100 μM chitohexaose in the DMAB assay (column 2), the *p*NP assay with *p*NP-GlcNAc₂ (column 5 and 9), and the *p*NP assay with *p*NP-GlcNAc₃ (column 7). Equilibrium dissociation constants (K_D , μM) derived from fluorescence quenching (Figure 3.38) are shown in column 3. The K_D values for wild-type chitinase and the mutants W275G and W397F in columns 4, 6 and 8 were derived from 3-parameter fits of the corresponding ITC experiments assuming one set of sites (model A). Values represent means \pm SD from at least three independent sets of the experiments.

1	2	3	4	5	6	7	8	9
	WT	WT	WT	WT	W275G	W275G	W397F	W397F
Inhibitor	IC_{50} DMAB	K_D Fluorescence	K_D ITC	IC_{50} <i>p</i> NP	K_D ITC	IC_{50} <i>p</i> NP	K_D ITC	IC_{50} <i>p</i> NP
DEQ	3.9 \pm 1.1	0.2 \pm 0.02	0.07	0.4 \pm 0.1	37	70 \pm 28	3.8	9 \pm 1
IDA	6.4 \pm 1.1	0.4 \pm 0.02	n.d. ^a	0.9 \pm 0.2	n.d.	270 \pm 33	n.d.	15 \pm 4
SAN	7.6 \pm 1.3	0.6 \pm 0.02	2.3	2.3 \pm 0.3	28	71 \pm 26	14	30 \pm 2
CHE	11 \pm 1.1	0.7 \pm 0.03	n.d.	2.2 \pm 0.01	n.d.	95 \pm 34	n.d.	48 \pm 4
IMI	21 \pm 1.5	1.0 \pm 0.1	n.d.	15 \pm 3.2	n.d.	160 \pm 78	n.d.	56 \pm 3
PEN	59 \pm 1.2	4.0 \pm 0.6	4.0	3.5 \pm 0.5	600	260 \pm 21	8.7	32 \pm 2
PRO	83 \pm 1.0	4.7 \pm 0.5	n.d.	3.7 \pm 0.9	n.d.	360 \pm 42	n.d.	66 \pm 5

n.d. = not determined.

4.5 A structural comparison between the WT-inhibitor complexes and W275G-inhibitor complexes

A summary of inhibitor bindings to wild-type and W275G is shown in Figure 4.1. The WT-inhibitor complexes revealed that most inhibitors bound at two hydrophobic areas in the active site of the wild-type enzyme. The first molecule bound at the aglycone sites was sandwiched by Trp397 and Trp275, while the second molecule at the glycone sites interacted mainly with Trp168 and Val205 via hydrophobic interactions. These binding behaviors were observed with the inhibitors SAN, PEN, PRO, and IMI in more or less similar places. In contrast, only one molecule of DEQ was bound in the active site of the wild-type enzyme, but its two 4-amino-2-methylquinolinium head group behaves like two inhibitor molecules, one of the aromatic head group occupied the aglycone sites and the other head group occupied the glycone sites (Figures 4.2A and 4.2B).

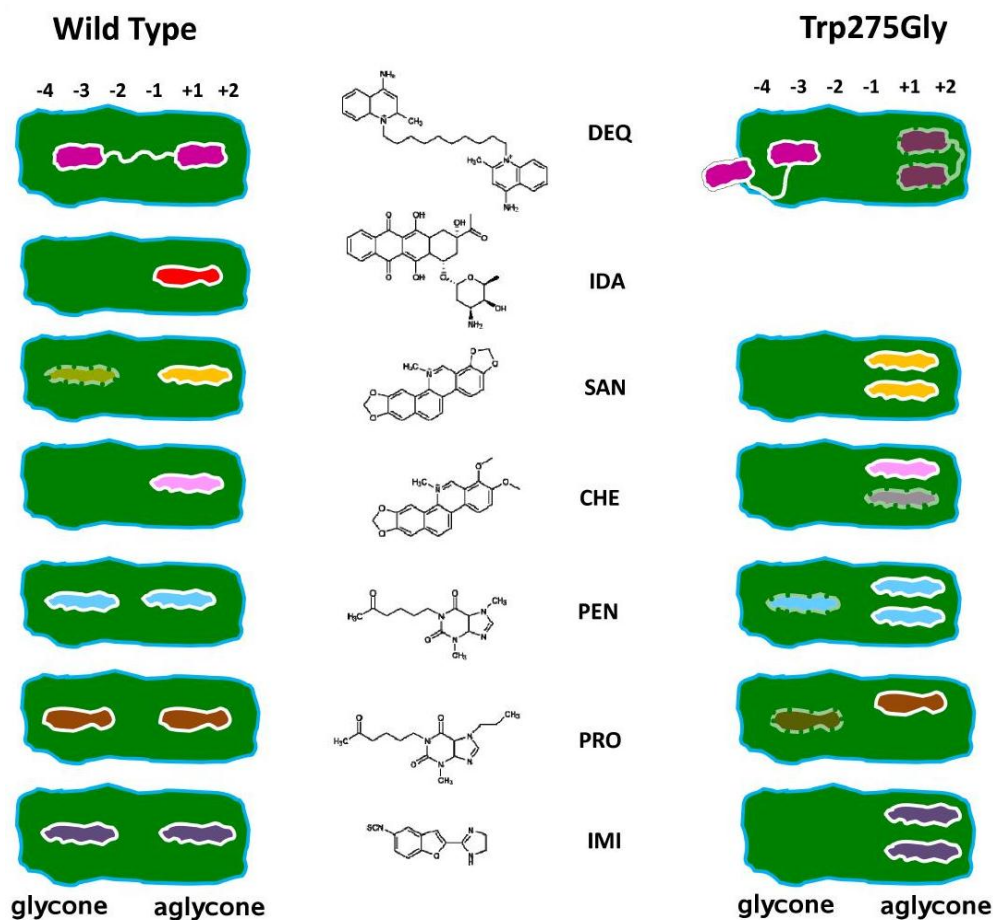


Figure 4.1 A summary of *VhChiA*-inhibitor interactions as revealed by crystallographic data.

W275G-IDA is the only missing structural complex. Only a single molecule of PRO was found in the aglycone sites of mutant W275G instead of two due to a possible steric clash as described in the text. Numbers -4, -3, -2, -1, +1, and +2 represent six substrate binding subsites of *VhChiA*, where subsite -4 is located at the glycone side and subsite +2 at the aglycone side. The inhibitor DEQ is indicated in magenta, IDA in red, SAN in yellow, CHE in pink, PEN in cyan, PRO in brown, and IMI in purple. The inhibitor molecules with very weak electron density are indicated as dashed lines.

The eliminated indole ring of Trp275 was found to significantly change the binding behavior of the enzyme. This was verified by the two inhibitor molecules forming a double stack with Trp397, one of which replaced the missing indole ring of Trp275 (Figure 4.2A). In the case of a W275G-PRO complex, only one molecule of PRO was found to stack against Trp397. This could be explained as a possible steric clash of the 7-propyl moiety that protrudes towards the site of the mutation of Trp275 to Gly. In case of binding of DEQ to W275G, its binding characteristic is notable for three reasons: 1) two DEQ molecules were bound to W275G, whereas only one molecule was bound in the active site of the wild-type enzyme (Figure 4.2B); 2) the first molecule of DEQ at aglycone sites of W275G behaved like two inhibitor molecules as its two 4-amino-2-methylquinolinium head groups folded onto itself; and 3) the second molecule of DEQ extended outside the active site towards the ChBD. Thorough inspection of the electron density map indicates that a third DEQ molecule may also bind, at the rear of the active site but its electron density is very weak.

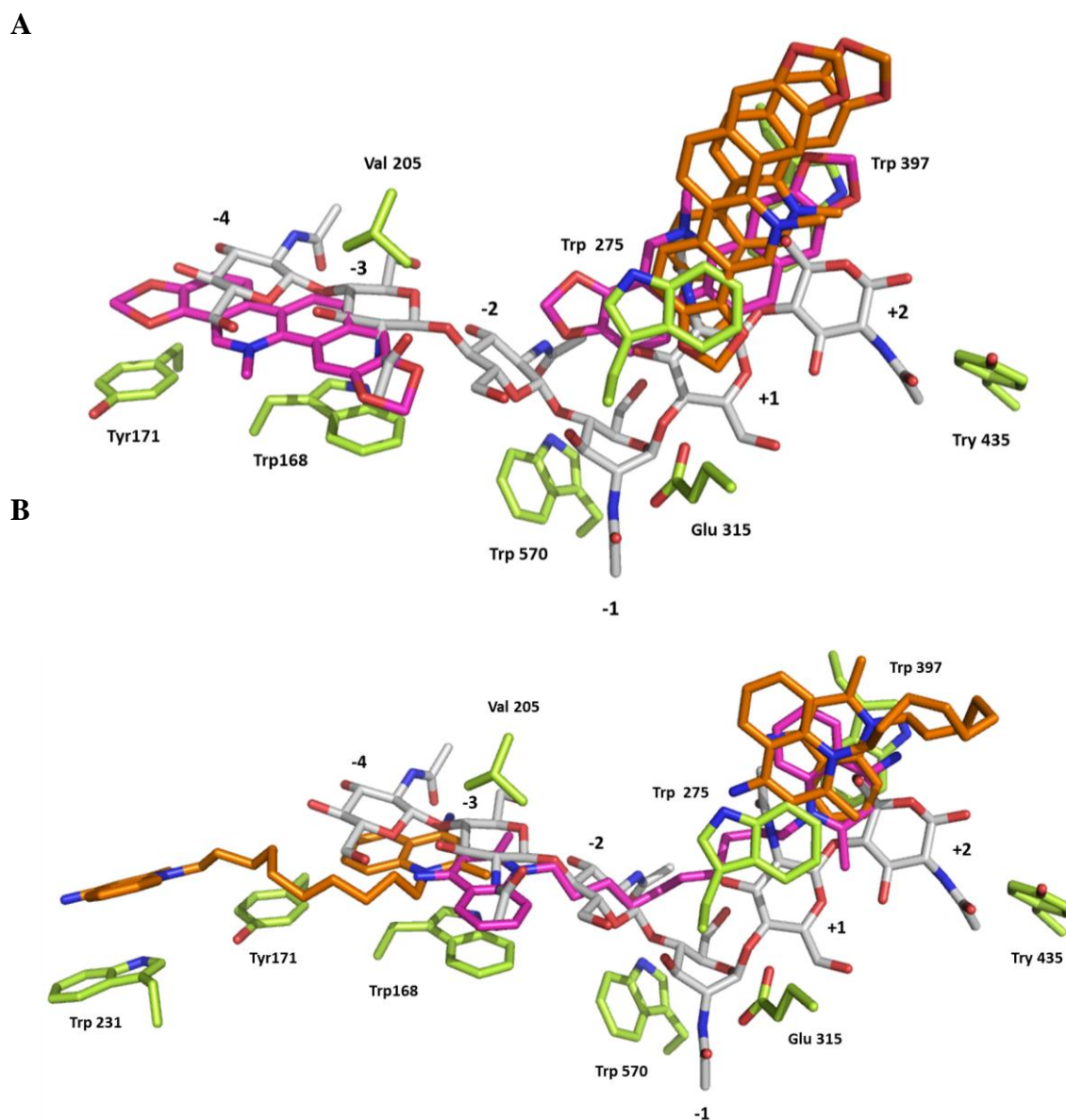


Figure 4.2 Different binding behaviors of the inhibitors in the active site of the wild-type and mutant W275G, comparing with the binding of GlcNAc₆.

Superposition of E315M- GlcNAc₆, with (A) WT or W275G with SAN; (B) WT or W275G with DEQ. The substrate binding residues, including catalytic residue (Glu315) are colored in green. Chitohexaose (GlcNAc₆) is colored in gray. The inhibitors bound with the wild type are shown in magenta, while the inhibitors bound with W275G are shown in orange.

The lack of occupancy around the glycone binding subsites as observed in the W275G is likely explained by backbone changes relative to the wild-type due to crystal packing. In wild-type, a loop containing Val205 forms one “wall” of the glycone side, and Trp168 acts as the counterpart on the other side. In the case of mutant W275G, the substrate binding cleft formed between those two residues is more open compared to the wild-type structures, thereby weakening the interactions of the potentially bound inhibitor molecules (Figure 4.3).



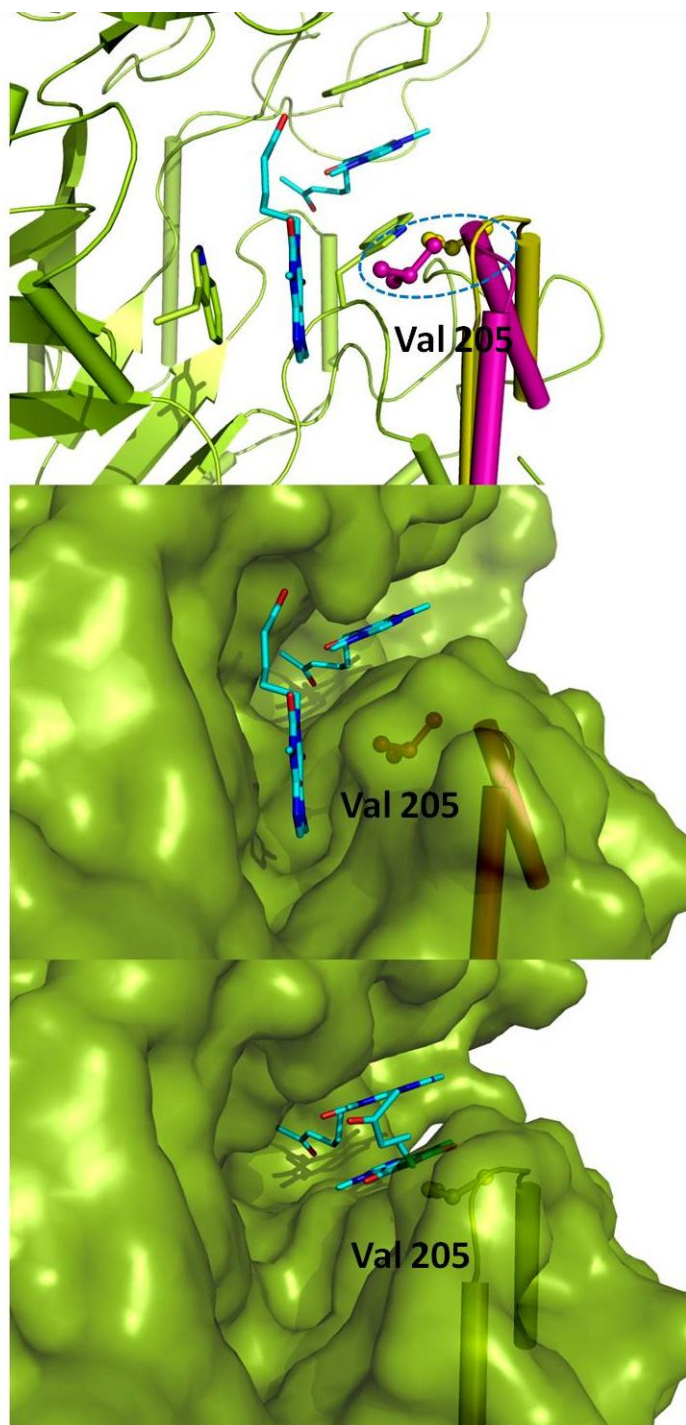


Figure 4.3 A comparison of the loop containing Val205 in the wild-type and the mutant W275G: Opening of the loop containing Val205 in the mutant due to changes in the backbone conformation leads to loss of potential interactions, thus empty the binding sites in the mutant structures.

4.6 A structural comparison between the wild-type bound with the substrate and with the the inhibitors.

The interactions of the enzyme to the identified inhibitors with *VhChiA* are entirely different from the interactions of the enzyme to the substrate GlcNAc₆. Bindings of the inhibitors are maintained exclusively at subsites -4, -3, -2, +1, and +2 by hydrophobic interactions with very few hydrogen bonds contributing to the binding affinity. Interactions of GlcNAc₆ within the substrate binding groove were made up by a number of hydrogen bonds and hydrophobic interactions with variable side-chains that surround the multiple binding sites. In addition, the transient sugar (-1GlcNAc) of the GlcNAc₆ chain embedded deeply at the bottom, where the cleavage site (between subsites -1 and +1) is located, while the inhibitor molecules were found to completely block the surface area of the active site.

In general, binding of all the inhibitors to the wild-type enzyme are associated tightly with two hydrophobic areas (the glycone area around subsites -4 to -2 and the aglycone area around subsites +1 and +2) (Figure 4.4A). The first inhibitor molecule at the aglycone sites was sandwiched by Trp397 and Trp275. The second inhibitor molecule at the glycone location interacted with the residues, Trp168 and Val205. Fluorescence titration of the intrinsic tryptophan with different concentrations of the inhibitors yielded significantly changes in the fluorescence intensity at emission wavelength between 330 - 350 nm, confirming that the tryptophan residues surrounding the active site play an important role in the inhibitor binding. A detailed comparison of interactions of the enzyme to the inhibitors and to the substrate GlcNAc₆ is clearly demonstrated as LIGPLOT (Figure 4.4B).

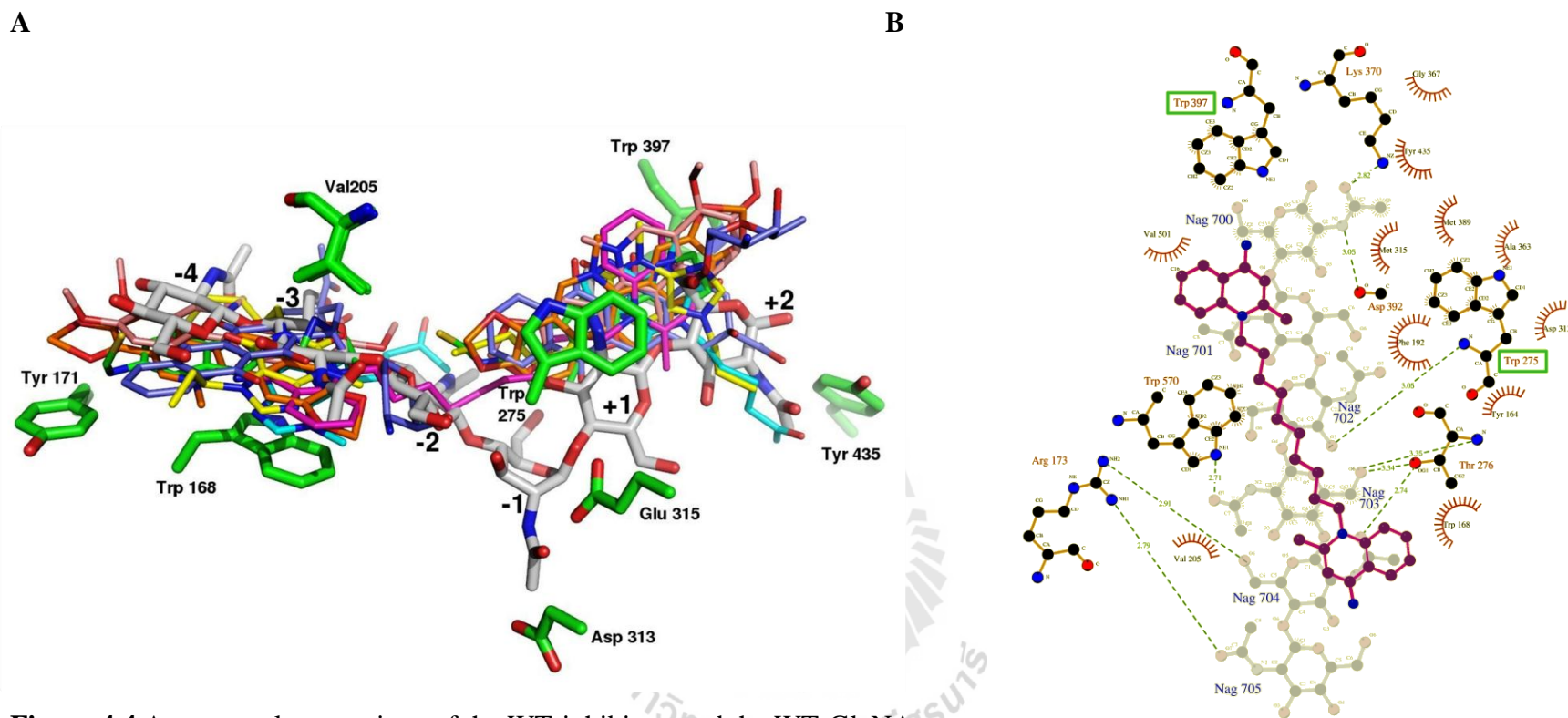


Figure 4.4 A structural comparison of the WT-inhibitors and the WT-GlcNAc₆.

(A) Superimposition of all the wild-type complexes with the inhibitors and the chitohexaose (shown in grey with the subsites labeled from (-4) to (+2) (B) The inhibitors are shown in magenta (DEQ), orange (SAN), cyan (PEN), yellow (PRO), red (CHE), green (IMI) and blue (IDA). The protein-ligand interaction of DEQ and chitohexaose was calculated by LIGPLOT.

4.7 Implications of structural and mechanistic studies of *VhChiA*-inhibitor complexes on therapeutics of asthma and inflammation

Recently, human acidic mammalian chitinase (AMCase), a family-18 chitinase homolog, was described in the serum of patients with asthma and allergic diseases (Donnelly *et al.*, 2004; Kawada *et al.*, 2007). This enzyme has been shown to contribute to the pathogenic process of such diseases through the recruitment of the inflammatory cells and a stimulation of the Th2 mediated immune responses (Mayumi *et al.*, 2007). For this reason, discovery of potent inhibitors against AMCase could offer an alternative for development of therapeutics against various forms of human inflammatory diseases.

Sequence analysis shows that AMCase (PDB code: 3FX Y) has 22% sequence identity to the CatD domain of *VhChiA*. Superposition of the CatD domain of *VhChiA* with the entire molecule of AMCase gave the R.M.S. deviation of 1.7 Å in the C α positions of 449 residues. Superposition of the 3D structure of AMCase with that of *VhChiA* showed that their active sites are relatively similar. The exception is that the loop containing Val205 in *VhChiA* is not present in AMCase. The aromatic residues (Tyr171, Trp168, Trp275, Trp397, and Trp570) that were identified to be the substrate binding residues of *VhChiA* are also found (Tyr34, Trp31, Trp99, Trp218, and Trp358, respectively) in AMCase. The catalytic residue Glu315 of *VhChiA* is seen as Glu140 in AMCase (Figure 4.5A). Fitting the electron density map of DEQ (the most effective inhibitor identified in this study) into the active site of AMCase (PDB code 3FX Y) could indeed accurately reproduce the binding mode found in *VhChiA* (Figure 4.5B). From a

chemical point of view, DEQ seems to be a good candidate for further development of an inhibitor-based drug against human allergic and other inflammatory diseases.

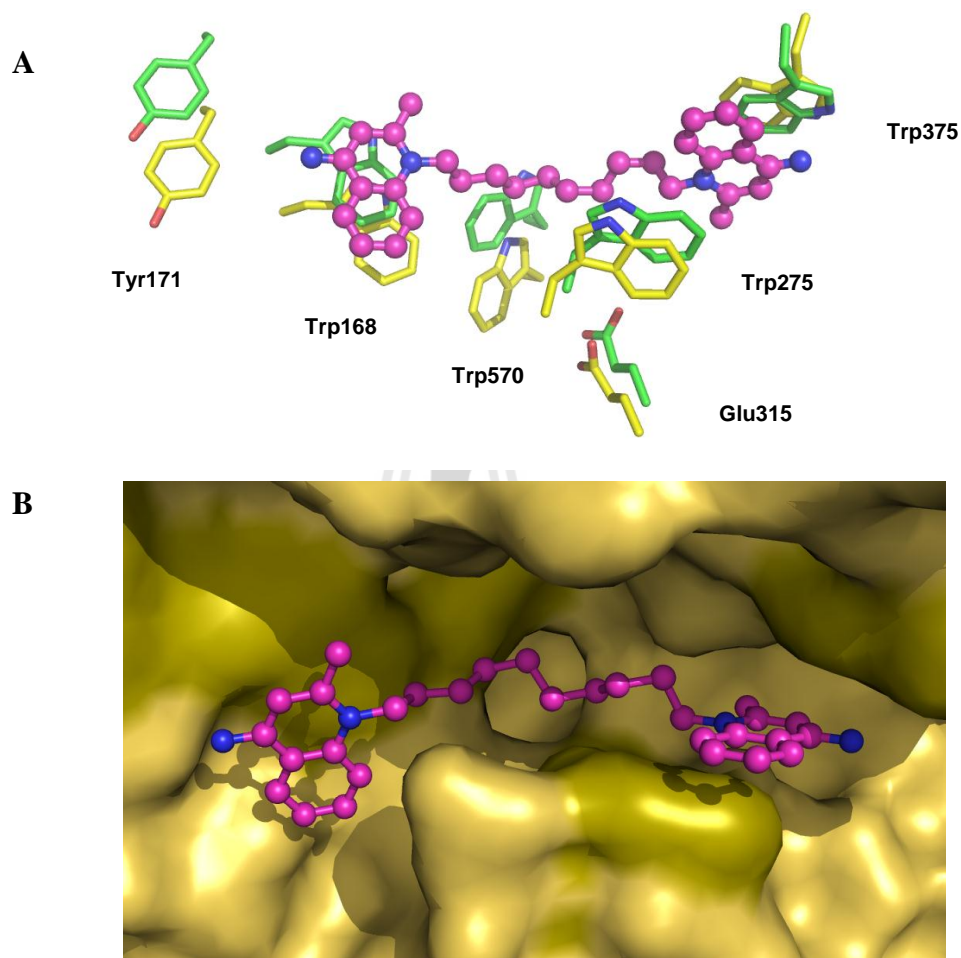


Figure 4.5 Superposition of structural complexes of WT-DEQ with the active site of AMCase.

(A) The stick model representation of active site superposition between AMCase and WE-DEQ. Carbon atoms of DEQ are shown in magenta. The binding residues of *VhChiA* and AMCase are shown in green and yellow, respectively. (B) Surface representation of the active site of AMCase superposed with WT-DEQ complex.

However, a comparison of the active site of *VhChiA* with that of the fungal chitinases (*AfChiB1*) (PDB code 2A3A for theophylline and 2A3C for PEN) and bacterial chitinases (*SmChiA*) PDB code 2WLY) gave less conserved binding residues in their active sites than the active site of human chitinase. Previous reports suggested that allosamidin derivatives (Rao *et al.*, 2003; Vaaje-Kolstad *et al.*, 2004), as well as theophylline, caffeine, and pentoxifylline (Rao *et al.*, 2005A) occupied active site of chitinase enzyme from subsites -3 to -1. Cyclopentapeptides, argifin and argadin occupied the subsites +1, -1, and -2 (Houston *et al.*, 2002B). While all the previously reported inhibitors mimick the reaction transition state (oxazolinium ion) by binding close to the critical subsite -1, all the inhibitors discovered in this study were found to occupy only the surface of the binding cleft of *VhChiA*.

Such findings suggest a novel concept for the synthesis of more potent chitinase inhibitors: i.e. two hydrophobic moieties like the quinolinium headgroups of dequalinium could be separated by a flexible linker with an allosamizoline analog at the perfect position to bind close to subsite -1. Such compounds should bind more tightly than either dequalinium or allosamidin alone. The inhibitors with high affinity and bifunctional, should be easy to compensate for small differences in the binding site by varying the lengths of the linker between the two hydrophobic moieties. An additional advantage is that this type of lead compound is not restricted to only one position in the active site, which offers more options for optimization.

CHAPTER IV

CONCLUSION

This research describes the enzyme-ligand interactions and the determination of the three dimensional structures of *Vibrio harveyi* chitinase A in complex with inhibitors newly identified from a commercially-available drug library. The studies are divided into two parts. The first part is focused on the investigation of the important roles of four conserved surface exposed residues located within or near the *N*-terminal ChBD. Site directed mutagenesis of such residues, including Ser33, Trp70, Trp231, and Tyr245, were carried out and then changes in binding and hydrolytic activities of *VhChiA* were assessed upon point mutations. Substitution of Trp70 to Ala caused a remarkable loss of binding and hydrolytic activities against soluble chitin, suggesting that Trp70, which is located at the *N*-terminal end of ChBD, is a crucial residue for insoluble chitin binding and hydrolysis. Ser33 located next to Trp70 also showed the effects in chitin binding and hydrolysis but to a lesser extent. The residues Trp231 and Tyr245, both located at the glycone binding subsites, were also involved in chitin hydrolysis as the substitution of Trp231 to Ala improved hydrolysis activity, whereas the mutation of Tyr245 to Trp showed inverse effects. Thus the aromatic side chains of Trp231 and Tyr245 cause a binding barrier around the entrance hall of the catalytic domain, instead of facilitating a chitin chain to get through the enzyme's active site.

The second part of this study involved identification of potential inhibitors for family-18 chitinases and determination of the enzyme-inhibitor binding mechanisms employing biochemical and protein crystallography approaches. Seven potent *VhChiA* inhibitors were identified from the LOPAC library using high throughput screening technique. Such compounds, including chelerythrine (CHE), dequalinium (DEQ), idarubicin (IDA), 2-(imidazolin-2-yl)-5-isothiocyanatobenzofuran methysergide (IMI), pentoxifylline (PEN), propentofylline (PRO), and sanguinarine (SAN), showed IC_{50} values as submicromolar concentrations, with dequalinium being the most potent inhibitor (K_i of 70 nM).

Crystallization experiments of *VhChiA* and mutants W275G and W397F were carried out by a microbatch method using commercially available screening kits. However, only crystallization of the wild-type enzyme and mutant W275G was successful. After optimization, single crystals of the wild-type enzyme were obtained from two conditions. The first condition was 16% (w/v) PEG 4000, 21% (v/v) propanol in 0.1 M sodium citrate tribasic dihydrate, pH 5.6, and the second condition was 1.1 M ammonium sulfate in 0.1 M Tris-HCl, pH 8.5. For the crystallization of W275G, single crystals were obtained from the condition containing 26% (w/v) PEG 4000 in 0.1 M sodium citrate tribasic dihydrate, pH 5.5. To obtain the structures of the complexes, the X-ray quality crystals of both wild-type and W275G were initially soaked with the seven potent inhibitors. Co-crystallization technique was also used if the electron density of inhibitors was not successfully obtained by the soaking experiment.

After collection of X-ray diffraction data collection and processing, the initial statistics revealed that the wild-type crystals belonged to the primitive monoclinic

space group $P2_1$ whereas the W275G crystals belonged to the orthorhombic space group $P2_12_12_1$. Both of the wild-type and W275G crystals contained the volumes of the asymmetric unit compatible with only one subunit.

The refined models of all the structures gave good fit with their electron density maps with average B-factor values of protein atoms between 12.1 \AA^2 and 23.3 \AA^2 . The refinement of all structures were completed with *R*-factor values of 14.3% to 19.8% and free *R*-factor values of 17.7% to 25.9%. These values indicate that all the structures were well refined. The geometry of the refined models was well verified and indicated most of the residues in the polypeptide chain are in the most favored regions. No residues lay in the disallowed Ramachandran regions.

These studies yielded two structures of the wild-type and W275G in apoform and fourteen structural complexes of wild-type and W275G with the newly identified inhibitors. Even though soaking and co-crystallization were tried, both methods failed to obtain the electron density of IDA. Therefore, W275G-IDA is the only missing complex in this study.

All *VhChiA*-inhibitor complexes revealed that the inhibitor molecules only occupied the upper part of the substrate binding cleft in two hydrophobic areas (glycone area around subsites -4 to -2 and the aglycone area around substies +1 and +2). In the wild-type enzyme, the interactions of the first inhibitors at the aglycone sites showed a clearly defined inhibitor density, and that the inhibitor was sandwiched by two important residues, Trp397 and Trp275. At the glycone sites, the second inhibitor molecule was found to interact with two consensus residues, Trp168 and Val205, with an ill-defined density and high B factor values, indicating lower affinity of binding at the glycone location.

For the structures of the complexes of W275G-inhibitors binding at the glycone sites, the electron density was even weaker than in the wild type. In the mutant complexes, the second molecule of the inhibitors (SAN, CHE, and IMI) was not observed at the glycone sites, but found to form a double sandwich with Trp397 and the first molecule of the inhibitors instead. Mutation of Trp to Gly significantly decreases the binding affinities and increases the IC_{50} values up to 300 times of the wild-type's values. The weakened affinities of the mutant W275G is likely due to the missing hydrophobic side chain of Trp275.

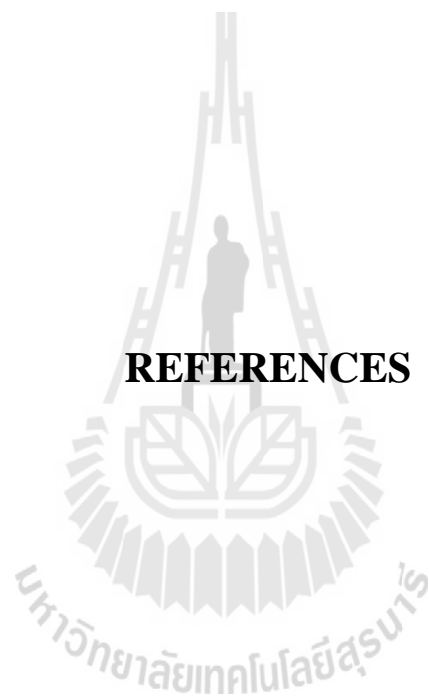
In good agreement with the structural data, the ITC data suggest that three different binding models for the occupation of the inhibitors in the active site of *VhChiA*. A single-site binding mode corresponds to the binding of one molecule of DEQ to the wild-type. A two-independent-site binding mode corresponds to binding of two molecules of the inhibitors to two locations (one at the glycone location and the other one at the aglycone location) of the wild-type enzyme. This binding mode is applicable for binding of two molecules of DEQ to the active site of W275G. For a two-sequential-site binding model, it corresponds to the structural complexes of the W275G-inhibitors displayed by two molecules of the inhibitors that formed a double sandwich between Trp397-inhibitor1-inhibitor2.

From previous reports, bindings of the known inhibitors to family-18 chitinases mimicked the reaction intermediate by part of the inhibitor molecules occupying deeply at the bottom of the substrate binding groove, mostly only one molecule being found to bind around subsites -3 to -1 or -2 to +1. In contrast, the newly identified inhibitors were shown to occupy on the upper part of the substrate binding cleft in two hydrophobic areas. This finding suggests a novel concept for the

synthesis of more potent chitinase inhibitors that includes two hydrophobic moieties separated by a flexible linker with an allosamizoline analog at the perfect position to bind close to subsite -1.

Superimposition of a human acidic mammalian chitinase (AMCase; a family-18 chitinase homolog) to *VhChiA*-inhibitor complexes showed that the active site of AMCase is very similar to *VhChiA* and that all the inhibitors were fitted reasonably well in the active site of the AMCase. Such data imply a potential development of the inhibitors identified in this study, as a therapeutic candidate for treatment of several forms of inflammatory diseases.





REFERENCES

REFERENCES

- Andersen, M. D., Jensen, A., Robertus, J. D., Leah, R., and Skriver, K. (1997). Heterologous expression and characterization of wild type and mutant forms of a 26-kDa endochitinase from barley (*Hordeum vulgare*). **The Biochemical Journal** 322: 815-822.
- Andersen, O. A., Nathubhai, A., Dixon, M. J., Eggleston, I. M., and van Aalten, D. M. F. (2008). Structure-based dissection of the natural product cyclopentapeptide chitinase inhibitor argifin. **Chemistry and Biology** 15: 295-330.
- Arai, N., Shiomi, K., Yamaguchi, Y., Masuma, R., Iwai, Y., Turberg A., Koelbl, H., and Omura, S. (2000). Argadin, a new chitinase inhibitor, produced by *Clonostachys* sp. FO-7314. **Chemical and Pharmaceutical Bulletin** 48: 1442-1446.
- Armand, S., Tomita, H., Heyraud, A., Gey, C., Watanabe, T., and Henrissat, B. (1994). Stereochemical course of the hydrolysis reaction catalyzed by chitinases A1 and D from *Bacillus circulans* WL-12. **FEBS Letters** 343: 177-180.
- Aronson, N. N., Halloran, B. A., Alexyev, M. F., Amable, L., Madora, J. D., Pasupulati, L., Worth, C., and van Roey, P. (2003). Family 18 chitinase-oligosaccharide substrate interaction: subsite preference and anomer selectivity of *Serratia marcescens* chitinase A. **The Biochemical Journal** 15: 87-95.

- Balsubramaniam, N., Juliet, A., Srikalaivani, P., and Lalithakumari, D. (2003). Release and regeneration of protoplasts from the fungus *Trichothecium roseum*. **Canadian Journal of Microbiology** 49: 263-268.
- Bhatnagar, R. K., Arora, N., Sachidanand, S., Shahabuddin, M., Keister, D., and Chauhan, V. S. (2003). Synthetic propeptide inhibits mosquito midgut chitinase and blocks sporogonic development of malaria parasite. **Biochemical and Biophysical Research Communications** 304: 783-787.
- Blaak, H. and Schrempf, H. (1995). Binding and substrate specificities of a *Streptomyces olivaceoviridis* chitinase in comparison with its proteolytically processed form. **European Journal of Biochemistry** 229: 132-139.
- Blattner, R., Furneaux, R. H., and Lynch, G. P. (1996). Synthesis of allosamidin analogues. **Carbohydrate Research** 294: 29-39.
- Blattner, R., Gerard, P. J., and Spindler Barth, M. (1997). Synthesis and biological activity of allosamidin and allosamidin analogues. **Pesticide Science** 50: 312-318.
- Boller, T. and Mauch, F. (1988). Colorimetric assay for chitinase. **Methods in Enzymology** 161: 430-435.
- Bortone, K., Monzingo, A. F., Ernst, S., and Robertus, J. D. (2002). The structure of an allosamidin complex with the *Coccidioides immitis* chitinase defines a role for a second acid residue in substrate-assisted mechanism. **Journal of Molecular Biology** 320: 293-302.
- Bradford, M. M. (1976). A rapid and sensitive method for the quantitation of microgram quantities of protein utilizing the principle of protein-dye binding. **Analytical Biochemistry** 72: 248-254.

- Brameld, K. A., Shrader, W. D., Imperiali, B., and Goddard, III W. A. (1998). Substrate distortion to a boat conformation at subsite -1 is critical in the mechanism of family 18 chitinases. **Journal of Molecular Biology** 280: 913-923.
- Breborowicz, A., Polubinska, A., Wu, G., Tam, P., and Oreopoulos, D. (2006). *N*-Acetylglucosamine reduces inflammatory response during acute peritonitis in uremic rats. **Blood Purification** 24: 274-281.
- Bruce, A., Srinivasan, U., Staines, H. J., and Highley, T. L. (1995). Chitinase and laminarinase production in liquid culture by *Trichoderma sp.* and their role in biocontrol of wood decay fungi. *International Biodeterioration Association; Biodeterioration Society* 35: 337-353.
- Brurberg, M. B., Nes, I. F., and Eijsink, V. G. H. (1996). Comparative studies of chitinases A and B from *Serratia marcescens*. **Microbiology** 142: 1581-1589.
- Brünger, A. T., Kuriyan, J., and Karplus, M. (1987). Crystallographic R factor refinement by molecular dynamics. **Science** 235: 458-460.
- Cantarel, B. L., Coutinho, P. M., Rancurel, C., Bernard, T., Lombard, V., and Henrissat, B. (2009). The Carbohydrate-Active EnZymes database (CAZy): an expert resource for glycogenomics. **Nucleic Acids Research** 37: 233-238.
- Chang, W., Chen, Y., and Jao, C. (2007). Antifungal activity and enhancement of plant growth by *Bacillus cereus* grown on shellfish chitin wastes. **Bioresource Technology** 6: 1224-1230.
- Cohen, E. (1993). Chitin synthesis and degradation as targets for pesticide action. **Archives of Insect Biochemistry and Physiology** 22: 245-261.
- Collaborative Computational Project, Number 4. (1994). The CCP4 suit: Programs for

- Protein Crystallography. **Acta Crystallographica** D50: 760-763.
- Davies, G. and Henrissat, B. (1995). Structures and mechanisms of glycosyl hydrolases. **Structure** 3: 853-859.
- D'Auria, F. D., Simonetti, G., and Strippoli, V. (1989). Antimicrobial characteristics of a tincture of dequalinium chloride. **Annali di Igiene** 1: 1227-1241.
- Della Casa, V., Noll, H., Gonser, S., Grob, P., Graf, F., and Pohlig, G. (2002). Antimicrobial activity of dequalinium chloride against leading germs of vaginal infections. **Arzneimittel forschung** 52: 699-705.
- DeNardis, D., Yeomans, D., Borucki, L., and Philipossian, A. (2006). Characterization of copper-hydrogen peroxide film growth kinetics. **Thin Solid Films** 513: 311-318.
- Derek, C. C., Olland, A. M., Jacob, J., Brooks, J., Bursavich, M. G., Czerwinski, R., DeClercq, C., Johnson, M., Joseph-McCarthy, D., Ellingboe, J. W., Lin, L., Nowak, P., Presman, E., Strand, J., Tam, A., Williams, C. M. M., Yao, S., Tsao, D. H. H., and Fitz, L. J. (2010). Identification and characterization of acidic mammalian chitinase inhibitors. **Journal of Medicinal Chemistry** 53: 6122-6128.
- Dickinson, K., Keer, V., Hitchcock, C. A., and Adams, D. J. (1989). Chitinase activity From *Candida albicans* and its inhibition by allosamidin. **Journal of General Microbiology** 135: 1417-1421.
- Dixon, M. J., Andersen, O. A., van Aalten, D. M. F., and Eggleston, I. M. (2005). An efficient synthesis of argifin: a natural product chitinase inhibitor with chemotherapeutic potential. **Bioorganic & Medicinal Chemistry Letters** 15: 4717-4721.

- Dixon, M. J., Nathubhai, A., Andersen, O. A., van Aalten, D. M. F., and Eggleston, I. M. (2009). Solid-phase synthesis of cyclic peptide chitinase inhibitors: SAR of the argifin scaffold. **Organic and Biomolecular Chemistry** 21: 259-268.
- Donnelly, L. E. and Barnes, P. J. (2004). Expression of heme oxygenase in human airway epithelial cells. **Trends in Pharmacological Sciences** 25: 509-511.
- Emsley, P. and Cowtan, K. (2004). Coot: model-building tools for molecular graphics. **Acta Crystallographica Section D** 60: 2126-2132.
- Fukamizo, T., Koga, D., and Goto, S. (1995). Comparative biochemistry of chitinases. Anomeric form of the reaction product. **Bioscience Biotechnology and Biochemistry** 59: 311-313.
- Fukamizo, T. (2000). Chitinolytic enzymes: catalysis, substrate binding, and their application. **Current Protein and Peptide Science** 1: 105-124.
- Fukushima, T., Kawai, Y., Urasaki, Y., Yoshida, A., Ueda, T., and Nakamura, T. (1994). Influence of idarubicinol on the antileukemic effect of idarubicin. **Leukemia Research** 12: 943-947.
- Fusetti, F., von Moeller, H., Houston, D., Rozeboom, H. J., Dijkstra, B. W., Boot, R. G., Aerts, J. M., and van Aalten, D. M. F. (2002). Structure of human chitotriosidase. Implications for specific inhibitor design and function of mammalian chitinase-like lectins. **The Journal of Biological Chemistry** 277: 25537-25544.
- Fusetti, F., Pijning, T., Kalk, K. H., Bos, E., and Dijkstra, B. W. (2003). Crystal structure and carbohydrate-binding properties of the human cartilage glycoprotein-39. **The Journal of Biological Chemistry** 278: 37753-37760.

- Geng, M., Zhao, Y., Bai, X., Liu, Y., Green, T.J. Luo, M., and Zheng, X. (2010). Structure of human stabilin-1 interacting chitinase-like protein (SI-CLP) reveals a saccharide-binding cleft with lower sugar-binding selectivity. **The Journal of Biological Chemistry** 285: 39898-39904.
- Hardta, M. and Roger, A. (2004). Mutation of active site residues in the chitin-binding domain ChBDChiA1 from chitinase A1 of *Bacillus circulans* alter substrate specificity: use of a green fluorescent protein binding assay. **Archives of Biochemistry and Biophysics** 426: 286-297.
- Hart, P. J., Puger, H. D., Monzingo, A. F., Hollis, T., and Robertus, J. D. (1995). The refined crystal structure of an endochitinase from *Hordeum vulgare* seeds at 1.8 Å resolution. **Journal of Molecular Biology** 248: 402-413.
- Hashimoto, M., Ikegami, T., Seino, S., Ohuchi, N., Fukada, H., Sugiyama, J., Shirakawa, M., and Watanabe, T. (2000). Expression and characterization of the chitin-binding domain of chitinase A1 from *Bacillus circulans* WL-12. **Journal of Bacteriology** 182: 3045-3054.
- Henrissat, B. (1991). A classification of glycosyl hydrolases based on amino acid sequence similarities. **The Biochemical Journal** 280: 309-310.
- Henrissat, B. and Davies, G. J. (2000). Glycoside hydrolases and glycosyltransferases. Families, modules, and implications for genomics. **Plant Physiology** 124: 1515-1519.
- Hiroshi, T., Hideyuki, O., Nao, B., Masahiro, M., Katsushiro, M., Masahide, Y., and Yoshihiko, I. (2002). Identification and characterization of the gene cluster involved in chitin degradation in a marine bacterium, *Alteromonas* sp. strain O-7. **Applied Environmental and Microbiology** 68: 263-270.

- Honda, Y., Tanimori, S., Kirihata, M., Kaneko, S., Tokuyasu, K., Hashimoto, M., Watanabe, T., and Fukamizo, T. (2000). Kinetic analysis of the reaction catalyzed by chitinase A1 from *Bacillus circulans* WL-12 toward the novel substrates, partially *N*-deacetylated 4-methylumbelliferyl chitobiosides. **FEBS Letters** 476: 194-197.
- Horn, S.J., Sørbotten, A., Synstad, B., Sikorski, P., Sørli, M., Vårum, K. M., and Eijsink, V. G. H. (2006). Endo/exo mechanism and processivity of family 18 chitinases produced by *Serratia marcescens*. **FEBS Journal** 273: 491-503.
- Hurtado-Guerrero, R. and van Aalten, D. M. F. (2007). Structure of *Saccharomyces cerevisiae* chitinase 1 and screening-based discovery of potent inhibitors. **Chemistry and Biology** 14: 589-599.
- Hult, E. L., Katouno, F., Uchiyama, T., Watanabe, T., and Sugiyama, J. (2005). Molecular directionality in crystalline beta-chitin: hydrolysis by chitinases A and B from *Serratia marcescens* 2170. **The Biochemical Journal** 388: 851-856.
- Houston, D. R., Eggleston, I., Synstad, B., Eijsink, V. G. H., and van Aalten, D. M. F. (2002A). The cyclic dipeptide CI-4 inhibits family 18 chitinases by structural mimicry of a reaction intermediate. **The Biochemical Journal** 368: 23-27.
- Houston, D. R., Shiomi, K., Arai, N., Omura, S., Peter, M. G., Turberg A., Synstad B., Eijsink, V. G. H., and van Aalten, D. M. F. (2002B). High-resolution structures of a chitinase complexed with natural product cyclopentapeptide inhibitors: Mimicry of carbohydrate substrate. **Proceedings of the National Academy of Sciences of the United States of America** 99: 9127-9132.

- Houston, D. R., Recklies, A. D., Krupa, J. C., and van Aalten, D. M. F. (2003). Structure and ligand-induced conformational change of the 39-kDa glycoprotein from human articular chondrocytes. **The Journal of Biological Chemistry** 278: 30206-30212.
- Houston, D. R., Synstad, B., Eijsink, V. G. H., Stark, M. J. R., Eggleston, M., and van Aalten, D. M. F. (2004). Structure-based exploration of cyclic dipeptide chitinase inhibitors. **Journal of Medicinal Chemistry** 47: 5713-5720.
- Huh, P. W., Kotasek, D., Jacob, H. S., Vercellotti, G. M., and Hammerschmidt, D. E. (1985). Mechanism of action of pentoxifylline in peripheral vascular disease: inhibition of platelet and granulocyte responsiveness. **Clinical Research** 33: 866-878.
- Ikegami, T., Okada, T., Hashimoto, M., Seino, S., Watanabe, T., and Shirakawa, M. (2000). Solution structure of the chitin-binding domain of *Bacillus circulans* WL-12 chitinase A1. **The Journal of Biological Chemistry** 275: 13654-13661.
- Ilnkovan, P., Hein, S., Ng, H. C., Trung, S. T., and Stevens, W. (2006). Production of *N*-Acetyl chitobiose from various chitin substrates using commercial enzymes. **Carbohydrate Polymers** 63: 245-250.
- Imai, T., Watanabe, T., Yui, T., and Sugiyama, J. (2002). Directional degradation of beta-chitin by chitinase A1 revealed by a novel reducing end labeling technique. **FEBS Letters** 510: 201-205.
- Iseli, B., Armand, S., Boller, T., Neuhaus, J. M., and Henrissat, B. (1996). Plant chitinases use two different hydrolytic mechanisms. **European Journal of Biochemistry** 11: 186-188.

- Itoh, Y., Watanabe, J., Fukada, H., Mizuno, R., Kezuka, Y., and Watanabe, T. (2000). Importance of Trp59 and Trp60 in chitin-binding, hydrolytic, and antifungal activities of *Streptomyces griseus* chitinase C. **Applied Microbiology and Biotechnology** 72: 1176-1184.
- Izumida, H., Imamura, N., and Sano, H. (1996). A novel chitinase inhibitor from a marine bacterium *Pseudomonas* sp. **Journal of Antibiotics** 49: 76-80.
- Je, J., and Kim, S. (2006). Antioxidant activity of novel chitin derivative. **Bioorganic and Medicinal Chemistry Letters** 16: 1884-1887.
- Jones, T. A., Zou, J. Y., Cowan, S. W., and Kjeldgaard, M. (1991). Improved method for building models in electron density maps and the location of errors in these models. **Acta Crystallographica** A47: 110-119.
- John, Hart P., Pfluger, H. D., Monzingo, A. F., Hollis, T., and Robertus, J. D. (1995). The refined crystal structure of an endochitinase from *Hordeum vulgare* L. seeds at 1.8 Å resolution. **Journal of Molecular Biology** 248: 402-413.
- John, M., Talent, M. S., and Robert, W. (1996). Pilot study of oral polymeric *N*-acetyl-*D*-glucosamine as a potential treatment for patients with osteoarthritis. **Clinical Therapeutics** 910: 1184-1190.
- Jones, J. D. G., Grady, K. L., Suslow, T. V., and Bedbrook, J. R. (1986). Isolation and characterization of genes encoding two chitinase enzymes from *Serratia marcescens*. **The EMBO Journal** 5: 467-473.
- Kabsch, W. (1993). The 2.2 Å crystal structure of the Ras-binding domain of the serine/threonine kinase c-Raf1 in complex with Rap1A and a GTP analogue. **Journal of Applied Crystallography** 26: 795-800.

- Kato, T., Shizuri, Y., Izumida, H., Yokoyama, A., and Endo, M. (1995). Styloguanidines, new chitinase inhibitors from the marine sponge *Stylotella aurantium*. **Tetrahedron Letters** 36: 2133-2136.
- Kawada, M., Hachiya, Y., Arihiro, A., and Mizoguchi, E. (2007). Chitinase 3-like-1 exacerbates intestinal inflammation by enhancing bacterial adhesion and invasion in colonic epithelial cells. **The Keio Journal of Medicine** 56: 21-27.
- Kaufman, A. Y. (1981). The use of dequalinium acetate as a disinfectant and chemotherapeutic agent in endodontics. **Oral Surgery, Oral Medicine, Oral Pathology, Oral Radiology, and Endodontology** 51: 434-441.
- Keyhani, N. O. and Roseman, S. (1999). Physiological aspects of chitin catabolism in marine bacterial. **Biochimica et Biophysica Acta** 1473: 108-122.
- Kim, S. and Rajapakse, N. (2005). Enzymatic production and biological activities of chitosan oligosaccharides (COS). **Carbohydrate Polymers** 62: 357-368.
- Koga, D., Isogai, A., Sakuda, S., Matsumoto, S., Suzukia, A., Kimura, S., and Ide, A. (1987). Specific inhibition of *Bombyx mori* chitinase by allosamidin. **Agricultural and Biological Chemistry** 51: 471-476.
- Koide, M. D. (1998). Chitin-chitosan: properties, benefits and risks. **Nutrition Research** 18: 1091-1101.
- Kolstad, G., Synstad, B., Eijsink, V. G. H., and van Aalten, D. M. F. (2002). Structure of the D140N mutant of chitinase B from *Serratia marcescens* at 1.45 Å resolution. **Acta Crystallographica Section D: Biological Crystallography** 58: 377-379.
- Kolstad, G., Houston, D. R., Rao, F. V., Peter, M. G., Synstada, B., van Aalten, D. M.

- F., and Eijsink, V. G. H. (2004). Structure of the D142N mutant of the family 18 chitinase ChiB from *Serratia marcescens* and its complex with allosamidin. **Biochimica et Biophysica Acta** 1696: 103-111.
- Kolstad, G. V., Houston, D. R., Riemen, A. H., Eijsink, V. G. H., and van Aalten, D. M. F. (2005). Crystal structure and binding properties of the *Serratia marcescens* chitin-binding protein CBP21. **The Journal of Biological Chemistry** 280: 11313-11319.
- Kumar, A. and Rao, M. (2010). A novel bifunctional peptidic aspartic protease inhibitor inhibits chitinase A from *Serratia marcescens*: Kinetic analysis of inhibition and binding affinity. **Biochimica et Biophysica Acta** 1800: 526-536.
- Laskowski, R. A., MacArthur, M. W., Moss, D. S., and Thornton, J. M. (1993). PROCHECK: a program to check the stereochemical quality of protein structures. **Journal of Applied Crystallography** 26: 283-291.
- Laemmli, U. K. (1970). Cleavage of structural proteins during the assembly of the head of bacteriophage T4. **Nature** 227: 680-685.
- Leslie, A. G. W. (1991). Recent changes to the MOSFLM package for processing film and image plate data. **Newsletters on Protein Crystallography** SERC Laboratory, Daresbury, UK.
- Linder, M. and Teeri, T. T. (1997). The roles and function of cellulose-binding domains. **Journal of Biotechnology** 57: 15-28.
- Li, Q., Wang, F., Zhou, Y., and Xiao, X. (2005). Putative exposed aromatic and hydroxyl residues on the surface of the N-terminal domains of Chi1 from

Aeromonas caviae CB101 are essential for chitin binding and hydrolysis.

Applied Environmental Microbiology 71: 7559-7561.

Li, Y., Irwin, D. C., and Wilson, D. B. (2007). Processivity, substrate binding, and mechanism of cellulose hydrolysis by *Thermobifida fusca* Cel9A. **Applied Environmental Microbiology** 73: 3165-3172.

Macdonald, J. M., Tarling, C. A., Taylor, E. J., Dennis, R. J., Myers, D. S., Knapp, S., Davies, G. J., and Withers, S. G. (2010). Chitinase inhibition by chitobiose and chitotriose thiazolines. **Angewandte Chemie International Edition** 49: 2599-2602.

Malíková, J., Zdarilová, A., Hlobilková, A., and Ulrichová, J. (2006). The effect of chelerythrine on cell growth, apoptosis, and cell cycle in human normal and cancer cells in comparison with sanguinarine. **Cell Biology and Toxicology** 22: 439-453.

Matthews, B. W. (1968). Solvent content of protein crystals. **Journal of Molecular Biology** 33: 491-497.

Matsumoto, T., Nonaka, T., Hashimoto, M., Watanabe, T., and Mitsui, Y. (1999). Three-dimensional structure of the catalytic domain of chitinase A1 from *Bacillus circulans* WL-12 at a very high resolution. **Proceedings of the Japan Academy** 75: 269-274.

Mayumi, K., Yuriko, H., Atsuko, A., and Emiko, M. (2007). Role of mammalian chitinases in inflammatory conditions. **The Keio Journal of Medicine** 56: 21-27.

- Merzendorfer, H. and Zimoch, L. (2003). Chitin metabolism in insects: structure, function and regulation of chitin synthases and chitinases. **The Journal of Experimental Biology** 206: 4393-4412.
- Montgomery, M. T. and Kirchman, D. L. (1993). Role of chitin-binding proteins in the specific attachment of the marine bacterium *Vibrio harveyi* to chitin. **Applied and Environmental Microbiology** 59: 373-379.
- Morimoto, K., Karita, S., Kimura, T., Sakka, K., and Ohmiya, K. (1997). Cloning, sequencing, and expression of the gene encoding *Clostridium paraputrificum* chitinase ChiB and analysis of the functions of novel cadherin-like domains and a chitin-binding domain. **Journal of Bacteriology** 179: 7306-7314.
- Miller, G. L. (1959). Use of dinitrosalicylic acid reagent for determination of reducing sugar. **Analytical Chemistry** 31: 426-429.
- Murshudov, G. N., Vagin, A. A., and Dodson, E. J. (1997). Refinement of macromolecular structures by the maximum-likelihood method. **Acta Crystallographica** D53: 240-255.
- Nakamura, T., Mine, S., Hagihara, Y., Ishikawa, K., and Uegaki, K. (2006). Structure of the catalytic domain of the hyperthermophilic chitinase from *Pyrococcus furiosus*. **Acta Crystallographica Section F: Structural Biology and Crystallization Communications** 63: 7-11.
- Navaza, J. (1994). Amore an automated package for molecular replacement. **Acta Crystallographica** A50: 157-163.
- Nishiyama, A., Tsuji, S., Yamashita, M., Henriksen, R., Myrvik, Q., and Shibata, Y. (2006). Phagocytosis of *N*-acetyl-*D*-glucosamine particles, a Th1 adjuvant, by

- RAW 264.7 cells results in MAPK activation and TNF- α , but not IL-10, production. **Cellular Immunology** 2: 103-112.
- Nishimoto, Y., Sakuda, S., Takayama, S., and Yamada, Y. (1991). Isolation and characterization of new allosamidins. **Journal of Antibiotics** 44: 716-722.
- Otwinowski, Z. and Minor, W. (1997). Processing of X-ray diffraction data collected in oscillation mode. **Methods in Enzymology** 276: 307-326.
- Pantoom, S., Songsiriritthigul, C., and Suginta, W. (2008). The effects of the surface-exposed residues on the binding and hydrolytic activities of *Vibrio harveyi* chitinase A. **BMC Biochemistry** 9 (2).
- Papanikolau, Y., Prag, G., Tavlas, G., and Vorgias, C. E., Oppenheim, A. B., and Petratos, K. (2001). High Resolution structural analyses of mutant chitinase A complexes with substrates provide new insight into the mechanism of catalysis. **Biochemistry** 40: 11338-11343.
- Papanikolau, Y., Tavlas, G., Vorgias, C. E., and Petratos, K. (2003). De novo purification scheme and crystallization conditions yield high-resolution structures of chitinase A and its complex with the inhibitor allosamidin. **Acta Crystallographica** 59: 400-403.
- Perrakis, A., Tews, I., Dauter, Z., Oppenheim, A. B., Chet, I., Wilson, K. S., and Vorgias, C. E. (1994). The crystal structure of a bacterial chitinase at 2.3 Å resolution. **Structure** 15: 1169-1180.
- Pace, C. N., Vajdos, F., Fee, L., Grimsley, G., and Gray, T. (1995). How to measure and predict the molar absorption coefficient of a protein. **Protein Science** 4: 2411-2423.

- Poole, D. M., Hazelwood, G. P., Huskisson, N. S., Virden, R., and Gilbert, H. J. (1993). The role of conserved tryptophan residues in the interaction of a bacterial cellulose binding domain with its ligand. **European Journal of Biochemistry** 106: 77-84.
- Prinz, H. and Schönichen, A. (2008). Transient binding patches: a plausible concept for drug binding. **Journal of Chemical Biology** 4: 95-104.
- Pruzzo, C., Crippa, A., Bertone, S., Panej, L, and Cadi, A. (1996). Attachment of *Vibrio alginolyticus* to chitin mediated by chitin binding proteins. **Microbiology** 142: 2181-2186.
- Qin, C., Li, H., Xiao, Q., Liu, Y., Zhu, J., and Du, Y. (2006). Water solubility of chitosan and its antimicrobial activity. **Carbohydrate Polymers**; 63:367-374.
- Ramachandran, G. N., Ramakrishnan, C., and Sasisekharan, V. (1963) Stereochemistry of polypeptide chain configurations. **Journal of Molecular Biology** 7: 95-9.
- Rao, F. V., Houston, D. R., Boot, R. G., Aerts, J. M., Sakuda, S., and van Aalten, D. M. (2003). Crystal structures of allosamidin derivatives in complex with human macrophage chitinase. **The Journal of Biological Chemistry** 22: 20110-20116.
- Rao, F. V., Andersen, O. A., Vora, K. A., DeMartino, J. A., and van Aalten, D. M. F. (2005A). Methylxanthine drugs are chitinase inhibitors: investigation of inhibition and binding modes. **Chemistry and Biology** 12: 973-980.
- Rao, F. V., Houston, D. R., Boot, R. G., Aerts, J. M. F. G., Hodkinson, M., Adams, D. J., Shiomi, K., Omura, S., and van Aalten, D. M. F. (2005B). Specificity and

- affinity of natural product cyclopentapeptide inhibitors against a fumigatus, human, and bacterial chitinases. **Chemistry and Biology** 12: 65-76.
- Robertus, J. D., Monzingo, A. F., Marcotte, E. M., and John, H. P. (1998) Structural analysis shows five glycohydrolase families diverged from a common ancestor. **The Journal of Experimental Zoology** 282: 127-132.
- Rodrigues, R. J. and Gamboa, D. N. (2007). Plasmodium berghei: in vitro and in vivo activity of dequalinium. **Experimental Parasitology** 115: 19-24.
- Rodrigues, R. J. and Gamboa, D. N. (2009). Effect of dequalinium on the oxidative stress in Plasmodium berghei-infected erythrocytes. **Parasitology Research** 104: 1491-1496.
- Rhodes, G. Crystallography made crystal clear. A guide for users of macromolecular models (2nd ed.). New York: Academic Press 2000; chapter 7: page 133-158.
- Sahai, A. S. and Manocha, M. S. (1993). Chitinases of fungi and plants: their involvement in morphogenesis and host-parasite interaction. **FEMS Microbiology Reviews** 11: 317-338.
- Sakuda, S., Isogai, A., Maysumoto, S., and Suzuki, A. (1987). Search for microbial insect growth regulators. II. Allosamidin, a novel insect chitinase inhibitor. **The Journal of Antibiotics** (Tokyo) 40: 296-300.
- Sakuda, S. and Sakurada, M. (1998). Preparation of biotinylated allosamidins with strong chitinase inhibitory activities. **Bioorganic & Medicinal Chemistry Letters** 8: 2987-2990.
- Schüttelkopf, A. W., and van Aalten, D. M. F. (2004). Prodr: a tool for highthroughput crystallography of protein-ligand complexes. **Acta Crystallographica D**60: 1355-1363.

- Schüttelkopf, A. W., Andersen, O. A., Rao, F. V., Allwood, M., Lloyd, C., Eggleston, I. M., and van Aalten, D. M. F. (2006). Screening-based discovery and structural dissection of a novel family 18 chitinase inhibitor. **The Journal of Biological Chemistry** 281: 27278-27285.
- Shimahara, K. and Takiguchi, Y. (1988). Preparation of crustacean chitin. **Methods in Enzymology** 161: 417-423.
- Shiomi, K., Arai, N., Iwai, Y., Turberg, A., Koelbl, H., and Omura, S. (2000). Structure of argifin, a new chitinase inhibitor produced by *Gliocladium sp.* **Tetrahedron Letters** 41: 2141-2143.
- Sikorski, P., Sørbotten, A., Horn, S. J., Eijsink, V. G., and Varum, K. M. (2006). *Serratia marcescens* chitinases with tunnel-shaped substrate-binding grooves show endo activity and different degrees of processivity during enzymatic hydrolysis of chitosan. **Biochemistry** 45: 9566-9574.
- Sinsabaugh, R. L. and Linkins, A. E. (1990). Enzymic and chemical analysis of particulate organic matter from a boreal river. **Freshwater Biology** 23: 301-309.
- Songsiriritthigul, C., Pantoom, S., Aguda, A. H., Robinson, R. C., and Suginta, W. (2008). Crystal structures of *Vibrio harveyi* chitinase A complexed with chitooligosaccharides: Implications for the catalytic mechanism. **Journal of Structural Biology** 162: 491-499.
- Suginta, W., Robertson, P. A. W., Austin, B., Fry, S. C., and Fothergill-Gilmore, L.A. (2000). Chitinases from *Vibrio*: activity screening and purification of Chi A from *Vibrio carchariae*. **Journal of Applied Microbiology** 89: 76-84.

- Suginta, W., Vongsuwan, A., Songsiriritthigul, C., Prinz, H., Estibeiro, P., Duncan, R. R., Svasti, J., and Fothergill-Gilmore, L. A. (2004). An endochitinase A from *Vibrio carchariae*: cloning, expression, mass and sequence analyses, and chitin hydrolysis. **Archives of Biochemistry and Biophysics** 424: 171-180.
- Suginta, W., Vongsuwan, A., Songsiriritthigul, C., Svasti, J., and Prinz, H. (2005). Enzymatic properties of wild-type and active site mutants of chitinase A from *Vibrio carchariae*, as revealed by HPLC-MS. **FEBS Journal** 272: 3376-3386.
- Suginta, W., Songsiriritthigul, C., Kobdaj, A., Opassiri, R., and Svasti, J. (2007). Mutations of Trp275 and Trp397 altered the binding selectivity of *Vibrio carchariae* chitinase A. **Biochimica et Biophysica Acta** 1770: 1151-1160.
- Suginta, W. (2007). Identification of chitin binding proteins and characterization of two chitinase isoforms from *Vibrio alginolyticus* 283. **Enzyme and Microbial Technology** 41: 212-220.
- Suginta, W., Pantoom, S., and Prinz, H. (2009). Substrate binding modes and anomer selectivity of chitinase A from *Vibrio harveyi*. **Journal of Chemical Biology** 2: 191-202.
- Sun, Y. J., Chang, N. C., Hung, S. I., Chang, A. C., Chou, C. C., and Hsiao, C. D. (2001). The crystal structure of a novel mammalian lectin, Ym1, suggests a saccharide binding site. **The Journal of Biological Chemistry** 276: 17507-17514.
- Svitil, A. L. and Kirchman, D. L. (1998). A chitin-binding domain in a marine bacterial chitinase and other microbial chitinases: implications for the ecology and evolution of 1,4- β -glycanases. **Microbiology** 144: 1299-1308.
- Suzuki, K., Taiyoji, M., Sugawara, N., Nikaidou, N., Henrissat, B., and Watanabe, T.

- (1999). The third chitinase gene (*chiC*) of *Serratia marcescens* 2170 and the relationship of its product to other bacterial chitinases. **The Biochemical Journal** 343: 587-596.
- Tabatabaia, M. A. and Bremner, J. M. (1969). Use of p-nitrophenyl phosphate for assay of soil phosphatase activity. **Soil Biology and Biochemistry** 1: 301-307.
- Tabudravu, J. N., Eijsink, V. G. H., Gooday, G. W., Jaspars, M., Komander, D., Legg, M., Synstad, B., and van Aalten, D. M. F. (2002). Psammaplin A, a chitinase inhibitor isolated from the fijian marine sponge *Aplysinella rhax*. **Bioorganic and Medicinal Chemistry** 10: 1123-1128.
- Tanaka, T., Fujiwara, S., Nishikori, S., Fukui, T., Takagi, M., and Imanaka, T. (1999). A unique chitinase with dual active sites and triple substrate binding sites from the hyperthermophilic archaeon *Pyrococcus kodakaraensis* KOD1. **Applied and Environmental Microbiology** 65: 5338-5344.
- Terwisscha, van Scheltinga, A. C., Kalk, K. H., Beintema, J. J., and Dijkstra, B. W. (1994). Crystal structure of hevamine, a plant defense protein with chitinase and lysozyme activity, and its complex with an inhibitor. **Structure** 2: 1181-1189.
- Terwisscha, van Scheltinga A. C., Armand, S., Kalk, K. H., Isogai, A., Henrissat, B., and Dijkstra, B. W. (1995). Stereochemistry of chitin hydrolysis by a plantchitinase/ lysozyme and x-ray structure of a complex with allosamidin: evidence for substrate assisted catalysis. **Biochemistry** 34: b15619-15623.
- Terwisscha van Scheltinga, A. C., Hennig, M., and Dijkstra, B. W. (1996).

The 1.8 Å resolution structure of hevamine, a plant chitinase/lysozyme, and analysis of the conserved sequence and structure motifs of glycosyl hydrolase family 18.

Journal of Molecular Biology 262: 243-257.

Tews, I., Terwisscha van Scheltinga, A. C., Perrakis, A., Wilson, K. S., and Dijkstra, B. W. (1997). Substrate-assisted catalysis unifies two families of chitinolytic enzymes. **Journal of the American Chemical Society** 119: 954-7959.

Tsujibo, H., Orikoshi, H., Shiotani, K., Hayashi, M., Umeda, J., Miyamoto, K., Imada, C., Okami, Y., and Inamori, Y. (1998). Characterization of chitinase C from a marine bacterium, *Alteromonas sp.* strain O-7, and its corresponding gene and domain structure. **Applied and Environmental Microbiology** 64: 472-478.

Tsujibo, H., Orikoshi, H., Baba, N., Miyahara, M., Miyamoto, K., Yasuda, M., and Inamori, Y. (2002). Identification and characterization of the gene cluster involved in chitin degradation in a marine bacterium, *Alteromonas sp.* strain O-7. **Applied and Environmental Microbiology** 68: 263-270.

Uchiyama, T., Katouno, F., Nikaidou, N., Nonaka, T., Sugiyama, J., and Watanabe, T. (2001). Roles of the exposed aromatic residues in crystalline chitin hydrolysis by chitinase A from *Serratia marcescens* 2170. **The Journal of Biological Chemistry** 44: 41343-41349.

Van Aalten, D. M. F., Komander, D., Synstad, B., Gåseidnes, S., Peter, M. G., and Eijsink, V.G.H. (2001). Structural insights into the catalytic mechanism of a family 18 exo-chitinase. **Proceedings of the National Academy of Sciences of the United States of America** 98: 8979-8984.

- Vaaje-Kolstad, G., Vasella, A., Peter, M. G., Netter, C., Houston, D. R., Westereng, B., Synstad B., Eijsink V. G. H., and van Aalten D. M. F. (2004). Interactions of a family 18 chitinase with the designed inhibitor HM508 and its degradation product. **The Journal of Biological Chemistry** 279: 3612-3619.
- Vagin, A. and Teplyakov, A. (1997). MOLREP: an automated program for molecular replacement. **Journal of Applied Crystallography** 30: 1022-1025.
- Vriend, G. (1990). WHAT IF: A molecular modeling and drug design program. **Journal of Molecular Graphics and Modelling** 8: 52-56.
- Wallace, A. C., Laskowski, R. A., and Thornton, J M. (1995). LIGPLOT: A program to generate schematic diagrams of protein-ligand interactions. **Protein Engineering** 8: 127-134.
- Watanabe, T., Ito, Y., Tadao, Y., Hashimoto, M., Sekine, S., and Tanaka, H. (1994). The roles of the C-terminal domain and type III domains of chitinase A1 from *Bacillus circulans* WL-12 in chitin degradation. **Journal of Bacteriology** 176: 4465-4472.
- Watanabe, T., Kimura, K., Sumiya, T., Nikaidou, N., Suzuki, K., Suzuki, M., Taiyoji, M., Ferrer, S., and Regue, M. (1997). Genetic analysis of the chitinase system of *Serratia marcescens* 2170. **Journal of Bacteriology** 179: 7111-7117.
- Watanabe, T., Ishibashi, A., Ariga, Y., Hashimoto, M., Nikaidou, N., Sugiyama, J., Matsumoto, T., and Nonaka, T. (2001). Trp122 and Trp134 on the surface of the catalytic domain are essential for crystalline chitin hydrolysis by *Bacillus circulans* chitinase A1. **FEBS Letters** 494: 74-78.
- Watanabe, T., Ariga, Y., Sato, U., Toratani, T., Hashimoto, M., Nikhidou, N., Kezuka, Y., Nonaka, T., and Sugiyama, J. (2003). Aromatic residues within

the substrate-binding cleft of *Bacillus circulans* chitinase A1 are essential for hydrolysis of crystalline chitin. **Biochemical Journal** 376: 237-244.

Wu, M., Chaung, Y., Chen, J., Chen, C., and Chang, M. (2001). Identification and characterization of the three chitin-binding domains within the multidomain chitinase Chi92 from *Aeromonas hydrophila* JP101. **Applied Environmental and Microbiology** 67: 5100-5106.

Yu, C., Lee, A. M., Bassler, B. L., and Roseman, S. (1991). Chitin utilization by marine bacteria. A physiological function for bacterial adhesion to immobilized carbohydrates. **The Journal of Biological Chemistry** 266: 24260-24267.

Yuli, E. P., Suhartono, T. M., Rukayadi, Y., Hwang, K. J., and Pyun, R. Y. (2001). Characteristics of thermostable chitinase enzymes from the Indonesian *Bacillus* sp. **Enzyme and Microbial Technology** 35: 147-153.

Zees, A. C., Pырpassopoulos, S., and Vorgias, C. E. (2009). Insights into the role of the (alpha+beta) insertion in the TIM-barrel catalytic domain, regarding the stability and the enzymatic activity of Chitinase A from *Serratia marcescens*. **Biochimica et Biophysica Acta** 1794: 23-31.

Zhu, Z., Zheng, T., Homer, R. J., Kim, Y. K., Chen, N. Y., Cohn, L., Hamid, Q., and Elias, J. A. (2004). Acidic mammalian chitinase in asthmatic Th2 inflammation and IL-13 pathway activation. **Science** 304: 1678-1682.



APPENDIX A

PREPARATION OF COMPETENT CELLS AND PLASMID TRANSFORMATION

1. Preparation of competent cells

1.1 Preparation of competent cells for CaCl₂ transformation

E. coli DH5 α and *E. coli* M15(pREP4) are the bacterial strains used for competent cell preparation. A single colony was picked from LB agar plate, then subjected to 2 ml of LB broth and incubated at 37°C for 5-6 hours with agitation of 200 rpm. Then, 10 μ l of the cell culture was transferred to 20 ml of LB broth and further incubated overnight at 37°C with shaking at 200 rpm. An overnight culture of 5 ml was transferred to 100 ml of LB broth (a ratio of the cell culture to the LB medium of 1:100) and incubated at 37°C until OD₆₀₀ reached 0.4-0.5. The cell culture was transferred to a polypropylene tube, which was pre-chilled on ice for 10 min, and the cell pellet was collected by centrifugation at 4,500 rpm at 4°C for 10 min. The cell pellet was gently re-suspended on ice in 10 ml of pre-chilled CaCl₂ solution (100 mM CaCl₂ and 15% (v/v) glycerol), then centrifuged at 4,500 rpm at 4°C for 10 min. The cell pellet was gently re-suspended again in 10 ml of pre-chilled CaCl₂ solution. The cell pellet collected by centrifugation was re-suspended in 4 ml of pre-chilled CaCl₂ and kept on ice for 10 min. Aliquots 80 μ l of the cell suspension were made in 1.5 ml microtubes.

The competent cells were snapped frozen in liquid nitrogen and stored at -80°C until used.

1.2 Preparation of competent cells for electroporation transformation

A single colony of *E. coli* DH5 α or *E. coli* M15(pREP4) cells picked from an LB agar plate was transferred to 2 ml of LB broth and incubated at 37°C for 5-6 hours with agitation of 200 rpm. The cells were grown as described in Section 1 to OD_{600} about 0.4-0.5, then collected by centrifugation at 4,500 rpm at 4°C . The harvested cells were kept on ice and re-suspended in 600 ml of 5% (v/v) sterilized glycerol, and then centrifuged at 4,500 rpm at 4°C for 15 min. The centrifugation step was repeated 4 times with the volume of the glycerol reduced to 400, 200, 50, and 1 ml respectively. In the final step, aliquots of 80 μl of cell suspension were transferred to 1.5 ml microtubes. After snap-freezing in liquid nitrogen, the competent cells were stored at -80°C until used.

2. Plasmid transformation

2.1 Heat shock method

The frozen competent cells (100 μl) were gently thawed and left on ice for 30 min, prior to being added with 10-100 ng of plasmid DNA. The mixture was immediately incubated at 42°C for 42 sec, and then rapidly placed on ice for 10 min. To allow the competent cell recover, 900 μl of pre-warmed LB broth was added into the transformed cells, and incubated at 37°C for 60 min. The cell were centrifuged at 4,500 rpm for 5 min, and then 900 μl of supernatant were removed. One hundred

microliters of the remaining transformed cells were then spread on an LB/Amp agar plate and then incubated at 37°C for 16 hour.

2.2 Electroporation method

Pre-chill the electroporation cuvette on ice. Then, 20 ng of the recombinant plasmid of pQE60-*VhChiA* was added into 70 μ l of the competent cells and gently mixed to avoid air bubbles. The sample mixture was transferred into the pre-chilled cuvette and placed into the cuvette holder equipped with the electroporator power source (Bio-rad Bio-Rad Laboratories, CA, USA). Transformation was done under the condition of 25 μ FD, 800 Ω , and 1.5 kV. The electroporation time was set at 1.6 msec. After electroporation, the transformed cells were immediately transferred into 1 ml of LB broth on ice and incubated at 37°C for 1 hour. The cells were diluted into 1:10, 1:100, and 1:1000 with LB medium and then spread on LB agar plate containing 100 μ g/ml ampicillin and 25 μ g/ml kanamycin then incubated at 37°C for 16 hours.

APPENDIX B

DETERMINATION OF PROTEIN CONCENTRATION

1. Determination of protein concentration

1.1 Bradford assay

A series of protein standards were prepared using BSA diluted with appropriate buffer to final concentrations of 0, 200, 400, 600, 800, and 1000 μg BSA/ml. The serial dilutions of the protein sample were also prepared to be measured. One hundred microliters of each of the above was added to a separate tube, and then added 900 μl of Bradford reagent to each tube and mixed by inversion and waited for 10 min. Then, the solution mixtures were measured at the wavelength of 595 nm, and the mixed solution contained the BSA concentration of 0 mg/ml was used as the blank. The protein concentrations were determined from BSA standard curve. The standard curve was plotted by the absorbance each BSA concentration against their concentration.

1.2 Intrinsic fluorescence emission assay

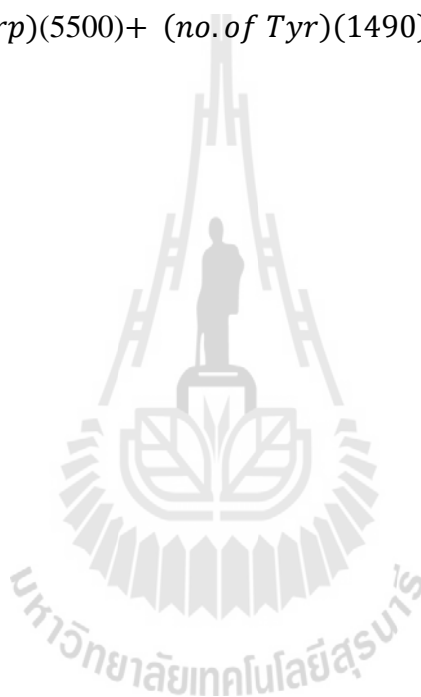
Dilutions of the protein samples with buffer were prepared. Then protein solutions were directly measured at a wavelength of 280 nm quartz cuvette. The solution containing only buffer was used as blank. The protein concentrations were estimated from its measured absorbance using the following equation.

$$A_{280} = \epsilon_{280} \times l \times c$$

A_{280} is the absorbance at 280 nm, l is the path length, which the most spectrometers is 1 cm, c is a concentration in the unit of mg/ml and ϵ_{280} is absorbance coefficient at 280 nm.

Since the amino acid composition of *VhChiA* has been known, the ϵ_{280} was predicted from the following equation (Pace *et al.*, 1995).

$$\epsilon_{280} = (\text{no. of Trp})(5500) + (\text{no. of Tyr})(1490) + (\text{no. of cystine})(125)$$



APPENDIX C

PREPARATION OF SOLUTIONS AND REAGENTS

1. Reagents for bacterial culture and competent cell transformation

1.1 Luria-Bertani (LB) broth containing 100 µg/ml of ampicillin

Dissolve 10 g Bacto tryptone, 5 g Bacto yeast extract and 5 g NaCl in 950 ml distilled water. Stir until the solute is dissolved. Adjust the volume of the solution to 1 liter with distilled water. The solution is then sterilized by autoclaving at 121°C for 15 min. The medium is allowed to cool down to 50°C before ampicillin is added to a final concentration of 100 µg/ml. The LB/Amp medium is freshly used or stored at 4°C until used.

1.2 LB agar medium containing 100 µg/ml of ampicillin

Dissolve 10 g Bacto tryptone, 5 g Bacto yeast extract, 5 g NaCl and 15 g Bacto agar in 950 ml distilled water. Stir until the solutes have been dissolved. Adjust the volume of the solution to 1 litre with distilled water. Sterilize by autoclaving the solution at 121°C for 15 min. Allow the medium to cool to 50°C before adding ampicillin to a final concentration 100 µg/ml. Pour the medium into petri-dishes. Allow the agar to harden, and keep at 4°C.

1.3 LB agar medium containing 25 µg/ml kanamycin

Dissolve 10 g Bacto tryptone, 5 g Bacto yeast extract, 5 g NaCl and 15 g Bacto agar in 950 ml distilled water. Stir until the solute is dissolved. Adjust the volume of the solution to 1 liter with distilled water. Sterilize the solution by autoclaving at 121°C for 15 min. The LB agar medium is allowed to cool to 50°C before kanamycin is added to a final concentration of 25 µg/ml. Pour the medium into petri-dishes. Allow the agar to harden, and keep at 4°C.

1.4 Antibiotic stock solutions

Ampicillin stock solution (100 mg/ml)

Dissolve 1 g of ampicillin in 10 ml sterile distilled water.

Kanamycin stock solution (50 mg/ml)

Dissolve 50 g of kanamycin in 10 ml sterile distilled water.

Both antibiotic solutions are filtered sterilized with a 0.2 µm filtration disc, and then stored at -30°C until used.

1.5 Isopropyl thio-β-D-galactoside (IPTG) stock solution (1 M)

Dissolve 2.38 g of IPTG in distilled water and make up a final volume to 10 ml. The stock solution is filtered sterilized, the aliquot to small volumes, and then stored at -30°C.

2. Reagents for competent *E. coli* cell preparation

2.1 CaCl₂ solution (100 mM CaCl₂ and 15% (v/v) glycerol)

To prepare 100 ml of CaCl₂ working solution, mix the stock solution as follows:

- 10 ml of 1 M CaCl₂ (14.7 g/100 ml, filtered sterilization)
- 15 ml of 100% (v/v) sterilized glycerol (autoclaved at 121°C, 15 min)

Add sterile distilled water to bring a volume to 100 ml. Store the solution at 4°C.

2.2 SOC media

Dissolve 20 g Bacto tryptone, 5 g Bacto yeast extract and 10 ml of NaCl (5.85 g/100 ml), 2.5 ml of 1M KCl (7.44 g/100 ml) in distilled water and make up a volume to 950 ml. Sterilize the solution by autoclaving at 121°C for 15 min. Allow the medium to cool down to room temperature, then add the sterilized medium with of 5 ml of 1M MgCl₂ 6H₂O (20.33 g/100 ml), 5 ml of 1 M MgSO₄ 7H₂O (12.30 g/100 ml) and 10 ml of glucose (36 g /100 ml). Store SOC medium at 4°C.

3. Reagents for plasmid purification

3.1 Plasmid extraction by QIAGEN Plasmid Mini Kit

3.1.1 Buffer P1 (cell suspension buffer)

50 mM Tris-HCl, pH 8.0

10 mM EDTA

50 µg/ml of RNase A

3.1.2 Buffer P2 (lysis buffer)

0.2 M NaOH and 1% (w/v) SDS

3.1.3 Buffer N3 (neutralization and binding buffer)

4 M guanidine hydrochloride (GuHCl)

0.5 M potassium acetate, pH 4.2

3.1.4 Buffer PB (wash buffer)

5 M guanidine hydrochloride (GuHCl)

20 mM Tris-HCl, pH 6.6

38% (v/v) ethanol

3.1.5 Buffer PE (wash buffer)

20 mM NaCl

2 mM Tris-HCl, pH 7.5

80% (v/v) ethanol

3.2 0.5 M EDTA, pH 8.0

Dissolve 18.6 g of EDTA (disodium ethylene diamine tetraacetate. $2\text{H}_2\text{O}$) in 70 ml distilled water. Adjust pH to 8.0 with 6M NaOH and make up a volume to 100 ml with distilled water. Sterilize by autoclaving the solution at 121°C for 15 min. Store the EDTA solution at room temperature.

4. Reagents for agarose gel electrophoresis

4.1 50 x TAE buffer for agarose gel electrophoresis

Mix 242 g Tris base, 57.1 ml glacial acetic acid, and 100 ml of 0.5 M EDTA, pH 8.0. Adjust the final volume to 1 liter with distilled water. Store the solution at room temperature.

4.2 6 x DNA loading solution (10 ml)

Mix 0.025 g Bromophenol blue and/or 0.025 g xylene cyanol and 3 ml of 100% (v/v) of glycerol. Adjust the final volume to 10 ml with distilled water and store at 4°C.

5. Solutions for protein expression and purification

5.1 20 mM Tris-HCl, pH 8.0 (1 L)

Dissolve 2.42 g of Tris Base in 800 ml distilled water. Adjust pH to 8.0 with 6 M HCl and bring the final volume to 1 liter with distilled water. Store the buffer at 4°C.

5.2 Equilibration buffer containing 20 mM Tris-HCl, pH 8.0 and 150 mM NaCl

Dissolve 8.77 g of NaCl in 20 mM Tris-HCl, pH 8.0. Adjust the final volume to 1 liter. Store the equilibration buffer at 4°C.

5.3 Wash buffer I containing 20 mM Tris-HCl, pH 8.0, 150 mM NaCl and 5 mM imidazole

Dissolve 0.34 g of imidazole in the equilibration buffer. Adjust the final volume to 1 liter. Store the wash buffer I at 4°C.

5.4 Wash buffer II containing 20 mM Tris-HCl, pH 8.0, 150 mM NaCl and 20 mM imidazole

Dissolve 1.36 g of imidazole in the equilibration buffer. Adjust the final volume to 1 liter. Store the wash buffer II at 4°C.

5.5 Elution buffer containing 20 mM Tris-HCl, pH 8.0 containing 150 mM NaCl and 250 mM imidazole

Dissolve 1.70 g of imidazole in the equilibration buffer. Adjust the final volume to 100 ml. Store the elution buffer at 4°C.

5.6 SDS-gel loading buffer (3×stock) containing 0.15 M Tris-HCl, pH 6.8, 6% (w/v) SDS, 0.1% (w/v) bromophenol blue and 30% (v/v) glycerol

Dissolve 6 g of SDS, 0.1 g bromophenol blue, 30 ml of glycerol and add 0.15 M Tris-HCl, pH 6.8 to bring a final volume to 100 ml. Store the SDS-gel loading buffer at -30°C. Before use add 20 µl of 2-mercaptoethanol to 40 µl of the buffer solution.

5.7 1.5 M Tris–HCl, pH 8.8

Dissolve 18.17 g of Tris base in 80 ml distilled water. Adjust pH to 8.8 with 6 M HCl and bring the final volume to 100 ml with distilled water. Store at 4°C.

5.8 1.0 M Tris–HCl, pH 6.8

Dissolve 12.10 g of Tris base in 80 ml distilled water. Adjust pH to 6.8 with 6 M HCl and bring the final volume to 100 ml with distilled water. Store at 4°C.

5.9 30% (w/v) Acrylamide solution

Dissolve 29 g acrylamide and 1 g *N, N'*-methylene-bis-acrylamide in distilled water to a volume of 100 ml. Mix the solution by stirring for 1 h until the solution is homogeneous, and then filter through a Whatman membrane No. 1. Store the acrylamide solution in the dark bottle at 4°C.

5.10 Tris-glycine electrode buffer (5×stock solution)

Dissolve 30.29 g of Tris base, 144 g of glycine, 5 g of SDS in distilled water. Adjust pH to 8.3 with 6M HCl and bring the final volume to 1 liter with distilled water.

5.11 Protein staining solution with coomassie brilliant blue R-250.

Mix 1 g of Coomassie brilliant blue R-250, 400 ml methanol, 500 ml distilled water and 100 ml glacial acetic acid and filter through a Whatman filter paper No. 1.

5.12 Destaining solution for the coomassie stain

Mix 400 ml methanol, 100 ml glacial acetic acid, and then add distilled water to a final volume of 1 liter.

5.13 10% (w/v) Ammonium persulfate

Dissolve 100 mg of ammonium persulfate in 1 ml distilled water. Store the solution at -30°C .

5.14 12% (w/v) Separating SDS-PAGE gel

Mix the solution as follows:

1.5 M Tris-HCl, pH 8.8	2.5 ml
Distilled water	3.3 ml
10% (w/v) SDS	0.1 ml
30% (w/v) acrylamide solution	4.0 ml
10% (w/v) ammonium persulfate	0.1 ml
TEMED	0.004 ml

Adjust the volume with distilled water to 10 ml

5.15 5% (w/v) Stacking SDS-PAGE gel

Mix the solution as follow:

0.5 M Tris-HCl, pH 6.8	0.63 ml
Distilled water	3.4 ml
10% (w/v) SDS	0.05 ml
30% (w/v) acrylamide solution	0.83 ml

10% (w/v) ammonium persulfate	0.05 ml
TEMED	0.005 ml

5.16 Bradford's reagent

Dissolve 0.01 g of Coomassie blue in 10 ml of 85% (v/v) phosphoric acid and 5 ml of ethanol and add distilled water to a final volume of 100 ml. Mix well and filter through a Whatman filter paper No. 1. Store the solution at 4°C.

6. Buffers and reagents for enzymatic studies

6.1 10 mM *p*-Nitrophenol

Dissolve 13.91 mg of *p*-nitrophenol in distilled water and make a final volume to 10 ml with distilled water.

6.2 100 mM Sodium acetate, pH 5.0 buffer

Dissolve 0.81 g of sodium acetate in 80 ml distilled water, and adjust pH to 5.0 with glacial acetic acid. Bring the final volume to 100 ml with distilled water.

6.3 1 M Na₂CO₃

Dissolve 5.30 g of Na₂CO₃ in distilled water, and adjust the final volume to 50 ml with distilled water.

6.4 10 mM 4-Methylumbelliferone

Dissolve 17.61 mg of 4-methylumbelliferone in distilled water, and adjust the final volume to 10 ml with distilled water.

6.5 0.4 M Citric acid

Dissolve 76.84 g of citric acid in distilled water, and adjust the final volume to 1 liter with distilled water.

6.6 0.4 M Sodium citrate tribasic dihydrate

Dissolve 117.76 g sodium citrate tribasic dihydrate in distilled water, and adjust the final volume to 1 liter with distilled water.

6.7 0.8 M Sodium dihydrogen phosphate monohydrate ($\text{NaH}_2\text{PO}_4 \cdot \text{H}_2\text{O}$)

Dissolve 110.39 g of sodium dihydrogen phosphate monohydrate in distilled water, and adjust the final volume to 1 liter with distilled water.

6.8 0.8 M Disodium hydrogen phosphate dihydrate ($\text{Na}_2\text{HPO}_4 \cdot 2\text{H}_2\text{O}$)

Dissolve 142.39 g of disodium hydrogen phosphate dihydrate in distilled water, and adjust the final volume to 1 liter with distilled water.

6.9 Dinitrosalicylic acid (DNS) reagent

Dissolve 5 g of DNS in 100 ml of 2 M NaOH, then add 250 ml of 60% (w/v) sodium potassium tartrate and distilled water to a final volume of 500 ml.

6.10 *p*-Dimethylaminobenzaldehyde (DMAB) (10x stock solution)

Dissolve 1.5 g of DMAB in glacial acetic acid and mix with 1.25 ml of 100 % (v/v) HCl and make up a final volume to 100 ml with distilled water. The solution is kept in a dark bottle at 4°C.

6.11 Stock solutions of chitinase substrates

The stock solutions of the substrates: *N*-acetyl-chitooligosaccharides (di-*N*-acetyl-chitobiose, tri-*N*-acetyl-chitotriose, tetra-*N*-acetyl-chitotetraose, penta-*N*-acetyl-chitopentaose, hexa-*N*-acetyl-chitohexaose), *p*-nitrophenyl-di-*N*-acetyl-chitobioside (*p*NP-GlcNAc₂), *p*-nitrophenyl-tri-*N*-acetyl-chitotrioside *p*NP-GlcNAc₃, 4-methylumbelliferyl β -*N,N'*-diacetylchitobioside (4MU-GlcNAc₂), and 4-methylumbelliferyl β -*N,N',N''*-triacetylchitotrioside (4MU-GlcNAc₃) were prepared as follows:

Dissolve 0.2212 mg of *N*-acetyl-glucosamine in 10 ml of distilled water, giving a final concentration of 100 mM *N*-acetyl-glucosamine.

Dissolve 50 mg of di-*N*-acetyl-chitobiose in 1,180 μ l of distilled water, giving a final concentration of 100 mM di-*N*-acetyl-chitobiose.

Dissolve 50 mg of tri-*N*-acetyl-chitotriose in 1,590 μ l of distilled water, giving a final concentration of 50 mM tri-*N*-acetyl-chitotriose.

Dissolve 50 mg of tetra-*N*-acetyl-chitotetraose in 1,200 μ l of distilled water, giving a final concentration of 50 mM tetra-*N*-acetyl-chitotetraose.

Dissolve 50 mg of penta-*N*-acetyl-chitopentaose in 1,930 μ l of distilled water, giving a final concentration of 25 mM penta-*N*-acetyl-chitopentaose.

Dissolve 50 mg of hexa-*N*-acetyl-chitohexaose in 2,000 μ l of distilled water, giving a final concentration of 20 mM hexa-*N*-acetyl-chitohexaose.

Dissolve 50 mg of *p*-nitrophenyl-di-*N*-acetyl-chitobioside in 2,000 μ l of distilled water, giving a final concentration of 20 mM *p*-nitrophenyl-di-*N*-acetyl-chitobioside.

Dissolve 25 mg of 4-methylumbelliferyl β -*N,N'*-diacetylchitobioside in 2,146 μ l of distilled water, giving a final concentration of 20 mM 4-methylumbelliferyl β -*N,N'*-diacetylchitobioside.

Dissolve 5 mg of 4-methylumbelliferyl β -*N,N',N''*-triacetylchitotrioside in 636 μ l of distilled water, giving a final concentration of 10 mM 4-methylumbelliferyl β -*N,N',N''*-triacetylchitotrioside.

All stock solutions were aliquoted and stored at -30°C.

6.12 Stock solutions of the chitinase inhibitors

Chelerythrine (CHE), dequalinium (DEQ), idarubicin (IDA), 2-(imidazolin-2-yl)-5-isothiocyanatobenzofuran (IMI), pentoxifyllin (PEN), propentofylline (PRO), and sanguinarine (SAN), methysergide (MET), 2-bromo- α -ergocryptine methanesulfonate (BRO) were purchased from Sigma-Aldrich, and prepared as follows:

Dissolve 1 mg of CHE in 0.13 ml of distilled water, giving a final concentration of 20 mM CHE.

Dissolve 21.1 mg of DEQ in 10 ml of DMSO, giving a final concentration of 4 mM DEQ.

Dissolve 10 mg of IDA in 0.94 ml of DMSO, giving a final concentration of 20 mM IDA.

Dissolve 5 mg of IMI in 0.51 ml of DMSO, giving a final concentration of 40 mM IMI.

Dissolve 27.8 mg of PEN in 1 ml of DMSO, giving a final concentration of 100 mM PEN.

Dissolve 25 mg of PRO in 2 ml of DMSO, giving a final concentration of 40 mM PRO.

Dissolve 5 mg of SAN in 0.68 ml of DMSO, giving a final concentration of 20 mM SAN.

Dissolve 2 mg of MET in 0.43 ml of DMSO, giving a final concentration of 10 mM MET.

Dissolve 25 mg of BRO in 1.67 ml of DMSO, giving a final concentration of 20 mM BRO.

All stock solutions were aliquoted and stored at room temperature.

7. Preparation of colloidal chitin

Colloidal chitin is prepared according to the modified method of Shimahara and Takiguchi (1988). Chitin flakes (10 g) are added into 200 ml of concentrated hydrochloric acid on ice. The suspension is vigorously stirred for 2 h on ice and kept overnight at 4°C. The suspension is filtered through cheesecloth and the filtrate is poured into 600 ml of 50% (v/v) ethanol on ice with stirring. After 1 h, the suspension is filtered with suction through a Whatman filter paper No. 1. The residual is washed thoroughly with distilled water through filtration until pH of the filtrate becomes neutral. The chitin is dried in oven and then weighed to obtain the estimated dry weight of the acid-treated chitin. The chitin suspension is stored at 4°C.

8. Preparation of buffers and reagents for protein crystallization

8.1 Crystallization precipitants

The stock solutions of polyethylene glycol (PEG), including PEG 1500, PEG 4000, PEG 8000 and PEG 20000, were prepared at the final concentration of 50% (w/v) by dissolving 50 g of PEG in 50 ml of ultra-pure water. The suspension was then heated at 60°C until the solutes were completely dissolved, and the final volume was brought to 100 ml with distilled water. For PEG 400, 50 ml of PEG 400 were diluted in ultra-pure water and were finally made to a final volume of 100 ml leading to final concentration of 50% (v/v). 50% (v/v) of ethylene imine polymer was prepared by adding 50 ml of ethylene imine polymer in ultra-pure water and made up a final volume of 100 ml.

8.2 Salts and buffers

For initial screening and optimization, the stock solution of various salts was prepared in ultra-pure water at desired concentrations. Buffers were adjusted to various pH using 6 M HCl or 5 M NaOH to obtain the desired pH, ranging from 4.7 to 9.0.

All of these solutions were filtered using a 0.45 μm MF-Millipore membrane filter connected with a vacuum pump. All of the stock solutions for protein crystallization were summarized below.

A summary of the stock solutions used for crystallization experiments.

Crystallization agent	Stock concentration
Precipitants	
PEG 400	40% (v/v)
PEG 1500	30% (v/v)
PEG 4000	40% (w/v)
PEG 8000	40% (w/v)
PEG 20000	40% (w/v)
2-methyl-2,4-pentanediol	100% (v/v)
Tert-butanol	100% (v/v)
Jeffamine M-600®	100% (v/v)
Ethylene imine polymer	50% (v/v)
Salts	
Ammonium phosphate monobasic	2 M
Ammonium acetate	2 M
Ammonium sulfate	2 M
Calcium acetate hydrate	2 M
Hexadecyltrimethylammonium bromide	1 M
Iron (III) chloride hexahydrate	0.1 M
Magnesium chloride hexahydrate	2 M
Sodium citrate tribasic dihydrate	5 M
Sodium cacodylate trihydrate	1 M
Sodium chloride	5 M

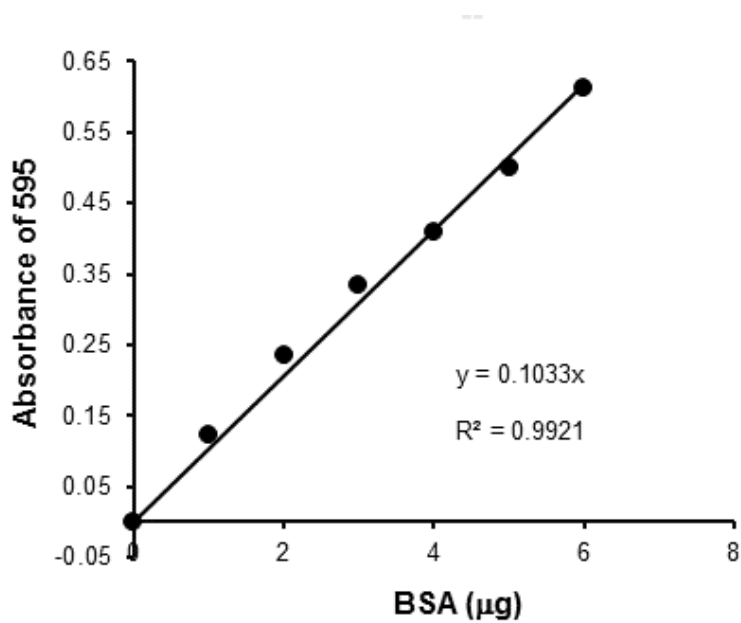
A summary of the stock solutions used for crystallization experiments (Continued).

Crystallization agent	Stock concentration
Buffers	
Sodium acetate, pH 4.7, 5.0, 5.5 and 6.0	1 M
Sodium citrate, pH 5.0, 5.6 and 6.0	1.M
Sodium cacodylate, pH 6.0, 6.5 and 7.0	1 M
MES, pH 5.5, 6.0 and 6.5	1 M
MOPS, pH 7.0 and 7.5	1 M
HEPES, pH 7.5	1 M
Tris-HCl, pH 7.0, 7.5,8.0, 8.5 and 9.0	1 M
PIPES, pH 7.0	
Inhibitors	20 mM
BRO	20 mM
CHE	4 mM
DEQ	20 mM
IDA	40 mM
IMI	10 mM
MET	100 mM
PEN	40 mM
PRO	20 mM
SAN	

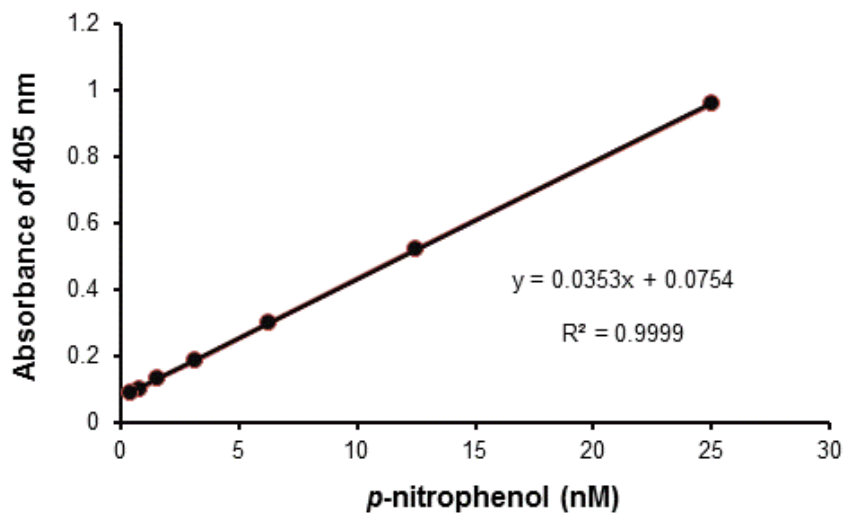
APPENDIX D

STANDARD CURVES

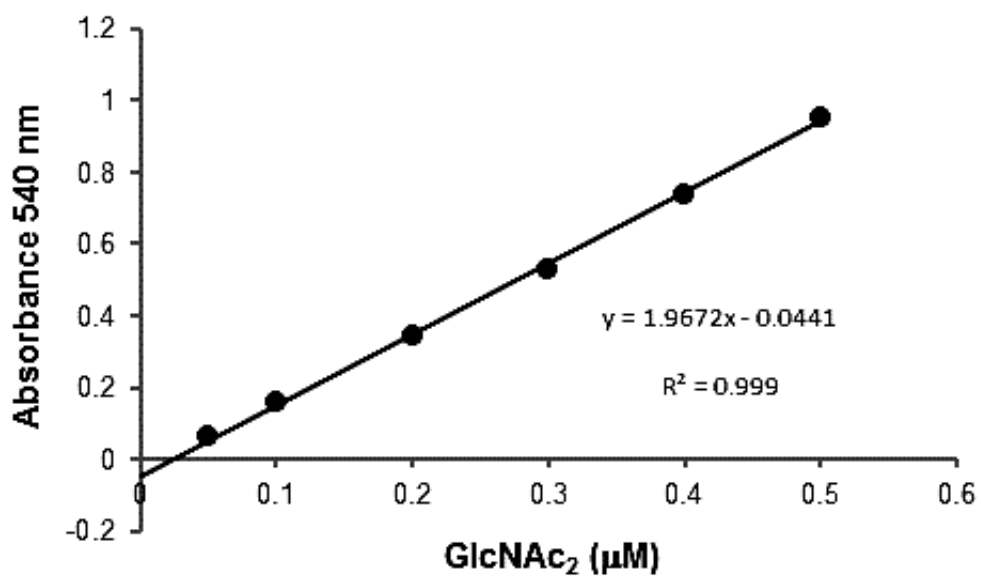
1. Stand curve of BSA by Bradford's method



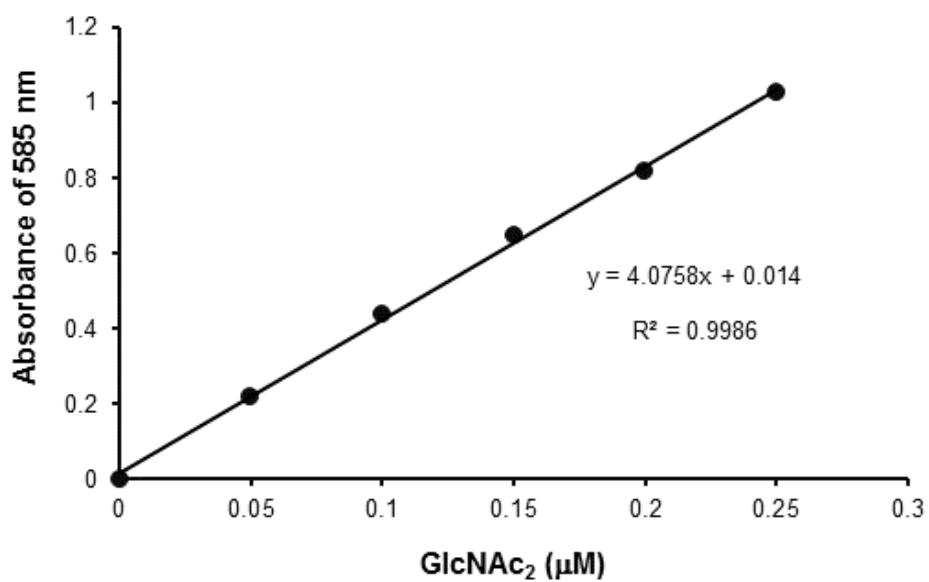
2. Standard curve of *p*-nitrophenol



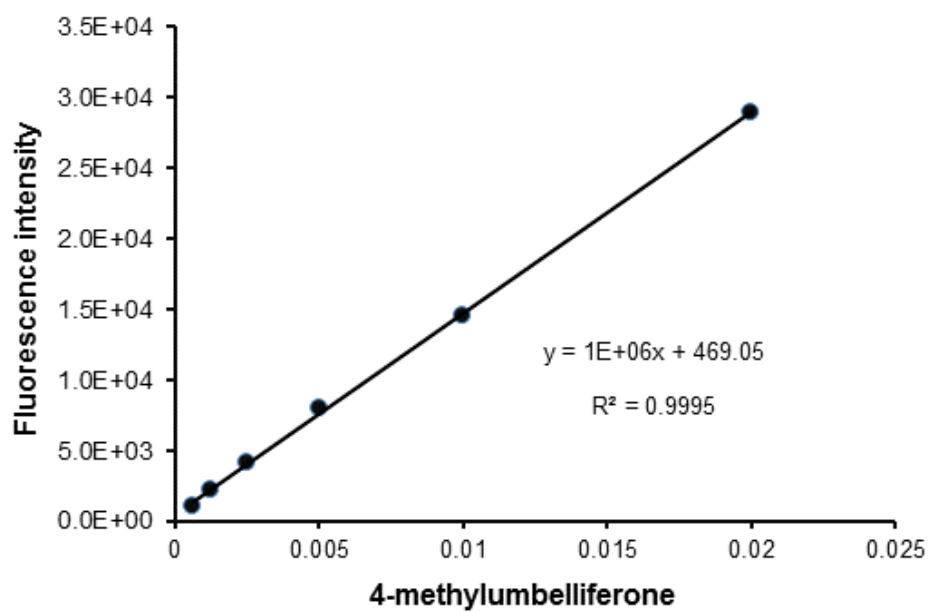
3. Standard curve of GlcNAc₂ for DNS assay



4. Standard curve of GlcNAc₂ for DMAB assay



5. Standard curve of 4-methylumbelliferone

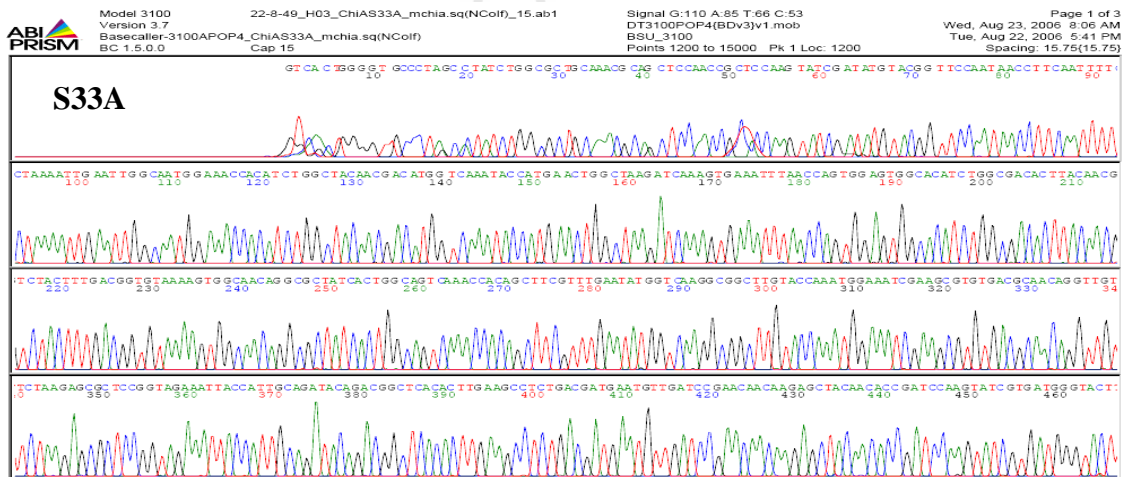


APPENDIX E

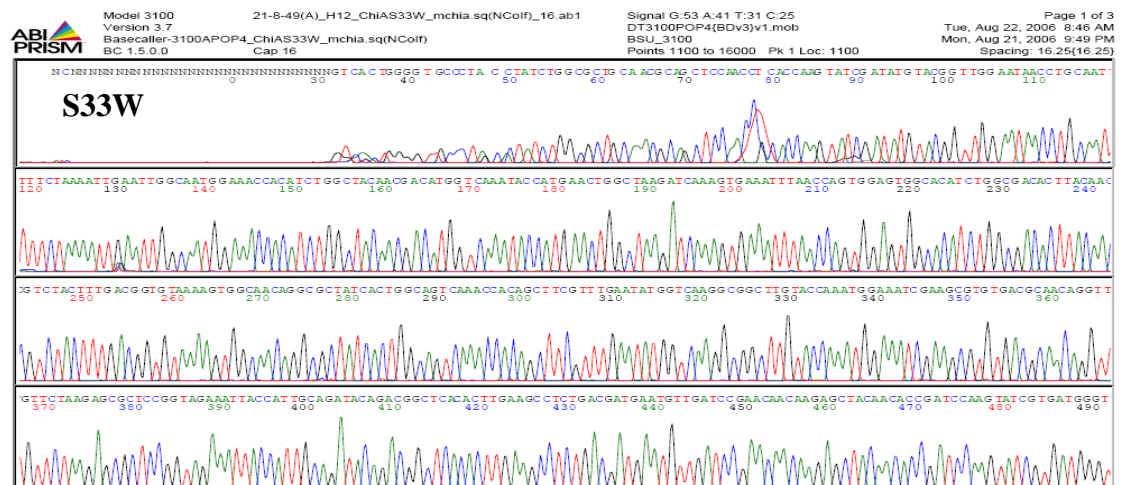
DNA SEQUENCING AND AMINO ACID SEQUENCE ALIGNMENT

1. DNA sequencing profile of the single point multinational.

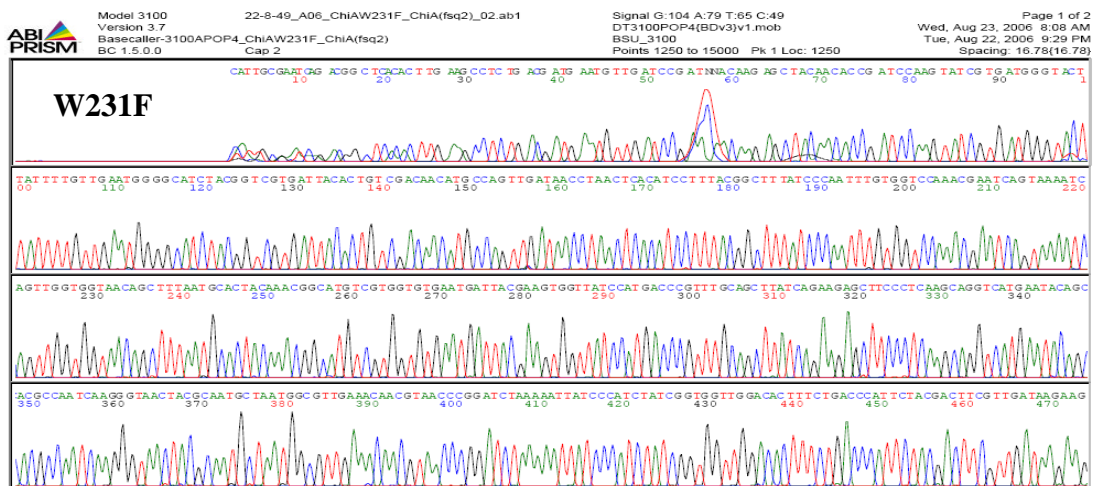
1.1 S33A



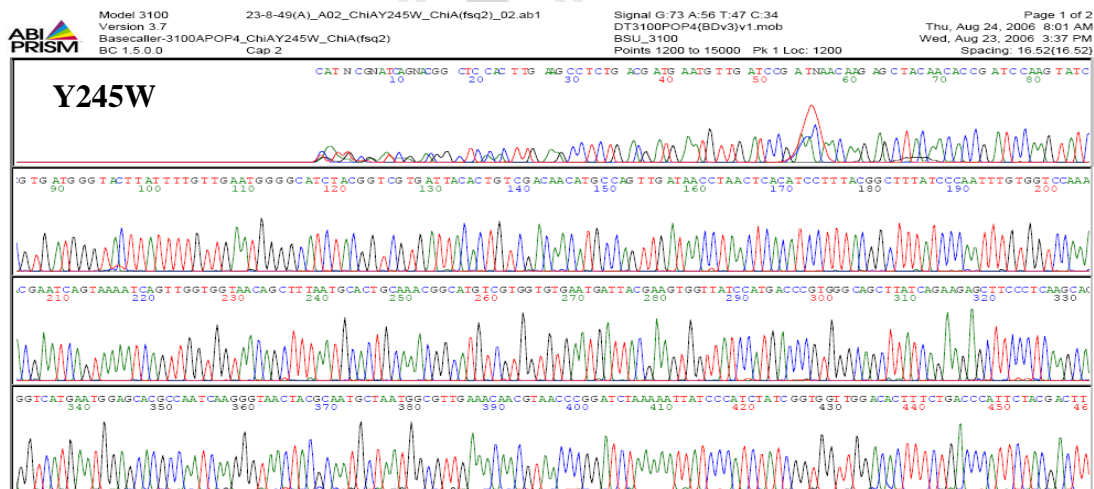
1.2 S33W



1.5 W231F



1.6 Y254W



2 Amino acid sequence alignment

A.

```

*          20          *          40          *          60          *
Wild-type : MIRFNLCAAGVALALS GAANAAPTAPSLDMYGSNNLQFSKIELAMETTSGYNDMVKYHELAKIKVKFNCGSST : 73
S33W      : -----SLDMYGSNNLQFSKIELAMETTSGYNDMVKYHELAKIKVKFNCGSST : 47
S33A      : -----GVALALS GAANAAPTAPSLDMYGSNNLQFSKIELAMETTSGYNDMVKYHELAKIKVKFNCGSST : 64
W70A      : -----LSGAANAAPTAPSLDMYGSNNLQFSKIELAMETTSGYNDMVKYHELAKIKVKFNCGSST : 59
          IDMYG NNLQFSKIELAMETTSGYNDMVKYHELAKIKVKFNQ SGT

*          80          *          100         *          120         *          140
Wild-type : SGGTYNVVYFDGKVKVATGAI TGSQTTASFEYGGGGLYQMEIEACDATGCSKSAPEVETIADTDGSHLKLPLTMNV : 146
S33W      : SGGTYNVVYFDGKVKVATGAI TGSQTTASFEYGGGGLYQMEIEACDATGCSKSAPEVETIADTDGSHLKLPLTMNV : 120
S33A      : SGGTYNVVYFDGKVKVATGAI TGSQTTASFEYGGGGLYQMEIEACDATGCSKSAPEVETIADTDGSHLKLPLTMNV : 137
W70A      : SGGTYNVVYFDGKVKVATGAI TGSQTTASFEYGGGGLYQMEIEACDATGCSKSAPEVETIADTDGSHLKLPLTMNV : 132
          SGGTYNVVYFDGKVKVATGAI TGSQTTASFEYGGGGLYQMEIEACDATGCSKSAPEVETIADTDGSHLKLPLTMNV

*          160         *          180         *          200         *          22
Wild-type : DENNKS YNTDPSIVMGT YFVWGIYGRDYTVDNMPVDNLTHILYGFIPICGPNESVKSVGGNSFNALQ TACRG : 219
S33W      : DENNKS YNTDPSIVMGT YFVWGIYGRDYTVDNMPVDNLTHILYGFIPICGPNESVKSVGGNSFNALQ TACRG : 193
S33A      : DENNKS YNTDPSIVMGT YFVWGIYGRDYTVDNMPVDNLTHILYGFIPICGPNESVKSVGGNSFNALQ TACRG : 210
W70A      : DENNKS YNTDPSIVMGT YFVWGIYGRDYTVDNMPVDNLTHILYGFIPICGPNESVKSVGGNSFNALQ TACRG : 205
          DENNKS YNTDPSIVMGT YFVWGIYGRDYTVDNMPVDNLTHILYGFIPICGPNESVKSVGGNSFNALQ TACRG

0          *          240         *          260         *          280         *
Wild-type : VNDYEVVIHDPWAAAYQKSF PQAGHEYSTPIKGNYAMLMALKQR-NPDLKTIIP-STIGGWTLSDFPFYDFV DKKNR : 290
S33W      : VNDYEVVIHDPWAAAYQKSF PQAGHEYSTPIKGNYAMLMALKQR-NPDLKTIIP-STIGGWTLSDFPFYDFV DKKNR : 264
S33A      : VNDYEVVIHDPWAAAYQKSF PQAGHEYSTPIKGNYAMLMALKQR-NPDLKTIIP-STIGGWTLSDFPFYDFV DKKNR : 281
W70A      : VNDYEVVIHDPWAAAYQKSF PQQVMNTARPSKGNYPVYKRAVENTVTPLEKNIPLNLEVGNLSPEI----- : 269
          VNDYEVVIHDPWAAAYQKSF PQ          P RGN Y M6 A6          PD K IP          G          LS P

```

B.



```

*          140         *          160         *          180         *          200
Wild-type : DGSHLKLPLTMNVDPNNKSYNTDPSIVMGT YFVWGIYGRDYTVDNMPVDNLTHILYGFIPICGPNES : 201
W231A    : -----SIVMGT YFVWGIYGRDYTVDNMPVDNLTHILYGFIPICGPNES : 44
W231F    : -----PSIVMGT YFVWGIYGRDYTVDNMPVDNLTHILYGFIPICGPNES : 45
Y245W    : -----PSIVMGT YFVWGIYGRDYTVDNMPVDNLTHILYGFIPICGPNES : 45
          DGSHLKLPLTMNVDPNNKSYNTDPSIVMGT YFVWGIYGRDYTVDNMPVDNLTHILYGFIPICGPNES

*          220         *          240         *          260
Wild-type : VKSVGGNSFNALQTACRGVNDYEVVIHDPWAAAYQKSF PQAGHEYSTPIKGNYAMLMALKQRNPDLKTI : 268
W231A    : VKSVGGNSFNALQTACRGVNDYEVVIHDPWAAAYQKSF PQAGHEYSTPIKGNYAMLMALKQRNPDLKTI : 111
W231F    : VKSVGGNSFNALQTACRGVNDYEVVIHDPWAAAYQKSF PQAGHEYSTPIKGNYAMLMALKQRNPDLKTI : 112
Y245W    : VKSVGGNSFNALQTACRGVNDYEVVIHDPWAAAYQKSF PQAGHEYSTPIKGNYAMLMALKQRNPDLKTI : 112
          VKSVGGNSFNALQTACRGVNDYEVVIHDPWAAAYQKSF PQAGHE5STPIKGNYAMLMALKQRNPDLKTI

*          280         *          300         *          320         *
Wild-type : IPSIGGWTLSDFPFYDFV DKKNRDTEVASVKKFLKTKWKFYDGVDIDWDFPGGGGAADKGDPEVNDGPA : 335
W231A    : IPSIGGWTLSDFPFYDFV DKKNRDTEVASVKKFLKTKWKFYDGVDIDWDFPGGGGAADKGDPEVNDGPA : 178
W231F    : IPSIGGWTLSDFPFYDFV DKKNRDTEVASVKKFLKTKWKFYDGVDIDWDFPGGGGAADKGDPEVNDGPA : 179
Y245W    : IPSIGGWTLSDFPFYDFV DKKNRDTEVASVKKFLKTKWKFYDGVDIDWDFPGGGGAADKGDPEVNDGPA : 179
          IPSIGGWTLSDFPFYDFV DKKNRDTEVASVKKFLKTKWKFYDGVDIDWDFPGGGGAADKGDPEVNDGPA

```

Amino acid sequence alignment of each a point mutation of with wild-type *VhChiA*

(A) Sequence alignment of a point mutation of S33A, S33W, W70A, and wild-type *VhChiA*. (B) Sequence alignment of a point mutation of W231A, W231F, Y245A, and wild-type *VhChiA*. Completely conserved regions are shaded in back.

APPENDIX F

PUBLICATIONS

- Pantoom, S., Songsiriritthigul, C., and Suginta, W. (2008). The effects of the surface-exposed residues on the binding and hydrolytic activities of *Vibrio harveyi* chitinase A. **BMC Biochemistry** 9(2) (published).
- Songsiriritthigul, C., Pantoom, S., Aguda, A. H., Robinson, R. C., and Suginta, W. (2008). Crystal structures of *Vibrio harveyi* chitinase A complexed with chitooligosaccharides: Implications for the catalytic mechanism. **Journal of Structural Biology** 2008 162: 491-499 (published).
- Suginta, W., Pantoom, S., and Prinz, H. (2009). Substrate binding modes and anomer selectivity of chitinase A from *Vibrio harveyi*. **Journal of Chemical Biology** 2: 191-202 (published).
- Pantoom, S., Vetter, I. R., Prinz, H., and Suginta, W. (2001). Potent family-18 chitinase inhibitors: X-ray structures, affinities and binding mechanisms. **The Journal of Biological Chemistry** 286: 24312-24323 (published).

Research article

Open Access

The effects of the surface-exposed residues on the binding and hydrolytic activities of *Vibrio carchariae* chitinase A

Supansa Pantoom¹, Chomphunuch Songsiririthigul² and Wipa Suginta*¹

Address: ¹School of Biochemistry, Suranaree University of Technology, Nakhon Ratchasima 30000, Thailand and ²National Synchrotron Research Center, Nakhon Ratchasima 30000, Thailand

Email: Supansa Pantoom - aon_biochem@hotmail.com; Chomphunuch Songsiririthigul - pook@nsr.or.th; Wipa Suginta* - wipa@sut.ac.th

* Corresponding author

Published: 21 January 2008

Received: 17 September 2007

BMC Biochemistry 2008, 9:2 doi:10.1186/1471-2091-9-2

Accepted: 21 January 2008

This article is available from: <http://www.biomedcentral.com/1471-2091/9/2>

© 2008 Pantoom et al; licensee BioMed Central Ltd.

This is an Open Access article distributed under the terms of the Creative Commons Attribution License (<http://creativecommons.org/licenses/by/2.0>), which permits unrestricted use, distribution, and reproduction in any medium, provided the original work is properly cited.

Abstract

Background: *Vibrio carchariae* chitinase A (EC3.2.1.14) is a family-18 glycosyl hydrolase and comprises three distinct structural domains: i) the amino terminal chitin binding domain (ChBD); ii) the (α/β)₈ TIM barrel catalytic domain (CatD); and iii) the $\alpha + \beta$ insertion domain. The predicted tertiary structure of *V. carchariae* chitinase A has located the residues Ser33 & Trp70 at the end of ChBD and Trp231 & Tyr245 at the exterior of the catalytic cleft. These residues are surface-exposed and presumably play an important role in chitin hydrolysis.

Results: Point mutations of the target residues of *V. carchariae* chitinase A were generated by site-directed mutagenesis. With respect to their binding activity towards crystalline α -chitin and colloidal chitin, chitin binding assays demonstrated a considerable decrease for mutants W70A and Y245W, and a notable increase for S33W and W231A. When the specific hydrolyzing activity was determined, mutant W231A displayed reduced hydrolytic activity, whilst Y245W showed enhanced activity. This suggested that an alteration in the hydrolytic activity was not correlated with a change in the ability of the enzyme to bind to chitin polymer. A mutation of Trp70 to Ala caused the most severe loss in both the binding and hydrolytic activities, which suggested that it is essential for crystalline chitin binding and hydrolysis. Mutations varied neither the specific hydrolyzing activity against pNP-[GlcNAc]₂, nor the catalytic efficiency against chitohexaose, implying that the mutated residues are not important in oligosaccharide hydrolysis.

Conclusion: Our data provide direct evidence that the binding as well as hydrolytic activities of *V. carchariae* chitinase A to insoluble chitin are greatly influenced by Trp70 and less influenced by Ser33. Though Trp231 and Tyr245 are involved in chitin hydrolysis, they do not play a major role in the binding process of crystalline chitin and the guidance of the chitin chain into the substrate binding cleft of the enzyme.

Background

Chitin is a homopolysaccharide chain of *N*-acetylglucosamine (GlcNAc or G1) units combined together with β -1,4 glycosidic linkages. Chitin is one of the most abundant biopolymers found in nature as constituent of fungal

cell walls and exoskeletons of crustaceans and insects. However, the β -GlcNAc units that generally form intra- and intermolecular H-bonds make chitin completely insoluble in water and its use is thus limited. Several strategies have been developed for converting chitin into small

soluble derivatives, which are more useful for applications in the fields of medicine, agriculture and industry. Enzymatic degradation of chitin using biocatalysts seems to be the method of choice since the type, quantity and quality of oligomeric products can be well controlled and the reaction occurs quickly and completely under mild conditions without generation of environmental pollutants.

Chitinases (EC3.2.1.14) are a diverse group of enzymes that catalyze the conversion of insoluble chitin to soluble oligosaccharides. They are found in a wide variety of organisms including virus, bacteria, fungi, insects, plants and animals [1-8]. In the carbohydrate active enzymes (CAZy) database <http://www.cazy.org/>, carbohydrate enzymes are first classified as glycosyl hydrolases (GH), glycosyl transferases (GT), polysaccharide lyases (PL), carbohydrate esterases (CE), and carbohydrate binding modules (CBM), and then further divided into numbered families with structurally-related catalytic and carbohydrate-binding modules. Following this classification, chitinases are commonly listed as family GH-18 and family GH-19 enzymes. Family-18 chitinases have the catalytic crevice located at top of the (α/β)₈-TIM barrel domain [9,10], whereas the catalytic domain of family-19 chitinases comprises two lobes, each of which is rich in α -helical structure [11]. Bacteria such as *Serratia marcescens*, *Bacillus circulans*, *Alteromonas sp.* and marine *Vibrios* produce chitinases to synergistically degrade chitin and use it as a sole source of energy [1,12-16]. The mechanism of chitin degradation by bacterial chitinases was mainly derived from the outcome of structural studies or site-directed mutagenesis [17-20]. Unlike chitoooligosaccharides, chitin polymer has been presumed to unidirectionally enter the substrate binding cleft of chitinases under the guidance of a few surface-exposed residues at the exterior of the substrate binding cleft [21,22]. Those residues were identified as Trp33, Trp69, Phe232, and Trp245 in *S. marcescens* Chi A [18], Ser33, Trp70, Trp232, and Trp245 in *Aeromonas caviae* Chi1 [23], and Trp122 and Trp134 in *B. circulans* Chi A1 [17]. Structurally, the latter two residues are located in the equivalent locations of Tyr245 and Trp231, respectively of *V. carchariae* chitinase A (Fig. 1 and ref [17]). We previously isolated chitinase A from a marine bacterium, *Vibrio carchariae* [24]. The enzyme was found to be highly expressed upon induction with chitin and was active as a monomer of 63 kDa. The DNA fragment encoding the functional chitinase A was subsequently cloned into the pQE60 expression vector that was compatible to be highly expressed in *E. coli* type strain M15 [25]. Mutational studies confirmed that the conserved Glu315 acts as the catalytic residue in the substrate-assisted mechanism [26,27], whereas the aromatic residues including Trp168, Tyr171, Trp275, Trp397 and Trp570 participated in direct interactions with chitoooligosaccharides [28]. In this study, site-directed mutagenesis

was employed in combination with following chitin binding assays and kinetic analysis to investigate the significance of the putative surface-exposed residues Ser33, Trp70, Trp231 and Tyr245 for the binding and hydrolytic activities of the *Vibrio* chitinase A.

Results

Homology modeling and sequence analysis

We previously reported gene isolation and sequence analysis of *V. carchariae* chitinase A precursor [25]. Site-directed mutation of the active site residues showed that Glu315 plays an essential role in catalysis [26]. On the other hand, the conserved aromatic residues (Trp168, Tyr171, Trp275, Trp397 and Trp570) located within the substrate binding cleft of the enzyme were found to be important in binding to chitoooligosaccharides [28]. Here, we have investigated the functional roles of four amino acid residues (Ser33, Trp70, Trp231 and Tyr245) at the surface of *V. carchariae* chitinase A. All of these residues have been proposed as functionally relevant to binding and hydrolysis of crystalline chitin [17,18]. Fig. 1 represents the modeled 3D-structure of *V. carchariae* chitinase A that was built based upon the crystal structure of *S. marcescens* chitinase A mutant E315L complexed with a chitohexamer [see Methods]. It can clearly be seen that the four residues linearly align with each other. Trp70 and Ser33 are positioned at the end of the N-terminal chitin binding domain (ChBD), whilst Trp231 and Tyr245 are found outside the substrate binding cleft where they are part of the TIM barrel catalytic domain.

When the amino acid sequences of several bacterial chitinases were compared, the *V. carchariae* chitinase A (Q9AMP1) exhibited highest sequence identity with chitinase A from *V. Harveyi* HY01 (A6AUU6) (93%), moderate identity with chitinase A from *S. marcescens* (P07254) and *Enteromonas sp.* (Q4PZF3) (47%), and low identity with chitinase A1 from *B. circulans* (22%). Surprisingly, extremely low sequence identity was observed when *V. carchariae* chitinase A was compared with chitinase A from *V. splendidus* (A3UMC6) (13%) and *V. cholerae* (A6ACY6) (11%).

A structure-based alignment of three chitinases, including *V. carchariae* chitinase A, *S. marcescens* chitinase A, and *B. circulans* WL-12 chitinase A1 was constructed and is displayed in Fig. 2A & 2B. Fig. 2A represents an alignment of the N-terminal ChBDs of the *Vibrio* and *Serratia* chitinases with the C-terminal fragment that covers the ChBD of the *Bacillus* chitinase A1 (ChBD_{ChIA1}). The ChBD_{ChIA1} consists of the residues 655 to 699 and deletion of this domain led to a severe loss in the binding activity to chitin as well as in the colloidal chitin-hydrolyzing activity, suggesting that this domain is essential for binding to insoluble chitin of this enzyme [29]. As shown in Fig. 2A, the residues

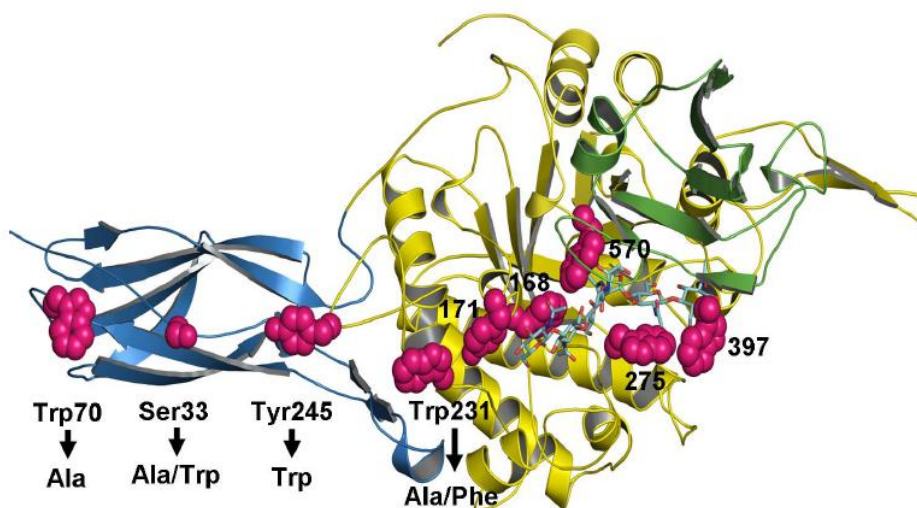


Figure 1
The Swiss-Model 3D-structure of *V. carchariae* chitinase A. A ribbon representation of the 3D-structure of *V. carchariae* chitinase A was constructed based on the x-ray structure of *S. marcescens* Chi A E315L mutant as described in the text. The N-terminal chitin binding domain is presented in cyan, the TIM barrel domain in yellow and the small insertion domain in green. The coordinates of [GlcNAc]₆ that are modeled in the active site of the *Vibrio* enzyme are shown as a stick model with N atoms in blue and O atoms in red. The mutated residues (Ser33, Trp70, Trp231 and Tyr245) and other substrate binding residues are also presented in stick model (magenta).

Trp656 and Trp687 of the ChBD_{chiA1} are well aligned with Ser33 and Trp70 of *V. carchariae* chitinase A. However, the determination of the solution structure of the ChBD_{chiA1} by Ikegami et al. [30] identified only Trp687 as a putative chitin binding residue, in addition to His681, Thr682, Pro689, and Pro693.

With respect to the alignment of the catalytic domain (Fig. 2B), Trp231 of the *Vibrio* chitinase is equivalent to Trp122 and to Phe232 of the *Bacillus* and *Serratia* chitinases. For Tyr245, this residue is replaced by Trp134 and Trp245 in the *B. circulans* and *S. marcescens* sequences, respectively. The sequence alignment additionally demonstrates the residues Ser33 and Trp70 within the flexible loops that join two strands in the chitin binding region. The residues Trp245 and Tyr231 are found as part of the catalytic (α/β)₈ TIM barrel, where Tyr245 is exposed on the loop that

joins helices 2(3) and 2(4) together and Trp231 is the only residue being found in an α -helix (helix 2(3)).

Expression and purification of chitinase A and mutants

To investigate the binding and hydrolytic activities of *V. carchariae* chitinase A, target residues as named above were mutated by site-directed mutagenesis. According to the employed system, the recombinant chitinases were expressed as the C-terminally (His)₆ tagged fusion protein (see Methods). After single-step purification using Ni-NTA agarose affinity chromatography, the yields of the purified proteins was estimated to be approx. 20 to 25 mg/ml per litre of bacterial culture. As analyzed by SDS-PAGE, all the mutated proteins displayed a single band of molecular weight of 63 kDa (data not shown), which is identical to the molecular weight of the wild-type enzyme.

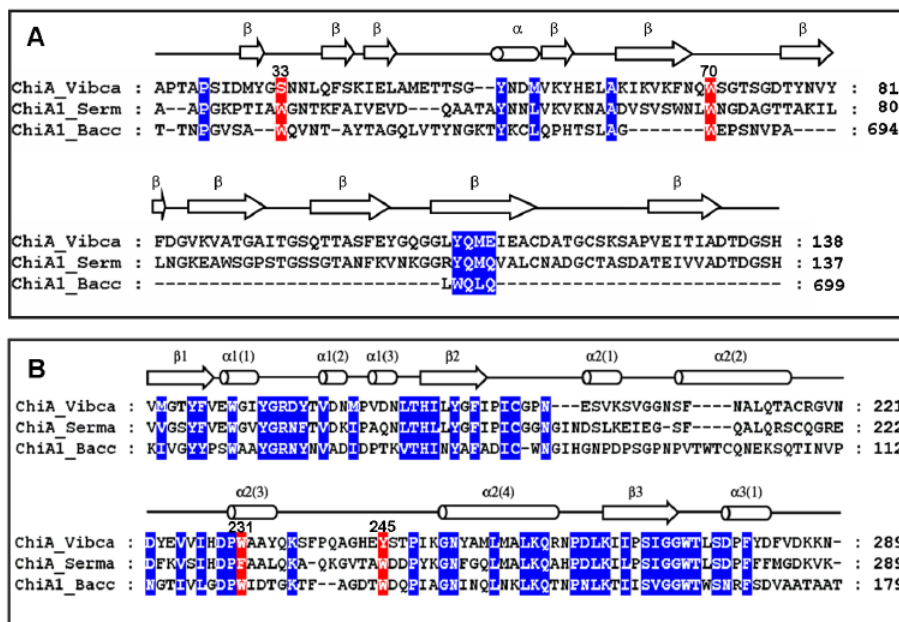


Figure 2

A structure-based alignment of *V. carchariae* chitinase A with *S. marcescens* chitinase A and *B. circulans* chitinase A1. A) The N-terminal ChBDs of *V. carchariae* chitinase A (residues 22–138) and *S. marcescens* chitinase A (residues 24–137) were aligned with the C-terminal fragment (residues 648–699), covering the ChBD of *B. circulans* WL-12 chitinase A1. B) An alignment of the catalytic domain of the three bacterial chitinases with residues 160 to 289 of *V. carchariae* chitinase A being displayed. The chitinase sequences were retrieved from the Swiss-Prot/TreEMBL protein databases, aligned using "MegAlign" in the DNASTAR package, and displayed in Genedoc. The secondary structure of *V. carchariae* chitinase A was predicted from the PHD method in PredictProtein using *S. marcescens* as template [see texts]. Conserved residues are shaded in blue, whereas the residues that are aligned with Ser33, Trp70, Trp231, and Tyr245 of *V. carchariae* chitinase A are shaded in red. ChiA_Vibca: *V. carchariae* chitinase A (Q9AMP1), ChiA_Serma: *S. marcescens* chitinase A (P07254), and ChiA1_Bacc: *B. circulans* chitinase A1 (P20533). β -strand is represented by an arrow, α -helix by a cylinder and loop by a straight line.

Effects of mutations on the chitin binding activities of chitinase A

To minimize hydrolysis, all the binding experiments were carried out on ice. Bindings of the wild-type chitinase and mutants to colloidal chitin were initially investigated as a function of time. After a removal of the enzyme bound to chitin, decreases in concentration of the unbound enzyme remaining in the supernatant was monitored discretely at different time points of 0 to 120 min. Fig. 3 demonstrates that the binding process took place rapidly and reached equilibrium within 5 min. The relative binding activity of each mutant to colloidal chitin is following the order W231A > S33W > WT \approx W231F > S33A > Y245W > W70A.

The binding activity of the individual mutants relative to the one of the wild-type enzyme was further examined with colloidal chitin and α -chitin polysaccharides at a single time point of 60 minutes. In general, the wild-type and mutant chitinases expressed greater binding activity towards colloidal chitin. A comparison of the level of binding of the engineered enzymes to the two substrates revealed a similar pattern (Fig. 4). For both polysaccharides, W70A and Y245W displayed lower binding activity than the wild-type enzyme. S33A and W231F showed a modest increase in binding to crystalline α -chitin and decreased level of binding to colloidal chitin. Mutants S33W and W231A, on the other hand, displayed higher

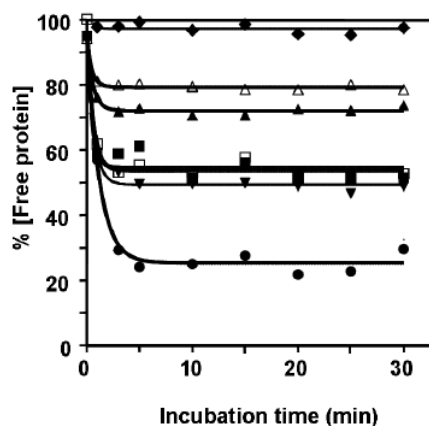


Figure 3
Time-course of binding of chitinase A and mutant enzymes to colloidal chitin. Chitinases (1 μmol in 100 mM sodium acetate buffer, pH 5.5) were incubated with 1.0 mg colloidal chitin at 0°C. Decreases in free enzyme concentration were determined at different time points from 0–30 min by Bradford's method. Each data value was calculated from triplicate experiments. Symbols: wild-type (black square); S33A (black upward-pointing triangle); S33W (black downward-pointing triangle); W70A (black diamond); W231A (black circle); W231F (open square); and Y245W (open triangle).

effectiveness in the binding to both substrates. Of all, mutant W231A displayed highest binding activity and W70A exhibited lowest activity. Especially, no detectable binding to crystalline α -chitin was observed with mutant W70A.

Adsorption isotherms of chitinase mutants to colloidal chitin were carried out relative to that of the wild-type enzyme. Fig. 5 represents a non linear plot of the adsorption isotherms obtained at a fixed concentration of colloidal chitin but varied concentrations of the enzyme (See Methods). In comparison to the wild-type enzyme, mutants S33W and W231A exhibited significantly higher binding activity, whereas mutants W70A, S33A, W231F and Y245W had a notably decreased binding activity. When the dissociation binding constants (K_d) were estimated from the non-linear regression function, it was found that the K_d value of wild-type ($0.95 \pm 0.11 \mu\text{M}$) was slightly larger than the K_d values of S33W ($0.84 \pm 0.09 \mu\text{M}$) and W231F ($0.88 \pm 0.09 \mu\text{M}$), but remarkably greater than the value of W231A ($0.26 \pm 0.03 \mu\text{M}$). In contrast,

significantly higher K_d values than the wild-type value were observed with S33A ($1.50 \pm 0.11 \mu\text{M}$), W70A ($2.30 \pm 0.25 \mu\text{M}$), and Y245W ($1.60 \pm 0.16 \mu\text{M}$). These estimated K_d values gave a notation of the enzyme's binding strength in the following order W231A > S33W > W231F > wild-type > S33A > Y245W > W70A, which is in absolute accordance with the binding activities determined by the chitin binding assay (see Fig. 4) and the kinetic data as described below.

Effects of mutations on the hydrolytic activities of chitinase A

The effects of mutations on the hydrolytic activity of *V. carchariae* chitinase A were further studied by exposing the wild-type and modified enzymes to pNP-[GlcNAc]₂, colloidal chitin and crystalline α -chitin. The specific hydrolyzing activity for the three different substrates was subsequently determined. From all the mutants, only W231A displayed a slightly reduced specific hydrolyzing activity against the pNP substrate (Table 1).

Unlike the pNP-glycoside, strong effects on the hydrolytic activities were observed with the insoluble polymeric substrates. The hydrolyzing activity against crystalline α -chitin was completely abolished in case of mutants S33A, W70A and W231A/F but improved for mutants S33W and Y245W at levels of 166% and 250% of the wild-type activity, respectively. A similar trend was also seen with colloidal

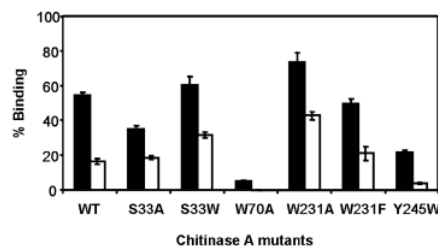


Figure 4
Binding of chitinase A and mutants to insoluble chitin. The binding assay set as described in the text was incubated with crystalline α -chitin or colloidal chitin for 60 min.

$$\text{The \% binding} = \left[\frac{E_t - E_f}{E_t} \right] \times 100; \text{ where } E_t \text{ is initial enzyme}$$

concentration and E_f is the free enzyme concentration after binding. Closed and open bars represent % binding to colloidal chitin and crystalline α -chitin, respectively. The presented data are mean values obtained from three independent sets of the experiment.

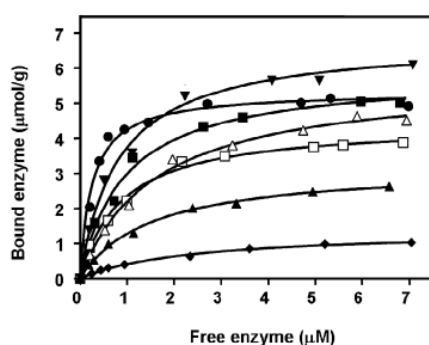


Figure 5
Equilibrium adsorption isotherms of wild-type and mutant chitinases A to colloidal chitin. The reaction assay (500 μ l) contained 1.0 mg chitin and varied concentrations of enzyme from 0 to 7.0 μ M. After 60 min of incubation at 0°C, the reaction mixture was centrifuged and concentrations of E_b and E_f were determined as described in the text. Symbols: wild-type (black square); S33A (black upward-pointing triangle); S33W (black downward-pointing triangle); W70A (black diamond); W231A (black circle); W231F (open square); and Y245W (open triangle).

dal chitin. However, for this substrate S33A, W70A and W231A/F not completely abolished but markedly decreased hydrolyzing activity, while S33W (119%) and Y245W (152%) again where the ones that displayed higher activity than wild-type enzyme. The most severe loss of the specific hydrolyzing activity towards colloidal chitin was detected for mutant W70A, which had a substitution of Trp70 to Ala.

Table 1: Specific hydrolyzing activity of chitinase A and mutants. The reducing sugar assay was carried out against crystalline and colloidal chitin. The release of the hydrolytic products was calculated from a standard curve of [GlcNAc]₂. On the other hand, the specific hydrolyzing activity against pNP-[GlcNAc]₂ was determined by the colorimetric assay. The release of pNP was estimated from a standard curve of pNP

Protein	Specific hydrolyzing activity (U/ μ mol protein) ^a		
	Crystalline chitin	Colloidal chitin	pNP-[GlcNAc] ₂
Wild-type	0.59 \pm 0.02(100) ^b	12.9 \pm 0.22 (100)	50.5 \pm 1.13 (100)
S33A	n.d. ^c	8.5 \pm 0.50 (66)	58.0 \pm 1.08 (115)
S33W	1.00 \pm 0.08 (166)	15.3 \pm 0.32 (119)	54.0 \pm 2.55 (107)
W70A	n.d.	4.3 \pm 0.17 (33)	52.8 \pm 2.14 (105)
W231A	n.d.	6.6 \pm 0.26 (51)	45.2 \pm 2.00 (90)
W231F	n.d.	9.2 \pm 0.49 (71)	54.3 \pm 2.85 (108)
Y245W	1.49 \pm 0.09 (250)	19.6 \pm 0.53 (152)	53.6 \pm 1.61 (106)

^a One unit of chitinase is defined as the amount of enzyme that releases 1 μ mol of [GlcNAc]₂ or 1 nmol of pNP per min at 37°C.

^b Values in parentheses represent relative specific hydrolyzing activities (%).

^c Non-detectable activity.

Steady-state kinetics of chitinase A and mutants

The kinetic parameters of the hydrolytic activity of chitinase A and mutants were finally determined with chito-hexaose and colloidal chitin as substrates. As presented in Table 2, mutations of the chosen residues led for the response of enzyme values towards the hexachitooligomer to concomitant decreases in both the K_m and k_{cat} values. For all the mutants, however, the overall catalytic efficiency (k_{cat}/K_m) was not much different to the value observed for the wild-type enzyme. In contrast, the kinetic properties of the enzyme against colloidal chitin were significantly modified by the mutations. The K_m values of S33A (2.07 10^1 mg ml⁻¹), W70A (2.26 10^1 mg ml⁻¹), and Y245W (1.82 10^1 mg ml⁻¹) were higher than the wild-type K_m (1.74 10^1 mg ml⁻¹) whereas S33W (1.58 10^1 mg ml⁻¹) and W231A (1.01 10^1 mg ml⁻¹) had considerably lower K_m compared to the reference value. Mutations that caused a large decrease in the enzyme's catalytic activity, k_{cat} , were Ser33 to Ala, Trp70 to Ala and Trp231 to Ala/Phe, whereas mutations of Ser33 to Trp and Tyr245 to Trp elevated k_{cat} values instead. The overall catalytic efficiency (k_{cat}/K_m) that was calculated for the hydrolysis of colloidal chitin was to more or less extent either reduced (for S33A, W70A, W231A and W231F) or increased (for S33W and Y245W).

Discussion

This study describes the possible role of Ser33, Trp70, Trp231, and Tyr245 in chitin binding and hydrolysis. Point mutations of these residues were introduced by site-directed mutagenesis and changes in the binding and hydrolytic activities of the enzyme as a result of the amino acid substitution were subsequently investigated for various substrates. Chitin binding assays (Fig. 3 & 4) demonstrate a decrease in the binding activity of mutants S33A, W70A and Y245W to various extents. However, the most severe effect was observed with W70A. A time course study displayed no binding activity of W70A but retained activ-

Table 2: Kinetic parameters of substrate hydrolysis by chitinase A wild-type and mutants. A kinetic study was carried out using 0–5% (w/w) colloidal chitin and 0–500 μ M chitohexaose as substrates. After 10 minutes of incubation at 37°C, the amounts of the reaction products were determined from a standard curve of [GlcNAc]₂

Chitinase A variant	Chitohexaose			Colloidal chitin		
	K_m (μ M)	k_{cat} (s ⁻¹)	k_{cat}/K_m (s ⁻¹ M ⁻¹)	K_m (10 ¹ mg ml ⁻¹)	k_{cat} (s ⁻¹)	k_{cat}/K_m (10 ⁻¹ s ⁻¹ mg ml ⁻¹)
Wild-type	218 ± 22.0	2.9	1.3 × 10 ³ (100) ^a	1.74 ± 0.1	1.2	0.7 (100)
S33A	171 ± 20.5	2.6	1.5 × 10 ³ (115)	2.07 ± 0.2	0.9	0.4 (57)
S33W	210 ± 15.4	2.8	1.3 × 10 ³ (100)	1.58 ± 0.2	1.4	0.9 (129)
W70A	185 ± 22.0	2.5	1.3 × 10 ³ (100)	2.26 ± 0.4	0.4	0.2 (29)
W231A	189 ± 13.2	2.6	1.4 × 10 ³ (108)	1.01 ± 0.2	0.6	0.6 (86)
W231F	163 ± 10.3	2.4	1.5 × 10 ³ (115)	1.70 ± 0.2	0.9	0.5 (71)
Y245W	201 ± 13.1	2.6	1.3 × 10 ³ (100)	1.82 ± 0.2	1.7	0.9 (129)

^a Relative catalytic efficiencies (%) are shown in parentheses.

ity of other mutants to colloidal chitin (Fig. 3). This strongly suggested that Trp70 is the major determinant for insoluble chitin binding. Sugiyama and colleagues previously employed the reducing-end labeling technique and the tilt micro-diffraction method [21,22] to illustrate the molecular directionality of crystalline β -chitin hydrolysis by *S. marcescens* chitinase A and *B. chitinase* chitinase A1. If the chitin polymer enters the substrate binding cleft of *V. carchariae* chitinase A from the reducing end as described for the *Serratia* and *Bacillus* enzymes, Trp70 will likely serve as a platform for the arrival of a chitin molecule. This idea is well complimented by the location of the residue at the end of ChBD. A remarkable loss of the specific hydrolyzing activity as well as the decrease in the rate of enzyme turnover (k_{cat}) that was observed for mutant W70A is hence explainable by the loss of the binding strength due to a substitution of Trp to Ala and an associated change in the hydrophobic interactions. A similar performance was seen for residue Ser33. Although to a lesser extent, a mutation of Ser33 to Ala also led to decreased binding activity, while its mutation to Trp improved binding activity. This finding provides additional evidence that binding of the chitin chain to the ChBD is cooperatively taken place via hydrophobic interactions and influenced by the molecular setting in this region.

The most striking observations were made with the residue Trp231. As demonstrated by the modeled 3D-structure (see Fig. 1), the residue Trp231 is placed at the outermost of the catalytic surface, thereby lying closest to the non-reducing end of the substrate binding cleft. The observed drastic improvement (rather than reduction) in the binding efficiency of mutant W231A could only be explained as a removal of the side-chain blockage. Hence, the reduced hydrolyzing activity of mutant W231A was unlikely influenced by changes in the binding activity as

a result of the alanine substitution of Trp231. Apparently, the same phenomenon was previously recognized in *S. marcescens* chitinase A [18], with which a mutation of Phe232 to Ala seriously diminished the hydrolyzing activity but left the binding activities to both colloidal chitin and β -chitin microfibrils unchanged.

When the next residue in line (Tyr245) (see Fig. 1) was mutated to a bulkier side-chain (Trp), inverse effects (reduced binding but improved hydrolysis) were observed. This complimented the idea of the binding barrier around the entrance hall of the catalytic domain by Trp231 and Tyr245. Similar findings were also recognized with a cellulose degrading enzyme, *Thermobifida fusca* endoglucanase (Cel9A) [31]. With this enzyme, it was observed that mutations of the surface-exposed cellulose binding residues Arg557 and Glu559 to Ala (mutant R557A/E559A) led to a severe loss in the hydrolytic activity against crystalline cellulose, but a change in the binding activity was not at all observed. Structurally, the residues Arg557 and Glu559 are found on the surface of the cellulose binding module (CBM), closest to the catalytic binding cleft of Cel9A. Therefore, the effects of Arg557 and Glu559 would be explained in analogy to those of Trp231 and Tyr245 in *V. carchariae* chitinase A.

In marked contrast, observations made with the *Vibrio* Trp231 mutation were different to the studies of Li et al. on *A. caviae* Chi 1 [23] and of Watanabe et al. on *B. circulans* Chi A1 [17]. Mutations of Trp232 and Trp245 (in *A. caviae* Chi 1) or Trp122 and Trp 134 (in *B. circulans*) to alanine resulted in a marked loss in both binding and hydrolyzing activities, especially against crystalline β -chitin. Therefore, the reduced hydrolytic activities were assumed to be associated with the weaker binding of the two corresponding residues. Based on their mutational data, the residues seemed to participate directly in binding

to crystalline chitin, and subsequently cooperatively assisting the chitin chain to penetrate through the catalytic cleft of *A. caviae* or *B. circulans* chitinase.

Indeed, the above-mentioned event that took place in the *A. carviae* and *B. circulans* chitinases did not seem to be the case for the *V. carchariae* chitinase A due to different behaviors of Trp231 and Tyr245 found for the *Vibrio* enzyme. Our data suggested that a possible action of *V. carchariae* chitinase A on insoluble chitin could proceed as follows: i) Initial binding of a chitin chain to the ChBD. This process is most influenced by the hydrophobic interaction set between the incoming sugar and residue Trp70, which is located at the doorway of the ChBD; ii) Further binding of GlcNAc units. However, binding through Ser33 remains inconclusive, since the mutational results revealed that Ser33 did not act as a powerful binding residue. Alternatively, this binding step might be made through a different surface-exposed aromatic residue located nearby; and iii) Sliding of bound sugar units of the chitin chain into the substrate binding cleft. Based on the 'slide and bend' mechanism proposed by Watanabe and others [17,21,32], the sliding process is achieved by cooperative interactions with other surface-exposed aromatic residues located close to the entrance of the substrate binding cleft. However, our data strongly suggested that the chitin chain movement most likely takes place via an interaction with different surface-exposed aromatic residues other than Tyr245 and Trp231.

When *p*NP-[GlcNAc]₂ was used as a substrate, hydrolyzing activities of the mutated enzymes and the wild-type enzyme were almost indistinguishable. This observation and the essentially unchanged catalytic efficiency (k_{cat}/K_m) of all mutants compared to wild-type enzyme clearly pointed out that Ser33, Trp70, Trp231 and Tyr245 do not play a major role in the process of hydrolysis of soluble chitooligosaccharides.

Conclusion

Point mutations of four surface-exposed residues of *V. carchariae* chitinase A and subsequent experiments on chitin binding and hydrolysis were performed. Trp70, which is located at the *N*-terminal end of the chitin binding domain, was identified as the most crucial residue in colloidal and crystalline chitin binding and consequently their hydrolysis. The residues Trp231 and Tyr245, both located nearer to the substrate-binding cleft, influenced chitin hydrolysis but not really insoluble chitin binding.

Methods

Bacterial strains and expression plasmid

Escherichia coli type strain DH5 α was used for routine cloning, subcloning and plasmid preparation. Supercompetent *E. coli* XL1Blue (Stratagene, La Jolla, CA, USA) was

the host strain for the production of mutagenized DNA. *E. coli* type strain M15 (Qiagen, Valencia, CA, USA) and the pQE 60 expression vector harboring *chitinase A* gene fragments were used for a high-level expression of recombinant chitinases.

A structural based sequence alignment and homology modeling

The amino acid sequence alignment was constructed by the program MegAlign using CLUSTAL method algorithm in the DNASTAR package (Biocompare, Inc., CA, USA) and displayed in Genedoc [33]. The amino acid sequence of the *V. carchariae* chitinase was aligned with five selected bacterial chitinase sequences available in the Swiss-Prot or TrEMBL database (see Results). The secondary structure elements of *V. carchariae* chitinase A were obtained by the PHD method available in PredicProtein [34]. The modeled tertiary structure of the *Vibrio* chitinase was built by Swiss-Model and displayed by Swiss-Pdb Viewer [35] using the x-ray structure of *S. marcescens* chitinase A E315L mutant complex with hexaNAG (PDB code: 1NH6) as structure template. The co-ordinates of [GlcNAc]₆ were modeled into the active site of the *Vibrio* enzyme and the target residues were located by superimposing the C α atoms of 459 residues of *V. carchariae* chitinase A with the equivalent residues of *S. marcescens* E315L complex, using the program Superpose available in the CCP4 suit [36]. The predicted structure was viewed with Pymol [37].

Mutation design and site-directed mutagenesis

Site-directed mutagenesis was carried out by PCR using QuickChange site-directed mutagenesis kit (Stratagene). The pQE60 plasmid harbouring chitinase A DNA lacking the residues 598–850 C-terminal fragment was used as DNA template [25]. The primers (Bio Service Unit, Thailand) used for the mutagenesis are summarized in Table 3. The success of newly-generated mutations was confirmed by automated DNA sequencing (BSU, Thailand). The programs used for nucleotide sequence analyses were obtained from the DNASTAR package (DNASTAR, Inc., Madison, USA).

Expression and purification of recombinant wild-type and mutant chitinases

The pQE60 expression vector harboring the DNA fragment that encodes wild-type chitinase A were highly expressed in *E. coli* M15 cells and the recombinant proteins purified as described elsewhere [28]. Briefly, the cells were grown at 37°C in Luria Bertani (LB) medium containing 100 μ g/ml ampicillin until OD₆₀₀ reached 0.6, and then 0.5 mM of isopropyl thio- β -D-galactoside (IPTG) was added to the cell culture for chitinase production. After 18 h of induction at 25°C, the cell pellet was collected by centrifugation, re-suspended in 15 ml of lysis buffer (20 mM Tris-HCl buffer, pH 8.0, containing 150

Table 3: Primers used for mutagenesis

Point mutation	Oligonucleotide sequence
Ser33→Ala	Forward 5'-CGATATGTA CGGTCCG •AATAACCTTCAATTTTC-3' Reverse 5'-GAAAATTGAAGGTTATT CGC ACCCTACATATCG-3'
Ser33→Trp	Forward 5'-CGATATGTA CGGTGG AATAACCTTCAATTTTC-3' Reverse 5'-GAAAATTG CAG GTATT CCA ACCCTACATATCG-3'
Trp70→Ala	Forward 5'-GAAAATTA ACCGCG AGTGGCACATCTG-3' Reverse 5'-CAGATGTGCCACT CGC CTGGTTAAATTTTC-3'
Trp231→Ala	Forward 5'-GTTATCCAT GATCCGCG Cgagcttacc-3' Reverse 5'-GATAAGCTG CCCGGAT CATGGATAAC-3'
Trp231→Phe	Forward 5'-GGTTATCCATG ACCCGIII GCAGCTTATCAG-3' Reverse 5'-CTGATAAGCTG CAAA CCGGTCATGGATAACC-3'
Tyr245→Trp	Forward 5'-CAGGTCA TGAG CACGCCAATCAAG-3' Reverse 5'-CTTGATTGGCGT GCTCCA TTCATGACCTG-3'

^a Sequences underlined indicate the mutated codons.

^b Sequences in bold represent the codon being modified to achieve the T_m value as required for QuickChange site-directed mutagenesis.

mM NaCl, 1 mM phenylmethylsulphonyl fluoride (PMSF), and 1.0 mg/ml lysozyme), and then lysed on ice using an Ultrasonic homogenizer. The supernatant obtained after centrifugation at 12,000 g for 1 h was instantly subjected to Ni-NTA agarose affinity chromatography following the Qiagen's protocol. After SDS-PAGE analysis [38], the chitinase containing fractions were pooled and then applied to Vivaspin-20 membrane filtration (Mr 10 000 cut-off, Vivascience AG, Hannover, Germany) to concentrate the protein and to remove imidazole. A final concentration of the protein was determined by Bradford's method [39] using a standard calibration curve constructed from BSA (0–25 µg).

Chitinase activity assays

The colorimetric assay was carried out in a 96-well microtiter plate using pNP-[GlcNAc]₂ (Bioactive Co., Ltd., Bangkok, Thailand) as substrate. A 100-µl assay mixture, comprising protein sample (10 µl), 500 µM pNP-(GlcNAc)₂, and 100 mM sodium acetate buffer, pH 5.5, was incubated at 37°C for 10 min with shaking. After the reaction was terminated by the addition of 1.0 M Na₂CO₃ (50 µl), the amount of p-nitrophenol (pNP) released was determined by A₄₀₅ in a microtiter plate reader (Applied Biosystems, Foster City, CA, USA). Molar concentrations of the pNP product were estimated from a calibration curve of pNP (0–30 nmol). Alternatively, chitinase activity was measured by a reducing-sugar assay. The reaction mixture (500 µl), containing 1% (w/v) colloidal chitin (prepared based on Hsu & Lockwood [40]), 100 mM sodium acetate buffer, pH 5.5, and 100 µg chitinase A, was incubated at 37°C in a Thermomixer comfort (Eppendorf AG, Hamburg, Germany). After 15 min of incubation, the reaction was terminated by boiling at 100°C for 5 min, and then centrifuged at 5,000 g for 10 min to precipitate the remaining chitin. A 200-µl superna-

tant was then subjected to DMAB assay following Bruce *et al.* [41]. The release of the reducing sugars as detected by A₅₈₅ was converted to molar quantity using a standard calibration curve of [GlcNAc]₂ (0–1.75 µmol). For crystalline α-chitin, chitinase activity assay was carried out as described for colloidal chitin with 400 µg of chitinase A included in the assayed mixture.

Chitin binding assays

Chitin binding assays were carried out at 0°C to minimize hydrolysis. For time course studies, a reaction mixture (500 µl), containing 1.0 µmol enzyme, and 1.0 mg of chitin in 20 mM Tris-HCl buffer, pH 8.0, was incubated to a required time of 0, 1.25, 2.5, 5, 10, 15, 20, 25, and 30 min, and then the supernatant was collected by centrifuging at 12000 g at 4°C for 10 min. Concentration of the remaining enzyme was determined by Bradford's method, while concentration of the bound enzyme (E_b) was calculated from the difference between the initial protein concentration (E_i) and the free protein concentration (E_f) after binding.

The chitin binding assay was also carried out with crystalline chitin and colloidal chitin (Sigma-Aldrich Pte Ltd., The Capricorn, Singapore Science Park II, Singapore) as tested polysaccharides. A reaction (set as above) was incubated for 60 min at 0°C, then the chitin-bound enzyme was removed by centrifugation, and the concentration of the free enzyme was determined. For adsorption isotherm experiments, the reaction assay (also prepared as described above) containing varied concentrations of protein from 0 to 7.0 µM was incubated for 60 min. After centrifugation, concentration of free enzyme in the supernatant was determined. A plot of [E_b] vs [E_f] was subsequently constructed and the dissociation binding constants (K_d) of wild-type and mutants were estimated using

a non-linear regression function in the GraphPad Prism software (GraphPad Software Inc., San Diego, CA).

Steady-state kinetics

Kinetic parameters of the chitinase variants were determined using chitohexaose or colloidal chitin as substrate. For chitohexaose, the reaction mixture (200 μ l), containing 0–500 μ M (GlcNAc)₆ and 50 μ g enzyme in 100 mM sodium acetate buffer, pH 5.5, was incubated at 37°C for 10 min. After boiling to 100°C for 3 min, the entire reaction mixture was subjected to DMAB assay as described earlier. For colloidal chitin, the reaction was carried out the same way as the reducing-sugar assay, but concentrations of colloidal chitin were varied from 0 to 5.0% (w/v). The amounts of the reaction products produced from both substrates were determined from a standard curve of [GlcNAc]₂ (0–1.75 μ mol). The kinetic values were evaluated from three independent sets of data using the nonlinear regression function obtained from the GraphPad Prism software.

Abbreviations

GlcNAc_n: β -1–4 linked oligomers of *N*-acetylglucosamine residues where *n* = 1–6; DMAB: *p*-dimethylaminobenzaldehyde; IPTG: Isopropyl thio- β -D-galactoside; PMSF: Phenylmethylsulphonylfluoride.

Authors' contributions

SP performed site-directed mutagenesis, recombinant expression, protein purification, and functional characterization. CS carried out the structure-based sequence alignment and the molecular modeling of the tertiary structure of *V. carchariae* chitinase A. WS initiated the ideas of research, was involved in primer design and site-directed mutagenesis, performed data analyses, and prepared the manuscript.

Acknowledgements

This work was financially supported by Suranaree University of Technology; The Thailand Research Fund (TRF) and The Thai Commission on Higher Education through a Research Career Development Grant to WS (grant no RMU4980028) and a TRF-Master Research Grant to SP (grant no MRG4955044).

References

- Yu C, Lee AM, Bassler BL, Roseman S: Chitin utilization by marine bacteria. A physiological function for bacterial adhesion to immobilized carbohydrates. *J Biol Chem* 1991, **266**:24260-24267.
- Rast DM, Horsch M, Furter R, Gooday GW: A complex chitinolytic system in exponentially growing mycelium of *Mucor rouxii*: properties and function. *J Gen Microbiol* 1991, **137**:2797-2810.
- Merzendorfer H, Zimoch L: Chitin metabolism in insects: structure, function and regulation of chitin synthases and chitinases. *J Exp Biol* 2003, **206**:4393-4412.
- Herrera-Estrella A, Chet I: Chitinases in biological control. *EXS* 1999, **87**:171-184.
- Melchers LS, Stulver MH: Novel genes for disease-resistance breeding. *Curr Opin Plant Biol* 2000, **3**:147-152.
- Patil RS, Ghormade VV, Deshpande MV: Chitinolytic enzymes: an exploration. *Enzyme Microb Technol* 2000, **26**:473-483.
- Donnelly LE, Barnes PJ: Acidic mammalian chitinase – a potential target for asthma therapy. *TRENDS in Pharmacol Sci* 2004, **25**:509-511.
- Wills-Karp M, Karp CL: Chitin checking-novel insights into asthma. *N Engl J Med* 2004, **351**:1455-1457.
- Terwisscha van Scheltinga AC, Kalk KH, Beintema JJ, Dijkstra BW: Crystal structures of hevamine, a plant defence protein with chitinase and lysozyme activity, and its complex with an inhibitor. *Structure* 1994, **15**:1181-1189.
- Perrakis A, Tews I, Dauter Z, Oppenheim AB, Chet I, Wilson KS, Vorgias CE: Crystal structure of a bacterial chitinase at 2.3 Å resolution. *Structure* 1994, **15**:1169-1180.
- Hart PJ, Pfluger HD, Monzingo AF, Hollis T, Robertus JD: The refined crystal structure of an endochitinase from *Hordeum vulgare* L. seeds at 1.8 Å resolution. *J Mol Biol* 1995, **248**:402-413.
- Watanabe T, Oyanagi W, Suzuki K, Tanaka H: Chitinase system of *Bacillus circulans* WL-12 and importance of chitinase A1 in chitin degradation. *J Bacteriol* 1990, **172**:4017-4022.
- Suzuki K, Sugawara N, Suzuki M, Uchiyama T, Katouno F, Nikaidou N, Watanabe T: Chitinases A, B, and C1 of *Serratia marcescens* 2170 produced by recombinant *Escherichia coli*: enzymatic properties and synergism on chitin degradation. *Biosci Biotechnol Biochem* 2002, **66**:1075-1083.
- Montgomery MT, Kirchman DL: Role of chitin-binding proteins in the specific attachment of the marine bacterium *Vibrio harveyi* to chitin. *Appl Environ Microbiol* 1993, **59**:373-379.
- Tsujibo H, Orikoshi H, Baba N, Miyahara M, Miyamoto K, Yasuda M, Inamori Y: Identification and characterization of the gene cluster involved in chitin degradation in a marine bacterium, *Alteromonas* sp. strain O-7. *Appl Environ Microbiol* 2002, **68**:263-270.
- Suginta W: Identification of chitin binding proteins and characterization of two chitinase isoforms from *Vibrio alginolyticus* 283. *Enzyme Microb Tech* 2007, **41**:212-220.
- Watanabe T, Ishibashi A, Ariga Y, Hashimoto M, Nikaidou N, Sugiyama J, Matsumoto T, Nonaka T: Trp122 and Trp134 on the surface of the catalytic domain are essential for crystalline chitin hydrolysis by *Bacillus circulans* chitinase A1. *FEBS Lett* 2001, **494**:74-78.
- Uchiyama T, Katouno F, Nikaidou N, Nonaka T, Sugiyama J, Watanabe T: Roles of the exposed aromatic residues in crystalline chitin hydrolysis by chitinase A from *Serratia marcescens* 2170. *J Biol Chem* 2001, **276**:41343-41349.
- Katouno F, Taguchi M, Sakurai K, Uchiyama T, Nikaidou N, Nonaka T, Sugiyama J, Watanabe T: Importance of exposed aromatic residues in chitinase B from *Serratia marcescens* 2170 for crystalline chitin hydrolysis. *J Biochem (Tokyo)* 2004, **136**:163-168.
- Itoh Y, Watanabe J, Fukada H, Mizuno R, Kazuka Y, Nonaka T, Watanabe T: Importance of Trp59 and Trp60 in chitin-binding, hydrolytic, and antifungal activities of *Streptomyces griseus* chitinase C. *Appl Microbiol Biotechnol* 2006, **72**:1176-1184.
- Imai T, Watanabe T, Yui T, Sugiyama J: Directional degradation of beta-chitin by chitinase A1 revealed by a novel reducing end labelling technique. *FEBS Lett* 2002, **510**:201-205.
- Hult EL, Katouno F, Uchiyama T, Watanabe T, Sugiyama J: Molecular directionality in crystalline beta-chitin: hydrolysis by chitinases A and B from *Serratia marcescens* 2170. *Biochem J* 2005, **388**:851-856.
- Li Q, Wang F, Zhou Y, Xiao X: Putative exposed aromatic and hydroxyl residues on the surface of the N-terminal domains of Chi1 from *Aeromonas caviae* CB101 are essential for chitin binding and hydrolysis. *Appl Environ Microbiol* 2005, **71**:7559-7561.
- Suginta W, Robertson PAW, Austin B, Fry SC, Fothergill-Gilmore LA: Chitinases from *Vibrio*: activity screening and purification of Chi A from *Vibrio carchariae*. *J Appl Microbiol* 2000, **89**:76-84.
- Suginta W, Vongsuwan A, Songsiririthigul C, Prinz H, Estubeiro P, Duncan RR, Svasti J, Fothergill-Gilmore LA: An endochitinase A from *Vibrio carchariae*: cloning, expression, mass and sequence analyses, and chitin hydrolysis. *Arch Biochem Biophys* 2004, **424**:171-180.
- Suginta W, Vongsuwan A, Songsiririthigul C, Svasti J, Prinz H: Enzymatic properties of wild-type and active site mutants of chi-

- tinase A from *Vibrio carchariae*, as revealed by HPLC-MS. *FEBS J* 2005, **272**:3376-386.
27. Tews I, Terwisscha van Scheltinga AC, Porrhakis A, Wilson KS, Dijkstra BW: Substrate-assisted catalysis unifies two families of chitinolytic enzymes. *J Am Chem Soc* 1997, **119**:7954-7959.
 28. Suginta W, Songsirithigul C, Kobdaj A, Opassiri R, Svasti J: Mutations of Trp275 and Trp397 altered the binding selectivity of *Vibrio carchariae* chitinase A. *Biochim Biophys Acta* 2007, **1770**:1151-1160.
 29. Watanabe T, Ito Y, Yamada T, Hashimoto M, Sekine S, Tanaka H: The roles of the C-terminal domain and type III domains of chitinase A1 from *Bacillus circulans* WL-12 in chitin degradation. *J Bacteriol* 1994, **176**:4465-4472.
 30. Ikegami T, Okada T, Hashimoto M, Seino S, Watanabe T, Shirakawa M: Solution Structure of the chitin-binding domain of *Bacillus circulans* WL-12 chitinase A1. *J Biol Chem* 2000, **275**:13654-13661.
 31. Li Y, Irwin DC, Wilson DB: Processivity, substrate binding, and mechanism of cellulose hydrolysis by *Thermobifida fusca* Cel9A. *Appl Environ Microbiol* 2007, **73**:3165-3172.
 32. Watanabe T, Ariga Y, Sato U, Toratani T, Hashimoto M, Nikaidou N, Kezuka Y, Nonaka T, Sugiyama J: Aromatic residues within the substrate-binding cleft of *Bacillus circulans* chitinase A1 are essential for hydrolysis of crystalline chitin. *Biodiem J* 2003, **376**:237-244.
 33. The National Resource for Biomedical Supercomputing (NRBSC) [<http://www.psc.edu/biomed/genedoc/>]
 34. PredictProtein [<http://www.predictprotein.org/>]
 35. Swiss-Model [<http://swissmodel.expasy.org/>]
 36. Collaborative Computational Project, No.4: The CCP4 suite: programs for protein crystallography. *Acta Crystallogr* 1994, **D50**:760-763.
 37. PyMol [<http://www.pymol.org/>]
 38. Laemmli UK: Cleavage of structural proteins during the assembly of the head of bacteriophage T4. *Nature* 1970, **227**:680-685.
 39. Bradford MM: A rapid and sensitive method for the quantitation of microgram quantities of protein utilizing the principle of protein-dye binding. *Anal Biochem* 1976, **72**:248-254.
 40. Hsu SC, Lockwood JL: Powdered chitin agar as a selective medium for enumeration of actinomycetes in water and soil. *Appl Microbiol* 1975, **29**:422-426.
 41. Bruce A, Srinivasan U, Staines HJ, Highley TL: Chitinase and laminarinase production in liquid culture by *Trichoderma* spp. and their role in biocontrol of wood decay fungi. *Int Biodeterior Biodegrad* 1995, **35**:337-353.

Publish with **BioMed Central** and every scientist can read your work free of charge

"BioMed Central will be the most significant development for disseminating the results of biomedical research in our lifetime."

Sir Paul Nurse, Cancer Research UK

Your research papers will be:

- available free of charge to the entire biomedical community
- peer reviewed and published immediately upon acceptance
- cited in PubMed and archived on PubMed Central
- yours — you keep the copyright

Submit your manuscript here:

http://www.biomedcentral.com/info/publishing_adv.asp





Contents lists available at ScienceDirect

Journal of Structural Biology

journal homepage: www.elsevier.com/locate/yjsbi

Crystal structures of *Vibrio harveyi* chitinase A complexed with chitooligosaccharides: Implications for the catalytic mechanism

Chomphonuch Songsiriritthigul^{a,b}, Supansa Pantoom^a, Adeleke H. Aguda^{c,d},
Robert C. Robinson^c, Wipa Suginta^{a,*}

^a School of Biochemistry, Suranaree University of Technology, Nakhon Ratchasima 30000, Thailand

^b National Synchrotron Research Center, Nakhon Ratchasima 30000, Thailand

^c Institute of Molecular and Cell Biology, Proteos, 61 Biopolis Drive, Singapore 138673, Singapore

^d Department of Biology, University of Virginia, Charlottesville, VA 22904, USA

ARTICLE INFO

Article history:

Received 13 December 2007
Received in revised form 14 March 2008
Accepted 18 March 2008
Available online xxx

Keywords:

Chitinase
Chitin oligosaccharide
Crystal structure
The slide-and-bend mechanism
Vibrio harveyi

ABSTRACT

This research describes four X-ray structures of *Vibrio harveyi* chitinase A and its catalytically inactive mutant (E315M) in the presence and absence of substrates. The overall structure of chitinase A is that of a typical family-18 glycosyl hydrolase comprising three distinct domains: (i) the amino-terminal chitin-binding domain; (ii) the main catalytic (α/β)₈ TIM-barrel domain; and (iii) the small ($\alpha + \beta$) insertion domain. The catalytic cleft of chitinase A has a long, deep groove, which contains six chitooligosaccharide ring-binding subsites (−4)(−3)(−2)(−1)(+1)(+2). The binding cleft of the ligand-free E315M is partially blocked by the C-terminal (His)₆-tag. Structures of E315M-chitooligosaccharide complexes display a linear conformation of pentaNAG, but a bent conformation of hexaNAG. Analysis of the final 2F_o − F_c omit map of E315M-NAG6 reveals the existence of the linear conformation of the hexaNAG at a lower occupancy with respect to the bent conformation. These crystallographic data provide evidence that the interacting sugars undergo conformational changes prior to hydrolysis by the wild-type enzyme.

© 2008 Elsevier Inc. All rights reserved.

1. Introduction

Chitin, a highly stable homopolysaccharide of β (1 → 4)-linked *N*-acetyl-D-glucosamine (GlcNAc or NAG)¹ is widely distributed in the shells of crustaceans; the cuticles of insects; the shells and skeletons of molluscs; and the cell walls of fungi. Chitin degradation is of considerable interest because the products have potential applications in the fields of biomedicine, agriculture, nutrition, and biotechnology. Chitinases (EC 3.2.1.14) are major enzymes that hydrolyse chitin into oligosaccharide fragments. These enzymes are found in organisms that possess chitin as a constituent or that use it as a nutrient source. Bacteria produce chitinases in order to utilise chitin as a source of carbon and nitrogen (Bhattacharya et al., 2007; Keyhani and Roseman, 1999). Fungal chitinases play a similar nutritional role but are additionally involved in fungal development and morphogenesis (Kuranda and Robbins, 1991; Sahai and Manocha, 1993). Plants produce chitinases as a defence mechanism against pathogenic fungi (Leah et al., 1991). Animal chitinases are involved

in dietary uptake processes (Jeuniaux, 1961). Human chitinases are responsible for hyperresponsiveness and inflammation of the airways of allergic asthma patients (Donnelly and Barnes, 2004; Kawada et al., 2007).

The carbohydrate active enzyme (CAZy) database (<http://www.cazy.org/>) classifies carbohydrate enzymes into functional families (glycosyl hydrolases, glycosyl transferases, polysaccharide lyases, carbohydrate esterases, and carbohydrate-binding modules), which are further subdivided into structurally related families designated by number. Following this classification, chitinases are listed as GH family-18 and GH family-19. These two families show no homology in both structure and mechanism. The catalytic domain of family-18 chitinases consists of an (α/β)₈-barrel with a deep substrate-binding cleft formed by loops following the C-termini of the eight parallel β -strands (Fukamizo, 2000; Hollis et al., 2000; Perrakis et al., 1994; Terwisscha van Scheltinga et al., 1996). In contrast, the catalytic domain of family-19 chitinases comprises two lobes, each of which is rich in α -helical structure (Hart et al., 1995). Family-18 chitinases are known to catalyse the hydrolytic reaction through the 'substrate-assisted' or 'retaining mechanism' (Brameld and Goddard, 1998a; Terwisscha van Scheltinga et al., 1995; Tews et al., 1997), whereas family 19 chitinases employ the 'single displacement' or 'inversion mechanism' (Brameld and Goddard, 1998b). The catalytic mechanism of family-18 chitinases involves protonation of the leaving

* Corresponding author. Fax: +66 44 224185.

E-mail address: wipa@sut.ac.th (W. Suginta).

¹ Abbreviations used: GlcNAc or NAGn, β -1-4 linked oligomers of *N*-acetylglucosamine residues where $n = 1-6$; pNP-[GlcNAc]_n, *p*-nitrophenyl- β -D-*N,N*-diacetylchitobioside; IPTG, isopropyl thio- β -D-galactoside; PMSF, phenylmethylsulphonyl fluoride; ChBD, the amino-terminal chitin-binding domain.

group by an absolutely conserved glutamic acid (equivalent to Glu315 of *Serratia marcescens* chitinase A), followed by substrate distortion into a 'boat' conformation at subsite -1 and the stabilisation of an oxazolinium intermediate by the sugar *N*-acetyl-amido group. The resultant bond cleavage yields the retention of anomeric configuration in the products (Armand et al., 1994; Fukamizo et al., 2001; Honda et al., 2004; Sasaki et al., 2002).

Chitinases from both families are further divided into exo- and endochitinases. Exochitinase activity represents a progressive action that starts at the non-reducing end of a chitin chain and successively releases diacetylchitobiose (NAG₂) units, where as, endochitinase activity involves random cleavage at internal points within a chitin chain (Robbins et al., 1988). The active sites of family-18 endochitinases, such as *S. marcescens* chitinase A and *Hevea brasiliensis* chitinase (hevamine), are groove-like structures with openings above and at both ends (Brameld and Goddard, 1998a; Hart et al., 1995). In contrast, the active sites of exochitinases, such as *S. marcescens* ChIB, have tunnel-like morphologies (Van Aalten et al., 2001).

We previously isolated the Chi A gene encoding the 95-kDa chitinase precursor (GenBank Accession No: Q9AMP1) from the genome of *Vibrio carchariae* type strain LMG7890. Based on genotypical and phenotypical features analysed by Pedersen et al. (1998), *V. carchariae* has been re-classified as a heterotypic synonym of *Vibrio harveyi*. To follow the new systematic taxonomy, *V. carchariae* will be referred to as *V. harveyi* in this and later studies. *V. harveyi* (formerly *V. carchariae*) is a marine bacterium that secretes high levels of a 63-kDa endochitinase A (Suginta et al., 2000). This family-18 glycosyl hydrolase shows greatest affinity towards chitoheptamer, which suggests the substrate-binding cleft of this enzyme that comprises an array of six GlcNAc-binding sites (Suginta et al., 2005), comparable to that of *S. marcescens* Chi A and hevamine (Papanikolaou et al., 2001; Perrakis et al., 1994; Terwisscha van Scheltinga et al., 1996). The gene that encodes chitinase A without the 253-aa C-terminal propeptide fragment was subsequently cloned and functionally expressed in *Escherichia coli* (Suginta et al., 2004). Substitution of Glu315 to Met/Gln completely abolished the hydrolysing activity against soluble and insoluble substrates, confirming that this residue is essential for catalysis (Suginta et al., 2005).

In this study, we describe the crystal structures of *V. harveyi* chitinase A and its catalytically inactive E315M mutant, as well as the E315M mutant soaked with NAG5 and NAG6. The overall structures of E315M with and without substrates are almost identical to the wild-type structure. However, the relative conformations of NAG5 and NAG6 bound to E315M are very different. These static structures provide hints to the conformational changes in chitoheptasaccharide conformation during binding and hydrolysis, allowing for a catalytic mechanism of the enzyme to be proposed.

2. Experimental procedures

2.1. Cloning, recombinant expression, and purification

Wild-type chitinase A (amino-acid residues 22–597) and mutant E315M were cloned into the C-terminal (His)₆ tag pQE60 expression vector, and were highly expressed in *E. coli* type strain M15 (Suginta et al., 2004). For protein purification, IPTG-induced bacterial cells obtained from 1-L culture were collected by centrifugation and then resuspended in 20 ml of 20 mM Tris-HCl (pH 8.0) containing 150 mM NaCl, 1 mg ml⁻¹ lysozyme, and 1 tablet of cOmplete EDTA-free, Protease Inhibitor Cocktail (Roche Diagnostics GmbH, Roche Applied Science, Germany). The cells were lysed on ice using a Misonix Sonicator 3000 (New Highway

Farmingdale, NY, USA) with a 20-mm-diameter probe. After the removal of cell debris by centrifugation, the supernatant was filtered through a SFCA membrane (0.2 μm pore size, Nalgene, Rochester, NY, USA) prior to application to two HisTrap HP 1-ml columns connected in series using an ÄKTApurification system (Amersham Biosciences, Piscataway, NJ, USA) and a flow rate of 2.8 ml min⁻¹. The columns were washed with 5 mM, followed by 20 mM, imidazole before being eluted with 250 mM imidazole in 20 mM Tris-HCl (pH 8.0), containing 150 mM NaCl. The protein-containing fractions were collected, concentrated using Vivaspin-20 membrane concentrator (Mr 10,000 cut-off, Vivascience AG, Hannover, Germany), and then further purified by an ÄKTApurification system using a HiLoad 16/60 Superdex 200 prep grade (Amersham Biosciences) with a flow rate of 1.2 ml min⁻¹. Chitinase-containing fractions were combined, exchanged into 10 mM Tris-HCl (pH 8.0), and concentrated to 10–20 mg ml⁻¹ using the Vivaspin membrane concentrator. All purification steps were carried out at 277 K. Protein concentrations were determined by the Coomassie Plus Kit (Pierce, Rockford, IL, USA) using a standard calibration curve constructed from BSA (0–20 μg). The purity of chitinase A was verified by SDS-PAGE (Laemmli, 1970). Chitinase activity was determined by colorimetric assay using pNP-[GlcNAc]₂ as substrate (Suginta et al., 2007) or by the reducing sugar assay using colloidal chitin as substrate (Bruce et al., 1995).

2.2. Protein crystallisation

Initial crystallisation trials of the wild-type chitinase A were set up using a Screenmaker 96+8TM Robot (Innovadyne Technologies, Inc., Santa Rosa, CA, USA) with sitting drop CrystalQuickTM plates (Greiner bio-one, Frickenhausen, Germany). For each crystallisation drop, 20 nl of freshly prepared enzyme (20 mg ml⁻¹) in 10 mM Tris-HCl (pH 8.0), was added to 20 nl of each precipitating agent obtained commercially (Crystal Screen HT & SaltRx HT from Hampton Research, Aliso Viejo, CA, USA, and JBScreen HTS I & II from Jena Bioscience GmbH, Jena, Germany). Crystal growth optimisation with macro seeding was carried out under several JBScreen HTS II precipitant conditions. Diffraction quality crystals, dimensions 230 × 100 × 15 μm³, were produced within two days at 288 K when a protein drop (5 mg ml⁻¹) was equilibrated in 1.2 M ammonium sulphate and 0.1 M Tris-HCl (pH 8.0). The E315M crystals were obtained from 20% (w/v) PEG 4000, 0.1 M ammonium sulphate and 0.1 M Tris-HCl (pH 7.5) and reached final dimensions of 100 × 30 × 50 μm³ after 1 week equilibration at 288 K. Prior to soaking experiments, single crystals of E315M grown under 16% (w/v) PEG 4000, 0.1 M MgCl₂ in 0.1 M HEPES (pH 7.0) were transferred to a cryoprotectant solution containing mother liquor with 20% (w/v) PEG 4000, and 10% (v/v) glycerol and 10 mM NAG5 or NAG6. The crystals were then soaked overnight at 288 K before being mounted directly into a nitrogen cryostream for data collection.

2.3. Data collection, processing, and structure determination

All the X-ray diffraction data were collected by a Rigaku/MSR FR-E Super Bright equipped with an R-AXIS IV++ imaging plate detector. Data processing was conducted with the program MOSFLM (Leslie, 1991) and molecular replacement was employed to obtain phase information using the program AmoRe from the CCP4 suite (Navaza, 1994). The E315M data set was solved using the crystal structure of *S. marcescens* chitinase A (PDB code 1CTN; 47% identical to *V. harveyi* chitinase A) as a search model. Alternate sessions of model rebuilding in O (Jones et al., 1991) and restrained refinement in REFMAC from the CCP4 suite (Collaborative Computational Project Number 4, 1994; Murshudov et al.,

1997) were continued until the values of the free *R*-factor converged. Crystallographic data and refinement statistics of the chitinase structures are summarised in Table 1.

The final model of E315M was employed as the model for the subsequent three data sets of E315M+NAG5, E315M+NAG6, and the wild-type enzyme. Sugar coordinates taken from the protein databank (PDB code 1NH6) were modelled into the $2F_o - F_c$ and $F_o - F_c$ maps, and further refined. During the model rebuilding process, the non-reducing end unit of NAG5 (–4NAG) showed poor electron density. Examination of the refined structure of E315M+NAG6 exhibited ambiguity in the electron density of the +1 NAG and –1NAG in the $2F_o - F_c$ omit map showing partial density for the NAG5 conformation. The final free *R*-factors from modelling NAG6, NAG5, or no ligand into the E315M+NAG6 data are 21.0%, 21.4%, and 21.7%, respectively.

Tight non-crystallographic symmetry restraints were initially employed in refining the wild-type structure but later released as judged by the free *R*-factor. The geometry of each final model was verified by PROCHECK (Laskowski et al., 1993). No residues lie in the disallowed regions of the Ramachandran plots. Three residues (590, 591, and 592) could not be modelled into the E315M structures due to their poor electron density. The C-terminal hexahistidine tag was clear in the electron density of the ligand-free E315M but absent from the other structures. The refined structures of the four enzyme forms were compared within the program Superpose and direct contacts determined in the program Contact (CPC4 suite). The structures and electron density maps were created and displayed by Pymol (www.pymol.org).

2.4. Fluorescence studies of chitooligosaccharide binding

The interactions of NAG5 and NAG6 with E315M/Q were studied by fluorescence spectroscopy. The purified proteins (0.25 μ M) were titrated with ligand (0.01–20 μ M) in 20 mM Tris–HCl (pH 8.0) and changes in the intrinsic tryptophan fluorescence (Srivastava et al., 2006) were directly monitored on an LS-50 fluorescence spectrometer (Perkin-Elmer Limited (Instruments & Life Sciences), Bangkok, Thailand). The measurements were conducted at 25 °C with an excitation wavelength of 295 nm and emission intensities collected over 300–450 nm. The excitation and emission slit widths were kept at 5 nm. Each protein spectrum was corrected for the buffer spectrum. The fluorescence intensity data were analysed by non-linear regression function available in GraphPad Prism version 3.0 (GraphPad Software, California, USA) using the following single-site-binding equation: where $F - F_0 = \frac{(F_b - F_0) \times (L_0)}{K_d + L_0}$. F and F_0 refer to the fluorescence intensity in the presence and absence of ligand, respectively; F_b refers to the maximum fluorescence signal of the protein–ligand complex; L_0 is the initial ligand concentration and K_d is the equilibrium dissociation constant.

3. Results and discussion

3.1. The overall structures of *V. harveyi* chitinase A

The overall structures of the native chitinase A, mutant E315M with and without substrates are essentially identical and closely

Table 1
Statistics of data and structural refinement

Crystal	Wild-type	E315M	E315M+NAG ₅	E315M+NAG ₆
<i>Data collection statistics</i>				
PDB code	3B8S	3B9E	3B9D	3B9A
Space group	P1	P2 ₁ 2 ₁ 2 ₁	P2 ₁ 2 ₁ 2 ₁	P2 ₁ 2 ₁ 2 ₁
Unit-cell parameters	<i>a</i> = 60.27 Å <i>b</i> = 64.28 Å <i>c</i> = 83.52 Å α = 91.74° β = 91.18° γ = 112.91°	<i>a</i> = 63.96 Å <i>b</i> = 83.11 Å <i>c</i> = 106.98 Å $\alpha = \beta = \gamma = 90^\circ$	<i>a</i> = 63.51 Å <i>b</i> = 83.08 Å <i>c</i> = 105.59 Å $\alpha = \beta = \gamma = 90^\circ$	<i>a</i> = 63.70 Å <i>b</i> = 83.32 Å <i>c</i> = 106.57 Å $\alpha = \beta = \gamma = 90^\circ$
Resolution range ^a (Å)	24.62–2.11 (2.00)	24.68–1.79 (1.70)	24.54–1.81 (1.72)	30–1.90 (1.80)
Solvent content (%)	46.9	44.85	43.70	44.55
Unique reflections	73693 (10404)	61563 (7880)	59561 (8247)	53131 (7564)
Observed reflections	292719 (41321)	607216 (59894)	406849 (45783)	452556 (63380)
Multiplicity	4.0 (4.0)	9.9 (7.6)	6.8 (5.6)	8.5 (8.4)
Completeness (%)	94.6 (91.9)	97.2 (87.2)	99.2 (95.6)	99.7 (99.0)
(<i>I</i> /sigma) ^b	19.5 (5.5)	26.9 (4.5)	26.3 (9.9)	26.3 (6.1)
<i>R</i> _{merge} ^{a, b} (%)	6.6 (22.8)	7.1 (36.1)	7.1 (12.3)	7.0 (31.2)
<i>Refinement statistics</i>				
<i>R</i> _{factor} ^c (%)	16.8	18.9	18.7	18.1
<i>R</i> _{free} ^d (%)	20.5	21.9	21.5	21.0
No. of amino acid residues	1134	581	567	567
No. of protein atoms	8708	4474	4353	4353
No. of carbohydrate atoms	–	–	57	85
No. of ordered waters	1091	740	664	690
<i>R.M.S. deviations</i>				
Bond length	0.007	0.006	0.006	0.006
Bond angle	0.968	0.932	0.962	0.990
<i>Mean atomic</i>				
B values Protein atoms	14.45	15.10	14.24	13.74
Substrate	–	–	19.82	21.79
Waters	24.46	25.69	24.92	25.42
Overall	16.19	16.60	15.70	15.45

^a Values in parentheses refer to the corresponding values of the highest resolution shell.

^b $R_{\text{merge}} = \frac{\sum_{hkl} \sum_i |I_i(hkl) - \langle I(hkl) \rangle|}{\sum_{hkl} \sum_i I_i(hkl)}$ where I_i is the intensity for the i th measurement of an equivalent reflection with indices hkl .

^c $R_{\text{factor}} = \frac{\sum |F_{\text{obs}} - F_{\text{calc}}|}{\sum F_{\text{calc}}}$ where F_{obs} and F_{calc} are the observed and calculated structure-factors.

^d $R_{\text{free}} = \frac{\sum |F_{\text{obs}} - F_{\text{calc}}|}{\sum F_{\text{obs}}}$ calculated from 5% of the reflections selected randomly and omitted from the refinement process.

Please cite this article in press as: Songsiririthigul, C. et al., Crystal structures of *Vibrio harveyi* chitinase A complexed with ..., J. Struct. Biol. (2008), doi:10.1016/j.jsb.2008.03.008

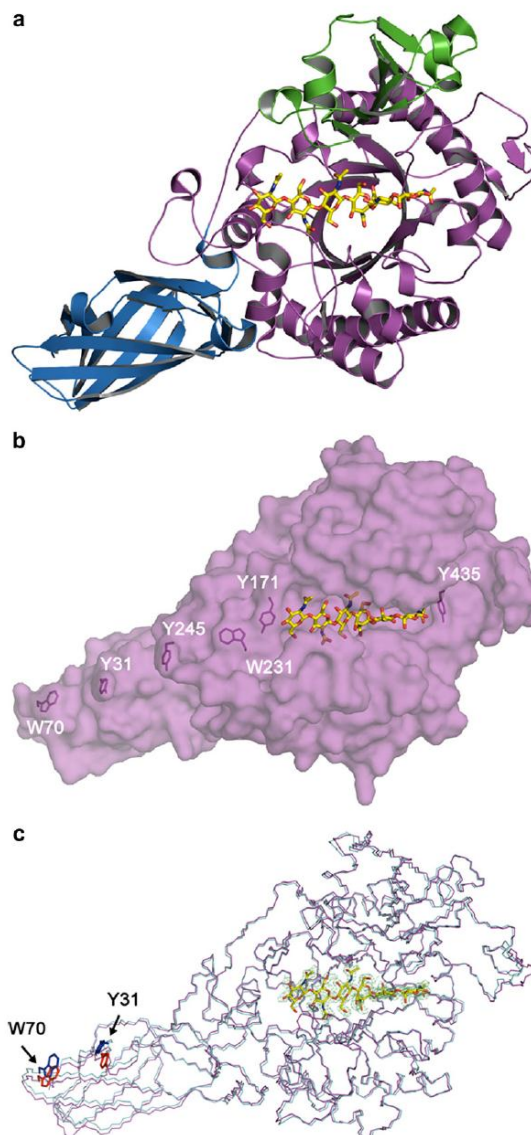


Fig. 1. The overall structure of *V. harveyi* chitinase A (a) The structure of catalytically inactive mutant E315M complexed with NAG₆. The N-terminal ChBD domain is in blue, the catalytic TIM-barrel domain in magenta, and the small insertion domain in green. (b) Surface representation of E315M showing the positions of the regularly spaced, surface-exposed hydrophobic residues. Y435 marks the reducing end of NAG₆ and Y171 marks the non-reducing end. The linear track of hydrophobic residues extending away from the non-reducing end of NAG₆ suggests the binding path for longer chain chitins. (c) A superimposition of wild-type chitinase A with E315M+NAG₆. The backbone structure of the wild-type is depicted in cyan and of E315M+NAG₆ in magenta. The residues Trp70 and Tyr31 located at the end of the ChBD and other aromatic residues located at the exterior of the TIM barrel domain (Y245, Trp231, Tyr171) and Tyr435 that marks the reducing end of the catalytic cleft are shown in blue for wild-type and red for E315M+NAG₆. Sugar units are shown as 2F_o - F_c map and sticks (yellow).

Please cite this article in press as: Songsirithigul, C. et al., Crystal structures of *Vibrio harveyi* chitinase A complexed with ..., J. Struct. Biol. (2008), doi:10.1016/j.jsb.2008.03.008

resemble those of chitinase A from *S. marcescens* and chitinase-1 from the pathogenic fungus *Coccidioides immitis* with minor dissimilarities in loop and helical regions (Perrakis et al., 1994; Hollis et al., 2000). Fig. 1a represents the structure of the chitinase A E315M mutant, which comprises three distinct domains, bound to hexaNAG. The amino-terminal chitin-binding domain (ChBD, blue) has a β -strand-rich fold formed by residues 22–138. This domain is connected to the core domain by a 21 amino-acid linker peptide (residues 139–159). The catalytic domain (magenta) has a $(\alpha/\beta)_8$ -TIM barrel fold consisting of eight β -strands (B1–B8) tethered to eight α -helices (A1–A8) by loops and is made up of two parts, referred to as Cat I (residues 160–460) and Cat II (residues 548–588). The catalytic residue (Glu315) is positioned in the loop of strand B4, which is part of a DxxDxDxE conserved motif. The $\alpha + \beta$ -fold insertion domain (green) connects strand B7 of Cat I and helix A7 of Cat II and is made up of five anti-parallel β -strands flanked by short α -helices (residues 461–547). This small domain provides a signature for subfamily A chitinases (Suzuki et al., 1999), although its function remains to be identified. As observed in this study, a few residues from this domain contribute to binding both NAG5 and NAG6 (Fig. 2).

The four structures exhibit three notable common structural features: (i) Tyr171 is detected in a generously allowed region in the Ramachandran plot and lines in the substrate-binding pocket; (ii) three cis peptide bonds are formed between the residues Gly191–Phe192, Glu315–Phe316, and Trp570–Glu571, all located at the exterior of the catalytic cleft; and (iii) three internal disulfide bonds are observed, one of which (Cys116–Cys121) is found at the end of the ChBD, and two others (Cys196–Cys217 & Cys409–Cys418) are present on the surface of the substrate-binding cleft. The existence of the conserved non-proline cis peptide bonds in the structures of *S. marcescens* chitinase A, *C. immitis* chitinase-1 and hevamine has been proposed to achieve essential conformational constraints (Hollis et al., 2000; Perrakis et al., 1994; Terwisscha van Scheltinga et al., 1996). The three non-proline cis peptide bonds, the two Cys196–Cys217 and Cys409–Cys418 disulfide bonds and residue Tyr171 define a general outline of the active site of the *Vibrio* chitinase (data not shown).

As in other family-18 chitinase 3D-structures (Fusetti et al., 2002; Hollis et al., 2000; Matsumoto et al., 1999; Perrakis et al., 1994; Terwisscha van Scheltinga et al., 1994; Van Aalten et al., 2000), the catalytic domain of *V. harveyi* chitinase A is an $(\alpha/\beta)_8$ -TIM barrel fold. The structure of E315M+NAG6 complex reveals the substrate-binding cleft as a long, deep groove with estimated dimensions of 33 Å (long) \times 14 Å (deep) \times 13 Å (wide), which contains six-binding subsites (–4)(–3)(–2)(–1)(+1)(+2), Fig. 1b and 2c. This subsite topology defines subsite –4 at the non-reducing end (NRE), subsite +2 at the reducing end (RE) and the cleavage site between –1 and +1 sites. Similar subsites have been identified for *S. marcescens* chitinase A (Aronson et al., 2003; Papanikolaou et al., 2001). In contrast, NAG5 occupies only four subsites (–3)(–2)(+1)(+2) of the binding cleft of E315M (Fig. 2a).

Four aromatic residues (Tyr31 & Trp70 from ChBD and Trp231 & Tyr245 at the edge of the non-reducing end of the substrate-binding sites) appear to line up in positions suitable for binding to longer chain chitins (Fig. 1b). Point mutations of these surface-exposed residues to Gly or Ala resulted in a notable decrease in the binding activity of *S. marcescens* Chi A, *B. circulans* Chi A1, and *Aeromonas caviae* Chi1 towards crystalline chitin (Li et al., 2005; Watanabe et al., 2001; Uchiyama et al., 2001). Our recent report further confirmed that Trp70 acts as the most crucial-binding residue for insoluble chitin, but had no effect on soluble chito oligosaccharides (Pantoom et al., 2008).

Superimposition of the four structures gives R.M.S. deviations in C $^{\alpha}$ positions of 0.63–0.77 Å for the 567 residues. Variation in the wild-type and the E315M+NAG6 structures is apparent as a

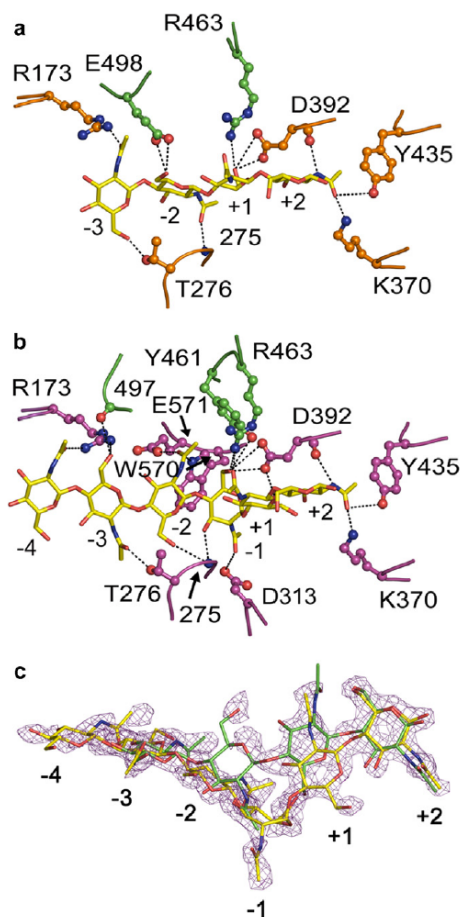


Fig. 2. Specific interactions within the substrate-binding cleft of E315M Interactions of (a) NAG5 and (b) NAG6. Hydrogen bonds are shown as dashed lines (...). The binding residues are depicted as ball-and-stick with the sugar residues in a stick model. Carbon atoms of the binding residues in the catalytic domain are colour-coded orange for NAG5 and magenta in NAG6. Green represents carbon in the small insertion domain and orange-yellow for sulphur. Sugar is coloured yellow for carbon; blue for nitrogen; and red for oxygen (c) The $2F_o - F_c$ OMIT electron density in the substrate-binding cleft of E315M, contoured at 1.0σ . NAG5 (green) and NAG6 (yellow) are modelled into the density. NAG6 fits well into the density, however, residual unexplained density suggests a partial occupancy of the NAG5 conformation. (For interpretation of color mentioned in this figure the reader is referred to the web version of the article.)

slight variation in the angle between the ChBD and the catalytic domain (Fig. 1c). The catalytic domains of the two structures superimpose well but leave their ChBDs offset, resulting in a relative displacement of C $^{\alpha}$ -Trp70 (the critical chitin-binding residue) of 1.46 Å and the C $^{\alpha}$ -Tyr31 of 2.03 Å. This tilt suggests some innate flexibility between the two domains and may be involved in the sliding mechanism (as proposed by Watanabe et al., 2003) of a chi-

tin polymer and in the bending process of long-chain chitooligomers.

Two additional residues (Tyr171 and Tyr435) are found at the edges of the catalytic cleft (Fig. 1b). Tyr171 appears to mark the non-reducing end of the hexasaccharide chain. Whereas, Trp435 marks the reducing end of the both the penta- and hexasaccharide chains (Fig. 2). Tyr435 located at the end of the +2 site seems to provide a partial barrier that may favour the ending of both sugar chains. However, inspection of the electron density map of the reducing-end subsites displays adequate space for the incoming oligomer to move beyond the +2 site, allowing various glycosidic bonds to approach the cleavage site. This explains how *V. harveyi* chitinase A hydrolyses a polymeric substrate in an endo manner at the same time favouring smaller substrates, such as hexaNAG (Suginta et al., 2005).

3.2. Specific interactions within the substrate-binding cleft of E315M

Fig. 3 depicts the relative positioning of the studied oligosaccharides inside the substrate-binding cleft of E315M. Four discernible sugar units of NAG5 (the GlcNAc residues in green) are bound to subsites –3, –2, +1, and +2, leaving the –1 site lying empty. NAG5 makes a number of interactions, either via hydrogen bonds (Fig. 2a) or via hydrophobic interactions, with residues in the substrate-binding cleft of E315M. As summarised in Table 2, five residues (Trp275, Lys370, Asp392, Trp397, and Tyr435) are directly involved in binding to +2NAG, whilst four residues (Trp275, Glu315 → Met, Asp392, and Arg463) contribute in binding to +1NAG and another five residues (Phe192, Gly274, Trp275, Glu498, and Trp570) to –2NAG. Specific interactions with –3NAG are made by Trp168, Arg173, Val205, Thr276, Trp497, and Glu498. The final non-reducing sugar of NAG5 could not be modelled into subsite –4 due to its poor electron density, probably reflecting a weak interaction in this conformation.

In relation to NAG5, NAG6 displays a more extensive set of interactions around the cleavage site extending to the reducing-end subsites (sites –1, +1, and +2) with its six sugar rings are entirely engaged with all the binding sites of E315M (the GlcNAc residues in yellow, Fig. 2b and 3a and b). Table 2 lists seven and six residues that participate in binding to +2NAG and +1NAG, respectively. These residues include all the residues that bind to NAG5, complemented by two extra (hydrophobic) interactions at each subsite (Phe316 and Gly367 at +2 site and Phe316 and Met389 at +1 site).

The mode of binding at the –1 site of E315M is particularly distinctive, since NAG6 interacts with twelve residues within this site, but there are no interactions with NAG5. To investigate further which conformation favours hydrolysis, the distances between the glycosidic oxygen and the OE1 atom of the γ -carboxyl side chain of catalytic Glu315 were estimated through superposition onto the wild-type structure. This distance is 2.98 Å for NAG6. The strained conformation of –1NAG combined with the twist of

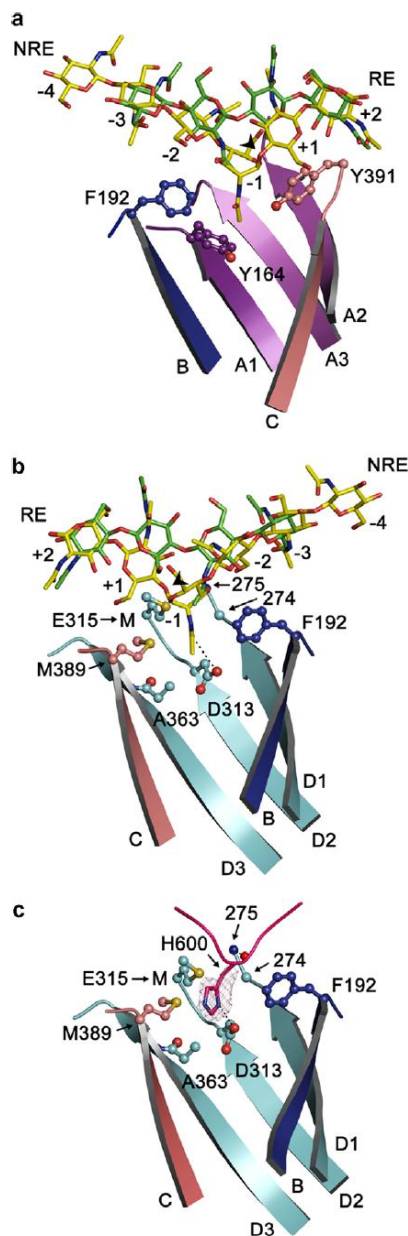


Fig. 3. A structural comparison of NAG₅ and NAG₆ in the catalytic cleft of E315M. (a) Superposition of E315M+NAG₅ onto E315M+NAG₆. Both sugars are shown along with interacting residues at the catalytic site. Only one protein chain is shown for clarity. (b) A 180° rotation of (a). Hydrogen bonds are shown as dashed lines (...). The eight β -strands are defined as A1 (residues 160–165); A2 (residues 455–460); A3 (residues 586–571); B (residues 186–192); C (residues 384–389); D1 (residues 267–273); D2 (residues 308–313) and D3 (residues 358–366). Carbon atoms of the labeled amino acids are coloured purple for strands A1, A2, and A3; Blue for strand B; deep salmon for strand C; pale cyan for strands D1, D2, and D3. The binding residues are depicted as ball-and-stick models and orange-yellow for sulphur. An arrow indicates the cleavage site. NRE and RE represent non-reducing end and reducing end, respectively. (c) The $2F_o - F_c$ map of the His600 residue calculated from the final refined model and contoured at 1.0 σ . Atoms in the histidine residue are labeled pink for carbon; blue for nitrogen and red for oxygen.

Table 2

A summary of the interactions between NAG₅ and NAG₆ and the binding residues in the substrate-binding site of E315M

Binding subsites	E315M-binding residues ^a	
	pentaNAG	hexaNAG
+2	Trp275 ^b , Lys370, Asp392, Trp397, Tyr435	Trp275, Phe316, Gly367, Lys370, Asp392, Trp397, Tyr435
+1	Trp275, Glu315 → Met, Asp392, Arg463	Trp275, Glu315 → Met, Phe316, Met389, Asp392, Arg463
-1	Not observable	Tyr164, Phe192, Trp275, Asp313, Glu315 → Met, Ala363, Met389, Tyr391, Asp392, Tyr461, Arg463, Trp570
-2	Phe192, Gly274, Trp275, Glu498, Trp570	Phe192, Trp275, Thr276, Trp570, Glu571
-3	Trp168, Arg173, Val205, Thr276, Trp497, Glu498	Trp168, Arg173, Thr276, Trp497
-4	Not observable	Tyr171, Arg173, Trp497

^a Direct contacts of each NAG with its adjacent residues were estimated, with the residues exhibiting a contact distance of ≤ 4 Å being considered as binding residues.^b Residues in bold are shared between E315+NAG₅ and E315+NAG₆.

the bonds between -1NAG and +1NAG in the structure of NAG6 appear to present the scissile bond of NAG6 to the catalytic residue. However, the longer distance for NAG5 (5.06 Å) indicates that the position of the scissile linkage is too far away from Glu315 for hydrolysis to occur (see Fig. 3b), hence, a non-productive (non-hydrolysable) conformation is adopted by this sugar.

Fewer residues are engaged in coordination at the non-reducing end of NAG6 (four for -3NAG and three for -4 NAG) (Table 2). The larger number of contacts in the reducing-end binding sites probably reflects stronger interactions which may be of particular importance in defining the primary-binding sites for the incoming chitooligomer. Point mutations of Trp275 (binds to -1 and +1 NAG) and Trp397 (binds to +2 NAG), which caused a complete change in the cleavage patterns of the enzyme towards various chitooligosaccharides (Suginta et al., 2007), confirmed the binding-selectivity role of the reducing-end residues.

Most of the contacts for both NAG5 (orange, Fig. 2a) and NAG6 (magenta, Fig. 2b) involve the amino acid residues located within the catalytic domain. However, residues that belong to the $\alpha + \beta$ insertion domain also contact the substrates (Glu498, Tyr461, Arg463, and Trp497, green, Fig. 2a and b). Partial contribution of this domain to substrate binding was also noticeable in the complex of *S. marcescens* E315Q+NAG8 as described by Papanikolaou et al. (2001).

Examination of the final structure of ligand-free E315M revealed that the catalytic cleft of the substrate-free enzyme is partially occupied by the six histidine affinity tag. These histidine residues are attached to the C-terminal end of a neighbouring chitinase molecule within the crystal and mimic the structure of the sugar rings. His600 particularly resembles -1NAG and makes most contact with the residues that bind to -1 NAG in the complex E315M+NAG6 (Fig. 3c).

3.3. Comparison of chitooligosaccharide-binding modes

The structures of the E315M complexes exhibited different conformations of NAG5 and NAG6. In addition to subsites -1 and +4 being unoccupied, the four sugar rings of NAG5 in the E315M+NAG5 complex do not fully lie on top of their corresponding sites in NAG6, with -2NAG and +1NAG (the sugar rings occupying the -2 and +1 subsites, respectively) being particularly displaced (Fig. 3a and b). As a result, the sugar oligomer may be expected to be interacting in a suboptimal manner. The glycosidic bond that joins -3NAG and -2NAG is twisted, causing the plane of -3NAG to lie perpendicular to the planes of the remaining sugars (Fig. 2a). Yet, the sugar chain maintains a linear form with no conversion of the chair configuration of any of the sugar residues. This linear confirmation may represent the initial step of binding, and therefore, it is referred to as the 'recognition' conformation.

A different substrate conformation is witnessed in the E315M+NAG6 complex. The $2F_o - F_c$ omit map (Fig. 2c) shows a

full span of NAG6 through the -4 to +2 subsites and a twist of the glycosidic bond between -1NAG and +1NAG (rather than between -3NAG and -2NAG as observed for NAG5) (Fig. 2b). As a result, the planes of the reducing-end disaccharide (+1NAG and +2NAG) are rotated by 90 degrees from the original plane. Additionally, the NAG6 units assume a 'bent' conformation due to geometric constraints at the -1 site causing the sugar (-1NAG) unit to be pulled down by 4.45 Å. This bending event probably takes place as an outcome of the sliding of the sugar chain towards the immobilized reducing-end subsites, enabling the non-reducing-end unit to interact at subsite -4. This process most likely occurs through swapping hydrogen bonds to allow the orientations of the sugars to be maintained while introducing the kink into the backbone (compare Fig 2a to b). For much longer oligosaccharides the flexibility of ChBD with respect to the catalytic domain may aid this sliding mechanism, as illustrated in Fig. 1c.

The binding characteristics of E315M to NAG5 and NAG6 were studied by the fluorescence spectroscopy. Excitation at 295 nm produced ligand-dependent changes in fluorescence intensity at the maximum emission wavelength of 338 nm. The wavelength of this maximum was not altered by the presence of NAG5 or NAG6. The fluorescence intensities were found to be substrate concentration dependent and saturable, which typically represents ligand binding to the proteins (Fig. 4a). The fluorescence intensity data were fitted reasonably well into the single-site-binding model of a non-linear regression function (Fig. 4b). The estimated K_d values of mutant E315M and E315Q against NAG5 (0.72 ± 0.24 and 0.76 ± 0.23 μ M) and NAG6 (0.09 ± 0.01 and 0.10 ± 0.01 μ M) are found to be indistinguishable. This provides evidence that the different conformations of NAG5 and NAG6 detected in the active site of E315M (Fig. 2a and b) were not structural artifact due to increased hydrophobicity arising from the methionine substitution of Glu315. The K_d values of E315M/Q against NAG5 are estimated to be eight times higher than the values against NAG6. These values are a reflection of the fewer interactions of the linear NAG5, which we suggest represents the recognition conformation of an oligosaccharide. Sliding and bending of the oligosaccharide into the NAG6 conformation would result in an increase in the number of interactions and is consistent with a slower off rate contributing to an overall higher affinity.

3.4. Proposed catalytic mechanism

Inspection of the final $2F_o - F_c$ omit map of E315M+NAG6 shows good density throughout the NAG6 chain. However, there remains unexplained density unaccounted for by the NAG6 model. Comparison with the NAG5 structure suggests a lower occupancy conformation of the NAG6 in which the sugar follows the path of the NAG5 sugar (see Fig. 2c). Hence, NAG6 appears to adopt two conformations in binding to the mutant E315M, the major form being bent and the minor form linear.

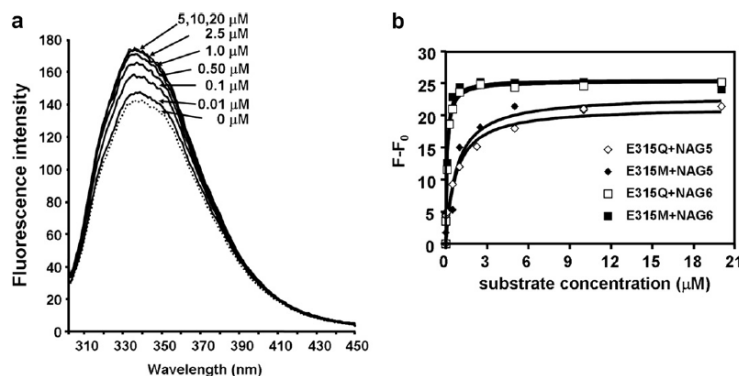


Fig. 4. Protein-ligand binding studies by fluorescence spectroscopy. (a) Effects of NAG₆ on the intrinsic fluorescence of E315M. Increased amounts of NAG₆ were added to 0.25 μM of the purified protein in 20 mM Tris-HCl (pH 8.0). The emission spectra were collected from 300–450 nm upon excitation of 295 nm. (b) The binding curves determined for NAG5 and NAG6 binding to mutants E315Q and E315M. Relative fluorescence intensity data ($F - F_0$) at 338 nm were fitted to a single-binding site model (see texts).

The distortion of –1NAG into a boat conformation and the twist of the scissile bond were predicted using molecular dynamics simulations (Brameld and Goddard, 1998a) and were verified by the crystal structures of *S. marcescens* chitinase, hevamine, or *S. marcescens* ChiA (Aronson et al., 2003; Papanikolaou et al., 2001; Terwisscha van Scheltinga et al., 1994; Tews et al., 1996; Tews et al., 1997). However, the partial density of the linear conformation in the electron density of NAG6 in E315M+NAG6 is the first crystallographic evidence for the occurrence of a recognition conformation that proceeds through a directed structural change to the catalytic conformation. Taking all the data obtained in this study together, *V. harveyi* chitinase A is presumed to catalyse the substrate hydrolysis following the ‘slide and bend mechanism’ as previously suggested for a long chain substrate (Watanabe et al., 2003). The proposed mechanism has four steps as shown in Fig. 5.

- Step 1. **Substrate recognition:** A linear form of chitooligosaccharide enters the substrate-binding cleft and its reducing end (dark filled circle) is primarily recognised by the +2 binding residues, such as Trp275, Asp392, Trp397, and Tyr435 (Table 2).
- Step 2. **Sliding and bending:** The sugar chain slides forward towards the reducing end distorting the chain especially in –1 NAG (green filled circle) and causing it to bend and take up a transient strained (boat) conformation. The increase in protein-sugar contacts in this conformation particularly in binding at the non-reducing end –4 site and at the catalytic site may drive this conformational change. Longer chitooligosaccharides may be aided in this movement by the flexibility in the ChBD relative to the catalytic domain.
- Step 3. **Bond cleavage:** The twist of the scissile bond, together with the bending of –1NAG, renders the linking glycosidic oxygen accessible to the catalytic residue Glu315 for cleavage. The stereoselective attack of the reaction intermediate (oxazolinium ion) by a neighbouring water leads to a retention of configuration of the anomeric product (Papanikolaou et al., 2001; Terwisscha van Scheltinga et al., 1994; Tews et al., 1997).
- Step 4. **Product release:** The cleaved components have lower binding energy, permitting the oligosaccharide (mainly NAG2, dark- and blue- filled circles) at the product side to diffuse away.

Steps

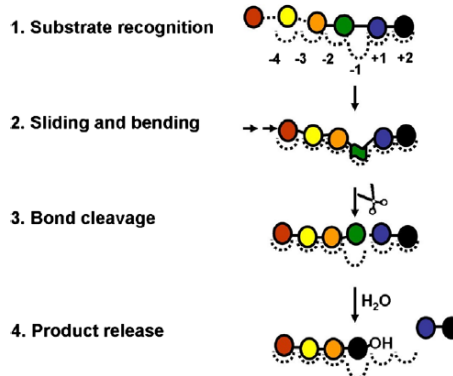


Fig. 5. The proposed catalytic mechanism of *V. carchariae* chitinase A. GlcNAc units are shown as filled, coloured circles. The reducing-end sugar is in black. Broken lines joining sugar rings represent free glycosidic bonds, solid lines depict constrained bonds. Curved dashed lines detail the binding subsites on the protein. Arrows signify the sliding of the sugar chain to allow the binding of the non-reducing end sugars (–4NAG) and for the green GlcNAc unit to adopt a boat conformation. (For interpretation of color mentioned in this figure the reader is referred to the web version of the article.)

4. Conclusions

This paper describes four crystal structures of *V. harveyi* chitinases A that have been solved to maximum resolution of 2.0–1.7 Å. The overall structure of chitinase A comprises three domains, which closely resembles chitinase A from *S. marcescens*. The structure of the ligand-free inactive mutant E315M displays blockage of the substrate-binding cleft by the C-terminal His6 residues from a second molecule. The structures of E315M bound to NAG5 and NAG6 provide key evidence that the interacting sugar undergoes conformational change to facilitate hydrolysis. Taking

all the data together, we propose that the *V. harveyi* chitinase A catalyses the hydrolytic reaction through a “slide and bend” mechanism.

Acknowledgments

This work is financially supported by The Thailand Research Fund (TRF) and The Thai Commission on Higher Education through Research Career Development Grant (RMU4980028), and the National Synchrotron Research Centre (NSRC), Thailand. R.C.R. and A.H.A. thank the Institute of Molecular and Cell Biology, Biopolis, Singapore and A*STAR, Singapore for their support.

References

- Armand, S., Tomita, H., Heyraud, A., Gey, C., Watanabe, T., Henrissat, B., 1994. Stereochemical course of the hydrolysis reaction catalysed by chitinases A1 and D from *Bacillus circulans* WL-12. *FEBS Lett.* 343, 177–180.
- Aronson Jr., N.N., Halloran, B.A., Alexyev, M.F., Amable, L., Madura, J.D., Pasupulati, L., Worth, C., van Roey, P., 2003. Family 18 chitinase-oligosaccharide substrate interaction: subsite preference and anomer selectivity of *Serratia marcescens* chitinase A. *Biochem. J.* 376, 87–95.
- Bhattacharya, D., Nagpure, A., Gupta, R.K., 2007. Bacterial chitinases: properties and potential. *Crit. Rev. Biotechnol.* 27, 21–28.
- Brameld, K.A., Goddard III, W.A., 1998a. Substrate distortion to a boat conformation at subsite -1 is critical in the mechanism of family 18 chitinases. *J. Am. Chem. Soc.* 120, 3571–3580.
- Brameld, K.A., Goddard III, W.A., 1998b. The role of enzyme distortion in the single displacement mechanism of family 19 chitinases. *Proc. Natl. Acad. Sci. USA* 95, 4276–4281.
- Bruce, A., Srinivasan, U., Staines, H.J., Highley, T.L., 1995. Chitinase and laminarinase production in liquid culture by *Trichoderma* spp. and their role in biocontrol of wood decay fungi. *Int. Biodeterior. Biodegrad.* 35, 337–353.
- Collaborative Computational Project, Number 4, 1994. The CCP4 suite: programs for protein crystallography. *Acta Crystallogr. D* 50, 760–763.
- Srivastava, D.B., Ethayathulla, A.S., Kumar, J., Singh, N., Sharma, S., Das, U., Srinivasan, A., Singh, T.R., 2006. Crystal structure of a secretory signalling glycoprotein from sheep at 2.0 Å resolution. *J. Struct. Biol.* 156, 505–516.
- Donnelly, L.E., Barnes, P.J., 2004. Acidic mammalian chitinase—a potential target for asthma therapy. *Trends Pharmacol. Sci.* 25, 509–511.
- Fukamizo, T., 2000. Chitinolytic enzymes: catalysis, substrate binding, and their application. *Curr. Protein Pept. Sci.* 1, 105–124.
- Fukamizo, T., Sasaki, C., Schelp, E., Bortone, K., Robertson, J.D., 2001. Kinetic properties of chitinase-1 from the fungal pathogen *Coccidioides immitis*. *Biochemistry* 40, 2448–2454.
- Fusetti, F., von Moeller, H., Houston, D., Rozeboom, H.J., Dijkstra, B.W., Boot, R.G., Aerts, J.M., van Aalten, D.M., 2002. Structure of human chitinase. Implications for specific inhibitor design and function of mammalian chitinase-like lectins. *J. Biol. Chem.* 277, 25537–25544.
- Hart, P.J., Pfleger, H.D., Monzingo, A.F., Hollis, T., Robertus, J.D., 1995. The refined crystal structure of an endochitinase from *Hordeum vulgare* L. seeds at 1.8 Å resolution. *J. Mol. Biol.* 248, 402–413.
- Hollis, T., Monzingo, A.F., Bortone, K., Ernst, S., Cox, R., Robertus, J.D., 2000. The X-ray structure of a chitinase from the pathogenic fungus *Coccidioides immitis*. *Protein Sci.* 9, 544–551.
- Honda, Y., Kitaoka, M., Hayashi, K., 2004. Kinetic evidence related to substrate-assisted catalysis of family 18 chitinases. *FEBS Lett.* 567, 307–310.
- Jeuniaux, C., 1961. Chitinase an addition to the list of hydrolases in the digestive tract of vertebrates. *Nature* 192, 135–136.
- Jones, T.A., Zou, J.Y., Cowan, S.W., Kjeldgaard, M., 1991. Improved methods for building models in electron density maps and the location of errors in these models. *Acta Crystallogr. A* 47, 110–119.
- Kawada, M., Hachiya, Y., Arihiro, A., Mizoguchi, E., 2007. Role of mammalian chitinases in inflammatory conditions. *Keio J. Med.* 56, 21–27.
- Keyhani, N.O., Roseman, S., 1999. Physiological aspects of chitin catabolism in marine bacteria. *Biochim. Biophys. Acta* 1473, 108–122.
- Kuranda, M.J., Robbins, P.W., 1991. Chitinase is required for cell separation during growth of *Saccharomyces cerevisiae*. *J. Biol. Chem.* 266, 19758–19767.
- Laemmli, U.K., 1970. Cleavage of structural proteins during assembly of head of bacteriophage T4. *Nature* 227, 680–685.
- Laskowski, R.A., MacArthur, M.W., Moss, D.S., Thornton, J.M., 1993. PROCHECK: a program to check the stereochemical quality of protein structures. *J. Appl. Crystallogr.* 26, 283–291.
- Leah, R., Tommerup, H., Svendsen, L., Mundy, J., 1991. Biochemical and molecular characterization of three anti-fungal proteins from barley seed. *J. Biol. Chem.* 266, 1564–1573.
- Leslie, A.G.W., 1991. Recent changes to the MOSFLM package for processing film and image plate data. CCP4 and ESRF-EACMB. Newsletters on Protein Crystallography. SERC Laboratory, Daresbury, Warrington, WA44AD, UK.
- Li, Q., Wang, F., Zhou, Y., Xiao, X., 2005. Putative exposed aromatic and hydroxyl residues on the surface of the N-terminal domains of Chi1 from *Aeromonas caviae* CB101 are essential for chitin binding and hydrolysis. *Appl. Environ. Microbiol.* 71, 7559–7561.
- Matsumoto, T., Nonaka, T., Hashimoto, M., Watanabe, T., Mitsui, Y., 1999. Three dimensional structure of the catalytic domain of chitinase A1 from *Bacillus circulans* WL-12 at a very high resolution. *Proc. Jpn. Acad.* 75, 269–274.
- Murshudov, G.N., Vagin, A.A., Dodson, E.J., 1997. Refinement of macromolecular structures by the maximum-likelihood method. *Acta Crystallogr. D* 53, 240–255.
- Navaza, J., 1994. AmoRe: an automated package for molecular replacement. *Acta Crystallogr. Sect. A* 50, 157–163.
- Pantoom, S., Songsiririthigul, C., Suginta, W., 2008. The effects of the surface-exposed residues on the binding and hydrolytic activities of *Vibrio carchariae* chitinase A. *BMC Biochem.* 9 (2).
- Papanikolaou, Y., Prag, G., Tavlas, G., Vorgias, C.E., Oppenheim, A.B., Petratos, K., 2001. High resolution structural analyses of mutant chitinase A complexes with substrates provide new insight into the mechanism of catalysis. *Biochemistry* 40, 11338–11343.
- Pedersen, K., Verdonck, L., Austin, B., Austin, D.A., Blanch, A.R., Grimont, P.A.D., Jofre, J., Kobravi, S., Larsen (IVP), J.L., Tjani, T., Vigneulle, M., Swings, J., 1998. Taxonomic evidence that *Vibrio carchariae* Grimes et al. 1985 is a junior synonym of *Vibrio harveyi* (Johnson and Shunk 1936) Baumann et al. 1981. *Int. J. Syst. Bacteriol.* 48, 749–758.
- Perrakis, A., Tews, I., Dauter, Z., Oppenheim, A.B., Chet, I., Wilson, K.S., Vorgias, C.E., 1994. Crystal structure of a bacterial chitinase at 2.3 Å resolution. *Structure* 2, 1169–1180.
- Robbins, P.W., Albright, C., Benfield, B., 1988. Cloning and expression of a *Streptomyces plicatus* chitinase (chitinase-63) in *Escherichia coli*. *J. Biol. Chem.* 263, 443–447.
- Sahal, A.S., Manocha, M.S., 1993. Chitinases of fungi and plants: their involvement in morphogenesis and host-parasite interaction. *FEMS Microbiol.* 11, 317–338.
- Sasaki, C., Yokoyama, A., Itoh, Y., Hashimoto, M., Watanabe, T., Fukamizo, T., 2002. Comparative study of the reaction mechanism of family 18 chitinases from plants and microbes. *J. Biochem. (Tokyo)* 131, 557–564.
- Suginta, W., Robertson, P.A., Austin, B., Fry, S.C., Fothergill-Gilmore, L.A., 2000. Chitinases from *Vibrio*: activity screening and purification of chiA from *Vibrio carchariae*. *J. Appl. Microbiol.* 89, 76–84.
- Suginta, W., Vongsuwan, A., Songsiririthigul, C., Prinz, H., Estibeiro, P., Duncan, R.R., Svasti, J., Fothergill-Gilmore, L.A., 2004. An endochitinase A from *Vibrio carchariae*: cloning, expression, mass and sequence analyses, and chitin hydrolysis. *Arch. Biochem. Biophys.* 424, 171–180.
- Suginta, W., Vongsuwan, A., Songsiririthigul, C., Svasti, J., Prinz, H., 2005. Enzymatic properties of wild-type and active site mutants of chitinase A from *Vibrio carchariae*, as revealed by HPLC-MS. *FEBS J.* 272, 3376–3386.
- Suginta, W., Songsiririthigul, C., Kobdaj, A., Opassiri, K., Svasti, J., 2007. Mutations of Trp275 and Trp397 altered the binding selectivity of *Vibrio carchariae* chitinase A. *Biochim. Biophys. Acta* 1770, 1151–1160.
- Suzuki, K., Taiyoji, M., Sugawara, N., Nikaidou, N., Henrissat, B., Watanabe, T., 1999. The third chitinase gene (chiC) of *Serratia marcescens* 2170 and the relationship of its product to other bacterial chitinases. *Biochem. J.* 343, 587–596.
- Terwisscha van Scheltinga, A.C., Kalk, K.H., Beintema, J.J., Dijkstra, B.W., 1994. Crystal structures of hevamine, a plant defence protein with chitinase and lysozyme activity, and its complex with an inhibitor. *Structure* 2, 1181–1189.
- Terwisscha van Scheltinga, A.C., Armand, S., Kalk, K.H., Isogai, A., Henrissat, B., Dijkstra, B.W., 1995. Stereochemistry of chitin hydrolysis by a plant chitinase/lysozyme and X-ray structure of a complex with allosamidin: evidence for substrate assisted catalysis. *Biochemistry* 34, 15619–15623.
- Terwisscha van Scheltinga, A.C., Hennig, M., Dijkstra, B.W., 1996. The 1.8 Å resolution structure of hevamine, a plant chitinase/lysozyme, and analysis of the conserved sequence and structure motifs of glycosyl hydrolase family 18. *J. Mol. Biol.* 262, 243–257.
- Tews, I., Perrakis, A., Oppenheim, A., Dauter, Z., Wilson, K.S., Vorgias, C.E., 1996. Bacterial chitinase structure provides insight into catalytic mechanism and the basis of Tay-Sachs disease. *Nat. Struct. Biol.* 3, 638–648.
- Tews, I., Terwisscha van Scheltinga, A.C., Perrakis, A., Wilson, K.S., Dijkstra, B.W., 1997. Substrate-assisted catalysis unifies two families of chitinolytic enzymes. *J. Am. Chem. Soc.* 119, 7954–7959.
- Uchiyama, T., Katouno, F., Nikaidou, N., Nonaka, T., Sugiyama, J., Watanabe, T., 2001. Roles of the exposed aromatic residues in crystalline chitin hydrolysis by chitinase A from *Serratia marcescens* 2170. *J. Biol. Chem.* 276, 41343–41349.
- Van Aalten, D.M., Synstad, B., Brurberg, M.B., Hough, E., Riise, B.W., Eijsink, V.G., Wierenga, R.K., 2000. Structure of a two-domain chitinoidase from *Serratia marcescens* at 1.9-Å resolution. *Proc. Natl. Acad. Sci. USA* 97, 5842–5847.
- Van Aalten, D.M., Komander, D., Synstad, B., Gaseidnes, S., Peter, M.G., Eijsink, V.G., 2001. Structural insights into the catalytic mechanism of a family 18 exochitinase. *Proc. Natl. Acad. Sci. USA* 98, 8979–8984.
- Watanabe, T., Ishibashi, A., Ariga, Y., Hashimoto, M., Nikaidou, N., Sugiyama, J., Matsumoto, T., Nonaka, T., 2001. Trp122 and Trp134 on the surface of the catalytic domain are essential for crystalline chitin hydrolysis by *Bacillus circulans* chitinase A1. *FEBS Lett.* 494, 74–78.
- Watanabe, T., Ariga, Y., Sato, U., Toratani, T., Hashimoto, M., Nikaidou, N., Kezuka, Y., Nonaka, T., Sugiyama, J., 2003. Aromatic residues within the substrate-binding cleft of *Bacillus Circulans* chitinase A1 are essential for hydrolysis of crystalline chitin. *Biochem. J.* 376, 237–244.

Please cite this article in press as: Songsiririthigul, C. et al., Crystal structures of *Vibrio harveyi* chitinase A complexed with ..., *J. Struct. Biol.* (2008), doi:10.1016/j.jsb.2008.03.008

Substrate binding modes and anomer selectivity of chitinase A from *Vibrio harveyi*

Wipa Suginta · Supansa Pantoom · Heino Prinz

Received: 26 February 2009 / Accepted: 7 May 2009
© Springer-Verlag 2009

Abstract High-performance liquid chromatography mass spectrometry (HPLC MS) was employed to assess the binding behaviors of various substrates to *Vibrio harveyi* chitinase A. Quantitative analysis revealed that hexaNAG preferred subsites -2 to +2 over subsites -3 to +2 and pentaNAG only required subsites -2 to +2, while subsites -4 to +2 were not used at all by both substrates. The results suggested that binding of the chitooligosaccharides to the enzyme essentially occurred in compulsory fashion. The symmetrical binding mode (-2 to +2) was favored presumably to allow the natural form of sugars to be utilized effectively. Crystalline α chitin was initially hydrolyzed into a diverse ensemble of chitin oligomers, providing a clear sign of random attacks that took place within chitin chains. However, the progressive degradation was shown to occur in greater extent at later time to complete hydrolysis. The effect of the reducing-end residues were also investigated by means of HPLC MS. Substitutions of Trp275 to Gly and Trp397 to Phe significantly shifted the anomer selectivity of the enzyme toward β substrates. The Trp275 mutation modulated the kinetic property of the enzyme by decreasing the catalytic constant (k_{cat}) and the substrate specificity (k_{cat}/K_m) toward all substrates by five- to tenfold. In contrast, the Trp397

mutation weakened the binding strength at subsite (+2), thereby speeding up the rate of the enzymatic cleavage toward soluble substrates but slowing down the rate of the progressive degradation toward insoluble chitin.

Keywords Chitin · Substrate binding mode · HPLC MS · *Vibrio harveyi* · Family-18 chitinase · Active-site mutation

Abbreviations

NAG _n	β -1-4 linked oligomers of <i>N</i> -acetylglucosamine residues where $n=1-6$
DNS	Dinitrosalicylic acid
IPTG	Isopropyl thio- β -D-galactoside
PMSF	Phenylmethylsulfonyl fluoride
HPLC-ESI-MS	High-performance liquid chromatography electrospray mass spectrometry
ChBD	Chitin-binding domain

Introduction

Chitin is a homopolymer composed of β -(1,4)-linked *N*-acetylglucosamine (GlcNAc or NAG) units and is mainly found as a structural component of fungal cell walls and exoskeletons of crustaceans and insects. A complete degradation of chitin requires chitinases (EC 3.2.1.14) and *N*-acetyl- β -glucosaminidases (EC 3.2.1.52). Chitinases are found in various organisms, and their physiological functions are dependent on the structural roles of chitin substrates existing in different species. Degradation of chitin by marine bacteria [1, 2] is crucial for maintaining the ecosystem in the marine environment [3]. In insects, chitinases are essential in the molting process and may also affect gut physiology through their involvement

W. Suginta (✉) · S. Pantoom
Biochemistry–Electrochemistry Research Unit,
School of Chemistry and Biochemistry, Institute of Science,
Suranaree University of Technology,
Nakhon, Ratchasima 30000, Thailand
e-mail: wipa@sut.ac.th

H. Prinz
The Max-Planck Institute of Molecular Physiology,
Otto-Hahn-Strasse 11,
44227 Dortmund, Germany

in peritrophic membrane turnover [4]. Plants produce chitinases as part of their defense mechanism against distinct pathogens [5, 6], whereas fungal chitinases participate in a number of morphogenetic processes, including spore germination, side-branch formation, differentiation into spores, and autolysis [7]. Human chitinases are involved in asthma and inflammatory conditions, but the endogenous substrate(s) and the pathogenic mechanism is not yet known [8–10].

Different bacteria seem to secrete different forms of chitinases [2, 11–17]. For example, *Serratia marcescens* produces three chitinases: ChiA, ChiB, and ChiC for a synergistic degradation of chitin [18, 19], whereas *Vibrio harveyi* (formerly *Vibrio carchariae*) mainly expresses chitinase A [2]. In the CAZy database (<http://www.cazy.org>), *V. harveyi* chitinase A is classified as a member of family-18 glycosyl hydrolases, comprising a $(\beta/\alpha)_8$ -barrel catalytic domain with a deep substrate-binding cleft and is known to catalyze the hydrolytic reaction through the ‘substrate-assisted’ or ‘retaining mechanism’ [20–26]. Most recently, the crystal structures of *V. harveyi* chitinase and its mutant E315M complexed with NAG₅ and NAG₆ were reported at 1.8–2.1 Å resolutions [27]. The structures revealed that chitooligosaccharides most likely interact with the multiple subsites of the enzyme using a linear conformation. Subsequently, the sugar chain develops a ‘kink’ conformation to facilitate bond cleavage. Such a movement is presumed to proceed via the ‘slide and bend’ mechanism [27]. The sliding motion of a chitooligomer resembles the feeding mechanism proposed by Watanabe and co-workers [28] for long-chain chitin. Either sliding or feeding, the process could be achieved only when a chitinase exhibits high processivity toward its substrates. The processivity has been described previously for other polysaccharide degrading enzymes, such as Chi A from *S. marcescens* [19, 28–30], cellobiohydrolases Cel6A from *Humicola insolens* [31], and Cel7A from *Trichoderma reesei* [32].

Insoluble substrates have been proposed to enter the active site of chitinases by the feeding mechanism and chitin oligomers by a random mechanism [28, 33]. Such a hypothesis probably holds true for most of the cases. However, a major point of concern remains the random cleavage of a chitin polymer by an endo action of chitinase A. We previously verified that *V. harveyi* chitinase A initially degraded insoluble chitins into NAG_{2–6} [20, 34]. Indeed, the production of the chitin oligomers other than NAG₂ cannot be explained as an outcome of the feeding mechanism. This is because the sliding following progressive degradation of chitin will only give rise to a single species of the product (NAG₂). In this study, we employed quantitative HPLC-MS as a direct and sensitive tool to investigate the binding behaviors of three different sub-

strates. Together with kinetic analysis, we also demonstrated that point mutation of the reducing-end binding residues (Trp275 and Trp397) affected the substrate specificity of the tested substrates and significantly altered the anomer selectivity of *V. harveyi* chitinase A. This enzyme belongs to family-18 chitinases, which are potential drug targets for the treatment of allergic asthma.

Experimental

Bacterial strains and chemicals

The pQE 60 expression vector harboring the DNA fragment that encodes chitinase A (amino acid residues 22–597, without the 598–850 C-terminal fragment) and *Escherichia coli* type strain M15 (Qiagen, Valencia, CA, USA) were used for a high-level expression of recombinant chitinases. Chitooligosaccharides were obtained from Seikagaku Corporation (Bioactive Co., Ltd., Bangkok, Thailand). Flake chitin from crab shells was the product of Sigma-Aldrich Pte Ltd. (The Capricorn, Singapore Science Park II, Singapore). Other chemicals and reagents (analytical grade) were obtained from the following sources: reagents for bacterial media (Scharlau Chemie S.A., Barcelona, Spain.); all chemicals for protein preparation (Sigma-Aldrich Pte Ltd., Singapore and Carlo Erba Reagenti SpA, Limite, Italy); and reagents for HPLC-MS measurements (J.T. Baker, Deventer, Holland and LGC Promochem GmbH, Wesel, Germany). Milli-Q water was used for preparations of reaction buffers and for HPLC MS measurements.

Instrumentation

HPLC was operated on a 150×2.1 mm 5 μm Hypercarb® column (ThermoQuest, Thermo Electron Corporation, San Jose, CA, USA) connected to an Agilent Technologies 1100 series HPLC system (Agilent Technologies, Waldbronn, Germany) under the control of a Thermo Finnigan LTQ electrospray mass spectrometer. The proprietary program Xcalibur (Thermo Finnigan, Thermo Electron Corporation, San Jose, CA, USA) was used to control and calibrate HPLC ESI/MS. For partial hydrolysis of colloidal chitin, the electrospray MS was conducted under a positive full scan mode with a range of the mass/charge ratio (m/z) of 200–1,400. Later, the HPLC MS was run under the single ion monitoring mode for improvement of signal/noise ratios. The selected masses for detection were m/z 424.5 for NAG₂, m/z 627.5 for NAG₃, m/z 830.3 for NAG₄, m/z 1034.16 for NAG₅, and m/z 1236.3 for NAG₆. The UV signals were detected by a diode array detector between 200 and 400 nm.

Site directed mutagenesis

Point mutations were introduced to the wild-type *chitinase A* DNA that was previously cloned into the pQE60 expression vector by polymerase chain reaction (PCR) technique [20], using the QuickChange Site-Directed Mutagenesis Kit. Mutations of Trp275 to Gly and Trp397 to Phe (so as to create mutants W275G and W397F, respectively) were generated using oligonucleotides synthesized from BioServiceUnit (BSU) (Bangkok, Thailand). The forward oligonucleotide sequence used for mutagenesis of Trp275 to Gly is 5'-CATCTATCGGTGGTGGAA-CACTTTCTGAC-3' and the reverse sequence is 5'-GTCA-GAAAGTGTTCACCAACCGATAGATG-3'. For mutagenesis of Trp397 to Phe, the forward sequence is 5'-GACTTCTACGGCGGCTTCAACAACGTTCC-3' and the reverse sequence is 5'-GGAACGTTGTTGAAGCCGCGG-TAGAAGTC-3'. Sequences underlined represent the mutated codons. The success of point mutations was confirmed by automated DNA sequencing (BSU, Thailand).

Recombinant expression and purification

The wild-type *chitinase A* with a C-terminal hexahistidine sequence was highly expressed in *E. coli* M15 cells [20]. *Chitinase A* mutants W275G and W397F were obtained by PCR-based site directed mutagenesis as described by Suginta et al. [35]. For recombinant expression and purification, the freshly transformed cells were grown at 37 °C in 500 mL of Luria–Bertani medium containing 100 µg·mL⁻¹ ampicillin until OD₆₀₀ reached 0.6. Then, the *chitinase* production was induced by the addition of 0.5 mM IPTG at 25 °C for 18 h. The cell pellet was harvested by centrifugation, re-suspended in 40 mL of lysis buffer (20 mM Tris/HCl buffer, pH 8.0, containing 150 mM NaCl, 1 mM PMSF, and 1 mg·mL⁻¹ lysozyme), and then lysed on ice using a Sonopuls Ultrasonic homogenizer with a 6-mm-diameter probe. The supernatant obtained after centrifugation at 12,000×g, 45 min was applied to a Ni-NTA agarose affinity column (1.0×10 cm) (Qiagen GmbH, Hilden, Germany), washed thoroughly with 5 mM imidazole, then eluted with 250 mM imidazole in 20 mM Tris/HCl buffer, pH 8.0. An eluted fraction (10 mL) was subjected to several rounds of membrane centrifugation using Vivaspine-20 ultrafiltration membrane concentrators (*M_r* 10,000 cut-off, Vivascience AG, Hannover, Germany) for a complete removal of imidazole and for concentrating the proteins. Protein purity was verified on sodium dodecyl sulfate polyacrylamide gel electrophoresis as described by Laemmli [36]. A final concentration of the protein was determined by Bradford's method [37] using a standard calibration curve of bovine serum albumin (0–25 µg). The

freshly prepared proteins were subjected to functional characterization or stored at -30 °C.

Partial hydrolysis of chitooligosaccharides by *V. harveyi* chitinase A

Partial hydrolysis of chitooligosaccharides by wild-type was carried out in a 50-µL reaction mixture, containing 0.1 M ammonium acetate buffer, pH 7.0, 500 µM substrate, and 100 ng purified enzyme. To minimize isomerization of the anomeric products, the reaction was performed on ice (0 °C) for 3 min, and then a 10-µL aliquot was transferred to a 200-µL sample vial and immediately subjected to HPLC MS analysis. The sample tray was kept at 4 °C, and the column was operated at 10 °C. A constant flow rate of 0.4 mL·min⁻¹ was applied with a run time set to 15 min using a 5–70% gradient of acetonitrile, containing 0.1% formic acid. The β/α ratios were calculated from the peak areas of the corresponding products using the program Xcalibur and applying an MS Genesis algorithm for peak detection.

Time courses of chitin hydrolysis

Time-course experiments were carried out on ice in a 100-µL reaction mixture, containing 0.1 M ammonium acetate buffer, pH 7.0, 10% (w/v) crystalline α chitin, and 50 ng purified enzyme. Aliquots of 10 µL were taken at 0, 3, 7, 20, 30, 60, and 180 min and analyzed immediately by HPLC MS as described for chitin oligosaccharides. The peak areas, which represent total ion counts of the hydrolytic products, were quantified using the program Xcalibur applying a MS Avalon algorithm for peak detection. Standard calibration curves of NAG moieties were constructed separately from a mixture of oligosaccharide containing 0.2–500 µM of NAG_{1–6}. These data points yielded a linear curve of each standard sugar with the *R*² values of 0.9995–1.0, thus allowing molar concentrations of chitooligosaccharides to be determined with confidence. For the determination of β/α contents of the chitooligosaccharide products, the reaction mixture, containing 250 ng purified enzyme in 0.1 M ammonium acetate buffer, pH 7.0, was incubated with 500 µM NAG₅ or NAG₆. Aliquots of a 100-µL reaction mixture were taken at specified times and analyzed immediately by HPLC MS. Amounts of β and α anomers of the hydrolytic products were derived from the corresponding peak areas using the standard calibration curves constructed as mentioned above.

Steady-state kinetics

Kinetic measurements were determined in a microtiter plate using NAG₅, NAG₆, and colloidal chitin as substrates. A

reaction mixture (100 μ L), containing 0–500 μ M substrate and chitinase (50 μ g wild type, 250 μ g W275G, or 0.4 μ g W397F) in 0.1 M sodium acetate buffer, pH 5.5 was incubated at 37 $^{\circ}$ C for 15 min. After boiling to 100 $^{\circ}$ C for 3 min, the entire reaction mixture was subjected to the reducing sugar assay using dinitrosalicylic acid (DNS) reagent as described by Miller [38]. For colloidal chitin, the reaction was carried out the same way as the reducing-sugar assay, but concentrations of colloidal chitin was varied from 0% to 5% (w/v) and amount of enzyme was used at 150 μ g wild type, 700 μ g W275G, or 200 μ g W397F. The amounts of the reaction products were determined from a standard curve of NAG₂ (0–500 nmol). The kinetic values were evaluated from three independent sets of data using the nonlinear regression function available in GraphPad Prism version 5.0 (GraphPad Software Inc., San Diego, CA).

Results

Structural evidence of hexaNAG in the catalytic cleft of *V. harveyi* chitinase A

We recently described four crystal structures of *V. harveyi* chitinase A and its catalytically inactive mutant E315M in complex with chitooligosaccharides (PDB codes 3BS8, 3B9A, 3B90, and 3B9E) [27]. Figure 1a is a surface representation of the catalytic domain of the mutant E315M, displaying six units of NAG (yellow) being embedded inside a long, deep-binding groove and interact specifically with various aromatic residues that stretch along the elongated cleft of the enzyme. Figure 1b represents a stick model underlying specific interactions between Tyr171 and –4NAG, Trp168 and –3 NAG, Trp275 and Trp570 and –1 to +1NAG, and Trp397 and Tyr435 with +2NAG. It is clear that the hydrophobic faces of the residues Trp275 and Trp397 stack against the heterocyclic rings of the reducing-end sugar units (+1 NAG and +2NAG; blue, Fig. 1a, b). We previously suggested that both residues are important for the primary interaction with soluble substrates [35]. We shall discuss later, in this study, that Trp275 and Trp397 are also crucial for the progressive degradation of insoluble chitin.

The structure in Fig. 1b also displays the cleavage site that is located between sites –1 and +1 (red arrow). Following the retaining mechanism, further cleavage would be expected to yield only β NAG₄ and β NAG₂. The released NAG₄ had two fates. It may diffuse into the reaction mixture and then rebind or it may slide forward to accommodate the next cleavage if remained attached to the active site. On the other hand, NAG₂ would dissociate from the product side (+1 and +2) and serves as the end product of hydrolysis.

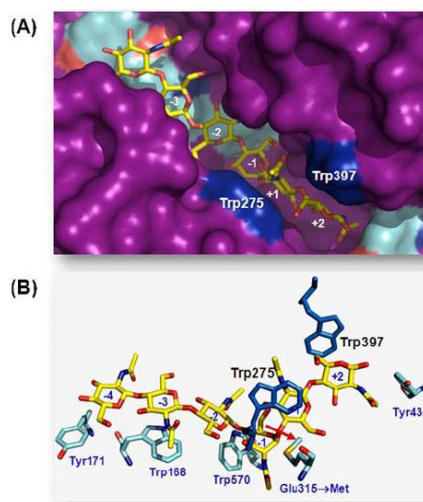


Fig. 1 The active site of *V. harveyi* chitinase A mutant E315M bound to hexaNAG. **a** A surface representation of hexaNAG that fully occupied subsites –4 to +2 within the substrate binding cleft of the enzyme. The sugar rings of NAG₆ are shown in sticks. **b** A stick model of the binding cleft of chitinase A mutant E315M complexed with NAG₆. N atoms are shown in blue and O atoms in red. C atoms are in marine blue for the amino acid residues and in yellow for the sugar residues. The cleavage site is indicated by an arrow, and Trp275 and Trp397 are represented in blue. The structure of E315M+NAG₆ complex is obtained from the PDB data base (PDB code, 3B9A) [24] and displayed by the program PyMol (<http://www.pymol.org>)

Investigation of the binding modes of soluble substrates

We employed quantitative HPLC MS to establish the binding modes of three substrates. Pursuing the idea of Uchiyama et al. [28] that chitooligosaccharides randomly enter the catalytic cleft of chitinase A, it is presumed that binding of the incoming sugar chain may begin at variable sites to allow various glycosidic bonds to be accessible to the cleavage site located between sites –1 to +1. Figure 2a and b represent three possibilities where soluble substrates could interact with the multiple binding subsites of the enzyme. For a NAG₅ substrate, the binding may begin at site –4 and end at site +1, leading to a complete formation of β NAG₄+ β NAG (Fig. 2a, bottom trace). Alternatively, the sugar chain may bind to subsites –3 to +2, subsequently generating β NAG₃+ β NAG₂ (Fig. 2a, middle trace) or only four units of NAG₅ bind to subsites –2 to +2, leaving the reducing-end NAG unbound at the exterior of the substrate binding cleft. As a result, β NAG₂ and either equilibrium ratio of β/α NAG₃ are expected (Fig. 2a, top trace).

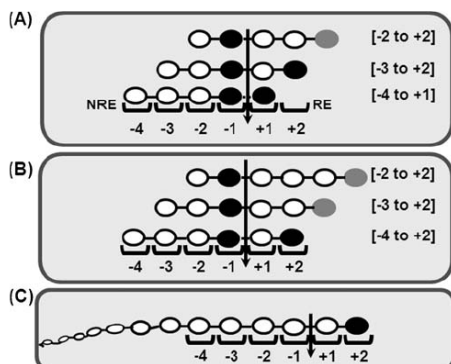


Fig. 2 Three possible models of chitin oligosaccharide bindings to the multiple binding subsites of *V. harveyi* chitinase A. Hydrolysis of a NAG_5 , b NAG_6 , and c crystalline α chitin. NAG unit with β configuration is shown in black circle, and NAG residue with α or β configuration with an equilibrium ratio is shown in gray circle. Types of the reducing-end anomers are predicted based on the retaining mechanism as suggested for family-18 chitinases

With respect to a NAG_6 substrate, it could interact with subsites (-4 to +2). This binding mode is seen in the structure of E315M+ NAG_6 , as shown in Fig. 1. The binding leads to a full occupancy of the six binding sites by chitohexaose (Fig. 2b, bottom trace). Subsequent bond cleavage results in the formation of $\beta\text{NAG}_4 + \beta\text{NAG}_2$, where βNAG_2 is released from the reducing-end subsites +1 to +2. A different binding event takes place when five units of NAG_6 bind to positions (-3 to +2) (Fig. 2b, middle trace), leaving the reducing-end NAG lying empty beyond the substrate binding cleft. As a result, a single cleavage of NAG_6 leads to the formation of two NAG_3 , one of which (the non-reducing end NAG_3) initially adopts β configuration, while the other NAG_3 possesses either β or α configuration. A third version of binding is that four units of NAG_6 symmetrically interact with subsites (-2 to +2), thereby letting the reducing-end NAG_2 remain unbound (Fig. 2b, top trace). This (-2 to +2) binding mode releases βNAG_2 from subsites (-2 and -1), whereas β or αNAG_4 is formed from the reducing-end side.

Assuming that the feeding mechanism is applicable, the binding characteristic of polymeric substrate is then depicted as Fig. 2c. After cleavage, a chitin chain remains attached to the active site before subsequently sliding forward toward the product side (+1 and +2), thereby allowing NAG_2 to be generated at a time. To investigate the preferred binding subsites of *V. harveyi* chitinase A, NAG_5 and NAG_6 (as a representative of soluble chitin) were partially hydrolyzed by the enzyme and the reaction mixtures analyzed immediately by HPLC MS. Partial

hydrolysis of the two substrates was carried out at 0 °C to stabilize the β and α isomers of initial products. For the assignment of the HPLC elution of α and β anomers acquired by our system, we referred to a separation profile of chito oligosaccharides obtained by reverse-phase HPLC and $^1\text{H-NMR}$ [39]. Figure 3 represents an HPLC MS separation of chitin intermediates derived from partial hydrolysis of NAG_6 . The β and α forms of an individual sugar were eluted at different retention times as a doublet. The preceding peak of the doublet is identified as β and the following peak α . Further mass detection by ESI-MS assigned m/z values of the two isomers of the same sugar to be identical. For instance, m/z 424.5 was seen for $\beta\alpha\text{NAG}_2$, 627.5 for $\beta\alpha\text{NAG}_3$, 830.3 for $\beta\alpha\text{NAG}_4$, and 1,236.5 for $\beta\alpha\text{NAG}_6$ (Fig. 3). Peak areas representing total ion counts of the corresponding oligomers were simply converted to molar concentrations using the standard calibration curves of NAG_{1-6} .

From Fig. 3, *V. harveyi* chitinase A degraded NAG_6 , yielding $\beta\text{NAG}_2 + \beta\text{NAG}_3$ as major isomers. This action was observed as early as 3 min. On the other hand, βNAG_4 and αNAG_4 were detected in comparable amounts, and NAG and NAG_5 were not observed at all (Fig. 3). With NAG_5 hydrolysis, two predominant products ($\beta\text{NAG}_2 + \alpha\text{NAG}_3$) were captured during the initial time (data not shown). No other product was seen. The preferred binding modes of the enzyme toward NAG_5 and NAG_6 were determined by comparing β content to α content of the same product (Table 1). The β contents of NAG_2 , NAG_3 , and NAG_4 obtained from NAG_6 hydrolysis were estimated as 90%, 65%, and 46%, respectively (Table 1, wild type). Such values do not at all fit with the β/α ratios calculated by a single binding mode as presented in Fig. 2b. Apparently, the values agree well with the values (data in

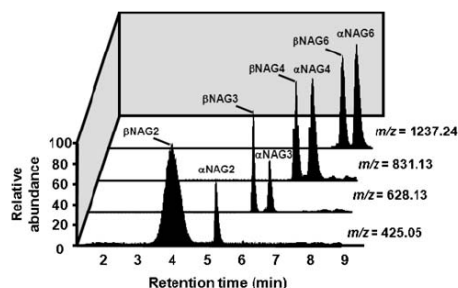


Fig. 3 An HPLC MS profile of the initial products obtained from partial hydrolysis of NAG_6 by wild-type chitinase A. The hydrolytic reaction (50 μL) was carried out on ice to minimize the rate of mutarotation. After 3 min, aliquots of 10 μL of the reaction mixture were subjected to HPLC MS analysis

Table 1 Quantitative HPLC MS analysis of partial hydrolysis of chitoooligosaccharides

Substrate	Enzyme	β content of initial products					
		NAG ₁	NAG ₂	NAG ₃	NAG ₄	NAG ₅	NAG ₆
pentaNAG (NAG ₅)	Wild-type	n.d. ^a	90±4.1(100) ^b	42±2.3(42)	n.d.	–	–
	W275G	n.d.	93±3.3	68±9.2	n.d.	–	–
	W397F	81±6.0	69±1.6	98±1.2	96±1.5	–	–
hexaNAG (NAG ₆)	Wild type	n.d.	90±2.2(100) ^c	65±3.0(71)	46±3.7(48)	–	–
	W275G	n.d.	92±4.9	63±0.7	79±2.8	–	–
	W397F	n.s. ^d	66±3.1	95±9.5	91±8.4	96±1.8	–
Crystalline α chitin	Wild type	n.d.	87±1.5(100) ^e	50±1.3(n.d.)	42±1.0(n.d.)	37±0.9(n.d.)	46±4.5(n.d.)
	W275G	n.d.	88±1.2	48±2.2	56±3.2	49±5.8	50±3.7
	W397F	n.s.	88±2.1	46±1.2	57±3.4	57±1.4	51±2.0

A reaction mixture (50 μ L), containing chitin substrates and chitinase A in 0.1 M ammonium acetate buffer, pH 7.0, was incubated on ice and then analyzed by HPLC ESI/MS after 3 min. The β contents were deduced from the peak areas of the corresponding products.

^a n.d. represents product is not detectable

^b The values in brackets are the expected values from the -2 to -2 binding mode for NAG₅ hydrolysis

^c The values in brackets are the expected values from a combination of the -3 to $+2$ and -2 to $+2$ modes for NAG₆ hydrolysis

^d n.s. represents non-separable between β and α anomer. The initial β contents were estimated from three independent sets of the experiment

^e The value is predicted from the progressive degradation of insoluble chitin

brackets, Table 1) derived from a combination of the -2 to $+2$ and -3 to $+2$ binding modes (top and middle traces, Fig. 2b). For NAG₅ hydrolysis, the β contents of NAG₂ and NAG₃ products were predicted as 90% and 42%. These values are consistent with a single -2 to $+2$ binding mode (top trace, Fig. 2a). When the hydrolytic reactions were performed at equilibrium (25 °C, overnight), the predominant form of all the sugars was α . The equilibrium β contents were calculated as 48% for NAG₂, 42% for NAG₃, 41% for NAG₄, 39% for NAG₅, and 43% for NAG₆ (data not shown).

Substrate binding preference toward crystalline α chitin

The substrate binding mode of natural substrate was further investigated. Figure 4a represents a time course of the hydrolytic products generated from crystalline α chitin hydrolysis by the wild-type chitinase. Similar to previous findings [20, 34], NAG₆ was degraded by *V. harveyi* chitinase A, yielding NAG₂ major products. Other intermediates (NAG₃₋₆) were also detected in the reaction mixture as early as 3 min although in much lower concentrations. The major isomer of NAG₂ products was found to be β , while other products gave equilibrium ratios of α/β (Table 2). NAG₂ was released at least sevenfold greater than the other products over the entire range of reaction times (Fig. 4a), indicating that the enzymatic cleavage preferably took place at the second bond from the chain ends. Nevertheless, the peaks corresponding to NAG₃₋₆ that were detected in the reaction mixture

simultaneously with NAG₂ verified the existence of a random attack occurring at internal points of a chitin chain.

The cleavage feature of a long-chain chitin was further elucidated. The values shown in Fig. 4b represent the cleavage ratios of NAG₂ to NAG₃–NAG₆. These values were compared when the reaction was carried out at initial time (3 min) and at equilibrium (180 min). In all cases, the cleavage ratios NAG₂ to other sugars were found to increase when the reactions reached equilibrium. For NAG₂/NAG₃, the ratio was enhanced by 1.5 times, for NAG₂/NAG₄ by nine times, for NAG₂/NAG₅ by five times, and for NAG₂/NAG₆ by six times. The lower cleavage ratios obtained at 3 min inferred that the internal attack proceeded at an early stage of reaction. The increased ratios represent the progressive action that took place at later time (i.e., at equilibrium).

Effects of point mutations on substrate bindings

Our recent data displayed a significant change in the cleavage patterns of NAG₄–NAG₆ hydrolysis when Trp275 was mutated to Gly and Trp397 to Phe. The 3D structure of chitinase A mutant E315M bound to NAG₆ has located Trp275 at the main subsites -1 , and $+1$, and Trp397 at subsite $+2$ (Fig. 1a, b, blue). Alterations of the cleavage pattern as a result of Trp275 and Trp397 mutations provided a hint that both residues are important in defining the primary binding of soluble substrates [35]. In this study, we explored further how Trp275 and Trp397 influenced the binding selectivity of the enzyme. When incubated briefly,

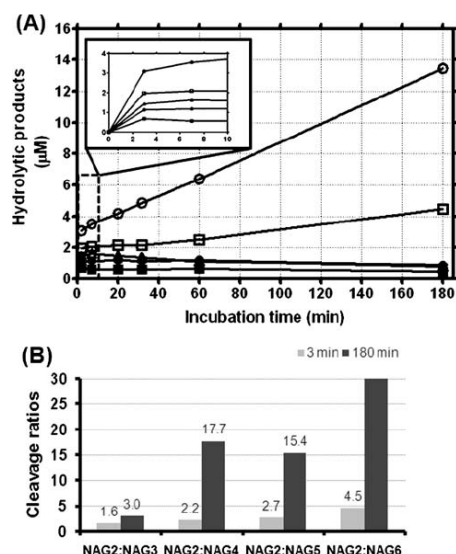


Fig. 4 Partial hydrolysis of crystalline α chitin by the wild-type chitinase A. **a** Time course of chitin hydrolysis. The hydrolytic reactions were carried out at on ice ($0\text{ }^{\circ}\text{C}$) from 0 to 180 min and were analyzed immediately by HPLC MS. Molar concentrations of the hydrolytic products were estimated using the standard curves of NAG_{1-6} . **b** The cleavage ratios of $\text{NAG}_2/\text{NAG}_{3-6}$ were calculated based on the molar concentration of each corresponding sugar. The reaction products generated during 0–10 min are indicated as an inset. Open circle dimers, open square trimers, open triangle tetramers; filled circle pentamers, filled square and hexamers

the mutant W275G was found to degrade NAG_5 into $\text{NAG}_2 + \text{NAG}_3$ with the value of βNAG_2 (93%) indistinguishable to the one formed by the wild-type enzyme (90%) (Table 1). However, the β content of NAG_3 (68%) produced by the mutated enzyme significantly increased when compared with the same product produced by the wild-type enzyme (42%). With mutant W397F, the initial products of NAG_5 hydrolysis by W397F were more varied from NAG to NAG_4 . The major form of all the products produced by W397F was β with observed values of 81% for βNAG , 69% for βNAG_2 , 98% for βNAG_3 , and 96% βNAG_4 (Table 1).

Partial hydrolysis of NAG_6 by mutant W275G generated three product species ($\text{NAG}_2 + \text{NAG}_3 + \text{NAG}_4$), all having β major isomer. The percentages of βNAG_2 (92%) and βNAG_3 (63%) were not similar to the wild-type value (Table 1). However, βNAG_4 formed by W275G (79%) was significantly greater than βNAG_4 formed by wild type (46%). Similarly, NAG_6 hydrolysis by mutant W397F released a full range of reaction intermediates (NAG –

NAG_5). The β contents for NAG_2 (66%), NAG_3 (95%), and NAG_4 (91%) were found to be different from that obtained from the non-mutated enzyme (Table 1).

Effects of point mutations on the kinetic properties

The steady-state kinetics of the hydrolytic activity of wild-type chitinase A and mutants W275G and W397F were investigated by using the DNS reducing-sugar assay (see “Experimental”). Table 2 represents the kinetic values of the three chitinase variants against NAG_5 , NAG_6 , and crystalline chitin. With NAG_5 hydrolysis, the K_m of W275G (315 μM) was only slightly decreased, but the K_m of W397F (476 μM) was 1.25-fold elevated from the K_m of wild type (380 μM). Similar results were observed with NAG_6 hydrolysis, where the K_m of W275G (238 μM) was twofold lower, whereas the K_m of W397F (460 μM) was 2.6-fold greater than the K_m of wild type (174 μM).

Mutations of Trp275 and Trp397 exhibited a more severe effect on the catalytic constant (k_{cat}) of the enzyme. With the NAG_5 substrate, the k_{cat} of W275G (0.04 s^{-1}) was fivefold lower than that of wild type (0.21 s^{-1}). In contrast, the k_{cat} of W397F (2.1 s^{-1}) was tenfold higher. Similar results were seen with the NAG_6 substrate by which W275G (0.06 s^{-1}) showed a threefold decrease, but W397F displayed a 16-fold increase in the k_{cat} compared to that of wild type (0.19 s^{-1}).

Both mutations gave a different outcome on insoluble substrate. The K_m of W275G (25 mg mL^{-1}) and W397F (19 mg mL^{-1}) toward colloidal chitin were higher than that of wild type (12 mg mL^{-1}). Both mutants displayed a 0.3–0.5-fold loss in the k_{cat} . The k_{cat}/K_m values of W275G toward all substrates were decreased five times toward NAG_5 and NAG_6 but ten times toward the crystalline chitin. In contrast, the k_{cat}/K_m values of W397F toward the short-chain substrates were increased by six- to eightfold but a fivefold decrease toward the long-chain chitin.

Effects of point mutations on the anomer selectivity

The effects of Trp275 and Trp397 mutations on the anomer selectivity of the oligosaccharide hydrolysis were further investigated. Determination of substrate decrease at different time points revealed that the wild-type enzyme degraded both β and α anomers at equal rates (Fig. 5a). However, the initial rate of the depletion of βNAG_5 by W275G (Fig. 5a) occurred about 1.4 times faster than the rate of αNAG_5 depletion. At 155 min of incubation, only half of αNAG_5 , but all of βNAG_5 , was degraded. βNAG_5 was also utilized by mutant W397F at a significantly higher rate than αNAG_5 ; however, the anomer consumption varied linearly over time of incubation (Fig. 5b). At the end of reaction, a substantial amount of αNAG_5 (> 50%) and only

Table 2 Kinetic parameters of *V. harveyi* wild-type chitinase A and mutants

Chitinase A variants	pentaNAG			hexaNAG			Colloidal chitin		
	K_m (μM)	k_{cat} (s^{-1})	k_{cat}/K_m ($\text{s}^{-1} \mu\text{M}^{-1}$)	K_m (μM)	k_{cat} (s^{-1})	k_{cat}/K_m ($\text{s}^{-1} \mu\text{M}^{-1}$)	K_m (mg mL^{-1})	k_{cat} (s^{-1})	k_{cat}/K_m ($\text{s}^{-1} \text{mg mL}^{-1}$)
Wild type	380±49 (1)	0.21 (1)	5.5×10^{-4} (1)	174±23 (1)	0.19 (1)	1.1×10^{-4} (1)	12±1.4 (1)	0.10 (1)	8.3×10^{-4} (1)
W275G	315±110 (0.8)	0.04 (0.2)	1.3×10^{-4} (0.2)	238±17 (1.4)	0.06 (0.3)	2.5×10^{-4} (0.2)	25±3.7 (2.1)	0.02 (0.2)	8.0×10^{-4} (0.1)
W397F	476±11 (1.3)	2.1 (10)	4.4×10^{-4} (8)	460±53 (2.6)	3.0 (16)	6.5×10^{-4} (6)	19±0.1 (1.6)	0.03 (0.3)	1.6×10^{-4} (0.2)

Kinetic measurements of the hydrolytic activity of wild-type chitinase A and mutants W275G and W397F were carried out using 0–500 μM pentaNAG, hexaNAG and colloidal chitin as substrates. After 15 min of incubation at 37 °C, the amounts of the reaction products were determined by DNS assay using a standard curve constructed from NAG₂

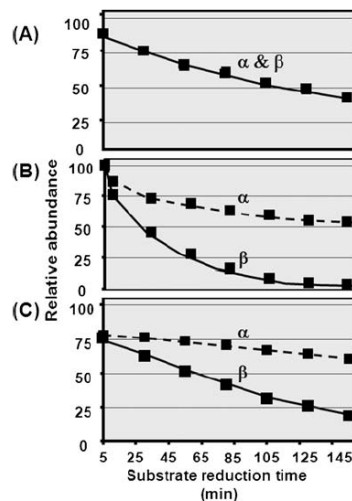


Fig. 5 Time-course of substrate consumption by chitinase A. Hydrolysis of NAG₅ by a wild type, b mutant W275G, and c mutant W397F. The hydrolytic reactions carried out at on ice (0 °C) from 0 to 155 min were analyzed by HPLC ESI/MS as described in texts. Rate of β anomer consumption is presented by a black line and rate of α anomer consumption by a broken line

a small amount of βNAG_5 (< 20%) remained in the reaction mixture.

With the NAG₆ substrate, similar patterns were observed (data not shown). The wild-type enzyme displayed no preferable selection toward a particular anomer of NAG₆. However, the initial rates of βNAG_6 degradation by both mutants were only slightly higher than that of αNAG_6 consumption. At the final stage of reaction, most of βNAG_5 and βNAG_6 (>80%) was used up.

Discussion

The 3D structures of the catalytically inactive mutant E315M complexed with NAG₅ and NAG₆ suggested that *V. harveyi* chitinase A most likely catalyzed chitin degradation through the 'slide and bend' mechanism [27]. From the mechanistic point of view, the sliding process can only be achieved by an enzyme with high processivity. Eijsink and colleagues reported previously that ChiA, ChiB, and ChiC from *S. marcescens* possessed different degrees of processivity [19, 29, 30]. ChiA was tested to be more processive than ChiB, whereas ChiC is a non-processive enzyme. The processive property explains how an enzyme processes its substrates. However, the mechanism

of how each substrate initially interacts with the enzyme depends entirely on the size of its substrate. Chitin oligomers are predicted to bind to the substrate-binding cleft by a random fashion. It implies that the sugar oligomer has freedom to bind to variable sites as far as the successful cleavage is concerned. In this study, three models are proposed for the productive binding of the soluble substrates (Fig. 1). NAG₅ may interact either with subsites (-4 to +1), (-3 to +2), or (-2 to +2) (Fig. 2a). Likewise, NAG₆ may bind to subsites (-4 to +2), (-3 to +2), or (-2 to +2) (Fig. 2b).

HPLC MS analysis of NAG₆ hydrolysis by wild-type chitinase gave rise to three species of reaction products (NAG_{2,3,4}). This happens only when the glycosidic cleavage takes place at least at two distinct locations. The presence of NAG₃ in the reaction mixture (Table 1) suggested that the enzymatic cleavage occurred in the middle of the chitin hexamer. When initial isomers of the degradation products were trapped at very low temperature (0 °C) for a short period of time (3 min), the estimated βNAG₃ (65%) agreed best to that of NAG₃ expected from the (-3 to +2) binding mode (71%) (the value in brackets, Table 1). Two other products (NAG₂ and NAG₄) could otherwise come from the interactions at subsites -4 to +2 or -2 to +2. However, the measured percentages of βNAG₂ (90%) and βNAG₄ (46%) were in conflict with the calculated values for the (-4 to +2) binding mode (100% for both βNAG₂ and βNAG₄). Instead, the obtained values agreed well with the 100% βNAG₂ and 48% βNAG₄ as calculated for the (-2 and +2) binding mode (Fig. 2b). This experimental outcome suggests binding of the chitin hexamer to either subsites -3 to +2 or -2 to +2, which emphasizes a dynamic process of interaction between an active enzyme and the substrate, and is in contrast with the occupation of the oligomer as observed in the static complex of the inactive enzyme (Fig. 1a, b). Previous quantitative HPLC MS analysis estimated the yield of NAG₃ to be 4 nmol when NAG₆ was incubated with native chitinase A for 5 min. This yield was half of NAG₂+NAG₄ yields (~8 nmol) obtained from the same reaction [34], and it indicated that NAG₆ favors the (-2 to +2) mode over the (-3 to +2) mode.

Limited hydrolysis of NAG₅ yielded only two products (NAG₂+NAG₃), meaning that the bond cleavage took place only at a single site either at positions -3 to +2 or -2 to +2 (see Fig. 2A). However, the observed percentages of βNAG₂ (90%) and βNAG₃ (42%) agreed more to that of βNAG₂ (100%) and βNAG₃ (42%) predicted for the (-2 to +2) binding mode. In contrast, 100% βNAG₂ and 100% βNAG₃ would be expected from the (-3 to +2) binding mode. No detection of NAG and NAG₄ in the reaction mixture implied that the (-4 to +1) mode was completely ignored by this substrate (see Table 1).

The binding characteristics of *S. marcescens* Chi A [40] and *Coccidioides immitis* chitinase-1 (CiX1) [41] were previously investigated by means of typical HPLC systems. Hydrolysis of NAG₆ by SmChiA that yielded 99% βNAG₂, 71% βNAG₃ and 48% βNAG₄ and hydrolysis of NAG₅ that yielded 100% βNAG₂ and 55% βNAG₃ represents the equivalent binding events as observed in this study. In CiX1, formations of α/βNAG₂ (9/1) and α/βNAG₄ (5/2) from NAG₆ hydrolysis supports the (-2 to +2) binding mode. Sasaki et al. [42] performed a comparative study of the reaction mechanism of rice and bacterial enzymes and concluded that microbial chitinases favors the (-2)(-1)(+1)(+2)(+3)(+4) subsites, while plant chitinases prefers the (-4)(-3)(-2)(-1)(+1)(+2) subsites. Binding of a chitooligomer to (-2) to (+4) sites would be comparable to the -2 to +2 binding mode described for *V. harveyi* chitinase A.

With partial hydrolysis of insoluble chitin, NAG₂ observed as the primary product during the course of reaction (from 0 to 180 min) was mostly derived from the progressive degradation of the second bond from a chain end of chitin polymer. Imai et al. [33] demonstrated previously that the degradation of β chitin microfibrils took place from the reducing end of the sugar chain. However, other products (NAG₃₋₆) that were observed in the reaction mixture, even as early as 3 min, and the equilibrium ratios of NAG₃₋₆ products obtained from a long-chain chitin hydrolysis (Table 1) were an indication of internal attacks that took place at variable positions within the chitin chain. This interpretation is further supported by the small cleavage ratios of NAG₂/NAG₃₋₆ intermediates. A dramatic increase in the ratios at later time of reaction is presumably achieved quite productively with the progressive action via the feeding and sliding mechanism.

The anomer analysis revealed no selectivity of the wild-type chitinase A in utilization of α or β substrates (Fig. 5a). No selectivity of binding by all means leaves the enzyme a lot more freedom to efficiently take up the β or α substrates that are present in the reaction equilibrium. This idea is well complimented by binding of NAG₅ to subsites (-2 to +2) and NAG₆ to subsites (-3 to +2) or (-2 to +2) as seen in Fig. 2a and b. For the structural point of view, *V. harveyi* chitinase A is shown to comprise a substrate binding cleft with a long, deep groove structure (Fig. 1). The reducing end of the binding groove is shown to be open, giving adequate space for the incoming sugar chain to move beyond the +2 site. As a consequence, various glycosidic bonds are accessible to the cleavage site. The open-end active site certainly fits the binding preference of NAG₅ and NAG₆ and the endo action of the enzyme toward chitin polymers.

We previously reported that the residues Trp275 and Trp397 positioned at subsites (-1, +1, and +2 sites) are particularly essential for defining the primary binding of

soluble chitooligosaccharides and Trp70 located at the N-terminal end of the ChBD is crucial for insoluble chitin degradation [35, 43]. In this study, the effects of mutations on the kinetic properties of the enzyme were evaluated. It was found that mutations of Trp275 and Trp397 to Gly and Phe, respectively, significantly changed the substrate specificity and the anomer selectivity of the enzyme. The structure of mutant E315M bound to NAG₆ showed that Trp275 could interact strongly with -1NAG and +1NAG [27]. Mutation of this residue was found to affect the kinetic properties involving the catalytic center by decreasing the k_{cat} and the k_{cat}/K_m toward NAG₅ and NAG₆ by a magnitude of 5 (Table 2). In addition, the mutation significantly increased the apparent rate of β consumption as shown in Fig. 5a. The event may be explained as a shift of the sugar chain toward the non-reducing end in the search for other available binding sites to compensate for the loss of interactions. The observed yields of β NAG₂ (93%) and β NAG₃ (68%) obtained from the cleavage of NAG₅ by W275G (Table 1) agrees well with the predicted yields of β NAG₂ (100%) and β NAG₃ (42–100%) of the model shown in Fig. 6a. A single move of the sugar chain toward the non-reducing end is predicted as further movement would likely be blocked by high affinity of binding between the reducing end of NAG₅ and Trp397 at subsite +2.

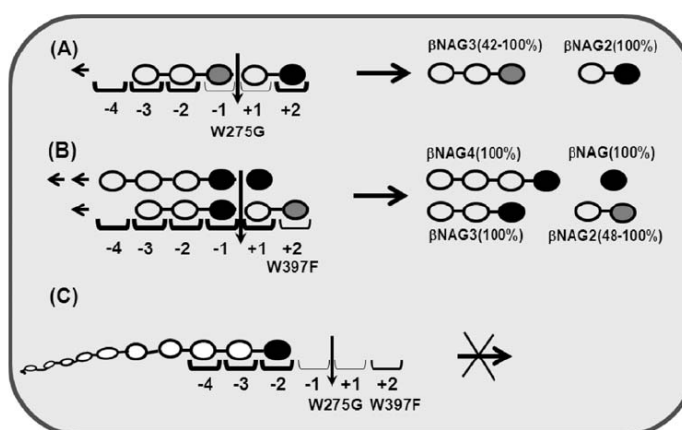
Different situations were observed with mutant W397F. Mutation of Trp397 to Phe led to an increase in the k_{cat} toward NAG₅ and NAG₆ by 10- and 16-fold, giving rise to an increase in the k_{cat}/K_m by a magnitude of 8 and 16, respectively. Trp397 is a crucial binding residue located at subsite +2, and it determines the primary binding of chitooligosaccharide substrates. A phenylalanine substitu-

tion appeared to weaken the binding strength of this subsite, enabling the sugar chain to move more freely and allowing various glycosidic bonds to be exposed to the cleavage sites. A full range of reaction intermediates seen in the reaction mixture of W397F (Table 1) supports the above assumption. Hydrolysis of NAG₅ by W397F, yielding 81% β NAG, 69% β NAG₂, 98% β NAG₃, and 96% β NAG₄ products agreed well with the yields proposed in Fig. 6b.

The residues Trp275 and Trp397 are found to be important for insoluble chitin hydrolysis, since the mutations showed a remarkable decrease in the k_{cat} value of the enzyme. The structure in Fig. 1 shows that both residues are located in a perfect position to be responsible for the feeding process by pulling the chitin chain toward the reducing end subsites, thereby permitting the next successive hydrolysis to occur (see Fig. 6c). A significant reduction of the k_{cat} and the k_{cat}/K_m values toward colloidal chitin (Table 2) seems to support the proposed roles of both residues (Table 2). Similar effects were also reported with ChiA1 from *B. circulans*, where mutations of Trp164 (equivalent to Trp275) and Trp285 (equivalent to Trp397) drastically reduced the hydrolytic activity of their enzymes toward colloidal chitin by 40–50% [44].

In conclusion, we employed quantitative HPLC MS to determine the binding modes of a family-18 chitinase from *V. harveyi* toward three substrates. Neither a random nor a progressive binding was entirely employed for a complete hydrolysis of the tested substrates. Nevertheless, soluble chitins seem to favor the -2 to +2 binding, but insoluble chitin preferred the progressive binding. Mutations of Trp275 and Trp397 were found to affect the anomer selectivity and the substrate specificity toward soluble substrates. The evaluation of the kinetic data suggested

Fig. 6 Plausible effects of point mutation on the substrate binding preference and the anomer selectivity. Binding of NAG₅ to a wild-type chitinase, b mutant W275G, and c mutant W397F. The β configuration is shown in *black circle*, NAG residue with α or β configuration with an equilibrium ratio is shown in *gray circle*, and NAG residue with α or β configuration that binds to a loosen-affinity binding site is shown in *gray-filled circle* in *dark circle*. The cleavage site is indicated by an *arrow*



that Trp275 and Trp397 are likely involved in the feeding process that facilitates a degradation of chitin polymer in a progressive manner. Ultimately, understanding of the binding mechanism of family-18 chitinases to their substrates may aid the drug-screening program to obtain effective inhibitors that act as therapeutic candidates for successful treatment of allergic asthma.

Acknowledgements This work is financially supported by Suranaree University of Technology, The Thailand Research Fund and The Thai Commission on Higher Education through a Research Career Development Grant to WS (grant no. RMU4980028). The Thailand Research Fund through the Royal Golden Jubilee PhD Program (grant no. PHD/0238/2549) to SP and WS is acknowledged.

References

- Hirono I, Yamashita M, Aoki T (1998) Note: molecular cloning of chitinase genes from *Vibrio anguillarum* and *V. parahaemolyticus*. *J Appl Microbiol* 84:1175–1178
- Suginta W, Robertson PA, Austin B et al (2000) Chitinases from *Vibrios*: activity screening and purification of chi A from *Vibrio carchariae*. *J Appl Microbiol* 89:76–84
- Keyhani NO, Roseman S (1999) Physiological aspects of chitin catabolism in marine bacteria. *Biochim Biophys Acta* 1473:108–122
- Merzendorfer H, Zimoch L (2003) Chitin metabolism in insects: structure, function and regulation of chitin synthases and chitinases. *J Exp Biol* 206:4393–4412
- Herrera-Estrella A, Chet I (1999) Chitinases in biological control. *EXS* 87:171–184
- Melchers LS, Stauver MH (2000) Novel genes for disease-resistance breeding. *Curr Opin Plant Biol* 3:147–152
- Goody GW, Zhu WY, O'Donnell RW (1992) What are the roles of chitinases in the growing fungus? *FEMS Microbiol Lett* 100:387–392
- Wills-Karp M, Karp CL (2004) Chitin checking—novel insights into asthma. *N Engl J Med* 351:1455–1457
- Kawada M, Hachiya Y, Arihiro A et al (2007) Role of mammalian chitinases in inflammatory conditions. *Keio J Med* 56:21–27
- Zhu Z, Zheng T, Homer RJ et al (2004) Elias acidic mammalian chitinase in asthmatic Th2 inflammation and IL-13 pathway activation. *Science* 304:1678–1682
- Watanabe T, Suzuki K, OyaGi W et al (1990) Gene cloning of chitinase A1 from *Bacillus circulans* WL-12 revealed its evolutionary relationship to *Serratia* chitinase and to the type III homology units of fibronectin. *J Biol Chem* 265:15659–15665
- Jones JDG, Grady KL, Suslow TV et al (1986) Isolation and characterization of genes encoding two chitinase enzymes from *Serratia marcescens*. *EMBO J* 5:6467–6473
- Roffey PE, Pemberton JM (1990) Cloning and expression of an *Aeromonas hydrophila* chitinase gene in *Escherichia coli*. *Curr Microbiol* 21:329–337
- Sitrit Y, Vorgias CE, Chet I et al (1995) Cloning and primary structure of The chiA gene from *Aeromonas caviae*. *J Bacteriol* 177:4187–4189
- Tsujibo H, Orikoishi H, Tanno H et al (1993) Cloning, sequence, and expression of a chitinase gene from a marine bacterium, *Alteromonas* sp. strain O-7. *J Bacteriol* 175:176–181
- Suginta W (2007) Identification of chitin binding proteins and characterization of two chitinase isoforms from *Vibrio alginolyticus* 283. *Enzyme Microb Tech* 41:212–220
- Itoi S, Kanomata Y, Koyama Y et al (2007) Identification of a novel endochitinase from a marine bacterium *Vibrio proteolyticus* strain No. 442. *Biochim Biophys Acta* 1774:1099–1107
- Suzuki K, Sugawara N, Suzuki M et al (2002) Chitinases A, B, and C1 of *Serratia marcescens* 2170 produced by recombinant *Escherichia coli*: enzymatic properties and synergism on chitin degradation. *Biosci Biotechnol Biochem* 66:1075–1083
- Sikorski P, Sörbotten A, Horn SJ et al (2006) *Serratia marcescens* chitinases with tunnel-shaped substrate-binding grooves show endo activity and different degrees of processivity during enzymatic hydrolysis of chitosan. *Biochemistry* 45:9566–9574
- Suginta W, Vongsuwan A, Songsiririthigul C et al (2004) An endochitinase A from *Vibrio carchariae*: cloning, expression, mass and sequence analyses, and chitin hydrolysis. *Arch Biochem Biophys* 424:171–180
- Perrakis A, Tews I, Dauter Z et al (1994) Crystal structure of a bacterial chitinase at 2.3 Å resolution. *Structure* 2:1169–1180
- Tews I, Terwisscha van Scheltinga AC, Perrakis A et al (1997) Substrate assisted catalysis unifies two families of chitinolytic enzymes. *J Am Chem Soc* 119:7954–7959
- Terwisscha van Scheltinga AC, Armand S, Kalk KH et al (1995) Stereochemistry of chitin hydrolysis by a plant chitinase/lysozyme and X-ray structure of a complex with allosamidin: evidence for substrate assisted catalysis. *Biochemistry* 34:15619–15623
- Hollis T, Monzingo AF, Bortone K et al (2000) The X-ray structure of a chitinase from the pathogenic fungus *Coccidioides immitis*. *Protein Sci* 9:544–551
- Brameld KA, Goddard WA III (1998) Substrate distortion to a boat conformation at subsite -1 is critical in the mechanism of family 18 chitinases. *J Am Chem Soc* 120:3571–3580
- Terwisscha van Scheltinga AC, Hennig M, Dijkstra BW (1996) The 1.8 Å resolution structure of hevamine, a plant chitinase/lysozyme, and analysis of the conserved sequence and structure motifs of glycosyl hydrolase family 18. *J Mol Biol* 262:243–257
- Songsiririthigul C, Pantoom S, Aguda AH et al (2008) Crystal structures of *Vibrio harveyi* chitinase A complexed with chitooligosaccharides: implications for the catalytic mechanism. *J Struct Biol* 162:491–499
- Uchiyama T, Katouno F, Nikaidou N et al (2001) Roles of the exposed aromatic residues in crystalline chitin hydrolysis by chitinase A from *Serratia marcescens* 2170. *J Biol Chem* 276:41343–41349
- Sörbotten A, Horn SJ, Eijsink VG et al (2005) Degradation of chitosans with chitinase B from *Serratia marcescens*. Production of chitooligosaccharides and insight into enzyme processivity. *FEBS J* 272:538–549
- Horn SJ, Sörbotten A, Synstad B et al (2006) Endo/exo mechanism and processivity of family 18 chitinases produced by *Serratia marcescens*. *FEBS J* 273:491–503
- Boisset C, Fraschini C, Schülein M et al (2000) Imaging the enzymatic digestion of bacterial cellulose ribbons reveals the endo character of the cellobiohydrolase Cel6A from *Humicola insolens* and its mode of synergy with cellobiohydrolase Cel7A. *Appl Environ Microbiol* 66:1444–1452
- Imai T, Boisset C, Samejima M et al (1998) Unidirectional processive action of cellobiohydrolase Cel7A on Valonia cellulose microcrystals. *FEBS Lett* 432:113–116
- Imai T, Watanabe T, Yui T, Sugiyama J (2002) Directional degradation of beta-chitin by chitinase A1 revealed by a novel reducing end labelling technique. *FEBS Lett* 510:201–205
- Suginta W, Vongsuwan A, Songsiririthigul C et al (2005) Enzymatic properties of wild-type and active site mutants of chitinase A from *Vibrio carchariae*, as revealed by HPLC-MS. *FEBS J* 272:3376–3386

35. Suginta W, Songsiririthigul C, Kobdaj A et al (2007) Mutations of Trp275 and Trp397 altered the binding selectivity of *Vibrio carchariae* chitinase A. *Biochim Biophys Acta* 1770:1151–1160
36. Laemmli UK (1970) Cleavage of structural proteins during the assembly of the head of bacteriophage T4. *Nature* 227:680–685
37. Bradford MM (1976) A rapid and sensitive method for the quantitation of microgram quantities of protein utilizing the principle of protein-dye binding. *Anal Biochem* 72:248–254
38. Miller GL (1959) Use of dinitrosalicylic acid reagent for determination of reducing sugar. *Anal Chem* 31:426–429
39. Armand S, Tomita H, Heyraud A et al (1994) Stereochemical course of the hydrolysis reaction catalysed by chitinase A1 and D from *Bacillus circulans* WL-12. *FEBS Lett* 343:177–180
40. Aronson NN Jr, Halloran BA, Alexyev MF et al (2003) Family 18 chitinase-oligosaccharide substrate interaction: subsite preference and anomer selectivity of *Serratia marcescens* chitinase A. *Biochem J* 376:87–95
41. Fukamizo T, Sasaki C, Schelp E et al (2001) Kinetic properties of chitinase-1 from the fungal pathogen *Coccidioides immitis*. *Biochemistry* 40:2448–2454
42. Sasaki C, Yokoyama A, Itoh Y et al (2002) Comparative study of the reaction mechanism of family 18 chitinases from plants and microbes. *J Biochem* 131:557–564
43. Pantoom S, Songsiririthigul C, Suginta W (2008) The effects of the surface-exposed residues on the binding and hydrolytic activities of *Vibrio carchariae* chitinase A. *BMC Biochem* 9:2
44. Watanabe T, Ariga Y, Sato U et al (2003) Aromatic residues within the substrate-binding cleft of *Bacillus circulans* chitinase A1 are essential for hydrolysis of crystalline chitin. *Biochem J* 376:237–244

CURRICULUM VITAE

NAME Miss Supansa Pantoom

DATE OF BIRTH September 30, 1982

PLACE OF BIRTH Khon Kean, Thailand

INSTITUTION ATTENDED

Khon Kean University, Khon Kean, Thailand, 2001-2005, Bachelor of Science (Biochemistry).

Suranaree University of Technology, Nakhon Ratchasima, Thailand, 2005-2010, Doctor of Philosophy (Biochemistry).

AWARDS AND SCHOLARSHIPS

Research Project for Undergraduate Students Award (RPUS), 2003-2004.

Second class honors, Khonkean Univerity, Khonkean, Thailand, 2005.

The Thailand Research Fund (TRF), 2005-2006.

Max-Planck Institute Fellowship, Dortmund, Germany, December 2009- April 2010.

The Royal Golden Jubilee Ph.D. Program scholarship, from the Thailand Research Fund 2008-2010.